DSE - Wings for Aid

Design an unmanned aircraft that can deliver 5 aid packages of 20 kg each with a range of 500 km.

Y. Bunk	4271408	M.J. Mollema	4284852
M.J. Faber	4294157	N. Pynaert	4277635
D.B. de Jong	4291506	B. Slangen	4278070
L.N. Lodder	4296990	B. Smit	4289692
L. M. van Loo	4211405	L. Vertonghen	4306716

Final Report

Design Synthesis Exercise

TU Delft Delft University of Technology

Aerospace Engineering

June 28, 2016

Preface

This report is the result of the Design Synthesis Exercise, and is the culmination of the Aerospace Engineering bachelor's programme at the Delft University of Technology. Ten students were assigned to design an unmanned aerial vehicle capable of delivering humanitarian aid for the Wings for Aid foundation.

We would like to thank Ir. J.A. Melkert, Ir R. van Gent, Dr. Ir. S. Hartjes and J. Nie, Msc. for their insights and guidance during the project. From VanBerlo we would like to thank D. Zeelenberg, A. Roseillier and W. Holtslag for their support during the design of the UAV. We would also like to thank B. Koperberg from the Wings for Aid foundation. We would like to thank E. Brouwer for his knowledge on aid distribution operations. We would like to thank A. Dekker from Smurfit Kappa for his knowledge on packaging design.

Summary

This report presents the results of the Design Synthesis Exercise for Wings for Aid. The aim was to design a cost effective, rapidly deployable and easily transportable cargo delivery UAV. A market analysis showed that there is a real need for reliable transportation in the last mile of humanitarian aid distribution. It also concluded that other UAVs currently capable of carrying out this mission are either expensive or have very limited payload capabilities.

To fill this market gap a UAV was designed with a cost price of just €15,000. In order to fulfill the stakeholder requirements a detailed look was taken at the aerodynamics and wing design, the performance, the stability and control and the structure. The UAV design is heavily inspired by kitplanes and general aviation propeller aircraft. A conventional take-off and landing aircraft with a puller engine configuration and a tricycle landing gear was deemed most efficient to carry out this mission, taking into account the short take-off and landing distances required on rough terrain.

The structure had to be designed in such a way that it was both lightweight and easy to produce, Therefore a foam wing core concept was developed, which will be covered by an aluminium skin. It is slightly heavier than more conventional options but easier to produce in larger quantities, and therefore more cost effective. For the fuselage a simple riveted construction was chosen, and a tail boom to mount the tail surfaces on. A simple solid spring landing gear is both easy to manufacture and low in parts. It is strong enough to take up the landing loads, yet still lightweight. Finally in order to increase the operational mobility of the aircraft the wing, tail surfaces and landing gear are all made detachable. The Wings for Aid UAV has a maximum take-off weight of 350 kg, an operational empty weight of 212 kg, a wingspan of 7.9 m, a wing area of 9.8 m^2 and a total length of 5.9 m. With a fuselage width of 0.58 m and by placing two UAVs in an opposite direction both UAVs can be placed in a standard 20 ft container. By removing the landing gear this increases to four UAVs per container

The turnaround time of every UAV during operation is 29 min, however due to an assembly line strategy, a UAV can take off and land every 6.4 min. This means that for a warzone mission a minimum of 53 UAVs and for a regular mission a minimum amount of 45 UAVs is required to reach the required capacity requirement of 22,500 kg delivered aid supply within 24 hours. The operational costs for the UAV are €27,423 to deliver 22,500 kg of goods to a location 500 km away from the ground site. This means that the Wings for Aid UAV can compete with the C-130 Hercules (€32,678) and the UH-1 Bell Huey (€897,000) from a cost perspective.

In aerodynamic design special care was paid first to the fuselage, where the optimal angle for fuselage closure was determined in order to minimize drag in cruise flight. Having the manufacturing freedom of foam, a custom airfoil was created by optimizing the NACA24012 airfoil for the flight conditions of our UAV, which increased the performance by 20%. A wing planform was also generated to approach an elliptical lift distribution to maximize the wing efficiency.

The operational aspect of the UAV was worked out in detail. Five hubs across the globe will serve as storage location for a fleet of UAVs, from where they can be rapidly deployed to almost any location on earth. Two different scenario's have been worked out, and in each scenario it is shown that the Wings for Aid UAV will offer better cost and time efficiency than traditional airlift methods, and therefore a very viable option for last mile humanitarian aid transportation.

Finally in post-DSE logistics plan was generated which explains the manufacturing and assembly method of the UAV, and the logistics which will bring the UAV from a preliminary design to final product integration into the market.

Table of contents

1 Introduction **11**

2 Market analysis **12**
2.1 The last mile in humanitarian aid distribution . . . 12
2.2 Currently available technology . . . 12

3 Final design process **15**

4 Final design **18**
4.1 Design considerations . . . 18
4.2 Design choices . . . 18
4.3 Final design parameters . . . 21
4.4 Internal lay-out . . . 21
4.5 CAD drawings . . . 23

5 Aerodynamics **26**
5.1 Wing design . . . 26
5.2 Wing planform design . . . 29
5.3 Fuselage drag . . . 34
5.4 UAV drag polar . . . 40
5.5 Verification and validation . . . 41

6 Performance and propulsion **42**
6.1 Flight envelope . . . 42
6.2 Mission profile . . . 42
6.3 Payload-range diagram . . . 43
6.4 Functional Flow of take-off and cruise . . . 45
6.5 Take-off, landing and general performance . . . 45
6.6 Total mission time . . . 46
6.7 Engine selection . . . 47
6.8 Propeller design . . . 51
6.9 Noise characteristics . . . 54
6.10 Verification and validation . . . 54

7 Stability and control **56**
7.1 Center of gravity range . . . 56
7.2 Control forces and control surface sizing . . . 56
7.3 DATCOM . . . 60
7.4 Longitudinal stability derivatives . . . 61
7.5 Symmetric state space system . . . 63
7.6 Symmetric eigenmodes . . . 64
7.7 Lateral stability derivatives . . . 65
7.8 Asymmetric state space system . . . 67
7.9 Asymmetric eigenmodes . . . 67
7.10 Propeller effects . . . 69
7.11 Verification and validation . . . 69

8 Structures **71**
8.1 Materials characteristics and selection . . . 71
8.2 Fuselage structure . . . 72
8.3 Wing structure . . . 77
8.4 Landing gear structure . . . 94
8.5 Tail structure . . . 98
8.6 Empennage structure . . . 101
8.7 Nose and tail cover . . . 102

9 Payload and dropping mechanism **105**
9.1 Drop mechanism design . . . 105
9.2 Drop maneuver . . . 105
9.3 Functional flow of dropping . . . 108
9.4 Verification and validation . . . 109

10 Auxiliary UAV systems **110**
10.1 Fuel system . . . 110
10.2 Exhaust gas temperature probe . . . 110
10.3 Wheels and braking systems . . . 111
10.4 Anti-icing systems . . . 111
10.5 Firewall . . . 112
10.6 Avionics . . . 112
10.7 Communication and navigation systems . . . 113
10.8 Collision avoidance . . . 114
10.9 Lighting . . . 115
10.10 Emergency systems . . . 115
10.11 Electrical systems . . . 116
10.12 Hardware and software . . . 118
10.13 Communication within system . . . 118

11 Operations and logistics concept **120**
11.1 Global logistics . . . 120
11.2 Local logistics . . . 125
11.3 Ground operations . . . 125
11.4 Operational cost estimate . . . 126
11.5 Wings for Aid deployability . . . 127
11.6 Scenarios . . . 127
11.7 Operational flow diagram . . . 129
11.8 Verification and validation . . . 130

12 Final design evaluation **132**
12.1 Cost budget . . . 132
12.2 Weight budget . . . 133
12.3 Requirement compliance analysis . . . 134
12.4 Risk evaluation and management . . . 134
12.5 Reliability, availability, maintainability and safety . . . 137
12.6 Sensitivity analysis . . . 141
12.7 Sustainability . . . 142

13 Post-DSE project plan **144**
13.1 Post-DSE project development . . . 144
13.2 Manufacturing and assembly plan . . . 144

14 Conclusion and recommendations **146**
14.1 Conclusion . . . 146
14.2 Recommendations . . . 146

A Total operational cost **149**

B DATCOM input file **150**

List of abbreviations

Abbreviation	Description
AC	Alternating Current
ADS-B	Automatic Dependent Surveillance-Broadcast
AoA	Angle of Attack
ATC	Air Traffic Control
CAD	Computer Aided Design
CFD	Computational Fluid Dynamics
CG	Center of Gravity
CS-LUAS	Certification Specifications for Light Unmanned Aerial Systems
CS-VLA	Certification Specifications for Very Light Aircraft
DC	Direct Current
DSE	Design Synthesis Exercise
EASA	European Aviation Safety Agency
ESC	Electronic Speed Controller
FAA	Federal Aviation Administration
GNSS	Global Navigation Satellite System
ht	Horizontal tail
IDC	Inter Drone Communication
IMU	Inertial Measurement System
LE	Leading Edge
LiDAR	Light Detection And Ranging
MAC	Mean Aerodynamic Chord
MTOW	Maximum Take-Off Weight
MZFW	Maximum Zero Fuel Weight
NACA	National Advisory Committee for Aeronautics
OEW	Operational Empty Weight
PMA	Parts Manufacturer Approval
RD	Rate of descent
ROC	Rate of climb
RON	Research Octane Number
SFC	Specific Fuel Consumption
SWOT	Strength, Weakness, Opportunities and Threats
TOP	Take-Off Parameter
TPM	Technical Performance Measurement
TRL	Technology Readiness Level
UAV	Unmanned Aerial Vehicle
USA	Up Sweep Angle
USAAF	United States Army Air Forces
VALID	Verifiable, Achievable, Logical, Integral and Definitive
vt	Vertical tail

End of list of abbreviations

List of symbols

Sign	Description	Unit
$\Lambda_{0.25c}$	Sweep at quarter chord	radians
$\Lambda_{0.5c}$	Sweep at half chord	radians
$\Lambda_{H.L.}$	Sweep at control surface hinge line	radians
$\Lambda_{max,t}$	Maximum airfoil thickness sweep	radians
α	Airfoil angle of attack	radians
α_0	Zero lift angle of attack	radians
β	Side-slip angle	radians
β	Prandtl compressibility factor	-
$\ddot{\theta}$	Pitch angular acceleration	rad/s^2
δ_R	Rudder deflection	radians
δ_a	Aileron deflection	radians
δ_e	Elevator deflection	radians
δ_f	Flap deflection	radians
η	Airfoil efficiency	-
η_p	Propeller efficiency	-
$\frac{(\alpha_\delta)_{C_L}}{(\alpha_\delta)_{C_l}}$	Ratio of 3-D flap-effectiveness parameter to 2-D flap-effectiveness parameter	-
γ	Flight path angle	radians
λ	Taper	radians
λ_v	Taper ratio vertical tail	-
μ	Friction coefficient	-
ν	Poission's ratio	-
ϕ	Roll angle	radians
$\sigma_{cr}(y$	Span-wise critical skin buckling stress	MPa
σ_{flange}	Span-wise normal stress in flange of the spar	MPa
$\sigma_{max}(y)$	Span-wise maximal normal stress	MPa
$\sigma_{skin}(y)$	Span-wise normal stress in wing skin	MPa
θ	Pitch angle	radians
ε_{flange}	Strain in flange of spar	-
A	Aspect ratio	-
a	Acceleration	m/s^2
a	Speed of sound	m/s
A_p	Propeller Area	m^2
A_w	Wetted area	m^2
b	Wing span	m
$b_{skin}(y)$	Span-wise distance between stiffeners	m
c	Chord length	m
c(y)	Span-wise chord length	m
c_a/c	Aileron chord over wing chord	-
C_D	Dimensionless 3-D drag coefficient	-
C_d	Dimensionless 2-D drag coefficient	-
C_{D_0}	Zero lift 3-D drag coefficient	-
C_{d_0}	Zero lift 2-D drag coefficient	-
C_F	Friction coefficient	-
$C_{F_{2D}}$	Basic friction coefficient	-

List continues on next page

Sign	Description	Unit
c_f/c	Flap chord over wing chord	-
C_L	Dimensionless 3-D lift coefficient	-
C_l	Dimensionless 2-D lift coefficient	-
C_{l_0}	Zero angle of attack 2-D lift coefficient	-
C_{L_α}	Lift gradient	1/radians
$C_{L_{\alpha_v}}$	Lift gradient of vertical tail	-
$C_{l_{\alpha_v}}$	Lift gradient of vertical tail airfoil	-
$C_{L_{\alpha_w}}$	Lift gradient of wing	-
C_{l_δ}	Lift effectiveness of plain flap	1/rad
$C_{l_{\delta_A}}$	Roll control derivative	-
$C_{L_{des}}$	Design 3-D lift coefficient	-
$C_{l_{des}}$	Design 2-D lift coefficient	-
$C_{L_{max}}$	Maximum 3-D lift coefficient	-
$C_{l_{max}}$	Maximum 2-D lift coefficient	-
C_m	Moment coefficient	-
C_{n_β}	Side-force-due-to-rudder derivative	-
$C_{n_{\delta_R}}$	Yawing-moment-due-to-side-slip derivative	-
C_p	Specific fuel consumption	kg/J
c_r	Root chord	m
c_{rudder}/c	Rudder chord over vertical tail chord	-
$C_{y_{\delta_R}}$	Side-force-due-to-rudder derivative	-
D	Drag	N
d_F	Diameter fuselage	m
d_p	Propeller diameter	m
e	Oswald factor	-
E_{al}	Young's modulus of aluminium alloy	MPa
E_{pl}	Young's modulus of plastic	MPa
e_{theo}	Theoretical Oswald factor	-
F	Force	N
g	Gravitational acceleration	m/s^2
I	Moment of inertia of the spar	m^4
I_p	Propeller mass moment of inertia	kgm^2
I_{xx}	Mass moment of inertia around x-axis	$kg \cdot m^2$
I_{yy}	Mass moment of inertia around y-axis	$kg \cdot m^2$
$I_{yy_{mg}}$	Pitching moment of inertia around main gear contact point	$kg \cdot m^2$
I_{zz}	Mass moment of inertia around z-axis	$kg \cdot m^2$
J_{climb}	Propeller advance ratio during climb	-
J_{cruise}	Propeller advance ratio during cruise	-
K_b	Flap-span factor	-
k_c	Skin buckling coefficient	-
K_f	Empirical correction for plain lift increment	-
K_q	Lift force distribution constant	N/m^2
L	Lift	N
$L'(y)$	Span-wise lift distribution	N/m
L_h	Lift force of horizontal tail	N
l_v	Longitudinal distance between center of gravity and vertical tail aerodynamic center	m
L_{wf}	Lift force of wing-fuselage	N
m	Mass	kg

List continues on next page

Sign	Description	Unit
M(y)	Span-wise moment	Nm
M	Mach number	-
$M_{ac_{wf}}$	Moment of wing-fuselage around aerodynamic center	Nm
n_{lim}	Limit load factor	-
n_{ult}	Ultimate load factor	-
p	UAV roll rate	rad/s
P_D	Propeller pitch	m
P_{ng}	Normal force on nose landing gear	N
P_{shaft}	Engine shaft power	W
q	Dynamic pressure	Pa
r	Radius	m
Re	Reynolds number	-
RPM	Engine revolutions per minute	min^{-1}
RPM_p	Propeller revolutions per minute	min^{-1}
s	Distance	m
S(y)	Span-wise shear force	N
S_{exp}	Exposed wing surface area	m^2
$S_{front}(y)$	Span-wise shear force on front spar	N
SFC	Specific fuel consumption	kg/J
$S_{flapped}$	Flapped area	m^2
$S_{rear}(y)$	Span-wise shear force on rear spar	N
S_v	Vertical tail surface area	m^2
S_w	Wing area	m^2
T	Torque	Nm
t/c	Airfoil thickness over chord ratio	-
$t_{skin}(y)$	Span-wise thickness of the wing skin	m
$\dot{u}$	Forward acceleration	m/s^2
V	Speed	m/s
V_a	Manoeuvre speed	m/s
$V_{approach}$	Approach velocity during landing	m/s
V_c	Cruise speed	m/s
V_d	Dive speed	m/s
V_{KTAS}	True airspeed in knots	kts
V_s	Stall speed	m/s
V_w	Crosswind velocity	m/s
W_f	Fuel weight	N
W_L	Landing weight	N
W_p	Payload weight	N
W_{TO}	Take-off weight	N
x_{ac_h}	X-location of the aerodynamic center of the horizontal tail	m
$x_{ac_{wf}}$	X-location of the aerodynamic center of wing-fuselage	m
x_{cg}	X-location of the center of gravity	m
x_{ng}	X-location of the nose landing gear	m
x_t	Longitudinal tail position	m
x_w	Longitudinal wing position	m
z_D	Z-location of the drag force	m
z_{mg}	Z-location of main landing gear	m
z_T	Z-location of the engine/propeller	m
z_v	Vertical distance between center of gravity and vertical tail aerodynamic center	m

End of list of symbols

Chapter 1

Introduction

Traditional means of transportation are often inadequate in inhospitable areas where humanitarian aid is required, such as in a warzone or following a natural disaster. One of the biggest challenges that humanitarian aid organizations face is the lack of infrastructure and logistical organization in the affected areas. These challenges make delivering sufficient aid in a timely manner extremely expensive. The Wings for Aid initiative aims to deliver aid to those in need in disaster areas quickly, efficiently and at a low cost through the use of a set of rapidly deployable unmanned aerial vehicles (UAVs).
The aim of these UAVs is to be able to transport five 20 kg packages over a distance of 500 km. The packages will contain food, water and blankets sufficient to provide relief to victims on the ground for several days. These goals resulted in a need statement and a mission statement for the wings for aid UAV:

Need statement There is a need to provide fast, low cost and accurate humanitarian aid in areas which are hard to reach by conventional aid transportation on a short notice.

Mission statement Wings for Aid will deliver accurate emergency humanitarian aid with a UAV within a 500 km range, in areas hard to reach for conventional transportation, with a lower operational cost than a helicopter and a unit cost price less than €15,000.

The conceptual and preliminary design of the Wings for Aid UAV was carried out in collaboration with the Wings for Aid consortium, and in particular with the engineers from VanBerlo. This report presents the results of the design of the Wings for Aid UAV. It contains details on the aerodynamics, performance, stability and control, and structures. It also analyzes the feasibility of the final design. Moreover, in collaboration with a Red Cross representative a detailed operational analysis was carried out, which will also be discussed.

Chapter 2

Market analysis

In this chapter humanitarian aid distribution will be discussed, with a focus on the last step in the supply chain, the last mile. First the current methods of aid distribution during the last mile will be discussed in Section 2.1. In Section 2.2 current possibilities of cargo delivery will be mentioned, identifying their capabilities and limits and thereby identifying the gap in the market the Wings for Aid drone aims to fill.

2.1 The last mile in humanitarian aid distribution

Emergency logistics is the most expensive part of any relief operation and the part that can mean the difference between a successful or failed operation [1]. The last mile is the final hurdle in the delivery of aid supplies from local warehouses to people in need. The most significant logistical problems in the last mile generally stem from the limitations related to transportation resources and emergency supplies, difficulties due to damaged transportation infrastructure, and lack of coordination among relief actors [2].

The sheer complexity of the operating conditions is the factor that differentiates private sector supply chain logistics from humanitarian aid logistics. It is for this reason that humanitarian aid relief requires robust equipment that can be set up and dismantled quickly, enabling them to be adaptable to highly dynamical circumstances [1].

In its current state humanitarian aid is often distributed by a combination of road, rail and air transport. The factors which determine the distribution method include accessibility of the area, urgency of supply and cost effectiveness of the route. In determining which of these factors is driving, a distinction must be made between sudden onset and slow onset disasters.

In case of slow onset disasters such as a drought, the existing infrastructure, though it may be limited, is not affected as much and is still usable for aid delivery. Therefore cost effectiveness becomes one of the driving factors, such that as many people as possible can be reached. In this scenario aid shipments can be split between different modes of transport. Usually a rail/road combination is most effective in this case, with just a few air lift operations for high-urgency shipments [3]. The exception is for slow onset disasters in areas where the roads and rail tracks are not safe such as, for example,+ Syria.

However in case of sudden onset disasters such as an earthquake, infrastructure is likely to be damaged and/or unusable and airlifts quickly can become the only viable method to be effective, especially in the critical first few days. In this case the amount of people that can be reached is purely dependent on the capacity of the airfields surrounding the disaster area. Four key areas determining capacity are warehousing, transport, material handling devices and human resources [4]. Due to a lack of ground equipment and size of the airport apron in remote areas, turnaround time and space for large aircraft quickly become the bottleneck in airlift operations [3]. Therefore the challenge in designing for Wings for Aid lies in avoiding these logistical challenges and maximizing capacity. The aim is to improve capacity by limiting the required material handling and human resources required, and by being operable regardless the state of ground infrastructure. In this manner, the capacity of Wings for Aid will be purely dependent on the number of drones deployed and the amount of supplies that are available on the distribution location.

2.2 Currently available technology

Having identified the challenge that the market faces, the current state of technology can be discussed. At present there are various ways to deliver aid to those in need. The most common and well known delivery method is through the use of military cargo aircraft such as the Hercules C-130. Other methods aid delivery are helicopters, drones and trucks.

Table 2.1: Wings for Aid and other UAVs with a payload around 100 kg or a range close to 500 km.

UAV	Unit cost [€]	MTOW [kg]	Payload [kg]	Range [km]
Schriebel Camcopter S-100[5]	430,000	200	50	200
MMIST CQ-10 Snowgoose[6]	290,000	635	272	300[7]
Elbit Hermes 450[8]	1,900,000	450	150	300
MQ-1 Predator[9]	4,000,000	1020	204	1100
AAI RQ-7 Shadow[10]	700,000	170	45	109
Wings for Aid	15,000	335	100	500

The Hercules C-130 makes a good aid delivery aircraft as it can haul heavy loads and it is able to land on and take off from a relatively short and unpaved runway. Furthermore it has a high cruise speed and a long range which means that it can travel to a disaster area from large distances if necessary. These benefits do come at an operation cost of around $18,500 per flight hour for the C-130H model[1] realized by the US air force.

Loading and unloading can be done swiftly if the right equipment and manpower is available. However, loading operations can take hours in places where no unloading devices are present and the manpower is limited. Additionally the C-130 falls short in the last mile as it can only transport the aid to an airport near the required area and not all the way to the people who need aid. The last mile is thus to be done by other means of transportation or dropping.

The last mile is where a helicopter can excel as it can land at each village requiring aid and distribute the aid to the doorstep of those who need it. However, helicopters are not always available in the affected area and can usually only be flown in from far away at a large cost. The operating costs of helicopters are also quite high at around $23,500 per flight hour for a UH-1H[2]. Per kilometer per ton this translates into 8,6 $€/km/ton$. Another downside of a helicopter is that it requires a skilled pilot to fly who will be subject to fatigue and therefore an helicopter can only be 24/7 operational if there are multiple pilots available.

Cargo UAVs are currently only used for medicine drops in remote areas and by the military to resupply soldiers in inaccessible areas. Examples are the Zipline medicine drone used in Rwanda[3] and the military MMIST CQ-10 Snowgoose used in the Middle East[4]. The medicine drones generally carry payloads smaller than 2 kg and have a high cruise speed to be able to deliver the medicines quickly. The military resupply drones either have a small range or small payload. The benefit of these UAVs is that they have very short take off distances, or are launched from a launcher.

Besides the cargo delivery UAVs the military extensively uses observational drones. These are large drones with a very large endurance and are designed to wait for an opportunity to engage a target. This type of UAVs, however, costs millions, fly at very high altitudes and they require long smooth runways to take off and land. They are therefore not representative for the mission of the Wings for Aid drones. The currently available UAVs that are the most similar to the Wings for Aid mission are listed in Table 2.1.

[1] URL `http://nation.time.com/2013/04/02/costly-flight-hours/` [Cited 28/04/2016]
[2] See Footnote 1
[3] URL `http://flyzipline.com/product/` [Cited on 20/06/2016]
[4] URL `http://www.mmist.ca/Media/Docs/Brochures/SnowGoose_Brochure.pdf` [Cited 26/04/2016]

The functionality of these UAVs measured as payload times range and the unit costs are plotted in Figure 2.1.

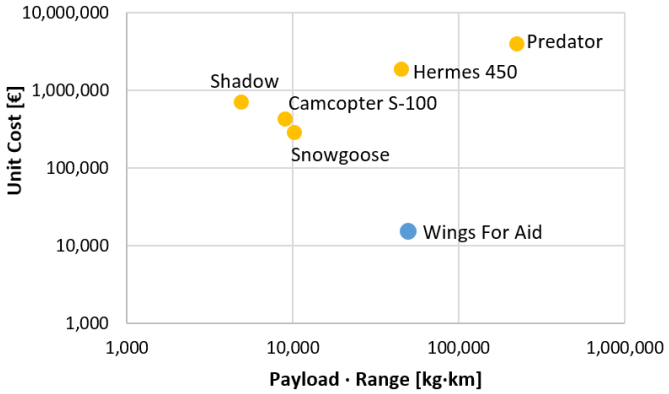

Figure 2.1: Functionality measured as payload times range vs the unit costs with logarithmic axes.

The use of trucks and trains to deliver goods to their final destination is on paper the cheapest option with trucks having an operational costs of 0.09 €/km/ton, based on an payload of 10 tons, fuel efficiency of 0.3 l/km, diesel price of 1.17 €/l and a ratio between the fuel and operating costs of 2.6[11]. However trucks and trains are not always the easiest to apply in practice. First of all, in case of a natural disaster, the local facilities can be damaged, and therefore out of service. This would render a train ineffective, as it can not move without rails. A truck could still make use of damaged roads, up to a certain point, depending on its size and weight. But driving on off road conditions will oblige a truck to go slower to make sure no mechanical failure occurs. Additionally, ground convoys are more prone to ambushes and being halted by locals and border control. Not only does it put the aid delivery at risk, but again slows down the process of getting the help at the intended destination. As the key point of aid delivery just after a disaster is the fast response, thus truck and train usage is not preferred.

With trucks and manned aircraft being unfeasible for crossing the last mile and helicopters being too expensive, a gap in the market is open for UAVs to fill. Currently there are UAVs available which have the payload and range to fill this gap, however they all have unit costs which are far above the budget of an aid organisation. Especially when considering that 50 to 100 drones will be required to keep up with the transporting capacity of a Hercules C-130. The cost difference is especially obvious from Figure 2.1. This means that there is a gap in the market for a cheap UAV that can deliver moderate payloads at a lower operating costs than a helicopter, that can be rapidly transported to the disaster area from a large distance and that can operate 24/7.

[5]URL https://schiebel.net/wp-content/uploads/2015/06/CAMCOPTER-S-100-Brochure-English.pdf [Cited 26/04/2016]
[6]See Footnote 4
[7]300 km range is with 34 kg payload
[8]URL https://www.elbitsystems.com/elbitmain/area-in2.asp?parent=3&num=32&num2=32 [Cited 26/04/2016]
[9]URL http://www.af.mil/AboutUs/FactSheets/Display/tabid/224/Article/104469/mq-1b-predator.aspx [Cited 26/04/2016]
[10]URL https://safety.army.mil/Portals/0/Documents/ON-DUTY/AVIATION/SHADOW/Standard/Shadow_4Apr2011.pdf [Cited 26/04/2016]
[11]URL http://www.atri-online.org/wp-content/uploads/2014/09/ATRI-Operational-Costs-of-Trucking-2014-FINAL.pdf [Cited op 28/04/2016]

Chapter 3

Final design process

A summary of the project management practise is given in the midterm report [5]. For the last phase of the project, the final design phase, a more detailed design procedure is made and explained in this chapter. The division in subsystems remains unaltered, however three more subsystems are added since these play also a major role in the project. These compartments are Operations, Systems/Avionics and Manufacturing.

The final design process is given in Figure 3.1. The output of the design tool developed in the conceptual design phase consists of preliminary design parameters based on first and second order estimations. It requires the chosen UAV configuration and related statistical data as input. The UAV configuration is discussed in Chapter 4. Verification has to be performed on the correctness of the design tool code checking whether the configuration with its parameters meets the system requirements. If the system requirements are not met, the parameters need to be reconsidered by putting different constraints in the design tool. The design parameters are iterated until the requirements are met.

If the design parameters meet the requirements a detailed subsystem design is initiated. This subsystem design is based on subsystem requirements and subsystem resources such as mass and cost. A detailed description of all subsystem requirements is given in Section 12.3. While designing the subsystems it is very important not to forget the global picture and the chief engineer is responsible for the interactions between the subsystems keeping the complete system in mind. Each compartment will have to validate its data and check if the subsystem requirements are met. If this is not the case this specific subsystem will need to be revised. Based on the detailed subsystem design the global system is updated. A CAD model is made to visualize its characteristics and evaluates further subsystem requirements in terms of special and dimensional constraints. In the end the global system will need to be validated against its requirements, especially the key stakeholder requirements.

If the key requirements are not met, something went wrong in the subsystem design and will need to be reconsidered. This is done after a revision of the resource allocation. When system requirements are met, the risk of the project has to be investigated. A quality control is performed assessing reliability, availability, maintainability, and safety (RAMS) characteristics. When the risk or quality assessments reveals possible improvements in the design, more iterations of the system design process are performed. When an optimal design is reached a manufacturing and assembly plan is made to prepare the UAV for production.

Previous described model represents a combination of the Spiral and V-model for systems design. Both iterations and verification and validation procedures are considered.

Of course the interfaces between all subsystems are more complex than described in the design process. All subsystems interact with each other. An interface definition is given by the N2 chart in Figure 3.2.

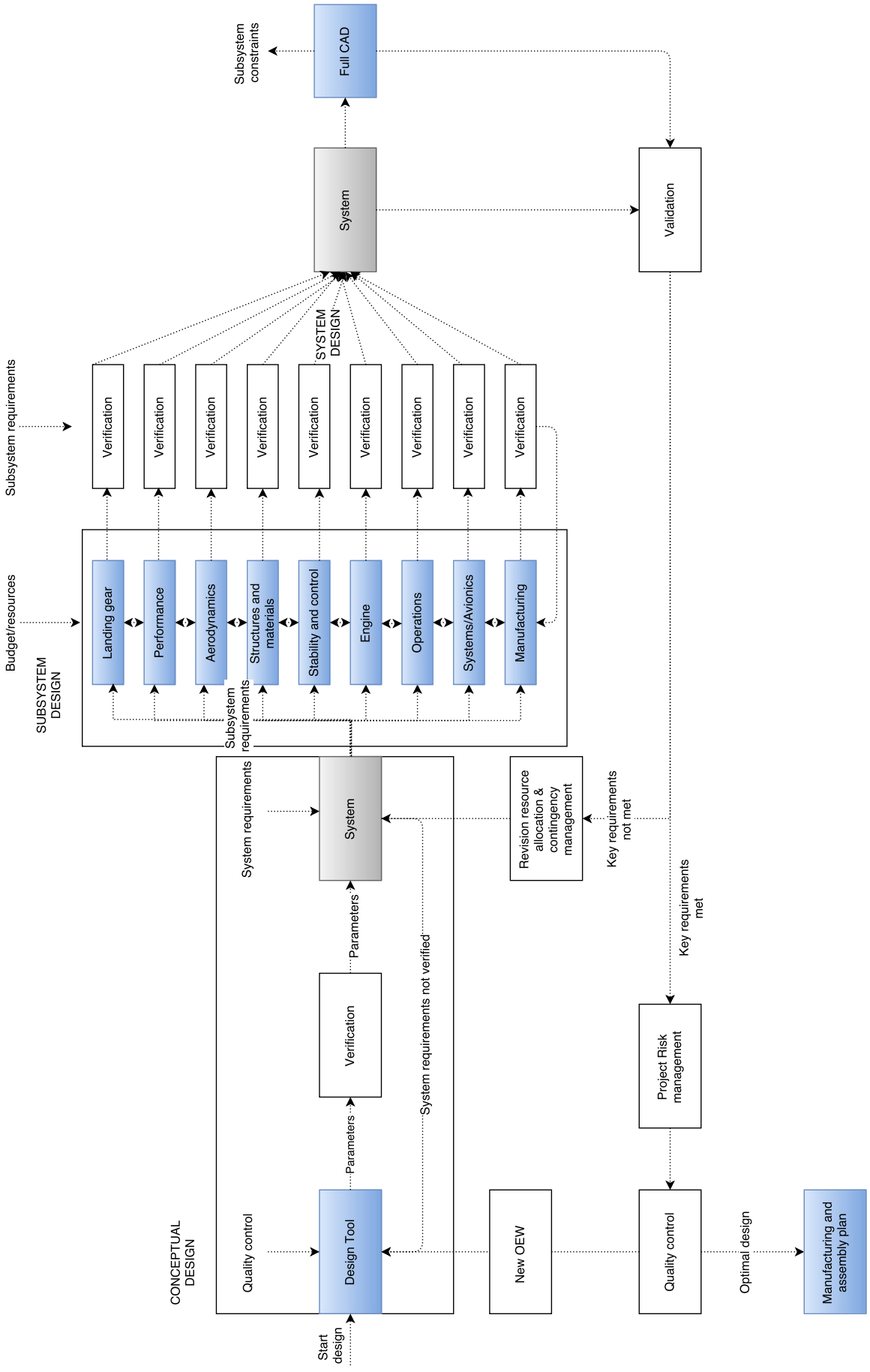

Figure 3.1: Final design process.

Aerodynamics	Wing planform	•Moment/lift characteristics •Stability derivatives •Planform dimensions	Lift/drag characteristics	•Landing •Take-off characteristic				Shape
Wing planform	**Structures and materials**	Tail planform	Weight	•Maintenance cost •Weight				Center of gravity location	Trinity
•Stability characteristics •Control Surfaces	•Location control surfaces •Tail length •Wing position •Control forces	**Stability and control**	Trim drag	Stability behaviour	Stability behaviour				
•Drag/lift characteristics •Cruise conditions	Load factor	Critical load cases	**Performance**	•Complexity operations •Cruise conditions •Climb performance	Propulsion system Fuel tanks	•Power requirement •Cruise conditions	Wing loading		
•Dropping manoeuvre •Payload dimensions	•Dropping mechanisms •Modularity	Dropping manoeuvre	Dropping manoeuvre	**Operations**	Manoeuvres				
	•Location systems •Electrical routing	Autopilot	Fuel system	Complexity operations	**Systems/avionics**				
	•Engine mounting •Engine thrust	Propeller dimensions	Fuel consumption	Fuel consumption	Power	**Engine**	Propeller diameter		
Landing gear dimension/shape	Landing gear location	Landing gear dimension					**Landing gear**		
•Surface finish •Shape	Trinity								**Manufacturing**

Figure 3.2: Interface definition subsystems.

Chapter 4

Final design

This chapter describes the outcome of the final design process. The design considerations, drivers and decisions taken after the midterm review are presented in Sections 4.1 and 4.2. Additionally the final design is presented in Section 4.3 and the internal layout in Section 4.4 complemented by CAD drawings in Section 4.5.

4.1 Design considerations

While designing the Wings for Aid UAV certain aspects were very important not only to the customer but also to the overall success of the UAV and aid delivery operation as a whole. Especially the low cost requirement was a major design driver, and specific considerations were taken to reduce the cost as much as possible. The various design considerations which made a significant impact on the Wings for Aid UAV are explained in this section.

Commonality

The design of the UAV is constrained to a strict cost requirement. The production of the UAV forms a significant amount of the unit cost. This cost can be decreased significantly by having as much common parts as possible. In the design of the UAV this is taken into account, and expressed in following design decision; The horizontal tail has the same planform as the vertical tail. The elevator and rudder are the same as well. The majority of the fuselage components and stiffeners are also identical.

Simple design

To meet the unit cost requirement, the design is made as simple as possible. This means the use of off-the-shelf components, standardized structural elements and cheap materials. Moving and complex systems are avoided.

Manufacturing

A third important driver is producibility and manufacturing. To decrease costs the installation of the components should be as easy as possible. This means that easy access during assembly is required. Furthermore the part manufacturing methods are to be considered as well. Cheap manufacturing is taken into account during all design trade-offs.

Maintainability

Maintainability is directly related to accessibility as easy access allows easy maintenance. Again the open structure of the fuselage will allow easy access to equipment. Furthermore the engine is placed in front and will be shielded by a cover which can be easily detached. This allows easy access to the engine. This consideration of an open fuselage structure has also a disadvantage. It will imply a higher overall weight for the structure, however the advantage in operation and maintainability ways up to this disadvantage in weight. To conclude an open structure is the optimal solution.

Modularity

The last driver considered is the modularity. The UAV will be made modular in the tail and wing. This means that two UAVs can be stored in a 20 ft container. Further more the transport is easy as the UAV can be rolled out of the container. If the landing gear is detached as well, loading becomes more difficult, however four UAVs can fit in a 20 ft container.

4.2 Design choices

In the conceptual phase of the project following design decisions were made.

- Take-off and landing will be conventional
- The UAV will have a conventional configuration
- The UAV will have a conventional tail
- The wing will be modular
- The wing won't have sweep

Please refer to the midterm report of the project [5] for a reasoning of these choices. The final configuration was not fixed yet in the midterm report, and therefore the final step was to determine position of the packages, wing and engine. These aspects will be discussed in this section.

Package dimension

Package dimensions were determined by the company VanBerlo. The cargo external dimensions are 380 by 380 by 600 *mm*, as in Figure 4.1. These dimensions were obtained by taking into account a crumple zone to absorb the impact of the fall. 50 *mm* around the package is accounted for as space for the dropping mechanism.

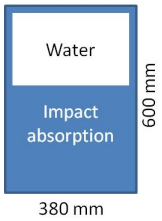

Figure 4.1: Package dimensions VanBerlo.

Wing Position

Basically there are three possibilities for the position of the wing: high, mid and low wing. A mid wing will limit the space available for packages and is therefore not optimal. Low and high wing do not cause this issue. A low non-swept wing may require dihedral to be stable which implies a more difficult wing structure and hence more expensive. A high wing however provides better stability and eases dropping from the bottom. For these reasons, a high wing is considered the most optimal solution.

Propeller configuration

Two possibilities were considered for the location of the engine and propeller. The propeller can be located in the front, a puller propeller, or in the back, a pusher propeller.

A pusher propeller is applied to UAVs that have no place in the front as it is reserved for avionics and payload. In this case the front could be used as cargo door to load the packages. This would imply easy loading and handling on the ground. The disadvantage of a pusher however is the possibility that little stones or dirt can be catapulted from the landing gear into the propeller and cause severe damage to it. In this setup there is also a higher risk of propeller strike during a conventional landing.

The other option, a puller propeller, does not suffer from last mentioned problems as landing gears are positioned after the propeller. Furthermore the propeller becomes more efficient as it is fed by clean air (no disturbances from the fuselage). There are no real disadvantages for the puller propellers.

It can be concluded that the puller propeller is a more safe solution and thus this concept is used for the UAV.

Loading

The decision was made to load all five packages at once by means of a rack which can be slid into the fuselage. The rack will be prepared beforehand. This will significantly reduce turn around time and ease the work for the people on the ground. The dropping mechanism will also be present and integrated in the rack and is connected to the UAV using an electrical connection which will send commands to the dropping mechanism.

As it is decided to have a puller engine, loading the rack from the front becomes unpractical as the engine would need to be removed or hinged. Loading the rack from the side is bothered by the wings. Loading from the back is therefore the most convenient solution. To ease loading the back of the fuselage needs to be opened and accessed easily. Some structural design decisions were made to make this happen. The tail structure is placed as high as possible such that the payload rack fits beneath it (see Figure 4.2). Furthermore the part of the tail cone structure which is avoiding direct access to the inside of the fuselage will be hinged on the side of the fuselage. For a more detailed description about the loading procedure and handling of the rack, please refer to Chapter 11.

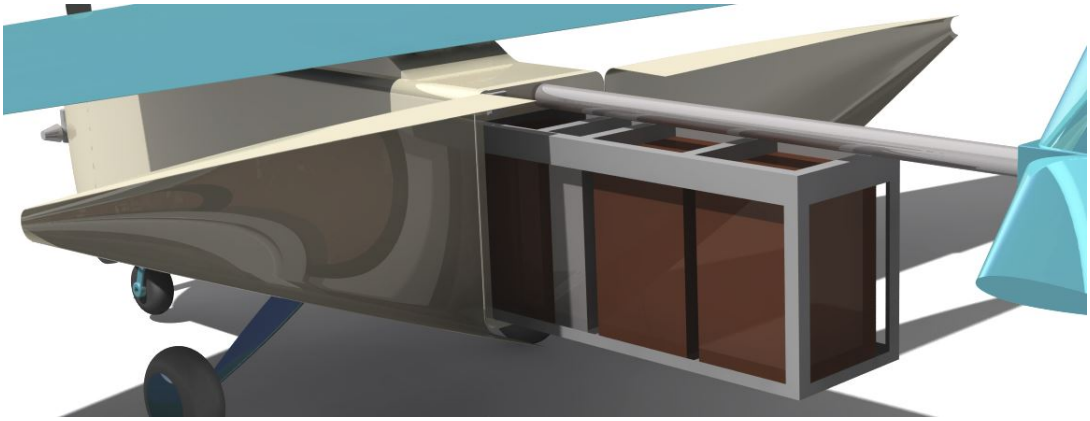

Figure 4.2: Back of the fuselage while loading.

Fuselage

During the design of the fuselage it is of utmost importance to consider the impact of aerodynamics, structure, payload, maintainability etc. in a qualitative sense. Furthermore the fuselage dimensions must be defined properly such that it will enclose all required internal components [6].

The design of fuselage is driven dominantly by the payload. This is in particularly true for cargo aircraft. For example the fuselage of Airbus Beluga with its bloated fuselage to house very large cargo and the reaper with a bulky 'head' to contain an antenna dish. The required cargo for the UAVs are five packages with dimensions given in Figure 4.1. It will be the main driver for the appearance of the UAV.

The packages will be placed in the fuselage with the impact absorption zone pointed below such that the package does not need to rotate while dropping. The fuselage cross-section is given in Figure 4.3. The fuselage contains the rack with packages. The rack accounts for the 50 mm necessary for the release mechanism. There is some place accounted aside and above the rack for the fuselage structure. On the upper side of the fuselage there is more place foreseen as to be able to house equipment such as the avionics and emergency parachute. See Chapter 8 for a detailed discussion about the fuselage structure. The width of the fuselage will be constrained by the dimensions of the engine and attachments which will be housed in the nose of the fuselage.

The packages will be placed as in Figure 4.3 one after each-other to minimize the front area and making the dropping mechanism as easy as possible. Besides the packages also the fuel tank will be placed into the payload rack. Placing the fuel tank into the payload rack has several advantages. It decreases turnaround time significantly as when the payload rack is slid into the UAV, the UAV is ready to go. It also provides more safety on the ground as fuelling can take place at a safe location separated from the base. This safety aspect is discussed more profoundly in Chapter 12. The connection between fuel tank and the carburettor of the engine should be made detachable. This also allows making the detachment of the engine easier in case of damage. It also gives challenges on the design as the detachment link should be made accessible in an easy way.

Besides the payload also aerodynamics is a major driver of the fuselage shape. The fuselage should be designed such that it does not generate excessive flow separation. This can be caused by blunt surface pointing to the back, sharp edges, external equipment etc. Furthermore lift losses can arise due to a poor wing fuselage arrangement. These matters will be treated more in dept in Chapter 5. The main aerodynamic driver on the fuselage shape is the minimization of wetted area. This is the complete area in contact with air. The higher the wetted area the more friction drag. As the payload is rectangle, the fuselage shape should also be rectangle and as close as possible to the dimensions of the payload to minimize the wetted area. However sharp edges can give rise to flow separations hence a fillet on the edge should be applied to avoid this phenomenon. Same counts for the longitudinal contours more specifically the transition from the main fuselage to nose and tail which should be as smooth as possible.

From a structures perspective the fuselage lay-out must provide an efficient load path. Weight of structural members can be reduced by providing the shortest, straightest load path possible [6]. This means

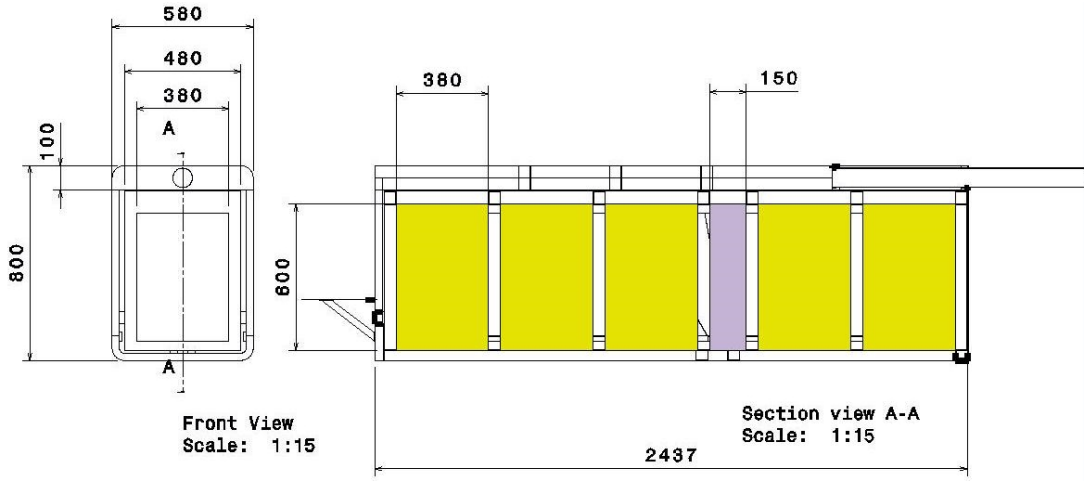

Figure 4.3: Payload distribution in fuselage.

that there should be as minimum interruption in the structure as possible. As the choice was made to have a high wing configuration the lift component acts on the upper part of the fuselage. To have the shortest load path to other components e.g. tail, engine, fuselage, their center of force should be as closest possible to this point. For the engine and fuselage this is quite challenging. The engine is off the shelf and the attachment point is on the lower side of the engine. The packages and fuel tank are also placed below the wing. The structure of these components will be treated more in dept in Chapter 8. The load path between tail and wing can be minimized by placing the tail at the same level of the structure where the wing is connected to. This also allows space to load the packages.

Landing gear configuration

Looking at the current UAV configuration it can be observed that a taildragger is more difficult to integrate. A long main landing gear would be necessary to have clearance with the ground. Furthermore for a taildragger the tail should be lifted up in order to load the UAV. The main benefit of a nose gear is easier loading, and it provides a higher degree of stability on the ground during take-off and landing, which is beneficial for the auto pilot. Nose landing gear has been proven to be able to land on rough terrain by the Twin Otter. Therefore a nose gear configuration has been chosen.

4.3 Final design parameters

In Table 4.1 the final design parameters of the Wings for Aid UAV can be found. Throughout the various chapters in this report the design of the UAV will be discussed in more detail. Table 4.1 is meant to give a summary of the final design parameters. Note that horizontal and vertical tail have the same planform.

4.4 Internal lay-out

Before the external lay-out is defined. Now, the internal lay-out, concerning the arrangement of all equipment in the UAV, is managed to fit into the external boundaries. An important start in the internal lay-out is the recognition of all systems that are necessary to successfully perform its mission. A complete overview of all these systems is given in Chapter 10. Their location in the fuselage will be described here. A successful lay-out should consider easy maintainability of all systems and consider, correct installation and physical limitations. Furthermore they should be located in a water free zone.

Flight control unit

The flight control unit is required to be located close to the center of gravity. This place is most likely to be taken by the payload packages. The best location of the flight control unit would be above the center of gravity as it than can be located in the symmetry plane of the UAV. Only the sense of the pitch rate will be a bit off but this can be corrected for. As the wing is located also above the center of gravity, the flight control unit should be integrated below the wing.

Table 4.1: The final design parameters of the Wings for Aid concept.

Parameter	Value
Maximum take-off weight [kg]	350.4
Operational empty weight [kg]	211.6
Payload weight [kg]	107.6
Fuel weight [kg]	31.2
Cruise speed [m/s]	43
Rate of climb[m/s]	6.5
Wing area [m^2]	9
Wing span [m]	7.9
Wing MAC [m]	1.2
Wing AR	6.9
Wing taper ratio	0.4
Wing airfoil thickness over chord ratio [%]	12.5
Horizontal tail area [m^2]	1.29
Horizontal tail span [m]	2.1
Horizontal tail MAC [m]	0.7
Horizontal tail AR	3
Horizontal tail taper ratio	0.45
Horizontal tail airfoil thickness over chord ratio [%]	12
Maximum power [kW]	40.23
Propeller diameter [m]	1.524

Cabling

To simplify production, routing of cables can be simplified through a provision of a clearly defined routing tunnel [6]. In most aircraft this tunnel runs through the lower part of the aircraft. As the belly of the fuselage is open and requires clearance to drop the package this is not a very convenient solution. This leaves two options. A tunnel running at the side of the fuselage or at the upper part of the fuselage. The routing tunnel should also take into account placement of internal equipment. A lot of cables run to and from the flight control unit, therefore the most optimal place for the router tunnel would be on the upper side of the fuselage. Therefore the other systems will also be placed on the upper part of the fuselage. Since the wings will be made modular, this equipment on top of the fuselage can be easy accessed once the wing is detached.

Accessibility

For the maintainability of the UAV accessibility to critical parts are very important. As discussed before, once the wing is detached, the flight control unit can be easy accessed. Other critical systems are avionics, engine, pumps, actuators and alternator. The avionics, transmitter, receivers and the battery are placed after the flight control unit where it can be accessed by a hinged cover plate. The engine, alternator and pumps will be placed in the nose of the UAV and can be accessed easily when the nose cone is made detachable. Actuators will be placed in the wing and access will be provided in the design of the wing.

Other critical equipment

Another important aspect is to place delicate equipment such as the avionics, far away from heat and vibration sources such as the engine. Therefore avionics shall be placed after the flight control unit and emergency equipment shall be placed between engine and flight control unit. The emergency equipment is a system which only needs to be activated from the outside and does not contain delicate sensors. A firewall is placed between the systems and engine to avoid possible flames from the engine entering the fuselage.

Lastly the magnetometer is very sensitive to electromagnetic induction and should be placed as far away from electronic equipment. The magnetometer will be mounted to the back of the fuselage where it can be accessed when the tail cover is removed. It will be placed to the side, where it is furthest removed from cables running through the tailboom.

Having all the systems in the wing or upper part of the fuselage also has the advantage that if the UAV should crash, expensive avionics are protected by the lower part of the fuselage. Furthermore it does allow for the same cross-section along the fuselage length, which decreases complexity in production.

The internal lay-out of the fuselage is depicted in Figure 4.4. The complete intern lay-out is given in Table 4.3.

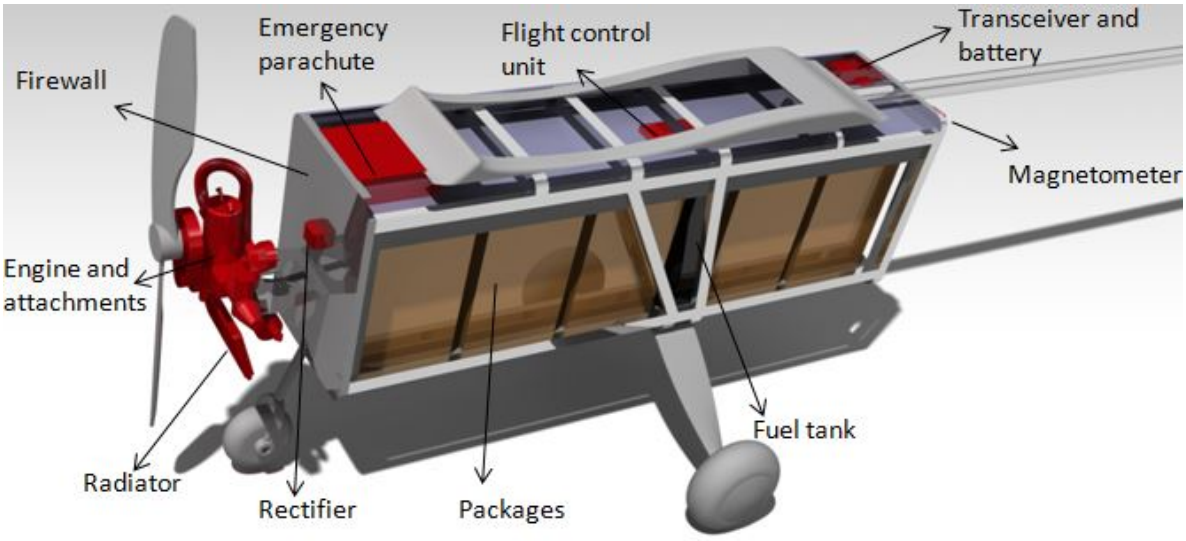

Figure 4.4: Fuselage internal lay-out.

4.5 CAD drawings

Every subcomponent was imported and placed into a full CATIA file. Having an approximation of the weight of each components and its location, the total mass, center of gravity and inertia matrix could be determined using CATIA. Furthermore the center of gravity shift could be observed while "dropping" payload. The most aft and foremost center of gravity was determined. The results are summarized in Table 4.2.

Table 4.2: UAV characteristics from CAD.

I_{xx} $[kgm^2]$	385.5
I_{xx} $[kgm^2]$	532.7
I_{xx} $[kgm^2]$	823.5
$x_{cg_{MOTW}}$ $[m]$ (from nose)	1.912
$x_{cg_{foremost}}$ $[m]$ (from nose)	1.912
$x_{cg_{aft}}$ $[m]$ (from nose)	1.978
$x_{cg_{MOTW}}$ $[\%MAC]$	46.5
$x_{cg_{foremost}}$ $[\%MAC]$	46.5
$x_{cg_{aft}}$ $[\%MAC]$	52.1

A bird's eye view of the UAV depicted in Figure 4.5. A side-view of the UAV can be found in Figure 4.6. Finally, the modularity of the wing, tail and landing gear is visualized in Figure 4.7. Furthermore a complete technical drawing with dimension is given in Figure 4.8. For more design details refer to the FullCAD CATIA file.

Table 4.3: Internal lay-out.

Location	Equipment
Nose	Engine
	Propeller
	Reduction drive (+ belt)
	Exhaust system
	Radiator
	Coolant piping
	Fuel piping
	Fuel pump
	Fuel filter
	Air filter
	Exhaust gas temperature probe
	Rectifier
Fuselage (upper part)	Emergency parachute
	Emergency Siren
	12V battery
	Flight control unit
	ADS-B transmitter
	ADS-B receiver
	GNSS receiver
	Magnetometer
Fuselage (rest)	Fuselage strobe lights (above and below)
	Packages
	Dropping mechanisms
Fuselage (rest) *continued*	Fuel tank
	Gascolator
	Fuel piping
	Fuel piping connection
Landing gear	Nose wheel
	Main wheels
	Hydraulics
Wings	ECSs (for flaps and ailerons)
	Servos (for flaps and ailerons)
	Strobe lights (both tips)
	Navigation lights (both tips)
	Pitot tube
	Radio altimeter
Tail boom	On/off switch
	Power plug
	USB port
Tail	ESCs (for elevators and rudder)
	Servos (for elevators and rudder)
	Strobe light
	Navigation light
Everywhere	Electricity and data cabling

Figure 4.5: Bird's eye view of the UAV.

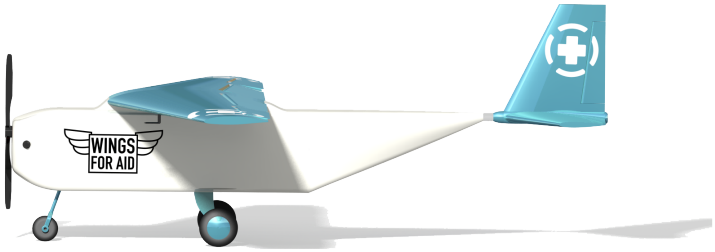

Figure 4.6: Side-view of the UAV.

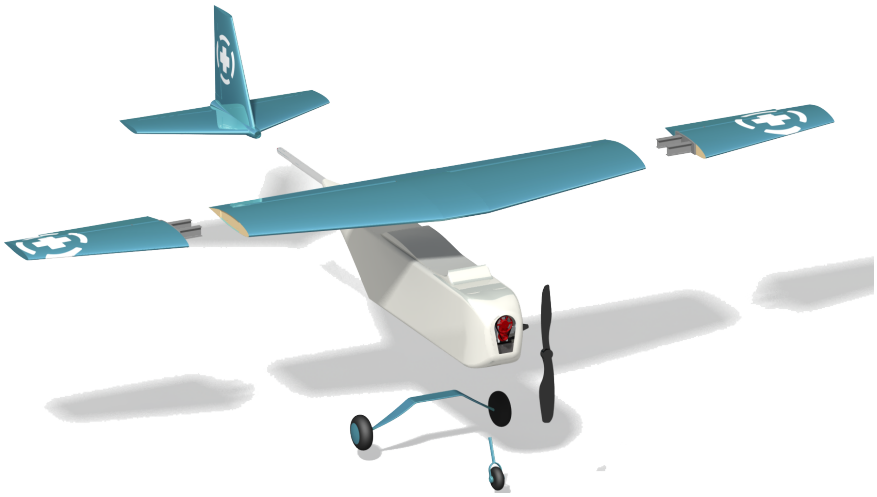

Figure 4.7: Modularity of the UAV.

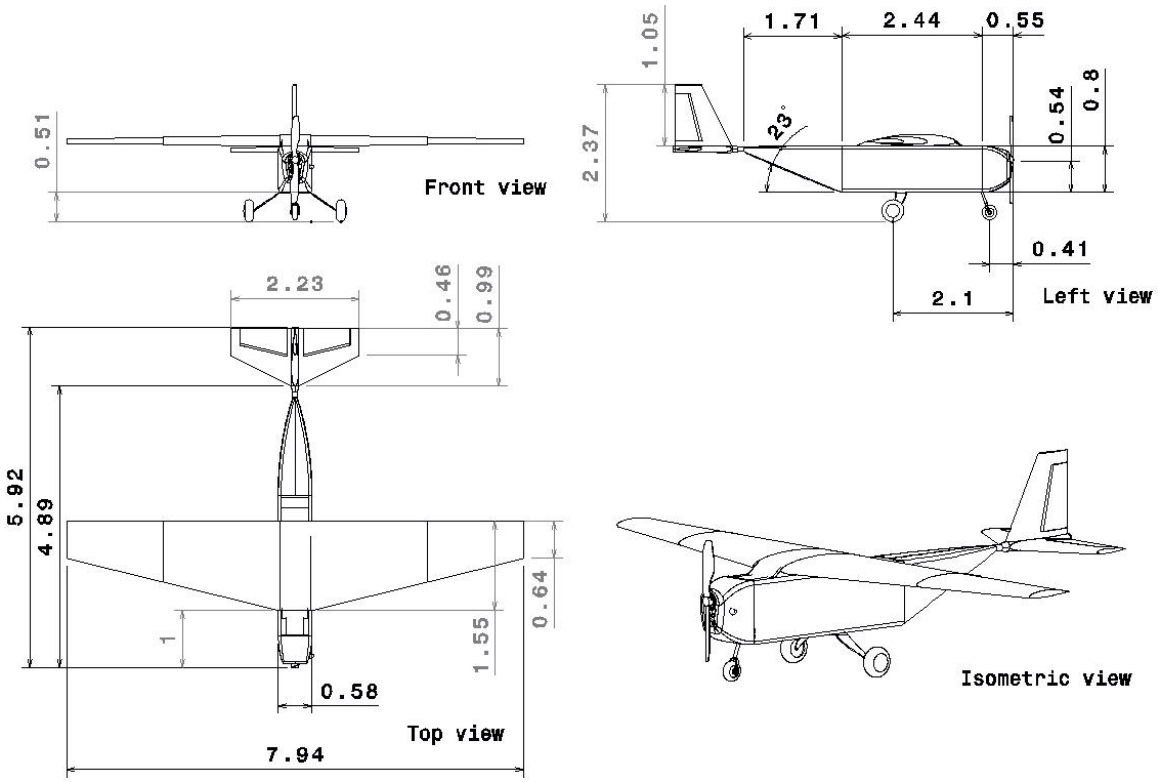

Figure 4.8: Technical drawing of the complete UAV.

Chapter 5
Aerodynamics

In this chapter the aerodynamics of the UAV will be discussed. First the design of the wing is considered, an optimization has been performed to maximize the lifting capacity and minimize the induced drag. Secondly the drag of the complete vehicle is considered. The aerodynamics around the fuselage is considered, more particularly around the tail. A estimation has been performed of the complete drag which completes the UAV drag polar. Finally a verification on requirements is performed.

5.1 Wing design

One of the main task of the aerodynamics department is the design of the wing. This includes the cross section or airfoil as well as the design of the wing planform. The wing must be designed in such a way that it satisfies all requirements set by the performance group. The requirements used for the design are summarized in Table 5.1. The design process of the complete wing is split in two parts. First the airfoil is selected in Section 5.1 and in the second part the wing planform is designed in Section 5.2.

Table 5.1: Wing design requirements.

Parameter	Value	Unit
S_w	9.0	m^2
b_w	7.9	m
$\frac{t}{c}$	> 0.12	-
$C_{L_{cruise}}$	0.35	-
V_{cruise}	43	$\frac{m}{s}$

Airfoil selection and characteristics

During the conceptual design phase a NACA 24012 airfoil was selected. This airfoil was selected for the following reasons: NACA 5 series airfoils are well documented airfoils, the digits of the airfoils already determine the design point and the shape of the airfoil and the thickness of the airfoil is 12% which is required by the structural department. The goal of the preliminary design phase was to develop an airfoil which has better characteristics than the NACA 24012, especially for cruise flight. This design process is explained in the next three sections. First the parameterization of the airfoil shape is discussed, in the second section the optimization process is presented and in the last section the airfoil is compared to the NACA 24012 airfoil.

Airfoil parameterization

In order to design an airfoil one needs a way to describe the surfaces. This description or parameterization can be done by single points which lay on the surface, by polynomials or by other functions. Having points describing the surfaces yields the most variable airfoil shape since the number of points can be increased almost infinitely. This also means that non smooth surfaces with kinks or jumps are possible. Polynomials on the other hand have usually less design variables, however the design variables can be chosen in such a way that they already describe properties of the shape. The NACA 5 series airfoils also have a polynomial to describe the surface. The five digits describe the design C_l, the position of the maximum camber and the maximum thickness as percentage of chord. For example the NACA 24012 airfoil has a design C_l of 0.3, the maximum camber position is at 40% of the chord and it has a thickness of 12%. This means that the airfoil shape can be much better controlled with the use of polynomials and kinks and jumps do not occur since polynomials are smooth and continuous functions.

Since the NACA 5 series does not have enough design parameters for a proper optimization other parameterization methods were investigated. In the end the Parsec parameterization was selected. The Parsec airfoil parameterization has eleven coefficients which are shown in Figure 5.1. These coefficients describe various surface properties of the airfoil such as nose radius, trailing edge angle or curvature. In the next section it will be described how these coefficients are determined.

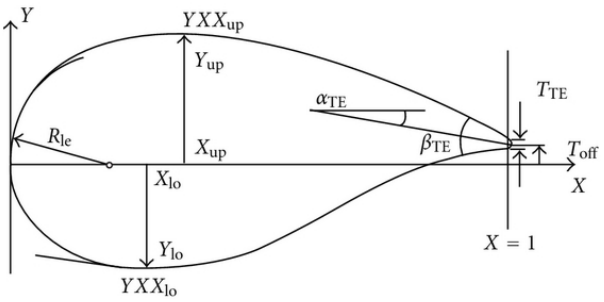

Figure 5.1: Parsec airfoil parameterization.

Airfoil optimization

The next design step consists of determining the selected Parsec coefficients. This was done with the help of an optimization process which is described in this section.

At the beginning of an optimization process the design variables, the cost function and constraints must be determined. The design variables are the already mentioned Parsec coefficients. However for the later optimization only nine variables were used. The trailing edge y and x position will be fixed since they have no significant influence on the performance but only change the chord length which is already set by the planform and the incidents angle which can still be changed during a later stage. The design parameters are combined to one design vector $\vec{x}$ during the optimization. The cost function is describing the performance of the airfoil. The main focus of this optimization is on the lift over drag ratio at cruise. The $C_{l_{max}}$ was not included in the cost function since it is computational wise expensive to estimate it and the method used for the airfoil analysis has limited accuracy at high angles of attack. To conclude, the cost function can be seen in Equation (5.1). $Cd(Cd(C_{l_{des}}, \vec{x}))$ is the drag coefficient of a certain design $\vec{x}$ at a certain C_l.

$$\begin{aligned} Cost(\vec{x}) = \quad & 0.5 \cdot Cd(C_{l_{des}}, \vec{x}) + 0.15 \cdot Cd(C_{l_{des}} + 0.1, \vec{x}) + 0.15 \cdot Cd(C_{l_{des}} - 0.1, \vec{x}) \\ & + 0.1 \cdot Cd(C_{l_{des}} + 0.2, \vec{x}) + 0.1 \cdot Cd(C_{l_{des}} - 0.2, \vec{x}) \end{aligned} \tag{5.1}$$

It can be noted that the drag was not only calculated at the $C_{l_{des}}$ but also at C_ls below and above this C_l. This was done to ensure that no mathematical singularities occur where the C_d of the airfoil is almost zero at the $C_{l_{des}}$ but drastically increases for a larger and smaller C_l than the $C_{l_{des}}$. In addition to that the cost function helps the overall performance of the aircraft since the weight changes a lot during flight due to the package dropping and fuel consumption the $C_{l_{cruise}}$ is therefore not constant. Last but not least two constraints were set on the airfoil. On one side the thickness of the airfoil was not allowed to be lower than 12% and on the other side the nose radius had to be larger than 0.01 in order to guarantee good stall behaviour.

After the design parameters, cost function and constraints are known, an algorithm or process for the optimization can be selected. In the end a gradient based optimizer was selected since the initial design is already close to the optimum and the design space is small which makes a swarm based optimization algorithm not necessary.

The algorithm works as follows. First an initial design is created by setting the Parsec coefficients. This can be done randomly or manually by the user. Then the algorithm enters the optimization loop. First the cost function gradient is calculated by using a central difference scheme which can be seen in Equation (5.2). By applying small perturbations $\vec{h}$ to each design coefficients separately the cost gradient vector can be assembled which contains the change in cost in each design direction.

$$\frac{\delta Cost}{\delta \vec{x}} = \frac{Cost(\vec{x} + \vec{h}) - Cost(\vec{x} - \vec{h})}{2 \cdot |\vec{h}|} \tag{5.2}$$

With the fully calculated cost gradient vector the design vector can be updated with Equation (5.3). Where the gradient is normalized to yield a unit direction vector and D is the step length which limits the change of the design during one optimization step.

$$\vec{x}_{i+1} = \vec{x}_i - D \cdot \frac{\frac{\delta Cost}{\delta \vec{x}}}{|\frac{\delta Cost}{\delta \vec{x}}|} \tag{5.3}$$

With this new design vector the cost gradient can be recalculated and the loop is repeated.

One major part of the optimization tool is the airfoil solver or the tool that calculates the airfoil characteristics. The programme chosen for the analysis is Xfoil. Xfoil can be used to analyse airfoils at low Reynolds numbers. It includes a boundary layer model to estimate not only pressure drag but also skin friction drag and separation. In addition Xfoil is command based which means it can be easily operated from outside programmes. The steps necessary to get to the airfoil characteristics are the following. First the design vector or Parsec coefficients are converted into the surface coordinates. With these airfoil coordinates Xfoil can be launched and the airfoil can be analyzed. The finished results are then exported and analysed by the optimizer. A flow chart of the optimization algorithm can be seen in Figure 5.2.

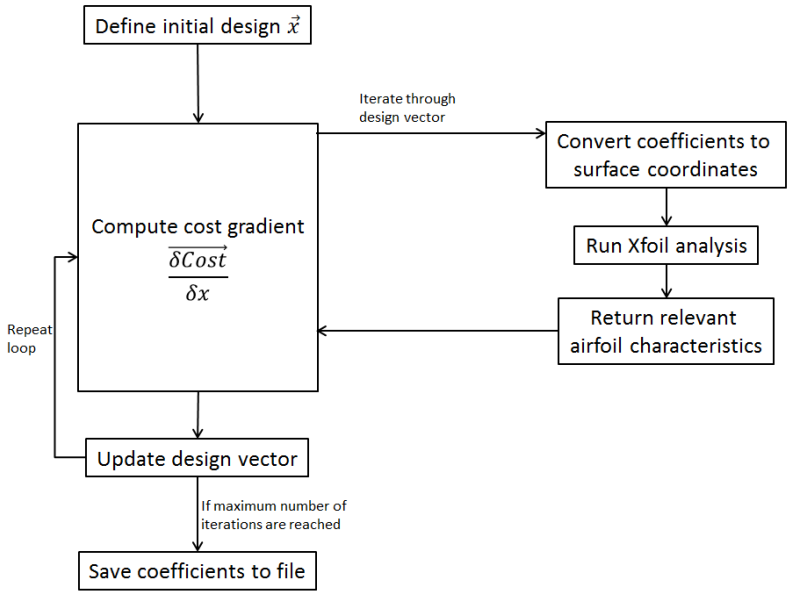

Figure 5.2: Airfoil optimization algorithm.

Results

The optimization tool was run with different starting designs to have a higher probability of converging to the global optimum, which is however never guaranteed. In this section the final airfoil will be presented and compared to the NACA24012. The nine design coefficient determined during the optimization process are summarized in Table 5.2.

Table 5.2: Optimized Parsec airfoil coefficients.

R_{le}	X_{lo}	Y_{lo}	$Y_{XX_{lo}}$	θ_{lo}	X_{up}	Y_{up}	$Y_{XX_{up}}$	θ_{up}	T_{TE}	T_{off}
0.01	0.36	-0.04	0.31	2.0	0.43	0.08	-0.45	-8.0	0.0	0.0

Figure 5.3 shows the polars of the Parsec airfoil and the most important characteristics are listed in Table 5.3.
Figure 5.4 was made to compare the NACA 24012 airfoil with the optimized Parsec airfoil. With the optimization the lift over drag ratio at the cruise C_l was increased by 48% from 64 to 95. This is partially due to a later transition of the flow from laminar to turbulent. The transition point of the NACA24012 airfoil is at 0.25c while the transition of the Parsec airfoil is at 0.8c. However due to the propeller the flow around the wing will probably be turbulent which means that the expected drag values during real flight conditions are expected to be higher.

Figure 5.3: Parsec airfoil polars.

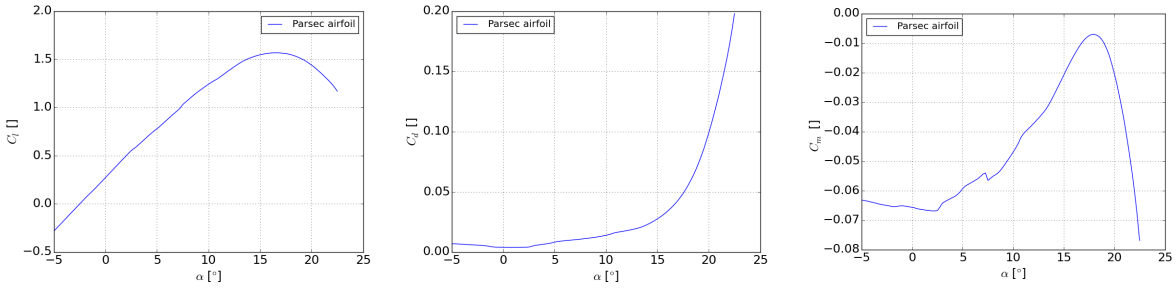

(a) C_l polar of Parsec airfoil. (b) C_d polar of Parsec airfoil. (c) C_m polar of Parsec airfoil.

Table 5.3: Parsec airfoil characteristics.

Parameter	Parsec	NACA 24012
C_{d_0}	0.0056	0.0072
C_{m_0}	-0.065	-0.017
$C_{l_{\alpha=0}}$	0.27	0.15
$C_{l_{max}}$	1.58	1.72
$\frac{L}{D}_{cruise}$	95	64

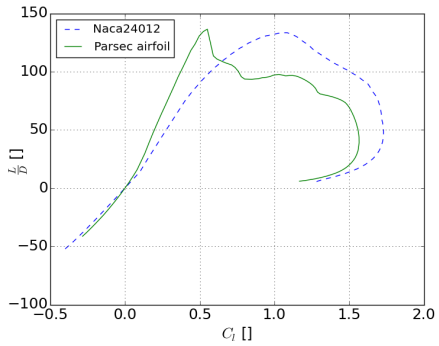

Figure 5.4: Lift over drag comparison between NACA 24012 and Parsec airfoil.

In conclusion the optimization process was successful by creating an airfoil which is optimized for the Reynolds numbers and flight condition the UAV will encounter during operations. This airfoil can now be used in the second step of the wing planform design.

5.2 Wing planform design

The second step of the wing design is the wing planform design. For this design three steps are required. First the control parameters which shape the planform are defined, which is similar to the parameterization of the airfoil in Section 5.1. Afterwards an analysis tool is selected which can calculate the performance of the selected planform and at last a design process is required which derives a planform which meets all requirements.

Wing planform parameterization

As for the airfoil parameterization there are again multiple ways to parameterize the planform of the wing. During the conceptual design phase the planform was described by three parameters, aspect ratio, taper and sweep. The structural design of the wing which will be presented in Section 8.3 showed that a fully variable planform is possible. Since the three parameters, aspect ratio, taper and sweep,

limit the design space to a large extent a different parameterization was selected. The selected parameterization method divides the planform in N elements. Each element is defined by a chord length and x position or sweep. In addition a twist angle or different airfoil can be selected per element.

Analysis tool

There are different methods to analyse the wing planform and 3D flow effects of the wing. These range from the analytical lifting line theory from Prandtl [7] to advanced CFD software packages. The lifting line theory can predict the lift curve and induced drag of high aspect ratio wings, however it does not include any form of viscous effects and it is not able to estimate stall. Modern CFD software packages are able to analyse all flow phenomena. However an exact drag prediction requires very fine meshes and a lot of computing power and time.

For the preliminary design a viscous drag prediction as well as a stall estimation is required. However the time and computing power necessary for CFD is not available. Therefore a method which combines the analytical approach from the lifting line method and the accuracy of CFD packages is required. Such a method is the non-linear lifting line method proposed by [7]. This method uses the non-linear data from airfoils and combines them with the lifting line method. The software package Xflr5 contains such a method. It uses the data obtained before by Xfoil to obtain the non-linear airfoil characteristics and contains multiple panel and lifting line approaches to estimate the finite wing characteristics.

Xflr5 is fast and reliable in obtaining the wing characteristics, however it is not command based and can therefore not be used for optimization where many interactions and automation procedures are required. Due to that reason it was decided to write a new code which is using the algorithm described in [7]. In the following section this code will be presented.

Lifting line code

As explained in the previous section it was decided to write a code which can analyse a wing using a non-linear lifting line algorithm. An illustration of the algorithm can be seen in Figure 5.5. This section will present a brief explanation of the code using Figure 5.5.

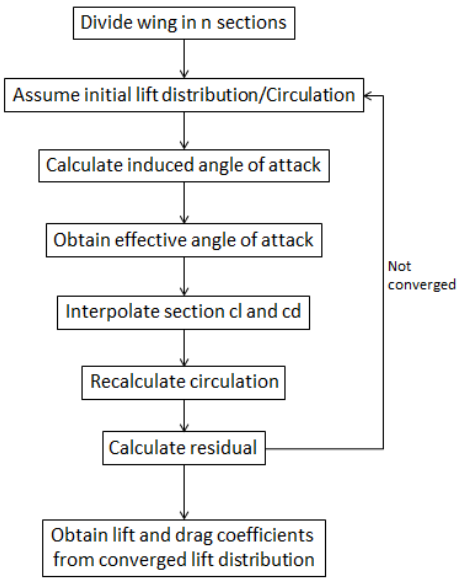

Figure 5.5: Non-linear lifting line algorithm.

The non-linear lifting line method first replaces the wing by a finite number of horseshoe vortexes. In the second step an initial lift distribution or circulation is assumed. In order to obtain a faster convergence an elliptical lift distribution is selected. Next the induced angle of attack is calculated at each element using Equation (5.4).

$$dV = \frac{\Gamma}{4\pi} \frac{dlxr}{|r|^3} \tag{5.4}$$

Using Equation (5.5) the effective angle of attack can be computed with the before determined induced

angle of attack.

$$\alpha_{eff} = \alpha - \alpha_i \tag{5.5}$$

Afterwards the airfoil section characteristics for each element are obtained using Xfoil. The airfoil computation with Xfoil can either be done before the wing analysis or during the wing analysis. From the C_l obtained from the Xfoil analysis a new lift distribution or circulation can be calculated with Equation (5.6).

$$\Gamma = \frac{1}{2} V_\infty c C_l \tag{5.6}$$

In the last step of the loop the residual is computed by taking the difference between the initial and new lift distribution. If the residual meets the required convergence, the loop is exited and the lift and drag coefficients are computed by integrating over the lift distribution. If the convergence requirement is not met a new initial lift distribution is calculated with Equation (5.7). Where D is the relaxation factor used to ensure stability.

$$\Gamma_{input} = \Gamma_{old} + D(\Gamma_{new} - \Gamma_{old}) \tag{5.7}$$

For a more detailed explanation of the lifting line theory and the non-linear lifting line algorithms see [7].

Optimization

The last tool which is required for the design of the planform is the tool that develops a planform which meets all requirements. Due to the good performance of the gradient based optimizer during the design of the airfoil it was decided to use the same method for the design of the planform. The gradient based optimizer does also have a large benefit for the computing time of the design perturbations since the already converge solution of a previous design can be used as an initial lift distribution of a new design. This showed a very large improvement in the converging time. It was decided to use the same airfoil along the span which means that only the sweep or x-position of an element and its chord are design variables. An illustration of the algorithm can be seen in Figure 5.6, however it is not further explained since it has large parallels to the airfoil optimization algorithm. The only difference between the airfoil and wing optimization is the cost function which was simplified to equation Equation (5.8), which means that only the C_{D_0} at cruise is grading the design.

$$Cost = C_D(\vec{x}, C_{L_{design}}) \tag{5.8}$$

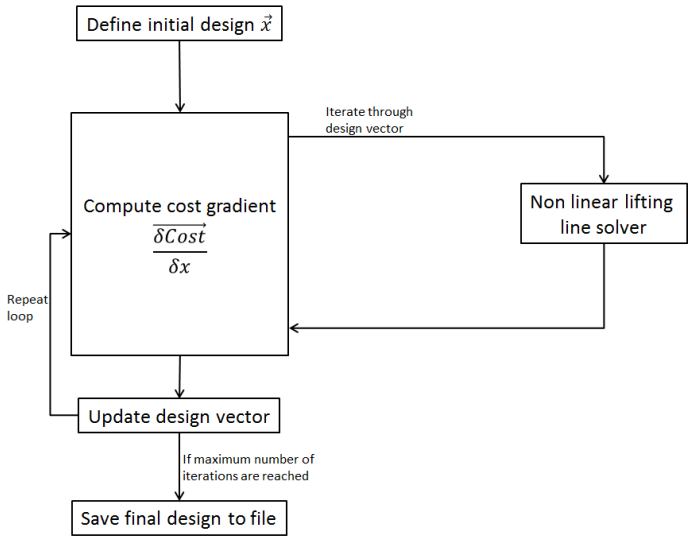

Figure 5.6: Wing planform optimization algorithm.

Results

As for the airfoil optimization the tool was run multiple times with different initial planforms. The best planform can be seen in Figure 5.7. It is noticeable that the wing planform is almost elliptical.

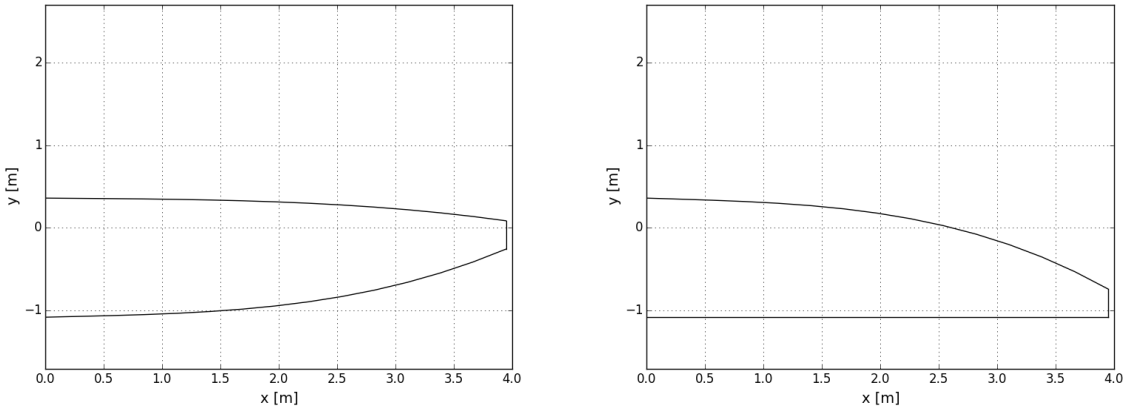

(a) Optimized wing planform.

(b) Final wing planform.

Figure 5.7: Wing comparison.

Looking at the lift distribution Figure 5.8 and the Oswald factor of the wing, one can say that with an Oswald factor of 0.999 the lift distribution is indeed elliptical and therefore resembles the theoretically optimal lift distribution derived by Prandl. For the final optimized planform however the planform was adapted. The curved trailing edge does complicate the installment of flaps and ailerons. It was therefore decided to straighten the trailing edge and only curve the leading edge. This increases the sweep and the Oswald factor decreases which will be shown later in the comparison. However the increased sweep yields an easier installment of the flaps and ailerons and it increases the stability of the overall aircraft.

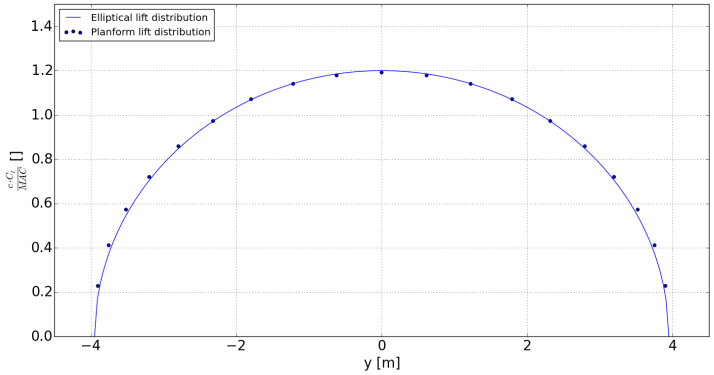

Figure 5.8: Optimized wing lift distribution.

More important than the elliptical lift distribution of the planform are the updated polars of the wing. The three most relevant polars can be seen in Figure 5.9 and the most important characteristics are summarized in Table 5.4. As expected from the finite wing the $\frac{L}{D}_{cruise}$ is lower than the $\frac{L}{D}_{cruise}$ of the airfoil. Also the $C_{L_{max}}$ is lower.

Wing planform trade-off

In order to find the final planform for the UAV three different planforms where analysed together with the structural department. These three planforms are the optimized planform which was described in the previous section, a rectangular planform where the tip chord is equal to the root chord and a tapered planform. To ensure that all characteristics are comparable and reliable all three planforms were analysed in Xflr5.

Figure 5.9: Wing polars.

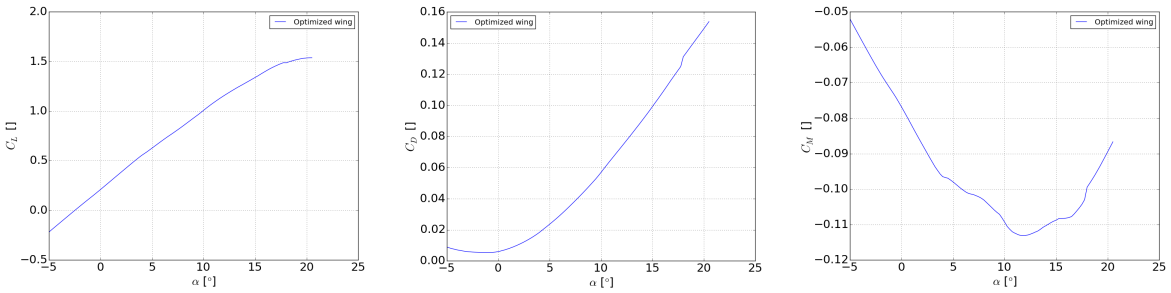

(a) C_L polar of wing. (b) C_D polar of wing. (c) C_M polar of wing.

Table 5.4: Parsec airfoil characteristics.

Planform	Optimized	Rectangular	Tapered
C_{D_0}	0.0057	0.0057	0.0057
C_{M_0}	-0.065	-0.0065	-0.065
$C_{L_{\alpha=0}}$	0.2	0.2	0.2
$C_{L_{max}}$	1.54	1.46	1.52
$\frac{L}{D}cruise$	37.8	36.0	37.6
e	0.999	0.950	0.996
$M_{root}C_{L_{max}}[Nm]$	12725	13925	12625

Figure 5.10: Wing comparison.

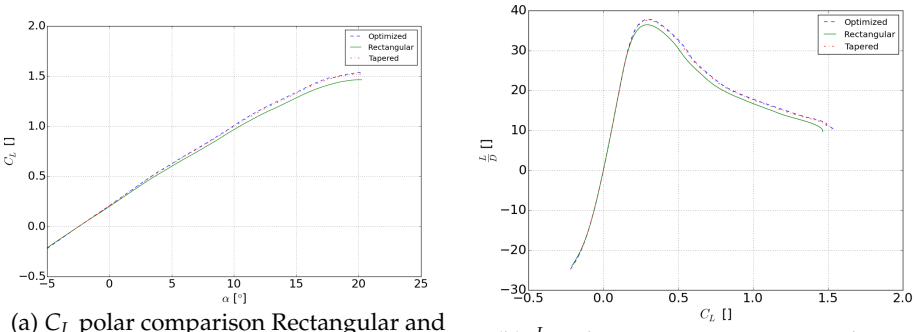

(a) C_L polar comparison Rectangular and Optimized planform.

(b) $\frac{L}{D}$ polar comparison Rectangular and Optimized planform.

Table 5.4 compares the most relevant values of the planforms which will be further discussed in the text. Starting with the lift over drag ratio of the planforms one can see only a minor increase in performance of 4.7% between the optimized and rectangular planform. The difference between the optimized and tapered planform in lift over drag ratio is even smaller with 0.5%. The lift over drag ratio is driven by two planform parameters the Oswald factor and the aspect ratio. The Oswald factor of all three planforms are already close to one and the aspect ratio was fixed during the optimization which explains the rather small increase in $\frac{L}{D}$. The $C_{L_{max}}$ on the other hand is increased by 0.08 or 5.4% for both tapered and optimized planforms, which is very beneficial for the landing, take-off and the flight conditions during dropping. One improvement not shown in the aerodynamic characteristics is the reduction of the root bending moment. The root bending moment was reduced by 8.6% for the optimized planform and by 9.3% for the tapered planform. In addition due to the longer root chord the optimized and tapered planforms have an increased moment of inertia which is beneficial for the structural design of the wing.

In conclusion the optimized wing planform might have better aerodynamic characteristics than the tapered and rectangular planform. However due to the structural complications of the curved leading edge, the higher root bending moment and the only minor increase in performance over the tapered wing, the tapered wing planform was selected as the wing planform of the final UAV. The dimensions of the planform can be seen in Figure 8.11

Verification and Validation

In order to ensure validity of the numerical results different verification and validation methods were used. For the airfoil design two tools needed to be verified and validated. First the analysis tool XFoil needed to be validated and second the optimization script needed to be validated.

Since the source code of XFoil was not available and no experimental data was available for airfoils the tool could not be verified and validated during the project. However during the aerospace bachelor wind tunnel test the tool was validated which showed very good agreement between experimental and XFoil results.

The validation of the optimization script was part of the results section of the airfoil design Section 5.1. The fact that the tool found a design which is performing better than the NACA24012 guarantee that the tool was working properly. For the Verification of the wing planform design tool, the non-linear airfoil characteristics were replaced by linear characteristics. Meaning the lift slope of the airfoil was 2π and there are no viscous forces acting on the airfoil. This means that the results for lift and induced drag must be equal to the values obtained from the analytical lifting line theory, which was indeed the case. For the validation no experimental data was available again. However data of other CFD codes as Xflr5 is available which was used for the validation of the wing planform analysis tool.

Conclusion

In conclusion during the wing design an airfoil was designed which meets the requirements set by the performance group and which optimized for the cruise performance. Next to that a wing planform was selected which not only has good aerodynamic characteristics but also decreases the loads encountered during flight. The tools which were used for the analysis of the airfoil as well as for the planform were verified where possible however a proper validation was not possible since experimental data is necessary for this validation.

Recommendation

During the design of the wing multiple characteristics for both the airfoil and planform were obtained. All these characteristics were gathered by use of models which model the flow and partially its viscous effects. Since assumption are used to create the models, they never represent the actual characteristics with 100% certainty. this means that some of the characteristics need further investigation.

During the design process especially two characteristics are questionable and require further investigation. The first one is the drag coefficient of the airfoil. The main reason for the low drag is the laminar flow region over the surface of the airfoil. This laminar flow region however might not occur during real world flight conditions. This low drag coefficient also explains the high Lift over drag ratio of the wing during cruise as well as higher angles of attack. The second questionable outcome is the $C_{l_{max}}$. Xfoil does estimate the $C_{l_{max}}$ however since it does not solve the complete flow field it has only limited capability of modeling separated flows and therefore accurately predicting the $C_{l_{max}}$ is difficult. Therefore the recommendation derived from the results are the following. To finalize the wing design and validation experimental data about the $C_{L_{max}}$ and drag coefficients has to be obtained with wind tunnel testing for both the airfoil as well as the final planform..

5.3 Fuselage drag

Different phenomena contribute to the drag. In low-speed flight conditions the drag consists of two components: parasite or zero-lift drag (C_{D_0}) and induced drag (C_{D_i}). The induced drag and zero-lift drag of the wing was considered in the previous sections while designing the wing. In this section the focus will be on the zero-lift drag of the fuselage.

As drag is an aerodynamic force, it consists of basically two components: drag produced by skin friction and a pressure differential along the body.

The skin friction is caused by the viscosity of air. Its magnitude depends on whether the flow is laminar

or turbulent. Laminar flow is beneficial for skin friction. The area in contact with air (wetted area) should be minimized to minimize skin friction drag. This was done by making the surface area of the fuselage as small as possible. As the propeller is in the front of the UAV, the turbulent flow it creates will have a negative effect on the skin friction.

Pressure drag is caused by velocity changes along the body. The most prominent pressure drag is caused by separation of flow, leaving behind a low pressure zone. For a well designed aircraft the drag consist mostly of skin friction drag. However as the UAV is not very slender compared to other aircraft and the design needs to be simple in nature, it is expected that the UAV will have a significant amount of pressure drag. Nevertheless pressure drag should be avoided as much as possible. Origins of pressure drag are separation near the tail (boat tail drag) and cut-offs at the back of the fuselage (base drag).

Furthermore interference in the flow between the aircraft components can increase both skin friction and pressure drag. Interference can cause transition from laminar to turbulent flow and encourage airflow separation [6].

While designing the UAV, previous considerations were taken into account to reduce drag as much as possible. In Chapter 4 it was already considered while designing the fuselage external lay-out. This section will treat the aerodynamic design of the tail and nose sections more in depth.

Tail cone design

Separation at the back of the aircraft can cause a very high pressure drag and should be avoided by designing the tail in such a way that the airflow is guided back to its original state. Since the structure does not allow for an aerodynamic shape at the tail, a plastic cover will make sure the flow is not heavily separating at the back. However the bigger this cover the more mass and the higher the costs. Therefore this cover should be as small as possible.

Separation is avoided by gradually decreasing the cross-section of the fuselage. In the final design of the UAV, consisting of a tail attached to a boom, the most convenient way is to gradually taper the fuselage cross-section to the cross-section of the tail boom. In this way the tail boom is partly inside the aerodynamic cover, reducing the friction drag over the boom. Furthermore it provides an attachment point for the cover. This will shape the tail cone such as in Figure 5.11. The flow is likely to separate at the start of the tail cone indicated as critical area in Figure 5.11. For higher upsweep angles (φ) the flow is expected to separate in this critical area. To limit the mass and cost of the cover however, the upsweep angle should be as high as the aerodynamics allows, hence no excessive separations.

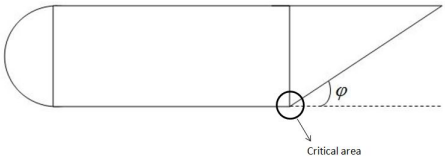

Figure 5.11: Tail upsweep angle.

From literature it can be found that to prevent separation of the airflow, the aft-fuselage deviation from the free stream direction should not exceed 10-12° [6]. However when the fuselage lower corners are fairly sharp, this causes a vortex-pattern which energizes the flow and postpones separation to upsweep angles of 25° [6].

A 2D CFD analysis using Fluent was performed to assess the effect of the upsweep angle using the flight conditions and configuration of the UAV. Analysing in 2D has the advantage that certain parameters can be optimized within a relatively short time frame. This is because of the limited amount of mesh cells and therefore computing time. Of course 3D effects will have a large influence on the aerodynamics around the tail. Therefore a couple of 3D simulations were performed to complement the results of the 2D analysis.

Set-up

The fuselage shape is analyzed using CFD codes provided by Ansys Fluent. To keep the simulations within the scope of the DSE, the rotating flow resulting from the propeller in front of the UAV is neglected. The rotational flow will cause a higher velocity magnitude of the flow increasing friction at the surface. However this component is normal to the direction of the drag and can therefore be neglected. The rotating component will also affect separation of the flow as it energizes the flow. It is assumed

that this energy is dissipated at start of the tail cone. The propeller will leave the flow turbulent and therefore the simulation will model the inflow as turbulent.

The model which will be simulated is shown in Figure 5.11.

The operation conditions are given in Table 5.5. Atmospheric conditions at sea level are taken as the UAV will fly at 150 m altitude. These conditions are most critical for drag. The intensity at the inlet is considered high as the propeller will result in turbulent flow. For high turbulence cases the turbulent intensity is typically between 5% and 20% [1].

Table 5.5: Operating conditions

Parameter	Value	Unit
Velocity	48	m/s
Angle of attack	0	deg
Density	1.225	kg/m^3
Pressure	$1.1013 \cdot 10^5$	Pa
Kinematic viscosity	$1.5 \cdot 10^{-5}$	m^2/s
Turbulent intensity	10	%

The domain in which the flow will be simulated consists of a rectangular box surrounding the fuselage. The inlet is taken 9 m in front of the fuselage and the outlet 25 m after. Upper and lower boundaries are taken 4 m from the fuselage. The boundaries must be sufficiently far away from the body to make sure that it does not influence the flow around the body. The operating conditions are applied as boundary conditions on the inlet. At the outlet a pressure is defined equal to the free stream pressure. The upper and lower boundaries are slip boundaries hence the velocity is not reduced to zero at these boundaries. On the inner body, the fuselage, a no slip condition is applied.

In order to select a suitable mesh and model, some initial information about the flow is required. The Mach number the UAV is flying is around 0.14. This means the flow can be assumed incompressible, therefore no compressibility effects should be modelled and no shock-waves are expected. The Reynolds number over the fuselage (characteristic length: 2.5 m) at cruise conditions is about 8,000,000. The boundary layer thickness for flow over a flat plate can be estimated by Equation (5.9) [8].

$$\delta = \frac{0.37x}{Re_x^{1/5}} = 0.0385m \tag{5.9}$$

In order for the solution to converge and to be accurate a minimum mesh size is required to simulate certain flow features. Inflation is applied to the boundary of the fuselage to capture the boundary layer. This inflation size has a total thickness of 0.0385m (thickness of boundary layer) and consists of eight layers. The mesh is refined on the nose of the fuselage to capture the strong velocity gradients. Furthermore the mesh is refined on the back to capture small eddies in the wake. The mesh used can be found in Figure 5.12.

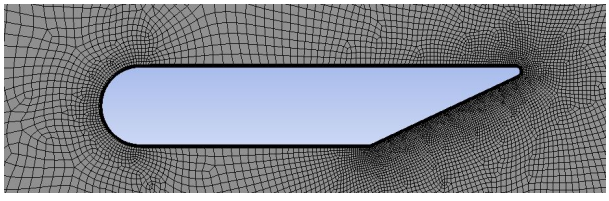

Figure 5.12: Mesh around fuselage 2D.

The solver used is a steady pressure-based solver that will use Reynolds Average Navier Stokes (RANS) equations. The Reynolds stresses in these RANS equations were modelled using the realizable k-epsilon

[1] URL `http://www.cfd-online.com/Wiki/Turbulence_intensity` [Cited on 15/06/2016]

model. Studies have shown that the realizable k-epsilon model provides good performance for separated flows and flows with complex secondary features [9]. Turbulence near wall is simulated using enhanced wall-treatment. The spatial discretization used to solve for pressure, momentum, turbulent kinetic energy and turbulent dissipation rate are all second order.

Verification

Verification is the practise of checking whether the equations are solved correctly. A correctly solved set of equation has the following characteristics:

- The residuals for all the equations show convergence.
- The solutions do not change anymore with more iterations.
- Conserved quantities are conserved
- Computed flow is independent of the mesh

Residuals, lift and drag coefficient have been observed to converge in the plotting interface of Fluent. Mass flow at the inlet found to be 529.20001 kg/s and at the outlet 529.19966 kg/s. Therefore it can be concluded that mass is conserved. The mesh has been adapted and not found to have significant influence on flow behaviour and force coefficients. Therefore it can be concluded that the equations in the simulation were solved correctly.

Results 2D

The pressure and skin friction drag was calculated for varying upsweep angles. The overall fuselage shape was kept the same, including fillets in order to have a valid comparison. The 2D drag coefficient, viscous drag coefficient and pressure drag are plotted for the various upsweep angles. To be able to compare 2D results with 3D results, the depth in the CFD analyses was defined as the width of the fuselage (500 mm) and the wing area (9.5 m^2). Note that these values have been changed troughout the design process. The result can be found in Figure 5.13.

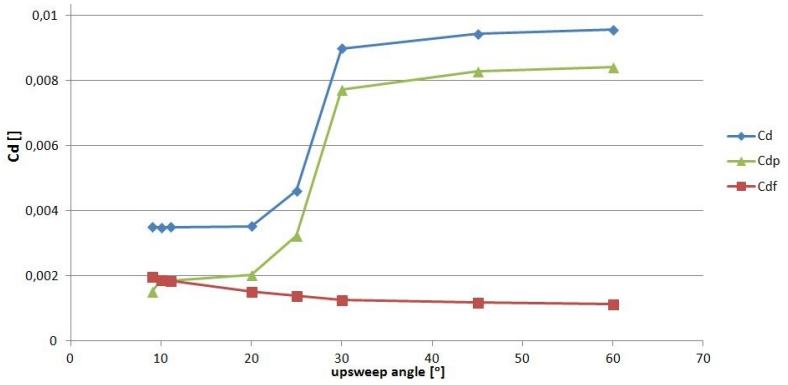

Figure 5.13: Drag coefficient vs. upsweep angle.

From Figure 5.13 it can be observed that an optimum drag coefficient of 0.0035 is reached for an angle of 10°. For lower angles the friction drag starts increasing more than the pressure drag decreases and therefore the total drag starts increasing. Between 10° and 20° the drag does not change much as in this region the pressure drag is basically exchanged for friction drag. When the upsweep angle becomes higher than 25°, the drag coefficient starts increasing significantly to a value of 0.0095. This reason of this sudden change became clear when plotting the velocity vectors of the flow in the simulated domain.

As can be seen in Figure 5.14 at 30° the flow separates at the critical area creating a low pressure zone behind the fuselage wherein the flow recirculates. This creates a very high pressure drag as the low pressure zone acts on the complete cross-sectional surface pushing the UAV back. Another way to look at it, is that these large eddies (recirculation) created behind the body take energy. As with tip-vortices at the wing this energy manifest itself as drag.

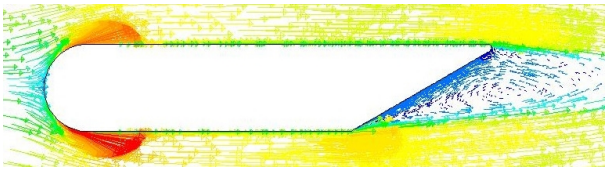

Figure 5.14: Velocity vectors of the flow at 30° upsweep angle.

At 20° (Figure 5.15) the flow stays attached to the fuselage. As the velocity is close to the free stream velocity (vectors have equal size) pressure should be equal to the free stream pressure according to Bernoulli's law. There is therefore no pressure pulling the UAV back as was the case in Figure 5.14.

Moreover it can be observed in Figure 5.15 that the velocity increases significantly at nose of the fuselage. Because the nose of the fuselage is very blunt in the simulation, the velocity around has to accelerate a lot. This acceleration costs energy and manifests itself as pressure drag. Another way to look at it is that the flow in front of the UAV is decelerated due the presence of the body. According to Bernoulli's law the pressure increase in this region. The flow is therefore pressing against the body which results in drag. Note that this does not represent the real nose cone, but was used as an illustration. A more slender nose would result in less pressure drag.

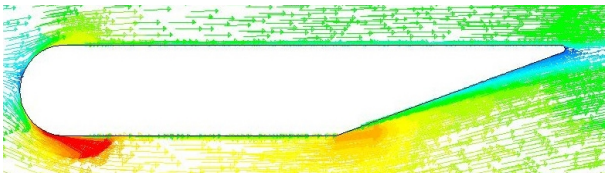

Figure 5.15: Velocity vectors of the flow at 20° upsweep angle.

Validation

A check has to be performed on the correctness of the results. Possible errors in the physical model have to be identified by comparing to experimental data or other models.

For an upsweep angle of 30° a simulation has been perform using a transition SST model. This model has four equations (compared to the two of the k-epsilon model). The transition SST model is based on the coupling of the SST k-omega transport equations with two other transport equations capable of simulation transition between laminar and turbulent flow. This simulation resulted in a drag coefficient of 0.0234 which is 18% more than the predicted value of the k-epsilon model. For the purpose of the simulation, this can be considered close enough to be valid.

Raymer [6] states that if lower corners are fairly sharp, 25° can be used as maximum upsweep angle. This in line with the results of the CFD analysis.

A numerical study of the Ahmed body [10] revealed a minimum drag coefficient for a rear slant angle of about 10°. This analysis is comparable to the upsweep angle of the UAV by following reasons. Reynolds number in both analysis is comparable. Velocity is about 40 m/s and sea level flight conditions are considered. The slant angle can be seen as a mirrored upsweep angle. The 2D analysis of the fuselage shows the same optimum as for the rear slant angle of the Ahmed body.

In conclusion the simulated behaviour of the flow for different upsweep angles can be validated as correct.

Results 3D

To see the effect of 3D flows, similar simulations on 3D models have been performed. Simulations have been performed on a model of the UAV for upsweep angles of 11°, 15°, 20° and 25° under an angle of attack of 4°. Simulation and verification of 3D fuselage is performed in the same way as of the 2D fuselage. The results are summarized in Figure 5.16.

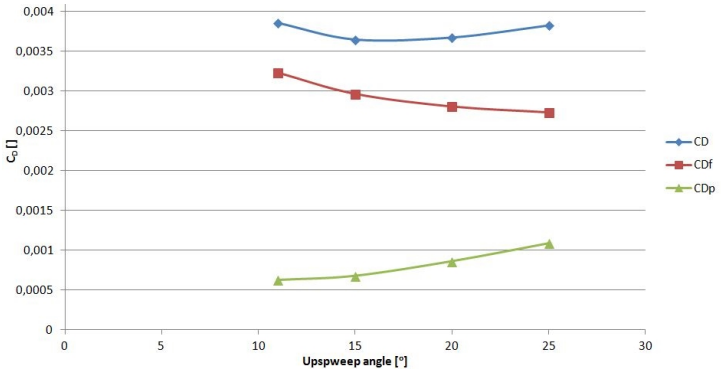

Figure 5.16: 3D Drag coefficient vs. upsweep angle.

It can be observed that the drag coefficient is not changing much over these three upsweep angles. Going from lower to higher upsweep angles, friction drag gets exchanged for pressure drag due to the separation over a higher surface area. The change in drag coefficient towards 25° is also not as sudden as what could be observed with the 2D analysis.

This can be explained by the creation of vortex-flow patterns which reduce the drag penalty for higher upsweep angles when the lower corner is fairly sharp [6]. This phenomenon has been observed by the simulation. The velocity vectors in the cross-sectional plane of the fuselage have been plotted at the start of the tail cone in Figure 5.17a and 1.7 *m* after in Figure 5.17b. At the start of the tail cone in the lower corner, the flow is turned into the back of the fuselage (large vectors at bottom) and this creates a vortex pattern which is clearly visible at 1.7 m from where it is initiated.

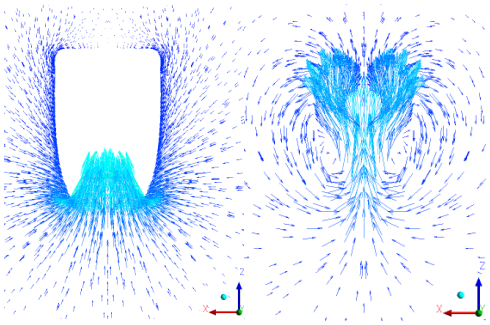

(a) Velocity projected to cross-sectional plane at start of the tail cone.

(b) Velocity projected to cross-sectional plane at 1.7 *m* after the start of the tail cone.

In Figure 5.18 the two cross-sectional planes (Figures 5.17a and 5.17b) are depicted in 3D along the fuselage.

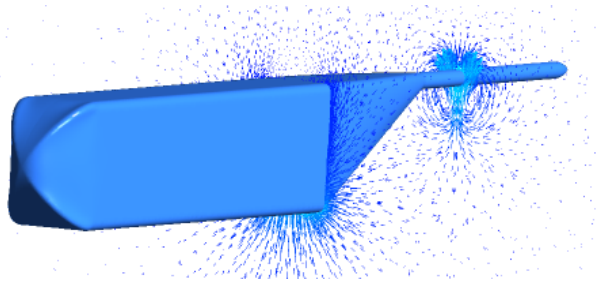

Figure 5.18: Velocity projected to cross-sectional plane at start of the tail cone and at 1.7 *m* after the start of the tail cone.

Conclusion

From the 2D analysis it became clear that upsweep angles of higher than 25° are unacceptable. The 3D analysis confirmed that drag does not decrease very much when the upsweep angle decreases to 10 °. After 25° the decrease in drag does not way up against the increase in size and hence cost of the tail cover. To be on the safe side, the tail cover will be designed with an upsweep angle of 23°.

Nose cone design

The design of the nose cone is mainly driven by the space required for the engine. As was observed from the 2D CFD analysis performed before, a slender nose results in less disturbance of the flow and hence less drag. However the length of the nose is limited by two sources. First the propeller which need to stick out of the nose. Since the propeller is directly detached to the engine, the location of the engine will limit the length of the nose cone. From a structures point of view, it is interesting to attach the engine as close as possible to the fuselage. Secondly the length of the nose cone was limited by the total length of the UAV as it needs to fit in a 20 ft container. Latter seemed to be more critical and the nose cone length was designed such that the UAV just fits in this container with a length of 5.9m. The length of the nose cone amounts 0.55 m. For the propeller to be as effective as possible, the flow behind it should be blocked as minimal as possible by the nose of the UAV. This has been a challenge given the size of the engine. Following solution had been come up with. The propeller axis is located above the center of the fuselage. Thereby there is a higher flow clearance for the propeller above its axis. Below the axis the flow enters the nosecone where it will cool the water streaming inside the radiator. The design of the nose cone is depicted in Figure 5.19. Note that the air filter is sticking out the nose cone. A recommendation for the post-DSE project was made to design a extra cover around it.

Figure 5.19: Design of the nose cone.

5.4 UAV drag polar

In the midterm report [5] a second order drag estimation is performed. The results of this method are completed with simulations to determine the total zero-lift drag (C_{D_0}). These results can be found in Table 5.6.

A CFD simulation of the fuselage estimated a drag coefficient of 0,0046 for the fuselage. This CFD simulation did not take into account 3D effects such as wrapping and super velocity. Also a rear-mounted door is not take into account. These attributions were estimated using the second order drag estimation method and added to the drag coefficient obtained from the CFD simulation. The total drag coefficient with corrections can be found under simulation in Table 5.6.

Trim drag can be calculated using Equation (5.10). The lift coefficient generated by the tail in trim condition during cruise is used. An Oswald factor of 0.65 has been taken for the tail.

$$C_{D_{trim}} = \left(\frac{V_h}{V}\right)^2 \frac{S_h}{S} \frac{C_{L_h}^2}{\pi A_t e_t} \tag{5.10}$$

The simulations performed in Section 5.1 revealed a C_{D_0} of 0.0057 for the wing only. This simulation did not take into account 3D effects such as super velocity and interference. Also the effect of flap gaps are not simulated. These contributions were estimated using the second order drag estimation method and added to the drag coefficient of the wing. The same is done for the simulated drag coefficient of the empennage which equals 0.0013. The drag coefficients of the landing gear obtained from the second order drag estimation is used in the simulation results to make the data complete. As can be seen in Table 5.6 the simulated drag coefficient gives a slightly smaller drag coefficient. To be conservative a drag coefficient of 0.0356 was used in performance calculations.

The Oswald factor of the wing has been determined in Section 5.1 and equals 0.996. This Oswald factor is corrected for fuselage, zero-lift drag and Mach number. The correction factor for the fuselage can be calculated using Equation (5.12). The correction factor for D_0 equals 0.804 for general aviation

Table 5.6: Drag prediction.

	Drag estimation	Simulation (with corrections)
Fuselage	0.0098	0.008631
Wing	0.0108	0.008321
Empennage	0.0023	0.0020
Trim drag	0.0012	0.00015
Landing gear	0.0115	0.0115
Total	0.0356	0.0306

[11]. The correction factor for Mach is ignored as the Mach number will be low ($k_{e,M} = 1$). Evaluating Equation (5.11) the Oswald efficiency number will be 0.775.

$$e = e_{wing} \cdot k_{e,F} \cdot k_{e,D_0} \cdot k_{e,M} \tag{5.11}$$

$$k_{e,F} = 1 - 2\left(\frac{d_F}{b}\right)^2 \tag{5.12}$$

With the C_{D_0}, the Oswald factor of the complete UAV and the aspect ratio, the drag polar can be defined. The drag polar is plotted in Figure 5.20.

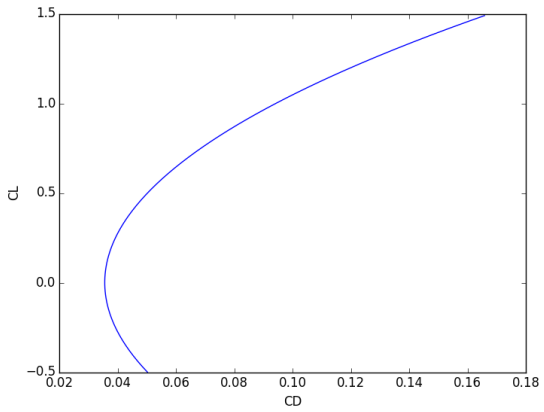

Figure 5.20: Drag polar for complete UAV.

.

5.5 Verification and validation

Subsystem requirement WFA-Sys-WFA-5.5-Aero-1 stated that the drag had to be minimized. This is a non-valid requirement as it cannot directly be verified. However drag minimization was taken into account in all decisions made during the design process. Wing and airfoil were optimized for minimum drag during cruise. The fuselage cross-section is designed as small as possible to decrease pressure drag. The length of the fuselage is minimized to decrease friction drag. The upsweep angle is chosen such that no detrimental flow separation occurs at the back of the fuselage.

Chapter 6

Performance and propulsion

In this chapter the performance and propulsion are treated, first the operational limits are determined in Section 6.1. After that the mission profiles and payload range diagrams are constructed in respectively Sections 6.2 and 6.3. To show the different functions happening during the take-off a functional flow diagram is given in Section 6.4. In Section 6.5 the take-off and landing performance are discussed and in Section 6.6 the total mission time is stated. Next the engine and propeller choice are explained in Section 6.7 and Section 6.8 respectively. This is then followed by the noise characteristics in Section 6.9 and the verification in Section 6.10.

6.1 Flight envelope

In order to give a overview of the loads on the UAV at the different parts of the mission a flight envelope has been constructed, as prescribed by the regulations in CS-VLA [12]. The flight envelope consists of two parts; one part is the loads due to maneuverability and the other part is the loads due to gust. The maximum load factor in the flight envelope is the limit load factor for which the UAVs wing should be designed.

The important speeds are the stall speed, maneuver speed, cruise speed and dive speed. The first one is just the minimum speed for the aircraft to fly at. The second one represents the transition between aerodynamic and load factor performance limitation. The cruise speed is the design speed used in the calculation. Lastly, the dive speed is the maximum speed of the aircraft during operation. It should be at least $1.25 \cdot V_c$, according to CS-VLA [12]. The calculations of the load factors can be seen in [5].

In Figure 6.1 the flight envelope is given for both maneuvering and gusts loads. As can be seen there are velocities where the maneuvering loads are limiting and a part where the gusts loads are limiting. A summary of the most maximum and minimum limiting load factors at V_c and V_d are given in Table 6.1. V_b is not considered in the CS-VLA [12] and is therefore not stated in Table 6.1. The ultimate load factors are the limiting loadfactors multiplied by 1.5 and are also given in Table 6.1.

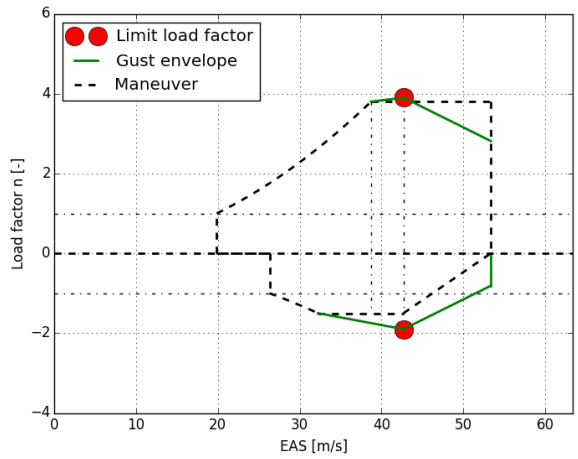

Figure 6.1: UAV flight envelope.

Table 6.1: Design load factors.

	V_c	V_d
n_{lim}	3.9	3.8
	-1.9	-.8
n_{ult}	5.85	5.7
	-2.85	-1.2

6.2 Mission profile

In Figures 6.2 and 6.3 the different mission profiles are shown. Differences between the mission profiles are due to the fact that the operation location is different, however it also depends on the different dropping schemes of the UAV. The difference in mission profile due to the operation location is because of the fact that UAV can be deployed in a warzone or in a natural disaster area. In order to avoid being shot down by small arms fire the cruise altitude of the UAV should be higher than 1 km when operating in a warzone. While with a normal disaster this risk is not present and the cruise altitude

will therefore be lowered to 150 m. The difference in cruise altitude has an effect on both the drag on the UAV and loiter time. The drag is increased when flying lower, however the loiter time for dropping will be shorter, which will be elaborated in Section 9.2. The mission profiles for deploying the UAV in a warzone can be seen in Figure 6.2 and for deployment for a natural disaster in Figure 6.3. The difference between the mission profiles depends on the difference between the dropping schemes. There are four different types of missions. The first type of mission is the generally executed dropping scheme, in this type all the packages are dropped in the first 250 km and after that the UAV will fly the 250 km back without any payload on board. The second dropping scheme is a scheme where the UAV drops the packages equally spaced over a distance of 500 km. Therefore the UAV will not return to the base where it started but will fly to another airstrip at a distance of 500 km. The third mission is also a mission where the UAV will not return to its original base however in this case the packages are dropped in the second part of the mission after 250 km flying. The last mission is a mission where the UAV is used to transport the packages to another airstrip 500 km away, however it assumed that the UAV does still have to fly the full loiter time for the dropping of the packages.

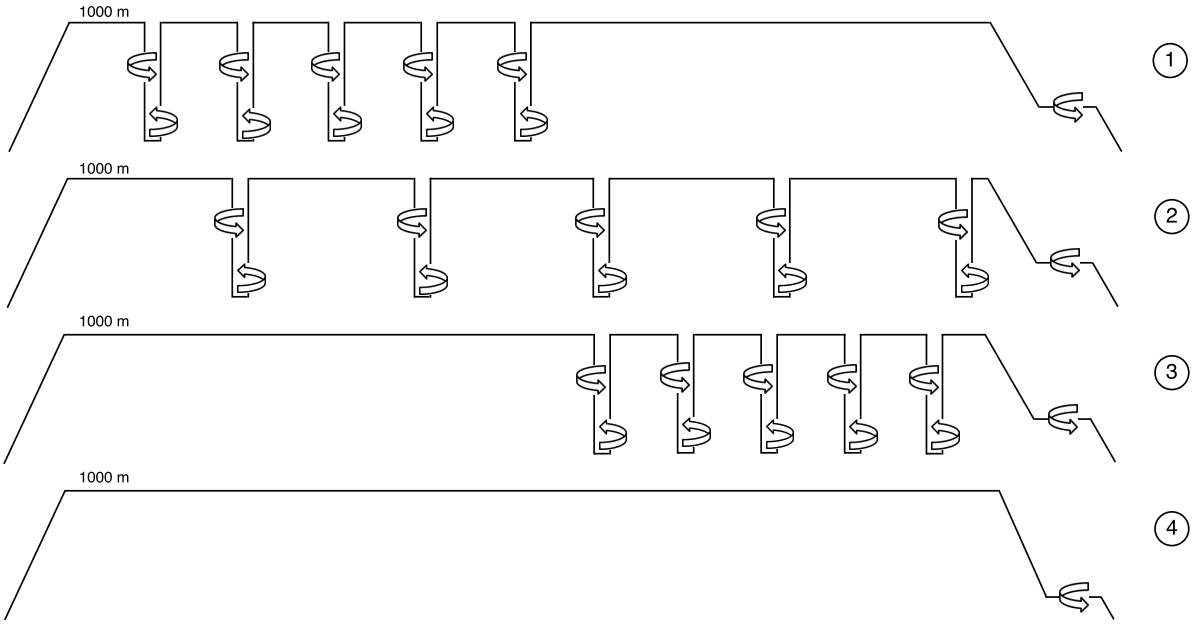

Figure 6.2: Mission profiles for different missions in case of a warzone.

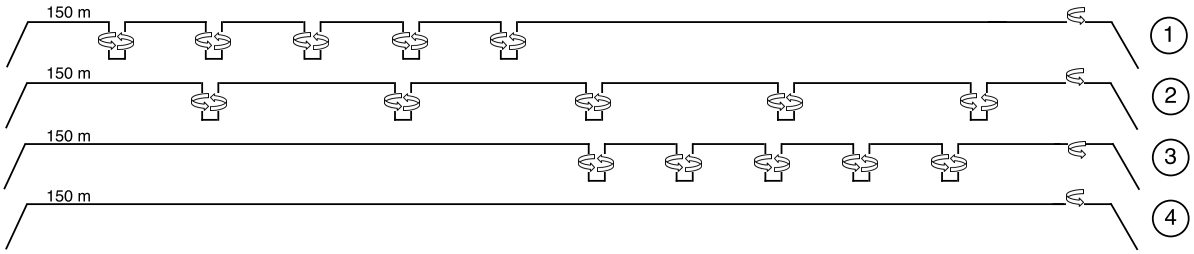

Figure 6.3: Mission profiles for different missions in case of a natural disaster.

6.3 Payload-range diagram

As said in Section 6.2 there are different mission profiles possible for the mission depending on the dropping locations of the packages and mission locations. Both of the dropping locations and the mission location have an effect on the range which can be flown by the UAV. In Figure 6.4 four different payload range diagrams can be seen for different dropping locations. All of these plots are made for the most critical mission location which is deploying the UAVs in a warzone. Deploying the UAVs in a warzone is critical for the range because the loiter time is much higher than the loiter time during a natural disaster mission. When looking at the plots the different mission profiles can be seen, every

jump is the result of a package drop. Looking at the maximum ranges of the diagrams it can be seen that there are a differences between the maximum ranges the UAVs are able to fly, this is the result of the different dropping moments in between the different mission profiles. Dropping the packages early in the mission result in a longer flight without payload and this results in a larger range. As a result of this the most limiting mission will be the transport mission where the packages are dropped at the very end of the mission. Here the maximum range is 500 *km* which is the minimum requirement for the UAV range.

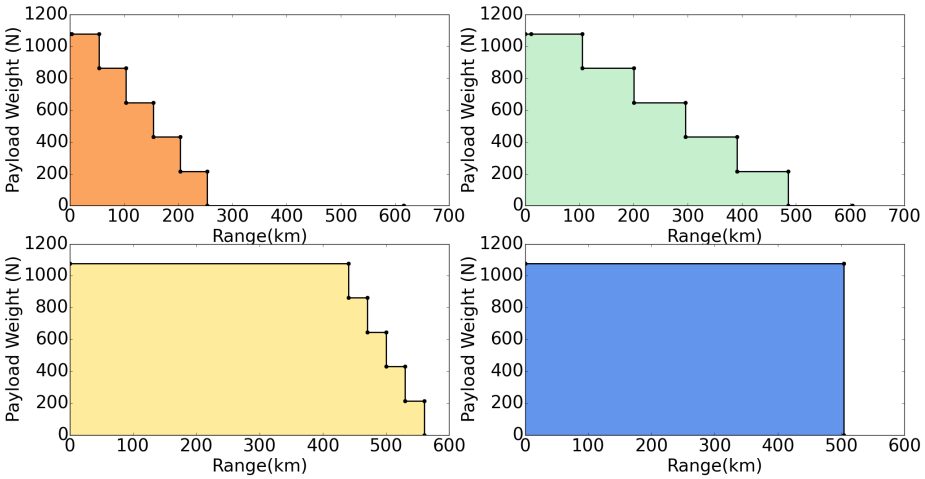

Figure 6.4: Payload-range diagram for four different mission profiles.

For the most limiting case where the packages are dropped at 500 *km* the full payload range diagram is computed. This payload range diagram can be seen in Figure 6.5. When looking at the diagram it can be noticed that there are three different parts: Maximum payload, FR1, FR2. The maximum payload part is the same part as in the fourth plot of Figure 6.4 and shows the maximum range with maximum payload which is 500 *km*. The second part is FR1, this is the first ferry range. This ferry range will be 825 *km*. The reason that this is such a large distance is because the UAV will fly with less payload but with no extra fuel and does not have to loiter an additional time of 69 *min* because there are no packages in the fuselage. FR2 is also a ferry range however this ferry range is the result of replacing all the payload mass with fuel mass. This ferry range will be 2550 *km*. Because the payload mass is a very large part of MTOW this range is large. It is chosen to make it not possible to trade a part of the payload for fuel because adding five extra fuel tank connections will be too expensive. So there will be one extra connection for connecting one large fuel tank with 100 *kg* of fuel. These ferry ranges are used to transport the UAV to other places to avoid demounting the UAV and transporting it with truck, trains or aircraft.

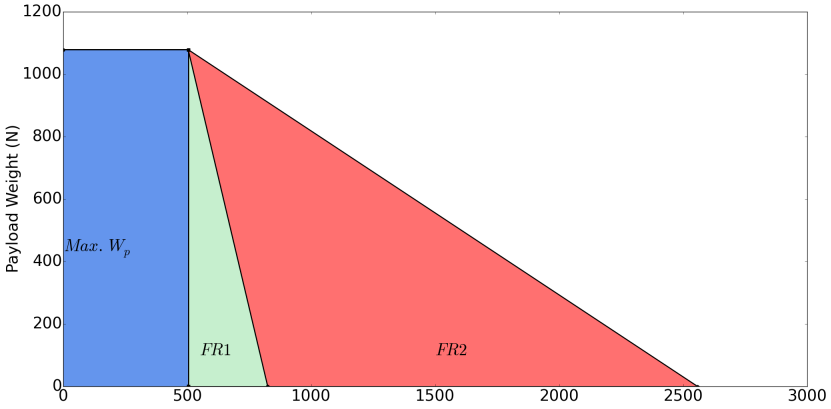

Figure 6.5: Full Payload-range diagram for the most critical mission.

6.4 Functional Flow of take-off and cruise

In this section the flow diagram of the take-off phase is given. As can be seen in Figure 6.6 at the top level other general functions of the UAV are worked out in flow diagrams. Assembling the UAV, loading and preparing the UAV, landing and turnaround and ending mission are stated in Section 11.7 because they are the most affected by the ground operations. The dropping maneuver is treated in the Section 9.3.

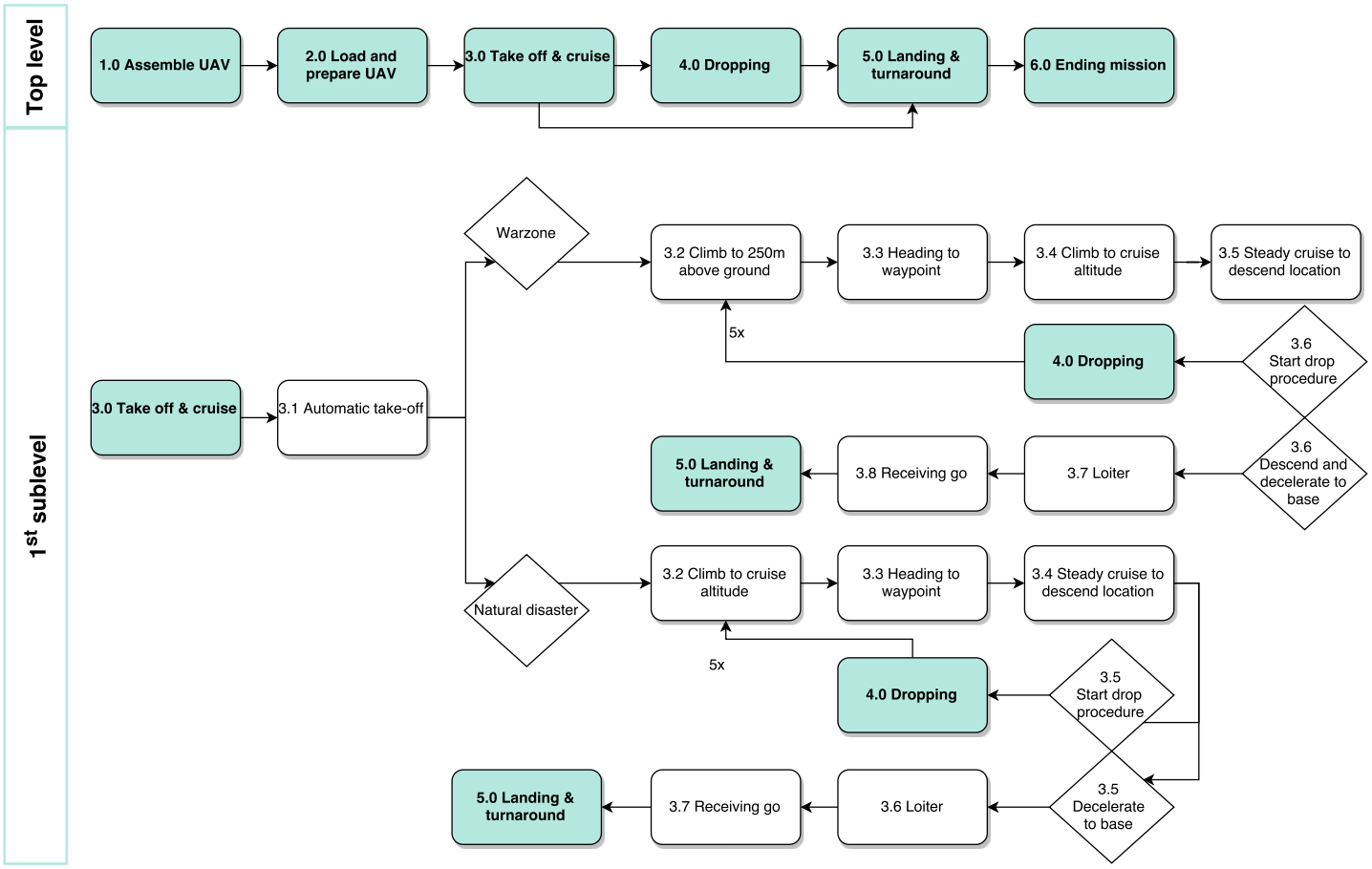

Figure 6.6: Flowchart of the take-off phase.

6.5 Take-off, landing and general performance

The take-off, landing and climb requirements were coded into the Python programme in the power loading versus wing loading diagram. For this Equation (6.1) was used to meet the take-off requirement of 150 m, Equation (6.2) for the 150 m landing distance [13]. Here TOP stands for take-off parameter and LP for landing parameter.

$$TOP = \left(\frac{W}{S}\right)_{TO} \left(\frac{W}{P}\right)_{TO} \frac{1}{C_{L_{max}}} \frac{\rho_0}{\rho} \qquad (6.1)$$

$$\left(\frac{W}{S}\right) = \frac{C_{L_{max}} \rho s_{land}}{2fLP} \qquad (6.2)$$

The statistical parameters, TOP and LP, were based on the performance of the RANS S6 Coyote STOL aircraft[1]. As this is not a very large statistical base to use, the take-off and landing were simulated in Section 6.10 to determine if the requirements are met.

The stall speed depends on altitude. The stall speed versus altitude graph is presented in Figure 6.7. the maximum rate of climb depends on altitude and can be reached at the point of minimum power required. At this point it is true that $dP_r/dV = 0$. The maximum climb rate is given by Equation (6.3).

[1]URL `http://www.rans.com/#!S-6ESSpecsPic.jpg/zoom/c1ibj/dataItem-igvcga0z` [Cited on 18/06/2016]

$$ROC = \frac{P_a - P_r}{W} \tag{6.3}$$

A decrease in density decreases the available power. This means that the climb rate will decrease as well as shown in Figure 6.8. The maximum climb rate is evaluated at the related optimal velocity.

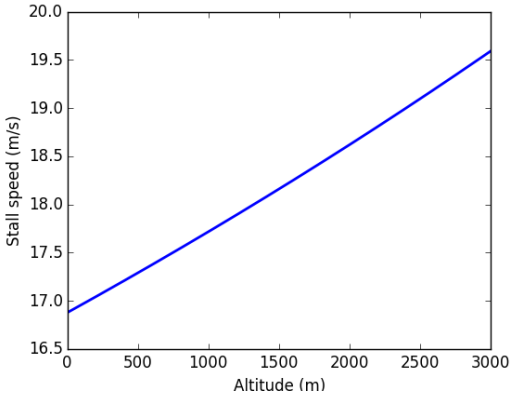

Figure 6.7: Stall speed vs. altitude at maximum C_L of 1.9.

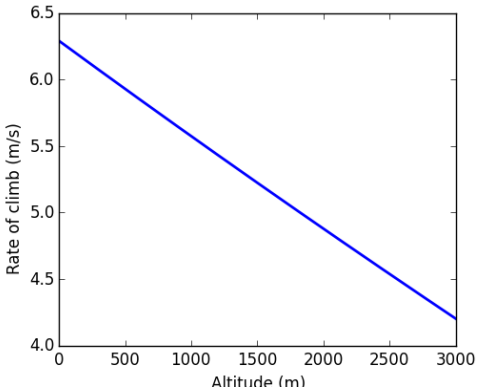

Figure 6.8: ROC at different altitudes ranging from 0 to 3000 m.

The stall speed varies from 16.9 m/s to 19.6 m/s depending on the altitude while the rate of climb varies between 6.3 m/s at sea level and 4.3 m/s at 3000 m altitude.

6.6 Total mission time

In this section the total mission time is computed as it is an important parameter for the capacity of the mission. In Section 9.2 the two different drop maneuvers are described and the corresponding durations are computed as well. The take-off and landing duration is computed in Section 6.10. The computation of the duration of the rest of the mission is presented in this section. After that the total mission duration is presented in Table 6.2.

First climb to cruise altitude

During warzone missions it is important that the UAV climbs as fast as possible to a safe altitude of 1000 m from where it can perform its mission. This is why a spiraling climb procedure at maximum rate of climb is recommended. The UAV will perform a climb similar to the climb described in Figure 9.7. This means that the UAV will climb with a climb rate of 4.2 m/s (assuming 3000 m altitude conditions) with a corresponding flight speed of 25 m/s. This climb will take 3.9 minutes.

During regular missions the UAV also climbs as fast as possible to reach a safe altitude for possible parachute deployment. This means that the UAV will climb at a 4.3 m/s climb rate towards 150 m cruise altitude. This procedure will take 0.5 minutes and while the UAV climbs a horizontal distance is covered as well. This distance is 680 m. For this computation it is assumed that the distance covered during climb is in the right direction considering the mission.

Final descent to runway

During warzone missions it is important that the UAV descents on the location of the ground station to perform its mission safely. The final mission will therefore consist of a spiraling descent towards 15 m similar to the descent described in Figure 9.2. This means that the UAV descends with a rate of 5.4 m/s and this maneuver will take 3.0 minutes. With a descent rate of 3.2 m/s and a flight speed of 23 m/s the distance covered during normal missions is around 960 m which will take about 42 sec.

Cruise duration

The cruise speed is 43 m/s or 155 km/hr. This means that the cruise duration for the warzone missions is 3.2 hr or 194 minutes.

Total time

In Table 6.2 the total mission time for both type of missions is presented.

Table 6.2: Total mission time for both types of missions.

Type of mission	Warzone mission	Normal mission
Take-off	4 min	1 min
Cruise	194 min	193 min
Dropping	69 min	23 min
Landing	3 min	1 min
Loiter time	15 min	15 min
Total	**4.75 hr**	**4.0 hr**

A loiter time is included because of possible waiting times that could arise due to the limited capacity of the ground station. This loiter time added is 30 minutes. This makes the total mission time to around 4.8 *hr* for the warzone mission and 4.0 *hr* for the regular mission.

6.7 Engine selection

With it being known from the midterm review [5] that the required propulsion will be obtained using a piston engine with a propeller and that this will be done by using a single engine, possible engines can be found. A full list of engines can be found in the midterm review [5]. Using the engines that cost less than €6,000, the dry engine weight is plotted against the power to compare weights in Figure 6.9. Several more engines are included here than in the midterm review. What is included in these weights can be slightly different between the various engines, so the weight can be solely the dry engine block, or also include a belt, exhaust, electronics and so forth. A vertical line is included at 48 *hp* to indicate the minimum power required from the second order estimation Python programme.

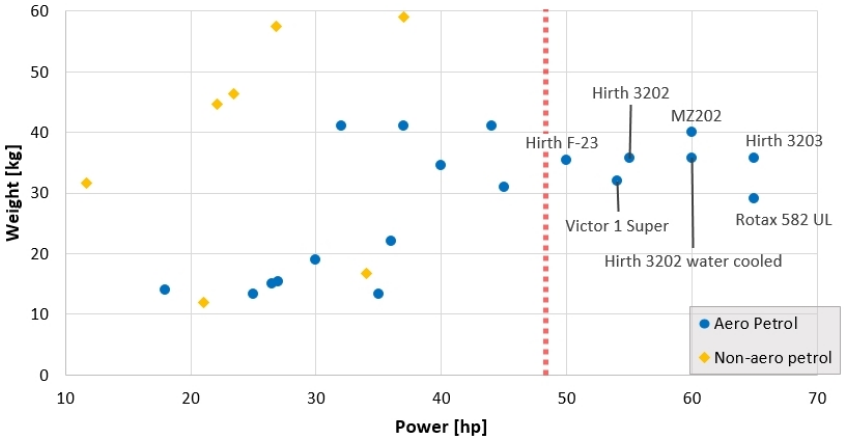

Figure 6.9: Weight against power graph for engines with a price below €6,000.

This shows that there are only a handful of feasible engines in the desired power range and that these engines all roughly have the same weight. From the Hirth engines only the cheapest and lightest engine, the F-23, is considered in the further analysis. Furthermore the MZ202 from CompactRadialEngines is not further considered as it is the heaviest engine and very little information about this engine is known with key information such as fuel consumption missing[2]. For the remaining engines, the F-23, Victor 1 Super and the Rotax 582 UL, a detailed weight and cost analysis is completed to determine the weight and cost of the whole set up. First the smallest engine, the Hirth F-23, is analysed in table Table 6.3. The fuel tank, propeller and battery are excluded from these detailed analyses. Next engine analyzed is the Victor 1 Super in Table 6.4 and then the Rotax 582 UL is analyzed in Table 6.5.

[2]CompactRadialEngines have been contacted about their engines, however no response followed.
[3]URL `http://www.recpower.com/` [Cited on 06/06/2016]
[4]Cost information from email correspondence with Simonini
[5]URL `http://www.rotaxservice.com/rotax_engines/rotax_582UL.htm` [Cited on 06/06/2016]

Table 6.3: F-23 detailed weight and cost analysis[3].

Component	Weight (kg)	Component	Cost (€)
Dry block, reduction unit, full exhaust and electric start	35.4	Engine, electric start and slide carburetor	4,451
		Multi-Groove belt drive	793
		Fuel pump	68
		Rotax regulator-rectifier	82
		Rotax/K&N dual carburetor air filter	41
Total	**35.4**	**Total**	**€5,435**

Table 6.4: Victor 1 Super detailed weight and cost analysis[4].

Component	Weight (kg)	Component	Cost (€)
Dry block, electric start and exhaust	32	Dry block, Bing 54 38mm carburetor, air filter, fuel pump, exhaust system, electric starter, Poly-V belt reduction and system to charge battery in flight	4,140
Radiator	1.1		
Coolant	3		
Cooling piping	0.3	Reservoir	56
		Radiator	65
Total	**36.4**	**Total**	**€4,261**

Table 6.5: Rotax 582 UL detailed weight and cost analysis[5].

Component	Weight (kg)	Component	Cost (€)
Dry block	29.1	Engine and exhaust	4,440
2 Carburetors	1.8	Reduction unit 'B'	554
Exhaust system	5.1	Electric starter	509
Electric starter	3.5	Fuel pump	68
Propeller speed reduction unit "B"	4.5	Rotax regulator-rectifier	82
Coolant	3	Rotax/K&N dual carburetor air filter	41
Coolant piping	0.3	Liquid circuit radiator set	410
Total	**47.3**	**Total**	**€6,104**

So the Victor 1 Super is the cheapest engine by far, however not the lightest. Before the final decision is made various other characteristics are looked at starting with the operational costs of the the Victor 1 Super in Table 6.6, then the Hirth F-23 in Table 6.7 and the Rotax 582 UL in Table 6.8. The fuel costs were estimated by using the fuel simulation in the Python programme using the fuel consumption of the Victor 1 Super. This resulted in the fuel weight for the worst case scenario including the maximum loiter time. Then this fuel weight was split into the petrol and the two-stroke oil and the price estimated by using 1 €/l for the petrol and 4 €/l for the motor oil. Furthermore the fuel use for the other engines were scaled using the specific fuel consumptions in Table 6.9 and the oil use scaled using the specific fuel consumptions and the different oil mixing ratios in Table 6.9. The maintenance intervals were obtained from the operators and maintenance manuals of the respective engines provided by the manufacturer. The maintenance costs were obtained by estimating a component cost and labour hours needed using a labour cost of €40 per hour for a certified engineer.

In particular the maintenance manuals of the Hirth and the Rotax are very detailed and contain too

much to completely include in the trade-off so a general type A and type B check are included in which many of the smaller tasks are included. The type A check is a mostly visual check of the engine, which includes inspecting at things such as the air filter, exhaust springs, inside of the exhaust, piping and various seals and also measuring belt tension. This check is estimated to take two hours and should be completed every 50 flight hours, or every 2.3 days when flying continuously with the minimum possible turn around time. The type B check should be done every 100 hours, or 4.6 days when flying continuously, and requires large parts of the engine to be disassembled to inspect and clean the inside of the engine and the various gaskets and is estimated to take six hours.

Table 6.6: Victor 1 Super operational costs[6].

	Cost (€)	**Flight hours**	**Cost (€/hr)**
Fuel use	40.0	4.75	8.42
Oil use	5.64	4.75	1.19
Replace spark plugs	100	200	0.50
Replace fuel filter	20	100	0.20
Replace fuel line	20	100	0.20
Replace air filter	50	250	0.20
Type A check	80	50	1.60
Type B check	240	100	2.40
Total overhaul	1,500	500	3.00
Total			17.7

Table 6.7: Hirth F-23 operational costs[7].

	Cost (€)	**Flight hours**	**Cost (€/hr)**
Fuel use	42.4	4.75	8.93
Oil use	4.0	4.75	0.84
Replace spark plugs	100	100	1.00
Replace fuel filter	20	100	0.20
Replace jet needle	50	100	0.50
Replace fuel line	20	100	0.20
Replace air filter	50	250	0.20
Top end overhaul	500	500	1.00
Type A check	80	50	1.60
Type B check	240	100	2.40
Total overhaul	1,500	1,000	1.50
Total			18.4

Table 6.8: Rotax 582 UL operational costs[8].

	Cost (€)	**Flight hours**	**Cost (€/hr)**
Fuel use	40.0	4.75	8.43
Oil use	3.8	4.75	0.79
Replace spark plugs	100	25	4.0
Replace fuel filter	20	100	0.20
Replace jet needle	50	150	0.33
Replace fuel line	20	100	0.20
Replace air filter	50	300	0.17
Top end overhaul	500	150	3.3
Type A check	80	50	1.6
Type B check	240	100	2.4
Total overhaul	1,500	300	5.00
Total			26.5

Next parameters such as such as engine and fuel type and fuel use are looked into. These parameters can be found in Table 6.9. Furthermore the weight and costs found above are summarized.

[6]Maintenance schedule based on URL `http://www.flyproducts.it/manuali/manualieng/VICTOR1ENG.pdf` [Cited on 14/06/2016]

[7]Maintenance schedule based on URL `http://hiwaay.net/~bzwilson/dragonfly/140406_engine/Operators_manual.pdf` [Cited on 14/06/2016]

[8]Maintenance schedule based on URL `http://flyrotax.com/portaldata/5/dokus/d00288.pdf` [Cited on 14/06/2016]

Table 6.9: Engine comparison between the Hirth F-23, Victor 1 Super and Rotax 582 UL

	Hirth F-23	**Victor 1 Super**	**Rotax 582 UL**
Engine type	Air cooled two-stroke	Water cooled two-stroke	Water cooled two-stroke
Cost (€)	5,435	4,261	6,104
Weight (kg)	35.4	36.4	47.3
SFC (10^{-7} kg/J)	1.13	1.07	1.07
Operational costs (€/hr)	18.4	17.7	26.5
Fuel type(s)	Min. 95 RON unleaded	Min. 91 RON unleaded	Min. 91 RON leaded or unleaded, AVGAS 100LL or E10
Oil mixing ratio	1:50	1:33 for 91 RON and 1:50 for 95 RON	1:50

The Victor 1 Super has a major cost advantage, so it will need to have other serious disadvantages to make it not be chosen. It is not the lightest engine, however only weighs 1 kg more than the Hirth F-23. Furthermore its fuel type is average, where the fuel can be a low RON level, however no alternative fuels are possible. Finally the oil mixture ratio is poor at 3% when normal unleaded petrol is used. The engine is water cooled so it will need coolant to be present to refill, which increases the complexity of the logistics. Furthermore it is another system that could fail. However it reduces the temperature range that the engine operates in allowing for reduced emissions and fuel use and also increases the longevity of the engine block by reducing fatigue and the change of damage by seizure. Furthermore water cooled engines are slightly more quiet. Finally for certification in the future the Rotax 582 would be the best decision as Rotax sells a certified version of the 582, which would allow for certification of the engine by simply swapping engines while using all of the same mounts. Another benefit for the Rotax and the Hirth is that they are older and have been updated several time to remove flaws, while the Victor 1 Super is newer and less reliable. Finally the Rotax 582 can run on a 10% ethanol blend which reduces overall emissions to increase the sustainability.

Although there are some disadvantages to the Victor 1 Super, the low price and operating costs are major advantages, therefore the Victor 1 Super engine is chosen.

Fuel consumption

The fuel consumption of various engines in the correct price and weight ranges from Figure 6.9 are shown in Figure 6.10. The fuel consumption of the Victor 1 Super could not be found, however the fuel consumption of the older model, the Victor 1 Plus, was found. The fuel consumption of the Victor 1 Plus is multiplied by 1.1 to estimate the Victor 1 Super fuel consumption. Furthermore, the fuel consumption graph of the Victor 1 Super is horizontal between 48 and 54 hp because the Victor 1 Plus had a maximum power of 48 hp, while the Victor 1 Super goes up to 54 hp.

The fuel consumption of the Victor 1 Super is suspiciously low indicating that the fuel consumption was most likely measured in unrealistically ideal conditions. To compensate for this the fuel consumption further in all calculations is the average of the Hirth F-23, Hirth 3203 and the Victor 1 Super. This line is indicated in Figure 6.10 as 'Average of F-23, 3203 and Super'. The average was taken of Victor 1 Super with the Hirth engines as these engines have the same compression ratio as the Victor 1 Super of 9.5. The Rotax 582 has a compression ratio of 11.5 and therefore should be more fuel efficient. One other consideration is the the Victor 1 Super is a considerably newer engine than the others and therefore should be slightly more advanced. An added benefit of this method is that the fuel consumption of the engine continues to climb between 48 and 54 hp.

[9]URL `http://www.flyrotax.com/files/Bilder/Produkte%20Rotax/Datasheets/Produktdatenblatt_582_65hp_RZ.pdf` [Cited on 06/06/2016]
[10]URL `http://www.simoniniusa.com/?page=Engines&Engine=Victor-1-Plus` [Cited on 06/06/2016]
[11]URL `http://www.recpower.com/hirth.htm` [Cited on 06/06/2016]

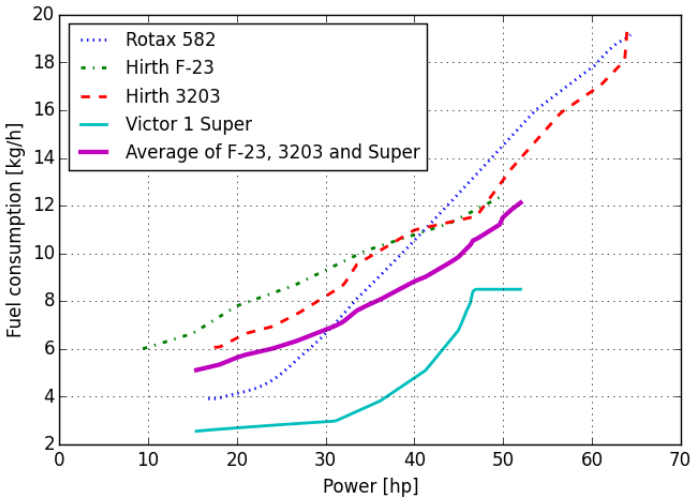

Figure 6.10: Fuel consumption of various engines[9] [10] [11].

At higher altitudes the power level producible by the engine drops and the engine needs to be at a higher setting, and therefore consumes more fuel, to obtain the same power output. This effect can be estimated using Equation (6.4) [13]. Here the P_{actual} is the actual power level of the engine needed to provide the required power output, $P_{required}$.

$$P_{actual} = P_{required} \cdot \left(\frac{\rho_0}{\rho}\right)^{3/4} \tag{6.4}$$

In the emissions aspect the Victor 1 Super is poor as it burns 3% two-stroke oil when using poor quality fuel of 91 RON. However this can be reduced to 2% oil if 95 RON fuel is used which is the standard in most first world countries. At half engine power the engine uses 0.20 kg of oil every hour when running 91 RON and uses 0.14 kg per hour when using 95 RON. Unfortunately all engines in the desired price and weight bracket from the market research are two-stroke engine that burn similar amounts of oil. Therefore the unit cost would have to be compromised to reduce the emission levels.

6.8 Propeller design

Propeller sizing

For the propeller design it is chosen that an off-the-shelf propeller set up should be used. To help find the correct propeller various propeller dimensions were calculated. However as the take-off requirement is so important a more accurate thrust equation than $T = P \cdot V$ was found to model the propeller thrust as very low speeds. The chosen equations result from modelling the propellers as an actuator disk which evenly increases the air velocity of the air passing through the disk by a ΔV and so produces a thrust. This can be seen in Equation (6.5) [14, p. 292]. Here the A_p is the area covered by the propeller.

$$P_{shaft} = \frac{T}{\eta_p}\left(V + \frac{1}{2}\Delta V\right) \qquad \Delta V = \sqrt{V^2 + \frac{2T}{\rho A_p}} - V \tag{6.5}$$

Combining the equations Equation (6.5) results in the static thrust equation with $V = 0$ in Equation (6.6).

$$T_{static} = \left(P_{shaft} \cdot \eta_p \cdot \sqrt{2\rho A_p}\right)^{\frac{2}{3}} \tag{6.6}$$

From this equation it is clear that a larger propeller diameter produces more thrust. Therefore, next, the maximum propeller diameter was determined using the fuselage and landing gear dimensions and a ground clearance of 22 cm per EASA regulations [12]. This resulted in a maximum feasible diameter of 1.52 m, which is chosen to be used in the design.

Next the geometric propeller pitch was determined using Equation (6.7) [15, p. 592] for optimal propeller efficiency during cruise if the propeller cuts perfectly through the air and does not slip at all. Here the $P_{D_{Geometric}}$ is the propeller pitch in inches, the V_{KTAS} is the true cruise airspeed in knots and RPM_p

is the propeller rotational speed during cruise. However some slip will be present and therefore the optimal pitch changes and can be calculated with Equation (6.8). Here the amount of slip between 0, for no slip at all, and 1, for full slip, is indicated as $slip$.

$$P_{D_{geometric}} = 1251.36 \left(\frac{V_{KTAS}}{RPM_p} \right) \quad (6.7) \qquad P_{D_{effective}} = P_{D_{geometric}} \cdot (1 - slip) \quad (6.8)$$

Finally the Mach number of the tip is calculated to verify that the speed of the blade tips does not come too close to the speed of sound, which would increase the noise significantly and also reduce the lifespan of the blades. The maximum tip Mach number is calculated using Equation (6.9).

$$M_{tip} = \frac{d_p \cdot \pi \cdot RPM_{p_{max}}}{60 \cdot a_{cruise}} \quad (6.9)$$

Furthermore the advance ratio for cruise and climb are calculated in Equations (6.10) and (6.11).

$$J_{cruise} = \frac{V_{cruise}}{RPM_{p_{cruise}}/60 \cdot d_p} \quad (6.10) \qquad J_{climb} = \frac{V_{climb}}{RPM_{p_{climb}}/60 \cdot d_p} \quad (6.11)$$

Using these advance ratios together with the 75% blade angle obtained from the effective pitch the propeller efficiency can be obtained using Figure 6.11.

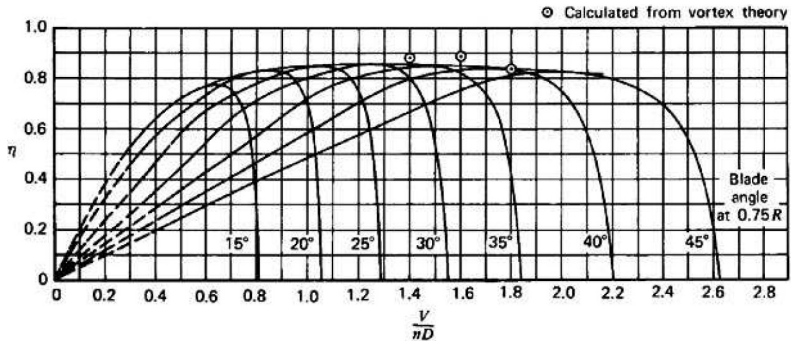

Figure 6.11: Propeller efficiency against advance ratio for different 75% blade angles [16].

Using these equations and figure the propeller is sized for two different reduction ratios. First 1:2.68, which is the lowest reduction ratio provided by the engine manufacturer, and 1:1.84 which is an optimized ratio. This optimized ratio is found by varying one of the pulleys in the belt drive using options provided by the manufacturer, Hutchinson transmissions, and then choosing the set up with first the highest cruise efficiency and then for equal cruise performance, then the highest climb performance. The minimum reduction ratio is set at 1:1.64 to prevent the blade tip spinning above Mach 0.9. Furthermore a slip of 15% is assumed. This resulted in a change of the large pulley from 182 mm diameter to 125 mm, which costs €65, and a change in belt to a 592 mm belt, which costs €12.20[12]. The comparison can be found in Table 6.10. For the static thrust levels it is assumed that the take-off propeller efficiency is equal to the climb efficiency and that the altitude is 1500 m.
The higher propeller efficiencies from using the optimized reduction drive reduce the fuel use by 200 g, or roughly €0.20, per mission. This means that the extra cost of the reduction drive will be earned back in 386 missions and additionally results in a more sustainable design. Furthermore, if the propeller climb efficiency is used in the take-off simulation from Section 6.10, the take-off distance is reduced by 12 meters at 1500 m altitude and 16 m at sea level. Therefore the optimized belt reduction set up is used.

Propeller selection

With the propeller sized, now a selection needs to be made of the off-the-shelf available propellers. The cheapest propellers turned out to be propellers designed for ultralights. These propellers have as additional benefit that they are designed for similar aircraft weights and speeds. The best two propellers resulting from research and email contact with manufacturers are the Ivoprop ultralight propeller and the Powerfin model "B" propeller with two blades. A comparison of the two propellers, both with a diameter of 1.52 m, can be found in Table 6.11. Pitch adjustable means that propeller angle can be changed.

[12]Belt drive information obtained from email correspondence with Hutchinson transmissions

Table 6.10: Propeller parameters for two different reduction ratios.

Parameters independent of slip				Parameters dependant on slip, using 15% slip			
Reduction ratio	**2.68**	**1.84**	**Unit**	**Reduction ratio**	**2.68**	**1.84**	**Unit**
M_{tip}	0.55	0.8	(-)	$P_{D_{effective}}$	2.01	1.38	(m)
J_{cruise}	1.51	1.04	(-)	Blade tip angle	25.6	17.0	(deg)
J_{climb}	1.05	0.72	(-)	75% blade angle	36.0	23.2	(deg)
$P_{D_{geometric}}$	2.37	1.63	(m)	$\eta_{p_{cruise}}$	0.84	0.85	(-)
				$\eta_{p_{climb}}$	0.73	0.78	(-)
				Static thrust	1437	1502	(N)

Table 6.11: Propeller comparison

Manufacturer	Ivoprop	Powerfin
Cost	€592	€542
Weight	3.6 kg	2.74 kg
Pitch adjustable	On ground	No
Separate blades and hub	No	Yes

So the Powerfin set up is cheaper and lighter, however the pitch can not be adjusted. The advantage of having an on ground adjustable pitch is that the pitch can be set to the optimal value for each mission and if the take-off strip is slightly too short, then the pitch could be reduced to increase the thrust and so trading cruise speed for a shorter take-off distance. The disadvantages are that it is an extra component that can fail and that needs to be maintained. The Powerfin has the advantage that the blades get bolted into the central hub providing propeller modularity and also allows for each damaged blade to be replaced separately. Whenever a blade is replaced the propeller will need to be rebalanced which is done by placing tape in a special cavity at the root[13]. The difficulty however is to determine the level of unbalance in the first place. For this we recommend using a dynamic prop balancer at each of the main hubs, which will cost around €1350[14] and a much cheaper and simpler bushing kit for determining the static balance in the field. The bushing kit is much cheaper at €270[15], however is less accurate and does not measure the dynamic unbalance. Overall the Powerfin propeller is seen as the best option it is cheaper, lighter, modular and easier for maintenance, even if the pitch can not be adjusted. Furthermore it is expected that the costs for the balancing devices will be offset by the savings from being able to reuse blades and hubs.

Lastly the propeller inertia of the chosen propeller is estimated using the beam approximation for the blades and a disk approximation for the hub, which results in Equation (6.12). This is to check that the propeller will not have too much inertia and so damage the belt drive.

$$I_p = m_p \cdot r_{CG_p}^2 \tag{6.12}$$

Using data provided by the manufacturer of a single blade weight of 0.77 kg, a hub weight of 1.2 kg and the CG distance to the center of rotation of 25 cm results in a propeller inertia of 1770 $kg \cdot cm^2$. This is well below the limit for many belt drives and small gearboxes of 3000 $kg \cdot cm^2$ for example the smallest Rotax gearbox, the type B gearbox[16]. So the large diameter does not cause an issue here either.

[13]URL `http://www.powerfin.com/balancing.html` [Cited on 26/06/2016]
[14]URL `http://www.aircraftspruce.com/pages/to/test_prop/dynavibe.php` [Cited on 26/06/2016]
[15]URL `http://www.aircraftspruce.com/catalog/appages/tool129bushkit05-12919.php?clickkey=4129` [Cited on 26/06/2016]
[16]URL `http://www.rotaxservice.com/rotax_engines/rotax_582UL.htm` [Cited on 16/06/2016]

6.9 Noise characteristics

The noise characteristics of the engine will be very poor as it is a two-stroke engine with a large single cylinder and the exhaust does not contain a muffler due to the extreme cost saving measures implemented in the design. Unfortunately the engine manufacturer does not provide engine noise levels. However some characteristics can still be derived. First the frequency of the engine noise can easily be derived due to the fact that it is a single cylinder, so the RPM of the engine is the same as the noise frequency. At the maximum power of 54 hp the engine turns at 6200 RPM and so produces a noise at 103 hertz at take-off. This is on the low end of the frequencies perceived by humans. Furthermore, the engine will sound similar to other single cylinder two-stroke devices with similar frequencies such as lawn movers and leaf blowers. If the noise level of the Hero product turns out to be unacceptably loud, then an after muffler can be added to the exhaust for €140 and an intake silencer can be included for €183 to reduce the noise coming out of the carburetter throat[17]. Using an intake silencer will reduce the power output by roughly 2%[18].

The propeller and engine noise will be dominant, however the other contributors to the overall noise levels should not be ignored. These are the aerodynamic noise from the wing tip vortices and the turbulence generated by the landing gear. This noise could be reduced by using wingtips and landing gear fairings, however due to cost saving these will not be implemented.

6.10 Verification and validation

Take-off performance

The take-off requirement of 150 meters will be achieved in the programme as it is a requirement in the power loading versus wing loading diagrams. The take-off requirement was one of the critical cases and uses a value called the Take-Off Parameter which is based on statistics, so a simulation is created to determine if the take-off requirement is truly achieved.

The amount of thrust is obtained using the actuator disk estimation in Equation (6.5). Furthermore a ground rolling friction coefficient of 0.05 for short grass [17, p. 40] was implemented to account for the poor terrain and a ground effect estimation from Roskam [18, p. 281 - 286] to estimate the increase in lift due to being close to the ground. Furthermore it is assumed that after the rotation speed was obtained the angle of attack becomes the alpha of $C_{L_{max}}$ and remains constant. Additionally the runway is assumed to be horizontal and wind is neglected.

This results in a take-off distance of 129 m at sea level and 155 m at 1500 m altitude. So the take-off requirement is considered met up to an altitude of 1250 m as long as the propeller efficiency of 0.78 from Section 6.8 is met[19]. Here the climb propeller efficiency is used as the take-off propeller efficiency. With a propeller efficiency of 0.66 the sea level take-off distance will still be 150 m.

Another issue with the take-off distance is the method of thrust calculation. Simonini claims that the Victor 1 Super can produce a static thrust of at least 130 kg[20]. This is 1275 N and is 15% below the estimated static thrust level of 1502 N indicating that the thrust could be overestimated. If it is overestimated, then this will be caused by either Equation (6.5) overestimating the thrust, or the propeller efficiency being overestimated. The thrust equations do use a actuator disk method, which ignores the effects of the air being accelerated unevenly and the generation of vortices. Using the propeller efficiency of 0.8, if the thrust equation over estimates the thrust by 12% then the take-off distance becomes 150 m for sea level and 180 m for at 1500 m altitude. If it is 15% overestimated, then the take-off distance is 160 m at sea level and 188 m at altitude.

Both the thrust level and propeller efficiency should be validated using real life testing at different speeds to determine what the thrust and propeller efficiency are in reality. Furthermore take-off tests should be conducted to validate if the take-off requirement is met, however for now it is considered verified.

[17] URL `http://www.rotaxservice.com/rotax_engines/rotax_582UL.htm` [Cited on 16/06/2016]

[18] See Footnote 17

[19] Powerfin have been contacted about the expected propeller efficiency, however, as they are a small company with a production of 20 units per week, they do not know this information.

[20] URL `http://www.flyproducts.it/manuali/manualieng/VICTOR1ENG.pdf` [Cited on 14/06/2016]

Landing performance

Similar to the take-off requirement the landing requirement of 150 m will be achieved in the programme as it is a requirement in the power loading versus wing loading diagrams. The landing requirement was not one of the critical cases, however was based on the Coyote aircraft. The Coyote has a taildragger set up, while the Wings for Aid UAV has a nose wheel. Furthermore there will not be any brakes on the nose wheel to cut costs, which will increase the landing distance. Therefore, again, a simulation is created to determine if the landing requirement is achieved.

First the maximum descent slope is determined while the aircraft does not accelerate. This is to minimize the horizontal distance covered when descending from the screen height of 15 m. And additional 0.6 m was added to the screen height to account for a 0.3 m uncertainty in the vertical direction. Using a three point landing and neglecting the flare, the braking distance can be found in Figure 6.12 for different values of the friction coefficient of the braking tires. Additionally the runway is assumed to be horizontal, the wind is neglected and a rolling friction coefficient for the non-braking wheel of 0.05 is assumed. Additionally it is assumed that two packages have been dropped, which will affect the operation as an emergency drop zone will be required near the take-off area to drop packages if the UAV is required to land shortly after take-off.

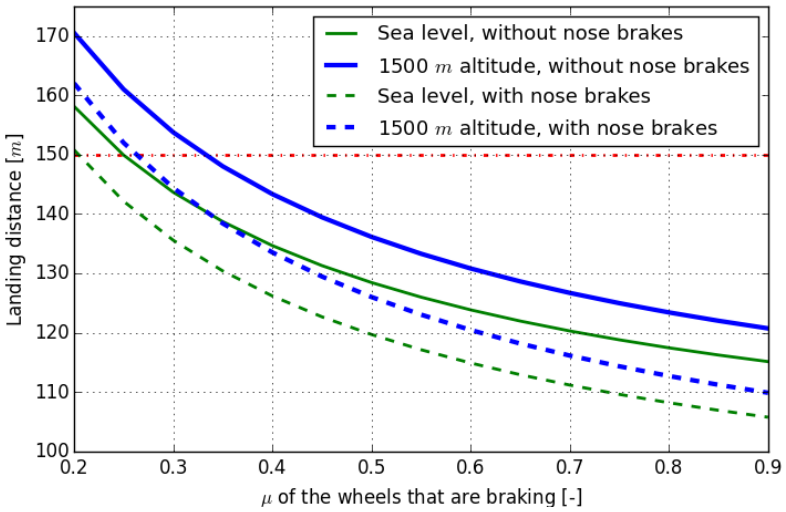

Figure 6.12: Landing performance for different maximum ground friction coefficients.

On a dry tarmac runway the maximum μ is between 0.7 and 0.8 and on a wet runway it varies roughly linearly between 0.4 at 100 km/h and 0.7 a 10 km/h [19, p. 317]. This means that the current UAV, without a nose gear brake, can land within 150 m on dry and wet tarmac. On a wet, grassy field the friction coefficient can be as low as 0.2 [20]. This makes it impossible to meet the landing distance requirement in a conventional manner. However if a bulldozer is used to clear the grass, then μ will increase to 0.35 for a gravel and dirt road or even 0.65 for loose moist dirt in which the tires can sink 5 cm [20]. Using the μ of 0.35 for the gravel road the landing distance becomes very tight on a 150 m field, however is still below 150 m, therefore the braking distance requirement is considered met. A nose brake will cost €190 extra and is not needed to meet the landing distance requirement, however could still be considered in the future for redundancy in the braking system.

Chapter 7

Stability and control

Keeping the UAV stable and being able to roll, pitch and yaw the UAV in a controlled manner is of great importance for safe flight. For the determination of the stability first of all the location of the center of gravity needs to be known. This location is calculated in Section 7.1. After this, control surfaces needed to control the UAV are sized in Section 7.2. Then, to analyze the stability and the behaviour of the UAV to control inputs, the stability and control derivatives of the UAV are calculated and implemented in a simulation, see Sections 7.3 to 7.9.

7.1 Center of gravity range

One important aspect for the stability and control of the UAV is the location of the center of gravity during all flight phases. The center of gravity is determined for different UAV configurations, for example for the UAV at OEW, or with three payload packages left. The center of gravity range is important since it gives limiting locations when sizing control surfaces, for example during take-off a more forward position of the center of gravity requires larger elevators.

The center of gravity locations are determined by using the full CATIA model of the UAV. The locations were first determined for OEW, OEW plus fuel, OEW plus payload and MTOW. After this, the best dropping procedure which results in the smallest range of center of gravity locations is determined. For this dropping procedure it can be noticed that the best solution would be to alternatively drop from the front and back, but the range of center of gravity locations then still depends on if the most forward or most aft package is dropped first. So the CATIA model is used to determine the center of gravity locations for both drop procedures. If the first package is indicated by 1 and the last package by 5, CATIA is used to simulate the dropping procedure of dropping package 1, then 5, then 2, then 4 and finally 3 and calculates the location of center of gravity at each configuration, both with fuel included and excluded. The CATIA model is then used to simulate the dropping procedure of package 5 first, then 1, then 4, then 2 and again finally 3 and also determines the center of gravity locations, again with fuel included and excluded. By looking at the results from both procedures the best dropping procedure is determined based on the smallest range of the location of the center of gravity.

The result of this simulation is that the front package should be dropped first. The range for the location of the center of gravity, including also center of gravity locations for OEW, OEW plus fuel, OEW plus payload and MTOW, is then [1.46, 1.53]. This range is given in meters and measured from the front of the fuselage. The range of the location of the center of gravity given in percentages of the MAC of the wing is [47.4, 53.1].

7.2 Control forces and control surface sizing

To control the UAV during all stages of the mission, control surfaces are required. These control surfaces include elevators, a rudder, ailerons and flaps and are sized in this section. This sizing is based on either Roskam [17][18], Raymer [6] or on "Aircraft Design: A Systems Engineering Approach" by M.H. Sadraey [21] and takes into account the most critical cases for the control surface. For some of the calculations values taken from figures are needed. Since designing the control surfaces is also an iterative process, these figures have been interpolated in Python.

Ailerons

To be able to roll the UAV in a controlled manner ailerons are used. The sizing is done based on the most critical case of CS-VLA specifications for rate of roll (CS-VLA 157) [12]. For the UAV the most critical case is during the approach at the specified airport altitude of 1,500 meters, where the specifications require the UAV to be able to roll from a steady 30° banked turn through an angle of 60°, so as to reverse the direction of the turn within four seconds from initiation of roll, with flaps extended, the landing gear extended, engine operating at idle power and engine operating at the power for level flight and trimmed at $1.3 \cdot V_{stall}$.

To determine the size of the aileron a time simulation has been made in Python. The simulation is based on Newton's second law for rotational motion: the summation of all applied moments is equal to the time rate of change of angular momentum (Equation (7.1)). The sum of the applied moments can be expressed in terms of the stability derivatives $C_{\ell_{\delta_a}}$ and C_{ℓ_p}, the aileron deflection and the actual roll rate, as can be seen in Equation (7.2). This sum of moments consists of the roll moment created by deflecting the ailerons and a counteracting moment induced by the roll damping.

$$\sum M_{cg} = I_{xx} \frac{\partial p}{\partial t} \tag{7.1}$$

$$\sum M_{cg} = C_{\ell_{\delta_a}} \cdot \frac{1}{2} \rho_{airport} \left(1.3 V_{stall}\right)^2 Sb \cdot \delta_a + C_{\ell_p} \cdot \frac{pb}{2 \cdot \left(1.3 V_{stall}\right)} \cdot \frac{1}{2} \rho_{airport} \left(1.3 V_{stall}\right)^2 Sb \tag{7.2}$$

The two stability derivatives are taken from DATCOM, a method for determining stability derivatives which will be explained in Section 7.3. This method takes into account the size of the ailerons. The inboard location of the aileron is taken at 2.3 m measured from the fuselage center-line (or 58% of semi-span) and an outboard aileron location of 3.56 m (or 90% of semi-span), with a chord ratio of 0.35. The outboard location is set at a maximum of 90% of the semi-span, since on the last 10% of the semi-span the control surfaces are not effective anymore due to wingtip vortices [6, p. 126]. These dimensions were determined in collaboration with the structures department and are the maximum size the ailerons can have.

With these dimensions the stability derivatives are determined using the DATCOM method. The rest of the input values for the simulation can be seen in Table 7.1.

Parameter	Value	Unit
$\rho_{airport}$	1.058	kg/m^3
V_{stall}	20.5	m/s
S	9.0	m^2
b	7.9	m
δ_a	-10	deg
C_{ℓ_p}	-0.432	-

Table 7.1: Input values for aileron calculations.

The results of the DATCOM method for the stability derivatives are a $C_{\ell_{\delta_a}}$ of -0.251 and a C_{ℓ_p} of -0.457. The result of the time simulation can be seen in Figure 7.1. As can be seen in this plot, the required roll angle of 30° is already reached before the maximum time of four seconds has passed, which means the UAV meets the CS-VLA requirement.

Flaps

Flaps are needed to provide extra lift during landing and take-off, of which take-off is the most critical case for the UAV since a larger ΔC_L is needed than for landing. This is the opposite of normal cases for airliners which is the result of the V_{stall} for which the UAV is designed. This V_{stall} is designed for safe gust loading and to reach this V_{stall} a smaller $C_{L_{max}}$ is needed than to reach the take-off requirement of 150 meters.

The ΔC_L required for the take-off requirement is 0.7. Of this 0.7 required ΔC_L 0.6 has to come from the flaps, the other 0.1 is achieved by deflecting the ailerons 10° downwards and use them as flaperons. With this aileron deflection of 10° and a required aileron deflection of 10° to easily meet the roll requirement there is still a 10° margin to the maximum deflection of 30°, as specified in Raymer [6, p. 420].

So the flaps are designed to give an increase in C_L of 0.6. The sizing for the flaps is based on a method described in Raymer [6, p. 490-493] (with this method also the ΔC_L which can be achieved by deflection of the ailerons was determined and found to be 0.1). This method determines the required $S_{flapped}/S_{ref}$ for a specified ΔC_L for plain flaps, which is also the type of flap the UAV will have since it is the simplest and cheapest design. The flapped area $(S_{flapped})_{flaps}$ is the area of the wing surface which is affected

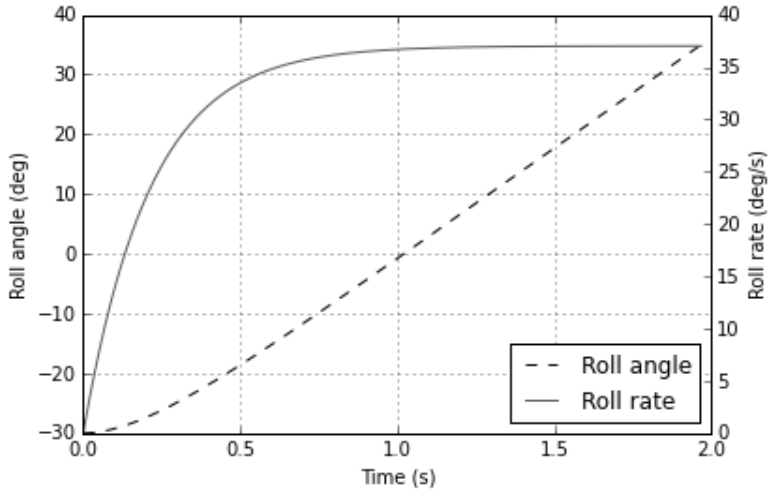

Figure 7.1: Roll angle and roll rate results.

by the flaps. Equations (7.3) to (7.5) show the formulas from Raymer which can be rewritten to express the required $(S_{flapped}/S_{ref})_{flaps}$ in required ΔC_L.

$$\Delta\alpha_{0L} = -\frac{\Delta C_L}{C_{L_\alpha}} \tag{7.3}$$

$$\Delta\alpha_{0L} = -\frac{1}{C_{L_\alpha}}\frac{\partial C_L}{\partial \delta_f}\delta_f \tag{7.4}$$

$$\frac{\partial C_L}{\partial \delta_f} = 0.9 K_f \left(\frac{\partial C_l}{\partial \delta_f}\right)_{airfoil} \left(\frac{S_{flapped}}{S_{ref}}\right)_{flaps} \cos\Lambda_{H.L.} \tag{7.5}$$

The rewritten equation can be seen in Equation (7.6).

$$\left(\frac{S_{flapped}}{S_{ref}}\right)_{flaps} = \frac{\Delta C_L}{0.9 K_f \left(\frac{\partial C_l}{\partial \delta_f}\right)_{airfoil} \cos\Lambda_{H.L.}\delta_f} \tag{7.6}$$

In this equation K_f and $\left(\frac{\partial C_l}{\partial \delta_f}\right)_{airfoil}$ are determined by interpolating figures from Raymer. To interpolate these figures, values for the ratio of flap chord and wing chord (c_f/c), flap deflection (δ_f) and thickness ratio (t/c) are needed.

The input values for both the figures from Raymer and Equation (7.6) can be seen in Table 7.2. The flap deflection and hinge line sweep should be inputted in radians, but are given in degrees for easier understanding.

Parameter	Value	Unit
c_f/c	0.3	-
δ_f	25	deg
t/c	0.125	-
$\Lambda_{H.L.}$	4.2	deg
ΔC_L	0.6	-

Table 7.2: Input values for Raymer figures and flap calculations.

With these inputs K_f is 0.662, $\left(\frac{\partial C_l}{\partial \delta_f}\right)_{airfoil}$ is 4.6 and the final output, $(S_{flapped}/S_{ref})_{flaps}$, is equal to 0.50. The span-wise position of the flaps has also been determined as a result of the required flapped area.

The inboard flap position is at 0.29 meters from the fuselage center-line, and the outboard position is at 1.96 meters. In percentages of the semi-span the locations are at 7.5% and 50% respectively.

Elevators

To control the pitch angle of the UAV during for example take-off and to trim the UAV during flight elevators are used. For the sizing of the elevators again the most critical case is defined, which is to rotate the UAV at MTOW and 80% of the rotation speed during take-off just before lift-off [6, p. 432][21, p. 673-674]. This has to be done at an angular acceleration of 10 deg/s^2 [17, p. 44]. After the sizing for this requirement is done, also the trim capability is checked by adding the elevators into the DATCOM analysis (Section 7.3).

To determine the lift force the elevator needs to generate during take-off rotation the forces and moments on the UAV during ground run need to be known. These forces and moments acting on the UAV can be seen in Figure 7.2. An expression of the moments around the main landing gear including these forces and moments can be seen in Equation (7.7). This equation can be rewritten to get an expression for the required lift force generated by the tail, see Equation (7.8). It is assumed that at the moment of initiation of the rotation the force on the nose wheel is zero, so P_{ng} is equal to zero.

It has to be mentioned that since the elevator is sized according to take-off rotation which takes place on the ground, the forces and moments acting on the UAV are affected by the ground-effect. The influences of this ground-effect on the forces and moments are determined according to Section 8.1.7 and Section 8.2.7 from Roskam [18].

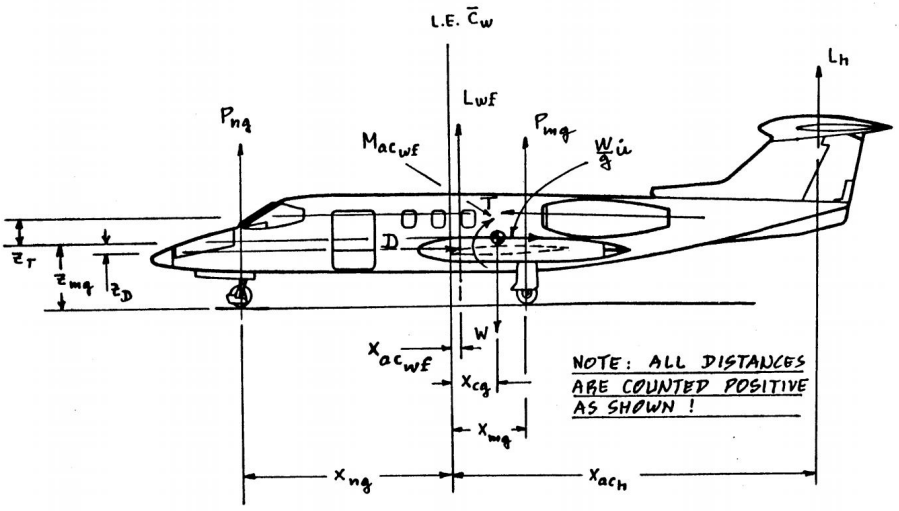

Figure 7.2: Longitudinal forces, moments and moment arms during the take-off ground run. [17]

$$M_{ac_{wf}} - T(z_{mg} + z_T) - W_{TO}(x_{mg} - x_{cg}) + P_{ng}(x_{ng} + x_{cg}) + L_{wf}(x_{mg} - x_{ac_{wf}}) + D(z_{mg} - z_D) + \\ + \frac{W_{TO}}{g}\dot{u}z_{mg} - L_h(x_{ac_h} - x_{mg}) = I_{yy_{mg}}\ddot{\theta} \quad (7.7)$$

$$L_h = \Big[M_{ac_{wf}} - T(z_{mg} + z_T) - W_{TO}(x_{mg} - x_{cg}) + P_{ng}(x_{ng} + x_{cg}) + L_{wf}(x_{mg} - x_{ac_{wf}}) + \\ + D(z_{mg} - z_D) + \frac{W_{TO}}{g}\dot{u}z_{mg} - I_{yy_{mg}}\ddot{\theta}\Big] / \left(x_{ac_h} - x_{mg}\right) \quad (7.8)$$

From this lift force a required tail lift coefficient can be determined by dividing by $\frac{1}{2}\rho V^2 S$, and since the lift coefficient for the horizontal tail without elevator deflection is known, also the required change in horizontal tail lift coefficient can be determined. This change in horizontal lift coefficient is induced by deflecting the elevators, which basically are again plain flaps. So with the known required $\Delta C_{L_{ht}}$, $(S_{flapped}/S_{ref})_{elevator}$ can be determined in the same manner as the $(S_{flapped}/S_{ref})_{flaps}$. The input values for the figures from Raymer for the elevator calculations can be seen in Table 7.3.

Parameter	Value	Unit
c_{elev}/c	0.25	-
δ_{elev}	20	deg
t/c	0.125	-
$\Lambda_{H.L.}$	8.6	deg

Table 7.3: Input values for Raymer figures and elevator calculations.

With these values for the input parameters K_f is 0.82, $\left(\frac{\partial C_l}{\partial \delta_f}\right)_{airfoil}$ is 4.2 and the final output, $(S_{flapped}/S_{ref})_{elevator}$, is equal to 0.71. Just as for the flaps, the span-wise location of the elevator has been determined. The inboard location is, measured from fuselage center-line, 0.12 m (or 11% of semi-span) and the outboard location is at 0.69 m (or 66% of the semi-span). After the implementation of these locations into DATCOM it was found that the UAV could not be trimmed to sufficient high angles of attack, so the elevator outboard location was extended to 90% of the span. The analysis was run again and showed that the trim for higher angles of attack was now also satisfied.

Rudder

Since it is decided that the horizontal and vertical tails will be the same because of easier and cheaper manufacturing the control surfaces on both tail surfaces will also be the same. This means that the sizing for the rudder was done concurrently with the sizing of the elevators. The sizing of the rudder is based on the requirement that it should be able to operate in the same conditions as a UH-1 helicopter. This requirement states that the UAV should be able to fly in crosswinds of 30 knots.

To design for this requirement, it is taken that the yawing moment created by deflecting the rudder should be able to counteract the yawing moment induced by a side-slip angle, as can be seen in Equation (7.9). The most limiting case with the largest side-slip angle and thus the largest yawing moment occurs when landing the UAV in a crosswind of 30 knots. The calculation for the side-slip angle can be seen in Equation (7.10).

$$C_{n_{\delta_R}} \cdot \delta_R = C_{n_\beta} \cdot \beta \qquad (7.9) \qquad \tan(\beta) = \frac{V_w}{V_{approach}} \qquad (7.10)$$

Where the approach speed is taken to be 1.3 times the stall speed, as specified in CS-VLA [12]. C_{n_β} is an output of the DATCOM analysis (discussed in Section 7.3) and $C_{n_{\delta_R}}$ can be determined from Equation (7.11) [18, p. 462]. $C_{y_{\delta_R}}$ from this equation can be determined with Equation (7.12) which is also from Roskam. In this equation several parameters are interpolated from figures from Roskam. These parameters can be seen in Table 7.4 next to the other inputs needed for the sizing of the rudder. For the value of $C_{l_\delta}/C_{l_{\delta_{theory}}}$ Figure 8.15 of Roskam is used. The input for this figure is the ratio of actual airfoil lift gradient over theoretical airfoil lift gradient, which was taken to be 1 since it is a symmetrical airfoil, which means that $C_{l_\delta}/C_{l_{\delta_{theory}}}$ is also 1.

$$C_{n_{\delta_R}} = -C_{y_{\delta_R}} * (l_v \cos\alpha + z_v \sin\alpha)/b \qquad (7.11) \qquad C_{y_{\delta_R}} = \frac{C_{L_{\alpha_v}}}{C_{l_{\alpha_v}}} K_f K_b \frac{(\alpha_\delta)_{C_L}}{(\alpha_\delta)_{C_l}} \frac{C_{l_\delta}}{C_{l_{\delta_{theory}}}} C_{l_{\delta_{theory}}} \frac{S_v}{S} \qquad (7.12)$$

With these input values $C_{y_{\delta_R}}$ is 0.117, $C_{n_{\delta_R}}$ is -0.050 and β is 30°, so the required rudder deflection is calculated to be 9.6°. This rudder deflection is smaller than the maximum deflection of 20° required for the elevator, which means the rudder is not limiting for the sizing of rudder/elevator. So the sizes for the rudder and elevator are the sizes stated in the elevator sizing section.

7.3 DATCOM

In order to further analyze the static and dynamic stability of the UAV it is required to calculate the stability derivatives of the concept. In order to do this the United States Air Force Stability and Control Digital DATCOM[1] was used. This programme requires an input file specifying the geometry of the concept and the specifications of the lifting surfaces of the UAV. While the DATCOM method is a

[1] URL `http://www.pdas.com/datcom.html` [Cited on 14/06/2016]

Parameter	Value	Unit	Parameter	Value	Unit
C_{n_β}	0.0158	-	$C_{l_{\alpha_v}}$	2π	1/rad
V_w	15.4	m/s	$\delta_{f_{max}}$	20	deg
$V_{approach}$	26.6	m/s	c_{rudder}/c	0.25	-
l_v	3.7	m	λ_v	0.45	-
z_v	1.2	m	η	0.58	-
α	3	deg	A_v	3.0	-
b	7.9	m	t/c	0.125	-
$C_{L_{\alpha_v}}$	2.03	1/rad	S_v	0.645	m^2

Table 7.4: Input values for Roskam figures and rudder calculations.

handy tool for the initial estimation of the dynamic and static stability derivatives there are some limitations. The body can only be modelled as a solid body without any inlets. In order to overcome this CFD or wind tunnel test should be done on the UAV to achieve more accurate results. It is also not possible to input a rudder to the programme. Therefore the stability derivatives for the rudder have been estimated using Sadraey [21] in Section 7.2. The input file used for this programme was rendered directly from the concept design tool output and made it possible to quickly analyze the stability of design iterations. The input file used for this programme can be seen in Appendix B. The input file can be explained as follows: the $FLTCON section specifies the flight conditions at which the UAV flies and at which angles of attack the concept should be tested for stability. Also, the Reynolds number at which the UAV flies is specified here. Next, the $SYNTHS specifies the locations of the different lifting surfaces of the UAV and the location of the center of gravity. The $OPTINS section defines the wing area, mean aerodynamic chord and the wing span. The $BODY section defines the geometry of the fuselage at different points. Also the nose length and tail section length are defined here. The $WGNPLNF, $HTPLNF and $VTPLNF specify the geometry of the wing, horizontal tail and vertical tail respectively. Also, the airfoil used for these planforms is specified in the line above each planform. For the wing the NACA-24012 was used to model the stability. Even though the UAV uses a custom airfoil this planform is used to model the stability. This airfoil was chosen because it has the same lift characteristics while having a higher drag coefficient. The $SYMFLP section defines the elevator surfaces which are located on the tail. The DELTA(1) parameter specifies the angles of attack at which the elevator is tested. The $PROPWR section defines the propeller power and geometry in order to take into account the propeller effect on the longitudinal stability derivatives. Lastly, in the $ASYFLP section the ailerons are specified. These are also tested at different angles of attack.

In order to get a better sense of the input specified in the input file the drawDATCOMaircraft[2] matlab script was used. A drawing of the input and the airfoils can be seen in Figure 7.3.

7.4 Longitudinal stability derivatives

In this section the longitudinal stability derivatives will be discussed. In the previous section the DATCOM input was discussed and in this section the output of the DATCOM method is analyzed.

Firstly, the longitudinal stability derivatives were determined for the Wings for Aid concept using the DATCOM output file. The C_{L_α} curve proved to be fairly inaccurate however in this output. This inaccuracy leads to inaccurate values of not only C_{Z_α} but also C_{X_α} and C_{M_α}. This can be explained due to the fact that DATCOM can not model the custom airfoil. Also, the position of the center of pressure and the position of the center of gravity have a major influence on these derivatives. Because the center of pressure can be more accurately determined with XFLR5, the result of this analysis was used as the center of pressure point. Also, the lift curve slopes for the wing and horizontal tail from XFLR5 were used instead of the one provided by the DATCOM output. The C_{X_α}, C_{Z_α} and C_{m_α} stability derivatives were therefore calculated according to the following equations respectively:

[2]URL `http://www.mathworks.com/matlabcentral/fileexchange/34035-drawdatcomaircraft` [Downloaded on 08/06/2016]

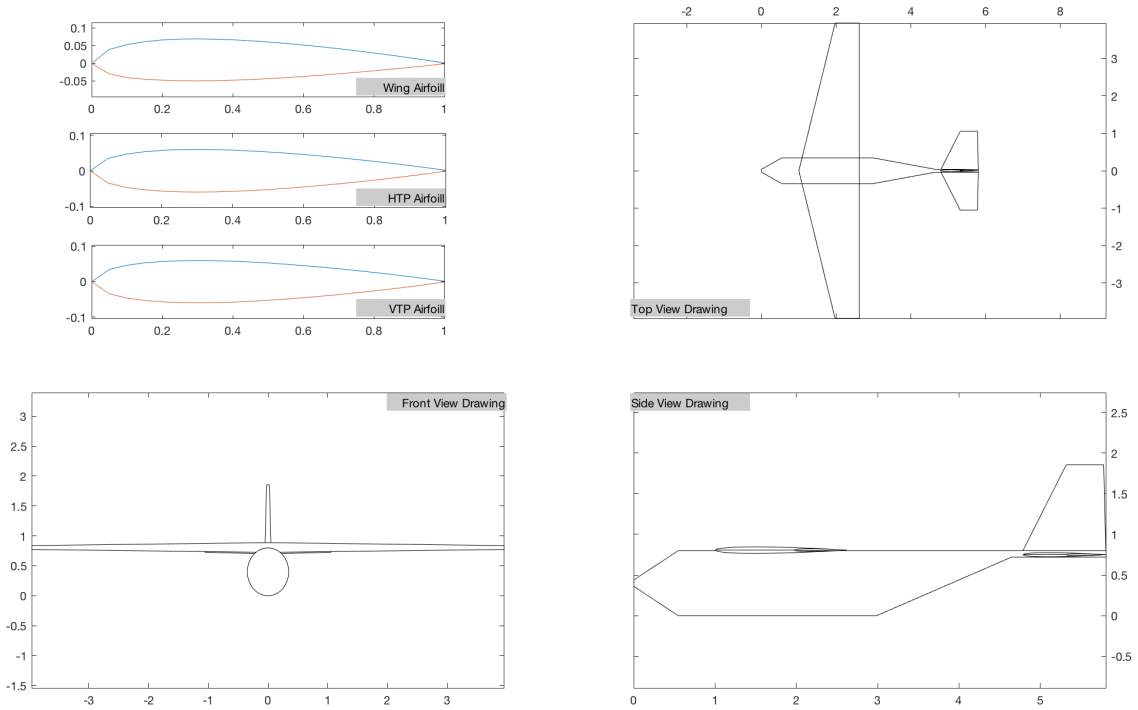

Figure 7.3: Input for the DATCOM programme.

$$C_{X_\alpha} = C_L \left(1 - \frac{2C_{L_\alpha}}{\pi A e}\right) \quad (7.13) \qquad C_{Z_\alpha} = C_L \sin\alpha - C_{L_\alpha} \cos\alpha - C_D \cos\alpha - C_{L_\alpha} \sin\alpha \quad (7.14)$$

$$C_{m_\alpha} = C_{N_{w\alpha}} \frac{x_{c.g.} - x_w}{\bar{c}} - C_{N_{h_\alpha}} \left(1 - \frac{d\epsilon}{d\alpha}\right) \left(\frac{V_h}{V}\right)^2 \frac{S_h l_h}{S\bar{c}} \quad (7.15)$$

These are the equations used in the lecture notes of the flight dynamics course AE3212-I [22]. These equations neglect the effect of the body and the landing gear on the stability derivatives. It is recommended that in the future a CFD analysis is run to study the influence of the landing gear and tires on the longitudinal stability derivatives. For the longitudinal stability derivatives with respect to acceleration also the equations given in the lecture notes [22] were used because the lift curve slope of the horizontal tail was also determined using XFLR5 and is more accurate than the lift curve slope DATCOM calculated. The equations used can be found in Equations (7.16) and (7.17).

$$C_{Z_{\dot{\alpha}}} = -C_{N_{h_\alpha}} \left(\frac{V_h}{V}\right)^2 \frac{d\epsilon}{d\alpha} \frac{S_h l_h}{S\bar{c}} \quad (7.16) \qquad C_{m_{\dot{\alpha}}} = -C_{N_{h_\alpha}} \left(\frac{V_h}{V}\right)^2 \frac{d\epsilon}{d\alpha} \frac{S_h l_h^2}{S\bar{c}^2} \quad (7.17)$$

Because the C_{X_α}, C_{Z_α} and C_{m_α} derivatives calculated by DATCOM were not accurate and proved to be too high the derivatives with respect to pitching velocity C_{X_q} and C_{m_q} were also not accurate. For these stability derivatives the equations from the lecture notes [22] were also used. The equations are as in Equations (7.18) and (7.19).

$$C_{Z_q} = -2C_{N_{h_\alpha}} \left(\frac{V_h}{V}\right)^2 \frac{S_h l_h}{S\bar{c}} \quad (7.18) \qquad C_{m_q} = -(1.1)C_{N_{h_\alpha}} \left(\frac{V_h}{V}\right)^2 \frac{S_h l_h^2}{S\bar{c}^2} \quad (7.19)$$

For the C_{Z_q} equation a factor 2 is applied because it is a rough estimate for the complete aircraft. For C_{m_q} the factor 1.1 is applied to account for the influence of the wing. Lastly, the C_{Z_u} and C_{X_u} stability derivatives were calculated by hand. The equations for these longitudinal stability derivatives are as follows in Equations (7.20) and (7.21) [22].

$$C_{X_u} = 2C_{X_0} + \frac{\partial C_X}{\partial V} V \quad (7.20) \qquad C_{Z_u} = 2C_{Z_0} + \frac{\partial C_Z}{\partial V} V \quad (7.21)$$

Where the derivative of the dimensionless force in x-direction with respect to airspeed are as in Equation (7.22).

$$\frac{\partial C_X}{\partial V} = \frac{\partial T_c'}{\partial V} - \frac{\partial C_D}{\partial V} \tag{7.22}$$

The dimensionless thrust coefficient variation with respect to airspeed was calculated using the engine data for the Victor 1 Plus engine supplied by the manufacturer.

The stability derivatives for the elevator were calculated using DATCOM. The stability derivatives were calculated for the cruise condition at an angle of attack of 2° with the most forward C.G. position. An overview of the longitudinal stability derivatives for the Wings for Aid concept can be found in Table 7.5. This can be compared to the stability derivatives of the Cessna 172 to get an initial estimation of the magnitude of the parameters. The longitudinal stability derivatives for the Cessna 172 can be seen in Table 7.6. As can be seen by comparison from the table the order of magnitude is fairly similar for both aircraft.

V	=	43.00 m/sec	m	=	350.40 kg	$\bar{c}$	=	1.20
S	=	9.00 m^2				μ_c	=	29.11
K_Y^2	=	1.049						
C_{X_0}	=	0	C_{Z_0}	=	-0.248			
C_{X_u}	=	-0.153	C_{Z_u}	=	-0.681	C_{m_u}	=	0
C_{X_α}	=	0.107	C_{Z_α}	=	-4.656	C_{m_α}	=	-0.949
$C_{X_{\dot{\alpha}}}$	=	0	$C_{Z_{\dot{\alpha}}}$	=	-1.016	$C_{m_{\dot{\alpha}}}$	=	-2.681
C_{X_q}	=	0	C_{Z_q}	=	-3.297	C_{m_q}	=	-5.617
$C_{X_{\delta_e}}$	=	0	$C_{Z_{\delta_e}}$	=	-0.229	$C_{m_{\delta_e}}$	=	-0.625

Table 7.5: Symmetric stability and control derivatives for the Wings for Aid UAV, Cruise

V	=	66.75 m/sec	m	=	1199.80 kg	$\bar{c}$	=	1.49
S	=	16.17 m^2				μ_c	=	44.70 m
K_Y^2	=	0.681						
C_{X_0}	=	0	C_{Z_0}	=	-0.310			
C_{X_u}	=	-0.093	C_{Z_u}	=	-0.620	C_{m_u}	=	0
C_{X_α}	=	0.180	C_{Z_α}	=	-4.631	C_{m_α}	=	-0.890
$C_{X_{\dot{\alpha}}}$	=	0	$C_{Z_{\dot{\alpha}}}$	=	-0.850	$C_{m_{\dot{\alpha}}}$	=	-2.600
C_{X_q}	=	0	C_{Z_q}	=	-1.950	C_{m_q}	=	-6.200
$C_{X_{\delta_e}}$	=	0	$C_{Z_{\delta_e}}$	=	-0.430	$C_{m_{\delta_e}}$	=	-1.280

Table 7.6: Symmetric stability and control derivatives for the Cessna 172, Cruise

7.5 Symmetric state space system

Now that the stability derivatives have been determined they can be used to create a state-space system from which eigenvalues can be calculated and the eigenmodes can be studied. In order to make this state-space system the linearized 'deviation equations' for the symmetric motions where $C_{X_q} = 0$ are used as a starting point[22], as seen in Equation (7.23).

$$\begin{bmatrix} C_{X_u} - 2\mu_c D_c & C_{X_\alpha} & C_{Z_0} & C_{X_q} \\ C_{Z_u} & C_{Z_\alpha} + (C_{Z_{\dot{\alpha}}} - 2\mu_C) D_c & -C_{X_0} & C_{Z_q} + 2\mu_c \\ 0 & 0 & -D_c & 1 \\ C_{m_u} & C_{m_\alpha} + C_{m_{\dot{\alpha}}} D_c & 0 & C_{m_q} - 2\mu_c K_Y^2 D_c \end{bmatrix} \cdot \begin{bmatrix} \hat{u} \\ \alpha \\ \theta \\ \frac{q\bar{c}}{V} \end{bmatrix} = \begin{bmatrix} -C_{X_{\delta_e}} \\ -C_{Z_{\delta_e}} \\ 0 \\ -C_{m_{\delta_e}} \end{bmatrix} \cdot \delta_e \tag{7.23}$$

This system is rewritten in the following form in order to obtain a linear differential equation (Equation (7.24)) which we can use to make a state system.

$$C_1\dot{\bar{x}} + C_2\bar{x} + C_3\bar{u} = \bar{0} \tag{7.24}$$

Where the symmetric state vector is dimensionalised and is as follows: $\bar{x} = [u, \alpha, \theta, q]^T$. Where u is the absolute dimensionalised deviation from the airspeed at which the system is linearized. The input vector is represented as $\bar{u} = [\delta_e]$. Rewriting the Equation (7.23) into Equation (7.24) gives the following matrices.

$$C_1 = \begin{bmatrix} -2\mu_c \frac{\bar{c}}{V^2} & 0 & 0 & 0 \\ 0 & \left(C_{Z_{\dot{\alpha}}} - 2\mu_c\right)\frac{\bar{c}}{V} & 0 & 0 \\ 0 & 0 & -\frac{\bar{c}}{V} & 0 \\ 0 & C_{m_{\dot{\alpha}}}\frac{\bar{c}}{V} & 0 & -2\mu_c K_Y^2 \frac{\bar{c}^2}{V^2} \end{bmatrix} \quad C_2 = \begin{bmatrix} \frac{C_{X_u}}{V} & C_{X_\alpha} & C_{Z_0} & C_{X_q}\frac{\bar{c}}{V} \\ \frac{C_{Z_u}}{V} & C_{Z_\alpha} & -C_{X_0} & \frac{\bar{c}}{V}\left(C_{Z_q} + 2\mu_c\right) \\ 0 & 0 & 0 & \frac{\bar{c}}{V} \\ \frac{C_{m_u}}{V} & C_{m_\alpha} & 0 & \frac{C_{m_q}\bar{c}}{V} \end{bmatrix}$$

$$C_3 = \begin{bmatrix} C_{X_{\delta_e}} \\ C_{Z_{\delta_e}} \\ 0 \\ C_{m_{\delta_e}} \end{bmatrix}$$

Rewriting the linearized symmetric equations of motions into this form allows us to make a state-space representation of the system of the following form in Equation (7.25).

$$\dot{\bar{x}} = A\bar{x} + B\bar{u} \qquad \bar{y} = C\bar{x} + D\bar{u} \tag{7.25}$$

Where $\bar{u}$ is the input vector and $\bar{x}$ represent the state vector. Also, the A and B matrices are defined as in Equation (7.26).

$$A = -C_1^{-1}C_2 \qquad B = -C_1^{-1}C_3 \tag{7.26}$$

7.6 Symmetric eigenmodes

Now that the state space matrices have been determined the MATLAB environment is used to create a state-space system. Using this state space system the eigenvalues can be calculated and input responses can be simulated. Firstly, the short period eigenmode will be discussed and secondly the phugoid eigenmode will be examined.

Using the MATLAB symmetric state space system the eigenvalues can be calculated with a simple MATLAB command. For the wings for Aid UAV the short period and phugoid eigenvalues can be found in Tables 7.7 and 7.8 respectively. Looking at these tables combined with Figure 7.4 it can be seen that for the symmetric non-dimensionalised eigenvalues the real part of the eigenvalues is more negative. Which means the symmetric eigenmodes of the Wings for Aid concept are relatively damped higher than the Cessna 172. Also, the damping ratio of both the phugoid and the short period is higher. This means for the symmetric eigenmodes the Wings for Aid concept is more stable than the Cessna 172. However, the time to damp half the amplitude for the short period is higher for the Cessna.

	WFA concept	Cessna 172
Eigenvalues	-0.106 ±0.102j	-0.097 ±0.100j
Dimensionalised eigenvalues	-3.777 ±3.657j	-4.345 ±4.452j
Time to half amplitude [s]	0.183	0.160
Period [s]	1.718	1.411
Damping ratio [-]	0.718	0.69
Undamped natural frequency [rad/sec]	5.257	6.221

Table 7.7: Characteristics of the short period eigenmode.

Using the symmetric state space system a step input for 1 second was used as input. The step input used was a deflection of the elevator of -0.01 radians. The time response of the Cessna 172 and Wings for Aid UAV to that step input of -0.01 radians elevator deflection can be seen in Figure 7.5 and Figure 7.6 for the short period and phugoid time response respectively. In these figures the pitch rate response

	WFA concept	Cessna 172
Eigenvalues	-0.001 ±0.006j	-0.0005 ±0.004j
Dimensionalised eigenvalues	-0.044 ±0.207j	-0.022 ±0.188j
Time to half amplitude [s]	15.679	31.501
Period [s]	30.374	33.419
Damping ratio [-]	0.209	0.116
Undamped natural frequency [rad/sec]	0.212	0.189

Table 7.8: Characteristics of the phugoid eigenmode.

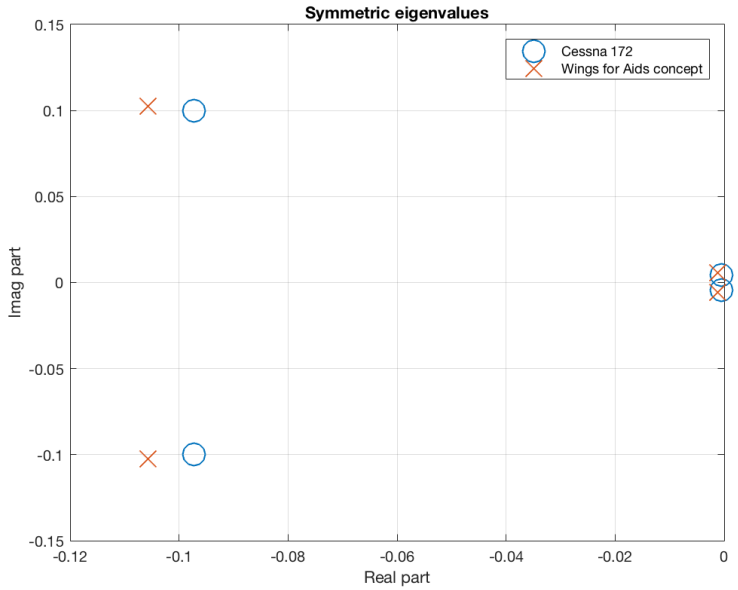

Figure 7.4: Symmetric eigenvalues of the Wings for Aid concept and the Cessna 172.

versus time is shown. As discussed before, the time to damp half the amplitude for the short period of the Cessna 172 is better while the phugoid is better damped for the Wings for Aid UAV.
The stability derivatives and eigenvalues computed here were calculated using the most forward C.G. position. The analysis was also run with the most aft possible C.G. position. The effect of this is that the poles of the short period eigenvalues move closer to the real axis and therefore the natural frequency decreased and the damping ratio increases. This is illustrated in Figure 7.7.

7.7 Lateral stability derivatives

In order to determine the lateral stability derivatives the DATCOM programme was used (again). With the option 'DAMP' the dynamic lateral stability derivatives of the input can be calculated. This output provided fairly realistic lateral stability derivatives except for some of the stability derivatives where the dominant contribution comes from the vertical stabilizer the results did not seem to be realistic (C_{Y_r}, C_{n_r} and C_{n_β}). Therefore Equations (7.27) and (7.28) have been used to approximate these stability derivatives[22].

$$(C_{Y_r})_v = 2C_{Y_{\beta_\alpha}} \left(\frac{V_v}{V}\right)^2 n \frac{S_v l_v}{Sb} \qquad (C_{n_r})v = -(C_{Y_r})_v \frac{l_v}{b} \tag{7.27}$$

$$(C_{n_\beta})_v = C_{Y_{\beta_\alpha}} \left(1 - \frac{d\sigma}{d\beta}\right) \left(\frac{V_v}{V}\right)^2 \frac{S_v l_v}{Sb} \tag{7.28}$$

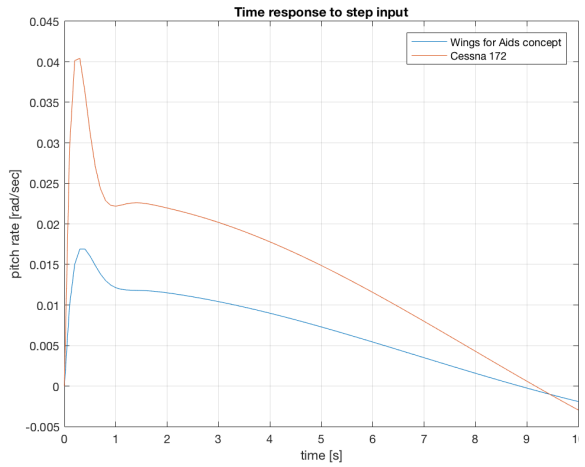

Figure 7.5: The short period time response.

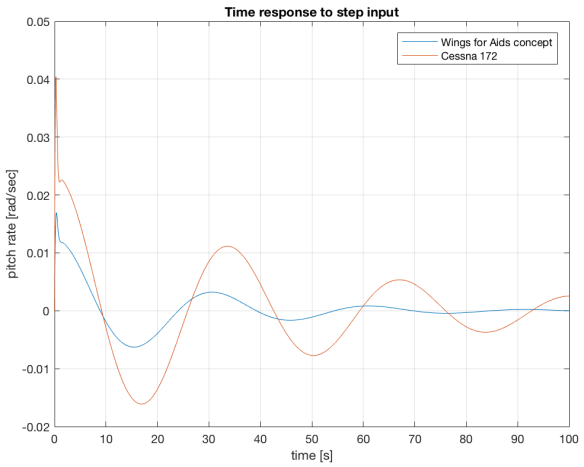

Figure 7.6: The phugoid time response.

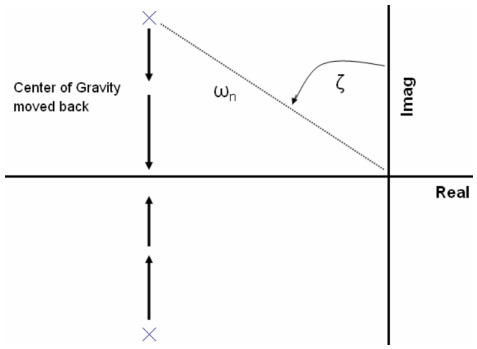

Figure 7.7: Effect of moving the center of gravity backward on the short period eigenvalues.[23, p. 84, Figure 6.1]

It is assumed that this calculation of these stability derivatives is off in the DATCOM method due to the incorrect approximation of the lift curve slope as mentioned before. Therefore the lift curve slope for the vertical tail calculated by XFLR5 will be used. It has been assumed for these stability derivatives that the dominant and only contribution is the vertical tail. For a first approximation this is valid but in order to get better results a CFD analysis is recommended. Also, the sidewash term ($\frac{d\sigma}{d\beta}$) has been calculated using Figure 8-22 from the lecture notes[22][p. 214]. The result of the calculations of the lateral stability derivatives can be seen in Table 7.9 and for the Cessna 172 in Table 7.10. For the Cessna 172 no stability derivatives for the rudder and ailerons could be obtained.

V	43.00 m/sec	m	350.40 kg	K_Z^2	0.038
S	9.00 m^2	μ_b	4.436	K_{XZ}	0
b	7.90 m	K_X^2	0.018		
C_{Y_β}	-0.341	C_{ℓ_β}	-0.067	C_{n_β}	0.067
C_{Y_p}	0.000	C_{ℓ_p}	-0.450	C_{n_p}	-0.018
C_{Y_r}	0.198	C_{ℓ_r}	0.060	C_{n_r}	-0.094
$C_{Y_{\delta a}}$	0	$C_{\ell_{\delta a}}$	-0.247	$C_{n_{\delta a}}$	-0.042
$C_{Y_{\delta r}}$	0.117	$C_{\ell_{\delta r}}$	0.007	$C_{n_{\delta r}}$	-0.050

Table 7.9: Asymmetric stability and control derivatives for the Wings for Aid UAV, Cruise.

V	66.75 m/sec	m	1199.80 kg	K_Z^2	0.018
S	16.17 m^2	μ_b	6.071	K_{XZ}	0
b	11.00 m	K_X^2	0.009		
C_{Y_β}	-0.310	C_{ℓ_β}	-0.089	C_{n_β}	0.065
C_{Y_p}	-0.037	C_{ℓ_p}	-0.470	C_{n_p}	-0.030
C_{Y_r}	0.210	C_{ℓ_r}	0.096	C_{n_r}	-0.099
$C_{Y_{\delta_a}}$	0	$C_{\ell_{\delta_a}}$	-0.178	$C_{n_{\delta_a}}$	-0.053
$C_{Y_{\delta_r}}$	0.187	$C_{\ell_{\delta_r}}$	0.015	$C_{n_{\delta_r}}$	-0.066

Table 7.10: Asymmetric stability and control derivatives for the Cessna 172, Cruise[3].

7.8 Asymmetric state space system

Now that the lateral stability derivatives have been determined they can again be used to create a state-space system from which eigenvalues can be calculated and the eigenmodes can be studied. This time the asymmetric equations of motions (7.29) are used as a starting point[22].

$$\begin{bmatrix} C_{Y_\beta} + (C_{Y_{\dot\beta}} - 2\mu_b)D_b & C_L & C_{Y_p} & C_{Y_r} - 4\mu_b \\ 0 & -\frac{1}{2}D_b & 1 & 0 \\ C_{\ell_\beta} & 0 & C_{\ell_p} - 4\mu_b K_X^2 D_b & C_{\ell_r} + 4\mu_b K_{XZ} D_b \\ C_{n_\beta} + C_{n_{\dot\beta}} D_b & 0 & C_{n_p} + 4\mu_b K_{XZ} D_b & C_{n_r} - 4\mu_b K_Z^2 D_b \end{bmatrix} \cdot \begin{bmatrix} \beta \\ \varphi \\ \frac{pb}{2V} \\ \frac{rb}{2V} \end{bmatrix} = \begin{bmatrix} -C_{Y_{\delta_a}} \\ 0 \\ -C_{\ell_{\delta_a}} \\ -C_{n_{\delta_a}} \end{bmatrix} \cdot \delta_a + \begin{bmatrix} -C_{Y_{\delta_r}} \\ 0 \\ -C_{\ell_{\delta_r}} \\ -C_{n_{\delta_r}} \end{bmatrix} \cdot \delta_r \quad (7.29)$$

Using this starting point the system has to be rewritten again as a linear differential equation as in Equation (7.24). After this it can be rewritten as the same state space system as found in Equation (7.25) only with a different state and output vector. The C1,C2 and C3 matrices for the asymmetric state space system can be found below.

$$C_1 = \begin{bmatrix} (C_{Y_{\dot\beta}} - 2\mu_b)\frac{b}{V} & 0 & 0 & 0 \\ 0 & -\frac{b}{2V} & 0 & 0 \\ 0 & 0 & -2\mu_b K_X^2 \frac{b^2}{V^2} & 2\mu_b K_{XZ} \frac{b^2}{V^2} \\ C_{n_{\dot\beta}} \frac{b}{V} & 0 & 2\mu_b K_{XZ} \frac{b^2}{V^2} & -2\mu_b K_Z^2 \frac{b^2}{V^2} \end{bmatrix} \quad C_2 = \begin{bmatrix} C_{Y_\beta} & C_l & C_{Y_p}\frac{b}{2V} & (C_{Y_r} - 4\mu_b)\frac{b}{2V} \\ 0 & 0 & \frac{b}{2V} & 0 \\ C_{\ell_\beta} & 0 & C_{\ell_p}\frac{b}{2V} & C_{\ell_r}\frac{b}{2V} \\ C_{n_\beta} & 0 & C_{n_p}\frac{b}{2V} & C_{n_r}\frac{b}{2V} \end{bmatrix}$$

$$C_3 = \begin{bmatrix} C_{Y_{\delta_a}} & C_{Y_{\delta_r}} \\ 0 & 0 \\ C_{\ell_{\delta_a}} & C_{\ell_{\delta_r}} \\ C_{n_{\delta_a}} & C_{n_{\delta_r}} \end{bmatrix}$$

The relation between A and B and the C1,C2 and C3 matrices is again given by Equation (7.26).

7.9 Asymmetric eigenmodes

Now that the asymmetric state space system has been made the asymmetric eigenmodes can be studied. The state-space system is again constructed with a simple command inside the MATLAB environment. In Table 7.11 the characteristics of the dutch roll, spiral and aperiodic roll moment can be found. In Figure 7.8 the eigenvalues of the Cessna 172 and the Wings for Aid concept can be found.

From this it can be concluded that the asymmetric eigenmodes are less stable for the Wings for Aid concept than the Cessna 172. For the dutch roll eigenmode the damping and eigenvalues are relatively close. In order to make the dutch roll even more stable the effective dihedral must either be increased or the vertical tail plane area S_v or vertical tailplane arm l_v should be increased. Increasing the tailplane arm is not an option because the requirements stipulate that the UAV should fit in a container. Increasing the vertical tailplane area would also lead to higher mass which will have a negative snowball effect on the airplane. Lastly, adding dihedral to the wing would greatly increase the complexity of the wing

	WFA concept	Cessna 172
Dutch roll eigenmode		
Eigenvalues	-0.044 $\pm$0.207j	-0.022 $\pm$0.188j
Time to half amplitude [s]	1.509	0.942
Period [s]	-2.505	-1.848
Damping ratio [-]	0.180	0.212
Undamped natural frequency [rad/sec]	2.550	3.478
Spiral eigenmode		
Eigenvalues	-0.0019	-0.0019
Dimensionalised eigenvalues	-0.0103	-0.0115
Time to half amplitude [s]	67.5874	60.019
Heavily damped aperiodic roll eigenmode		
Eigenvalues	-1.4474	-2.189
Dimensionalised eigenvalues	-7.8783	-13.282
Time to half amplitude [s]	0.088	0.052

Table 7.11: Characteristics of the dutch roll eigenmode.

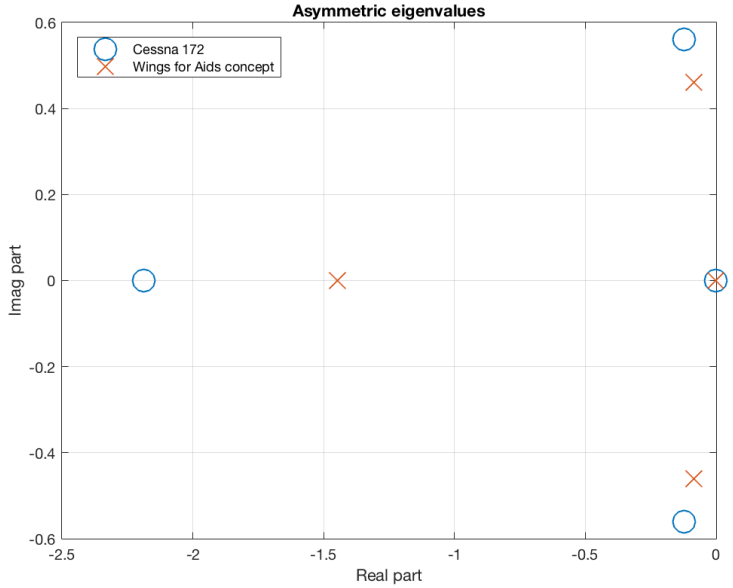

Figure 7.8: Asymmetric eigenvalues of the Wings for Aid concept and the Cessna 172.

structure and also the mass. Therefore, because the airplane is already sufficiently stable (the damping ratio is fairly close to that of the Cessna 172) the choice is made to not further alter the configuration to make the UAV unnecessarily heavy. Also, the spiral eigenvalue is negative this means the spiral mode is also damped and the UAV is also spirally stable. Lastly, the aperiodic rolling moment is also lower than the Cessna 172. This can be verified using Figure 8-30 from the Flight dynamics lecture notes [22][p. 220]. The formula for the heavily damped aperiodic rolling eigenvalue is as follows [22][p.158].

$$\lambda_{b_1} = \frac{C_{\ell_p}}{4\mu_b K_X^2} \tag{7.30}$$

This figure estimates that for a wing with similar characteristics as to the Wings for Aid UAV the value

of C_{ℓ_p} will be about -0.4 . Looking at Table 7.9 it can be seen that this estimate is quite close to the calculated value of -0.47 . As can be calculated from Table 7.9 and Table 7.10 the term $\mu_b \cdot K_X^2$ is larger for the Wings for Aid UAV and thus the eigenvalue of the Cessna 172 is more negative. Increasing this stability derivative for the Wings for Aid concept would mean either choosing a lower taper ratio or choosing a higher aspect ratio for the wing. Choosing a lower taper ratio would lead to a decrease in aerodynamic efficiency and choosing a higher aspect ratio for the wing would increase the total structural weight of the wing. Therefore also for this eigenmode the choice is made to not perform any modifications on the UAV to meet the Cessna 172 stability requirement.

Another explanation for the difference in eigenmode behaviour comparing the larger Cessna 172 to the smaller Wings for Aid UAV is the fact that smaller airplanes tend to have lower inertias. The result of this is that smaller airplanes tend have higher natural frequency for their eigemodes than large airplanes [23][p. 67] except for the dutch roll eigenmode. This also holds when comparing the dutch roll and phugoid eigenmode of the Wings for Aid UAV to the Cessna 172.

Lastly, the lateral stability derivatives shown here were also computed using the most forward possible center of gravity. An analysis for the most aft center of gravity was also run. This made the dutch roll less stable because the damping ratio decreased to a value of 0.1665 . This can be explained due to the shorter arm of the center of gravity to both the horizontal and vertical tail. This means the complete tail is less effective in the damping of the rolling and the yawing of the aircraft. The more aft center of gravity also causes the half-time amplitude of the spiral eigenmode to increase to 219.47 seconds. The change in the center of gravity did not have any (noteworthy) influence on the aperiodic roll eigenmode.

7.10 Propeller effects

The propeller of the UAV has an influence on various aspects of the airplane dynamics. Firstly, the spiraling slipstream of the propeller causes a rotational motion of the slipstream behind the propeller. For the tail this means the total resultant flow at the tailplane will be affected in such a way that the vertical tailplane produces more lift and thus the propeller slipstream causes a yawing moment. The magnitude of this moment varies with propeller thrust, engine setting etcetera. Therefore this effect should be studied more thoroughly using CFD, wind tunnel test and/or flight testing. Secondly, if the airflow is not perpendicular to the propeller then the propeller will produce asymmetrical thrust and thus will also cause a yawing moment. This is called the P-factor [4]. This effect should also be studied in more detail later. Because this effect is also dependent on numerous factors. The result of the propeller effect is that the rudder needs to constantly produce a side force in order to counteract the yawing moment created due to the two propeller effect. If the rudder is counteracting this sufficiently to keep the plane straight the net result will be that the aircraft is constantly translating to the left.This can be seen on the left side in Figure 7.9. In order to make sure the aircraft does not translate the plane must fly at a slight sideslip angle so the body also produces a small force in the opposite direction. This can be seen on the right side in Figure 7.9 and this way the aircraft does not translate. Lastly, the torque produced by the propeller also contributes to the aircraft dynamics. This is because the torque created by the propeller needs to be counteracted by the ailerons and the ailerons themselves. This adds more drag and also the ailerons themselves produce a yawing moment.

In conclusion, the propeller effects should be studied further using CFD, wind tunnel test and/or flight testing. The propeller effect will most likely need to be countered by placing the control devicess on a certain neutral point in order to cope with the effects of the propeller.

7.11 Verification and validation

The methods used for determining the center of gravity range and the sizing of the control surfaces also had to be verified and validated. The verification of the methods consisted of both code verification and calculation verification. The code verification was done in the same manner for all programmes. After a programme was written, it was compiled. If the programme contained syntax errors, the compiler would give error messages indicating the error so it could be fixed. After this was done and the code compiled correctly, the code was checked for for example incorrectly used for-loops or divisions by zero or infinity by printing intermediate values. Any interpolated figures were also checked by printing the value determined by the programme and then looking up the value from the actual used reference to see if the interpolation was done correctly.

[4]URL `https://www.aircraftspruce.com/catalog/pdf/13-09032.pdf` [Cited on 18/06/2016]

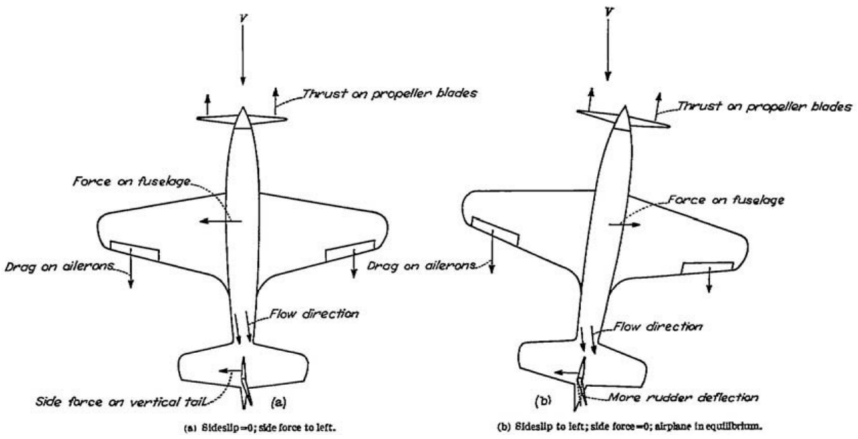

Figure 7.9: The propeller effect on the aircraft dynamics[5].

Printing intermediate values was also used for most of the calculation verification. These intermediate values were checked using engineering sense to see if they were feasible and the programme did not return unlikely big or small values. For the center of gravity calculations for example, it was clear that the center of gravity should be more to the front of the UAV since the payload, wing and engine are located to the front. It was also checked that if a package aft of the center of gravity was dropped, the center of gravity would shift even more forward.

The flap calculations were also verified by implementing reference data of a Cessna 172 aircraft[6] in the programme and then comparing the calculated required flap area with the actual area of the flaps. Using these methods, the programmes used for determining the center of gravity range and the sizing of control surfaces were found to be verified.

The validation of the programmes is rather difficult to do at the moment, since there is no prototype or wind-tunnel scale model yet which can be used for the validation. Once either one of these two is available, it can be used to conduct experiments needed to validate the programmes. During these experiments it has to be checked if the control surfaces actually generate the forces and moments for which their size has been determined and if the center of gravity is actually in the calculated location.

This location of the center of gravity can be determined by placing the nose and main landing gears of the UAV on scales to measure the weight on each landing gear. Then Equation (7.31) can be used to determine the location of the center of gravity. The flaps have to be validated to see if they generate a change in lift coefficient of 0.4 when deflected 20°. Checking the ailerons can be done by deflecting the ailerons by 10° when at a wing-level position and determining the time it takes to reach a bank angle of 30°. The validation of the elevators can be done in a manner similar to that of the flaps, it has to be checked if they actually generate the required lift to rotate the UAV during its ground-run. And finally, for the validation of the rudder it is the easiest to put the UAV side-ways in a wind-tunnel to simulate crosswinds and then checking if the rudder deflection of 20° is enough to keep the UAV stable and controllable.

$$CG = \frac{\sum W_i \cdot x_i}{\sum W_i} \tag{7.31}$$

The obtained stability derivatives for the Wings for Aid UAV have been verified by comparison to not only the Cessna 172 but also other reference aircraft like the Fokker F-27 as given in the Flight dynamics lecture notes [22]. The calculation of the eigenvalues has been verified by using the analytical solutions for the eigenmodes as specified in chapter 5 and 6 of the flight dynamics lecture notes [22][p. 117-160] for the symmetric and asymmetric eigenmodes respectively. Using the less coarsest approximations available the eigenvalues obtained from the state-space system were verified using the eigenvalues obtained from the analytical approximate equations. The difference between these 2 solutions proved to be less than 5% and therefore the state-space system is considered verified. The eigenvalues and stability derivatives have not yet been verified however. This should be performed with flight testing and is something which is recommended for the post-DSE period.

[6]URL `http://temporal.com.au/c172.pdf` [Cited on 18/06/2016]

Chapter 8

Structures

This chapter elaborates on the complete structural design and the structural design choices made during the project. In Section 8.1 the materials which will be used in the structural design will be selected. After this Section 8.2 shows the design steps of the fuselage. Subsequently to the fuselage design, Section 8.3 explains the development of the wing structure. The landing gear design is explained in Section 8.4 and the tail structural design is shown in Section 8.5. Finally, Section 8.7 elaborates on the design of the nose and tail cone.

8.1 Materials characteristics and selection

For any structural design, the trinity concept should be followed, meaning that the material selection, manufacturing and the structure are correlated. To start, a material selection was performed, whilst keeping the 2 other aspects in mind.

Material selection

Once the main different sections among the UAV structure have been defined, an initial material selection can be performed. A graph with materials which can be used for this design is shown in Figure 8.1. This graph is made in CES Edupack [24]. The material families chosen for this graph are indicated by the coloured areas. The maximum price for the materials in the graph is 5.00 €/kg, because very expensive materials cannot be used. The materials at the most top right position are the strongest and cheapest materials. It is therefore not unusual that this position is taken by iron and steel alloys which are the blue ovals in the top right corner of the graph. Even though these alloys score well according to the graph, due to production limits of sheets and beams these materials will be too heavy to use for UAV parts. The density of iron and steel alloys is approximately three times as large. Therefore, due to due minimum thickness of sheets and beams parts made of these alloys are often heavier than parts made of aluminium alloys. For the final determination of the material, more aspects such as environmental durability have to be investigated.

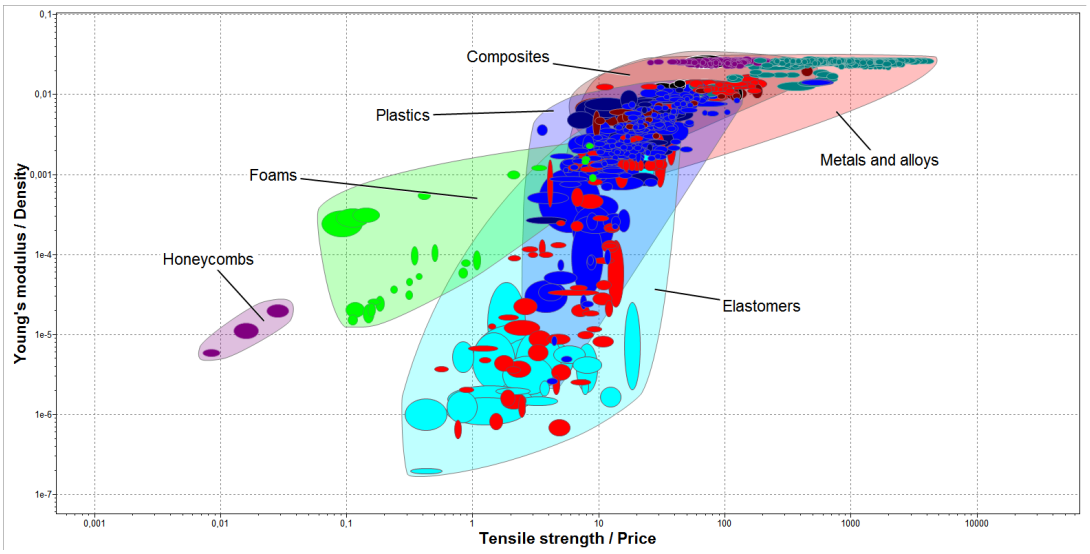

Figure 8.1: Graph with possible useful materials for the wing structure.

The aluminium alloys at the top right of the graph are mainly aluminium 2000, 5000, 6000, and 7000 series. The 2000 series alloys are very useful for aerospace design, however these series are susceptible to stress corrosion cracking. This UAV should be able to fly in multiple environmental conditions which also includes the sea. This environment is very corrosive, so a material in which stress corrosive cracking can occur is not suitable for this UAV. Furthermore, the 5000 series have good corrosion properties

and are cost effective, lightweight and strong. Due to the good performance in corrosive environments this alloys series is chosen for the skin. From this series the 5182-H19 alloy is chosen, because this alloys has the best fit for the design requirements.

From the 6000 and 7000 series the 6061-T6 and 7075-T6 are chosen to be used for the spars and load bearing structure when spars are used. This is due to the fact that the 5000 series alloys are rarely used for extrusion, because extruding 5000 series is a difficult process [25]. Furthermore, the 6061-T6 and 7075-T6 alloys are very common in aerospace design, so the reliability of the wing will be higher than for alloys which are uncommon in aerospace engineering.

Furthermore, in Section 8.3 also the foam core concept is introduced. For this concepts it is also needed to determine which foam will be used. It is possible to use PS foam types, however these foam cores need CNC milling to be made into their final shape. CNC milling is very time consuming and expensive. Therefore, expandable foam types are investigated and this showed promising results. Some polyurethane foam types are stiff and can carry some load. The functions of the foam is to maintain the wing shape and carry the shear loads. According to the Italian company DUNA-Corradini it is possible to use expandable polyurethane foams for a wing.

The selected materials to use during the trade-off are displayed in Table 8.1. The plastic and aluminium material values are based on values from CES Edupack.[24]

Table 8.1: Selected materials for wing design.

	Young's Modulus (GPa)	σ_{ult} (MPa)	μ (-)	ρ (kg/m^3)	price (€/kg)
PU foam [26]	0.025	1	0.25	53	2.20
PCT (40 % short glass fiber)	11.3	138	0.34	1550	6.40
Al 5182 H19	70.0	420	0.33	2650	2.20
Al 6061 T6	68.9	310	0.33	2700	2.40
Al 7075 T6	71.7	460	0.33	2800	4.60

8.2 Fuselage structure

The part that connects and supports all systems of the UAV is the fuselage. This section presents the methods and paths taken for the design and analysis of the fuselage structure.

Load cases

As mentioned in the introduction, the fuselage is supporting every system of the UAV such as payload, wing, landing gear or engine. This also means that there are various load cases for the fuselage structure. The most critical load cases for the fuselage are listed below.

- One point landing: A landing where only one of the main landing gears is touching the ground as stated in CS-VLA 483.
- Two point landing: A landing where only the two main wheels are touching the ground as stated in CS-VLA 479.
- Three point landing: A landing where all wheels are touching the ground simultaneously as stated in CS-VLA 479.
- Three point landing with side slip: A two point landing with an additional side slip as stated in CS-VLA 477.
- Rear wheel braking: Only the main wheel brakes are applied.
- wing gust/pull-up maneuver: Maximum gust or pull up maneuver as defined in CS-VLA 333.
- Horizontal tail load: The maximum upwards or downwards force introduced from the horizontal tail surface CS-VLA42X.
- Vertical tail load: The maximum sidewards force introduced by the vertical tail surface CS-VLA44X.

The load cases were taken from the CS-VLA [12] and will not be explained here in more details. However in Section 8.2 the loads, stresses and displacements due to those load cases are presented.

Fuselage structure option

There are numerous available structural concepts. In this section three concept which were made partially together with VanBerlo are presented.

Concept one consists of one single beam which is supporting the whole structure. This beam would go from the engine to the tail and can be produced by extrusion. The skin in this concept does not carry any load. All subsystems like wing and engines are attached to the beam with different types of brackets.

Concept two uses a frame structure for the support of the subsystems. Similar to the single beam structure the skin of the fuselage does not carry load. The preferred manufacturing method for this structure is welding. This also implies that steel is the preferred material since it as better welding characteristics than aluminium. For the tail connection two concepts are possible. The truss structure can be continued until the tail or the truss structure can go over into a single beam. The tail structural design is discussed in Section 8.5.

The last concept uses the skin as a load carrying part. The sides of the fuselage are thin aluminum plates which are supported by stiffeners. All loads will be introduced into the skin by brackets. This concept is widely used in the aerospace industry. It is used for the design of large passenger and transport aircraft's as well as for kit planes like the Zenith CH 650. The connection between stiffeners, brackets and skin is done by use of rivets.

Trade-off

In order to reduce development time. The trade off between the structure was done without a detailed stress analysis. This section discusses the advantages and disadvantages of the different structural concepts.

The first concept of a single beam which is supporting all subsystems has one main advantage. Since the beam is covering the complete length of the UAV only one main structural element is necessary. In addition the beam can be extruded which reduces the production costs. However there also many disadvantages for the single beam concept. One structural part also means a single point of failure meaning that if the beam fails the whole UAV is unsupported and will fail. In addition all subsystems need special attachments to the beam. Last but not least the skin is carrying no load which makes the concept heavier than a skin carrying concept. Due to the complication for the attachments of subsystems especially the attachment of landing gear, engine and wing. The structural concept was ruled out and not further analyzed.

The second concept which uses a truss structure as load carrying part is also used in light aircrafts and kit planes. It has more advantages over the single beam structure. The structure can be easily made fail safe due to the larger number of beams and struts and the possibility of placing zero force members into the structure. In addition the load paths for the landing gear or engine can be significantly improved over the single beam which decreases the weight of the structure. Unfortunately the production materials is preferable steel which does not have good specific properties when compared to aluminium. In addition the welding spot weakens the material. This weakening is hard to predict which means that additional safety factors should be used for the design.

Last but not least the structural advantages and disadvantages of the third concept are discussed. Given that the skin is carrying a major part of the load yields large advantages for the weight of the structure. As for the truss structure, the structure can be designed in such a way that it optimizes the load paths of landing gear, engine and wing. Having the possibility of using aluminium instead of steel reduces the weight further. In addition as said before this concept is widely used in the aerospace industry and seems to have cost benefits for kitplanes since all parts can be produced out of sheet metal. On the disadvantage side the torsional stiffness of the fuselage is lower for a skin carrying concept since the bottom side of the fuselage is open. This means that the stiffeners need to be larger, increasing the overall cost and weight of the concept. Last but not least the labour cost might be more expensive than the truss structure due to the amount of rivets.

In conclusion due to the lower weight and the ability to use the skin as load carrying part. The skin carrying concept was taken. The disadvantages of this structure were reduced during the design of the fuselage by using the same part for multiple locations. This will be further discussed in the following

section.

Structural fuselage design

This section presents how the final fuselage structure was developed. The structural design was split into three parts. First an initial concept was worked out on how the parts such as brackets or the attachment of the tail beam should look like and how they could be produced. Secondly the structure was analysed analytical and with a FEM model to check if it can withstand all load cases. From the obtained analysis results the structural design was updated in order to improve the weak points. Afterwards the production methods were finalized and a cost estimation was made which will be discussed in later sections.

The goal of the fuselage design was to use the same part as many times as possible and to design it in such a way that it is easily producible. This drove the design to use sheet metal parts which could be formed into the desired shape and to use brackets and stiffeners which have the same profile.

It was decided to use U profiles for the stiffeners as well as the brackets for landing gear and wing. However for the bracket one additional production process is required since the ends need to be bend in order to attach them to the skin. The side skin itself is a single aluminium sheet. The right and left side can be made out of the same shape, however during post processing the rivet holes have to be drilled differently. The firewall is also used as a structural part by supporting the engine and the front landing gear. This reduces the amount of parts and therefore also reduces the weight and cost.

Table 8.2: FEM stress analysis.

Load case	Maximum stress [MPa]	Location
One point landing	340	Main landing gear bracket
Two point landing	360	Tail clamp
Three point landing	210	Tail clamp
Three point landing with side slip	580	Main landing gear bracket
Rear wheel braking	480	Main landing gear bracket
Gust loading/ pull up maneuver	380	Firewall engine mount
Horizontal tail load	2000	Tail bracket
Vertical tail load	9756	Tail bracket

The FEM stress analysis showed the following results for the different load cases in Table 8.2. It showed that the landing gear bracket, the tail bracket and the engine mount needed to be redesigned. For the main landing gear attachment an additional bracket was introduced. Together with the first bracket the moment from braking and the forces from landing are better introduced into the skin. The tail beam attachment was reinforced with additional stiffeners as well as an additional top plate to increase the torsional rigidity. For the front landing gear an additional stiffener was placed onto the firewall. In addition stiffeners were placed on the upper edge of the fuselage to reduce skin buckling. These measurements brought the design to its final stage which can be seen in Figure 8.2. In addition the updated stress estimations are shown in Table 8.3.

Next to the stress estimation a first estimate for the rivet spacing of the brackets was made. The wing brackets were designed to take an ultimate load of around 16,000N which occurs during a gust. It is assumed that the load will be distributed equally over the three brackets and therefore equally over the six skin bracket attachments, see Figure 8.2. This yields a load of around 2,700N per rivet bond. An illustration of the simplified load case with the most relevant dimension can be seen in Figure 8.3. In addition it was decided to organize the rivets in two rows. For the analysis the following failure modes for the rivet and sheet were analysed.

- Shear fracture of the rivet.
- Bearing fracture of the sheet
- Skin shear failure

The failure load for each load case is given by Equations (8.1) to (8.3).

Table 8.3: FEM stress analysis.

Load case	Maximum stress [MPa]	Location
One point landing	160	Main landing gear bracket
Two point landing	240	Tail clamp
Three point landing	180	Tail clamp
Three point landing with side slip	260	Main landing gear bracket
Rear wheel braking	180	Main landing gear bracket
Gust loading/ pull up maneuver	170	Firewall engine mount
Horizontal tail load	220	Tail bracket
Vertical tail load	238	Tail bracket

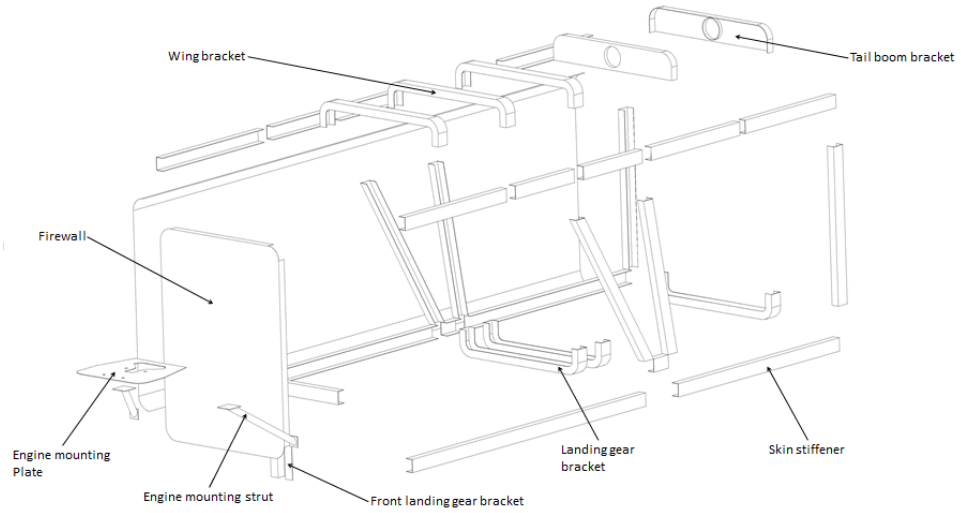

Figure 8.2: Exploded view of final fuselage structure.

$$F_{Rivet_shear} = 2n \cdot \alpha \cdot \frac{\pi D^2}{4} \tau^{rivet}_{fracture} \quad with \quad \alpha = 1 - 0.04(\frac{D}{t} - 3) \tag{8.1}$$

$$F_{Bearing_{fracture}} = 2n \cdot p_b D_{hole} t_{sheet} \tag{8.2}$$

$$F_{Skin_shear} = (w - nD) \cdot t_{sheet} \sigma_{sheet} \tag{8.3}$$

The equation have three unknowns which are $F_{failure}$, D and n. By varying the diameter D and the number n of rivets per row an optimum failure load was reached where the different failure modes occur at a similar applied loads. With an optimum diameter of $D = 2.4mm$ and $n = 4$ rivets per row an ultimate failure load of 6200N was found which is well above the ultimate load encounter during a gust. The calculation assumed a ultimate tensile strength of 310MPa taken from Table 8.1, the bearing strength was assumed to be 810MPa [27], the Rivet shear strength 210MPa [27] and the sheet thickness is $t_{sheet} = 0.5mm$. For all other brackets and attachments such as tail beam and landing gear a similar analysis can be performed. In addition to the mentioned failure modes an additional inter rivet buckling analysis should be performed for the stiffeners.

Production

As mentioned before special attention was given the production methods of the fuselage. The production of the parts can be split into four parts; part production, assembly pretreatment, assembly and post treatment.

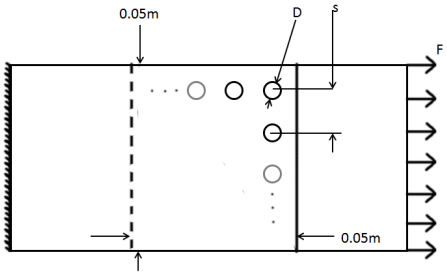

Figure 8.3: Wing bracket rivet load case.

For the part production of the stiffeners either extrusion or roll forming can be used. Due to the low thickness of 1-2 *mm* for the stiffeners and brackets roll forming is preferred. Roll forming is a cheap option which, similar to extrusion produces the part in an continuous way. The skin can be produced by various kinds of forming. Since the profile of the skin does not change from beginning to end the roll forming is an attractive option again.

The assembly pretreatment phase consist out of multiple steps. First the stiffeners and skins have to be cut into the required length. Additionally the ends of the bracket for landing gear and wing have to be bend into the correct shape. Afterwards the holes for rivets have to be drilled for every part this can be done manually with a template or with a CNC machine.

After all parts have been pretreated they can be assembled. The assembly only consists of riveting all parts together. No additional steps as applying adhesive layers or curing is necessary. In the post processing step coatings for paint or protection can be applied to the material.

Cost estimation

In order to arrive at the total production cost of the fuselage a cost estimation was performed for each part. This cost estimation included the raw material cost, the production cost, the assembly pretreatment cost and the final assembly cost. Table 8.4 lists these costs for the different parts. The total production cost of the fuselage is €775. This assumes that the assembly and pretreatment of the parts will take less than twelve hours for one worker. The raw material cost was estimated by multiplying each part weight with its material price per kilogram. For parts which are bought off-the-shelves the selling price was taken as raw material price. Due to the use of cheap manufacturing methods such as roll forming the production cost of the fuselage is €88. The production cost of off-the-shelve parts is zero since their costs are already included in the raw material cost. The main costs comes from the labour costs for assembly and pretreatment. The hourly labour cost is €40 which includes the overhead costs as well. Due to the high amount of cutting in drilling, which is required for the final assembly, the assembly pretreatment costs are with €380 the highest. The pretreatment costs were estimated by estimating the required labour time based on the size and work steps necessary. For the final assembly time four hours were estimated which were evenly distributed over each part in Table 8.4.

Conclusion and Recommendation

In conclusion it was shown how the final fuselage structure was developed and why the skin carrying structure was most favorable for the design. In addition it was proven that a rivet bond between the skin and bracket does resist the maximum load encountered during flight. However the structure is still not in its final stage and ready for production. All selected parts, production methods and cost estimates do need further investigation to obtain a higher accuracy. Many simplification and assumption were taken for the FEM model which include that all load cases were treated as quasi static and that rivet connection can be modelled as a tie constraints. As presented in the rivet sizing paragraph the analysis was only done for the wing bracket and needs to be applied all other connections withing the fuselage. Even though the skin carrying structure is a proven concept and is used in many application within the aerospace industry experimental testing with real scale models or final parts is essential to validate all outcomes of the analysis.

Table 8.4: Fuselage production cost.

Part	Instances	Mass (kg)	Material cost (€)	Machining cost (€)	Pretreatment cost (€)	Assembly cost (€)
Skin	2	1.1	2.7	10.9	80.0	16.0
Bracket	6	2.4	5.9	23.4	72.0	16.0
Stiffener	23	1.8	4.4	17.7	184.0	16.0
Front landing gear bracket	1	0.4	0.6	3.0	4.0	16.0
Tail beam bracket	2	0.8	2.0	11.8	16.0	16.0
Engine mounting plate	1	1.3	1.8	17.8	4.0	16.0
Engine support strut	2	0.5	0.7	3.4	8.0	16.0
Mounting plate	1	2.7	75.0	-	4.0	16.0
Top plate	2	1.4	24.0	-	8.0	16.0
Rivets	400	0.3	30.0	-	-	16.0
Sum	-	12.7	147.1	88.0	380.0	160.0
Total Cost						775.1

8.3 Wing structure

The planform and the airfoil of the wing are selected in Section 5.2 and Section 5.1. Now the lay-out aspects of the wing are known, a structure which can carry all the loads should be designed. For the design of the internal structure of the wing first some possible concepts have to be selected. After these concepts are selected, they are investigated further and finally a trade-off will be performed. After the trade-off a more detailed design phase is reached in which the elements of the inner structure are sized.

Structural concept selection

The structure of the wing has to comply to multiple requirements. For example, it should fit within the budget and it should be able to withstand the ultimate load of a 5.85 g longitudinal gust load. For the possible concepts a few criteria are kept in mind. For example, the stringent budget and the mass.

The parameters which affect the cost are the materials, ease of assembly, complexity of parts, amount of parts and manual labor time. The least expensive materials which are useful for the construction will be used, so titanium and carbon fibers, for example, will not be used. The materials should be light, strong, stiff and cost effective. Furthermore, parts of the structure are preferred to be as simple as possible, because parts that require complicated or time consuming production methods are often more expensive. Also, a small amount of parts could probably cause a small assemble time. The assemble time requires man-hours and the cost can become large if much man-hours are needed.

Secondly, the mass of the wing is preferred to be equal or lower than the mass which it should have according to the mass budget. This might be impossible, because very lightweight and strong materials such as carbon fiber composites cost too much. This means that other strong and lightweight materials need to be used. Aluminium alloys are often used in aerospace design and can still be used for the design of this UAV.

Wing box concept

The most common strategy for a wing structure is a wing box. The wing box is a very efficient design to withstand the banding, shear and torsion loads. However, this design normally requires many parts and many manual labor hours and this probably drives the cost of the wing box to an unfeasible extend. Therefore, the wing box concept will not be considered.

I-beam and box-beam spar concept

Other possible concepts are the I-beam spar concept and the box-beam spar concept. I-beam spars will be used to take the bending and shear loads and two spars can also take the torsion loads acting on the wing. This concept is similar to the wing box concept, but requires less manual labor time, because

the spars and stiffeners can be attached to the skin. However, the spars can become more expensive when the wing is tapered. The spars cannot be extruded when using a tapered wing and this affects the cost. This concept can be changed to use only one box-beam spar. This spar has a closed section and therefore it is more efficient for counteracting torsional loads. This concept is also more expensive to produce for tapered wings, because extrusion is impossible.

Extrusion of the spars will be very cost effective for the structure. However, this requires the spar to be designed for the worst load case. This is inefficient for the mass of the structure and therefore it is possible that a structure based on these concepts can become too heavy.

Sandwich structure concept

A sandwich structure with an load bearing skin and a foam core is also an possibility. This design is successfully used in remote control aircraft and could probably be as effective for this wing design. it requires a foam core, skin and inserts for control actuators. This concept is also more flexible with regard to the wing planform. The foam can be made in a large variety of shapes, so a tapered or elliptical planform are both feasible. The foam core can be made by moulds. The mould itself is more expensive, however multiple foam cores can be manufactured with this mould. Furthermore, the skin can be a sheet which is pressed in the needed shape.

From these concepts it is decided to further investigate the I-beam spar, box-beam spar and sandwich structure concepts. These concepts are very promising concerning the cost. The mass of these concepts could end up higher than the estimated mass of the mass budget. However, this is a result of the requirement that the design has to be very cost effective.

Load case

An aircraft is subjected to many loading configurations during its lifetime. Among all those loadings, one will always be the most critical for the structure. To find that most critical one, first so called load cases are constructed. These load cases are based on the regulation given in CS-VLA [12], and give a set of inputs happening at the same time on the structure and must be considered to make sure it is strong enough. A list of different load cases for the entire aircraft is listed next.

- Pull-up: this is the maximum lift created by the wings, as prescribed by the maximum positive load factor given in the flight envelope.
- Pull-down: this is the maximum downwards lift generated by the wings, as prescribed by the maximum negative load factor given in the flight envelope.
- Tip-over: in case of bad landing, and the aircraft were to tip over, the structure shall cope with load factor of at least those prescribed in CS-VLA 561 (d). The structure is not mandatory made compliant with this rule, as no pass angers are on board the UAV.
- Parachute deployment: this is the load the emergency recovery system puts on the aircraft when being deployed. It depends on the chosen parachute.
- Control surface deflection: this is the extra load all the control surfaces (rudder, aileron, flaps, elevator) do apply on the structure within the flight envelope.

Among those load cases, two are driving the design of the wing, being the pull-up and pull down. In both those conditions, the lift and drag distribution along the span of the wing is multiplied by the ultimate load factor to size the wing's structure. Both lift and drag will result in shear torsion and bending of the wing.

To be able to calculate the structure for an initial trade-off, a common load case was used. This load case was taken to be a constant lift distribution along the span, corresponding to a loading given by Equation (8.4).

$$q = \frac{n_{ult} m g}{b} \tag{8.4}$$

Using a constant distributed load will not change the maximum shear stress at the root section, but will put the point of application of the total lift further away from the center line. This will result in a higher root moment, and therefore higher bending stresses. However, as neither the torsion due to lift, nor the bending and shear due to drag, nor the bending relieve due to the wing's own weight are considered, and that the drag is less than a tenth than the lift, this assumption holds relatively well, and allows to take a margin which will cover those other loads.

Wing structure concepts

This section elaborates further on the concepts selected in Section 8.3. The concepts will be worked out with the loads described in Section 8.3. The mass and cost of each concepts will be estimated. For this stage the cost will only be estimated according to the material cost.

I-beam spar concept

This concept is calculated for a non-tapered wing planform, partially tapered, and a tapered wing planform. To determine the loads on the planform, first the lift distribution had to be estimated. The lift distribution along the span, L'(y), is determined according to Equation (8.5)[1].

$$L'(y) = K_q \cdot c(y) \qquad (8.5) \qquad K_q = \frac{MTOW \cdot n - W_w \cdot n}{S_w} \qquad (8.6)$$

Where K_q is a constant factor which is determined by Equation (8.6) and $c(y)$ is the chord of the airfoil along the span. The n in Equation (8.6) is the load factor. The load factors considered for the conceptual design are the ultimate load and limit load factors. This method estimates the lift distribution along the span according to the chord. Although it does not take the induced angle of attack into account, it determines a rather accurate lift distribution. For the purpose of conceptual trade-off this lift distribution is considered accurate enough. The shear forces and moment along the span can be determined by integrating the lift distribution and shear forces along the span.

$$S(y) = \int_y^{b_w/2} L'(y)dy \qquad (8.7) \qquad M(y) = \int_y^{b_w/2} S(y)dy \qquad (8.8)$$

In these equations S is the span wise shear force and M the span wise moment. Furthermore, b_w is the span of the main wing. The shear forces and moments are determined from the root, so therefore the upper limit of the integrals is at half the span. Ones the moment along the span is known the stresses can be determined. However, the locations of the spars have to be known first. For wing design the locations of the spars are normally at about 20% of the chord for the spar in the front of the wing and and around 55% of the chord for the spar at the back of the wing. For this design stage, these values for the locations of the spar in the front and back of the wing are used. The forces which act on the spars are determined according to their location. Furthermore, the locations of the spar also determine the height of the spar and this is important for the maximum stress calculations which will be performed later.

To determine the forces acting on each spar, the location where the lift distribution acts has to be known. From aerodynamics it is known that the aerodynamic center on an airfoil is approximately at 25% of the chord. The forces on the spars are determined by moment equilibrium and the resulting forces in the spars are shown in Equations (8.9) and (8.10)

$$S_{front}(y) = \frac{0.55 - 0.25}{0.55 - 0.2} \cdot S(y) \qquad (8.9) \qquad S_{rear}(y) = \frac{0.25 - 0.2}{0.55 - 0.2} \cdot S(y) \qquad (8.10)$$

The moment in the spars can be determined by the same method as used in Equation (8.8).

Now the forces on the spars and the height of the spars are known, it is possible to determine the stresses in the spars. First the normal stresses are considered. The maximum normal stresses are at the location which is furthest from the neutral point of the cross section. In this case that is the flange of the I-beam, which is half the distance of the spar height away from the neutral point. The stress in the spar is determined by Equation (8.11).[28]

$$\sigma_{max}(y) = \frac{M(y) z_{max}}{I_{xx}} \qquad (8.11) \qquad I_{xx} = \frac{1}{12} t_w h_w^3 + 2 \cdot \left(\frac{1}{12} l_f t_f^3 + (l_f t_f) \left(\frac{h_w}{2} + \frac{t_f}{2} \right) \right) \qquad (8.12)$$

Where $\sigma_{max}(y)$ is the maximum normal stress in the spar, z_{max} is the location furthest away from the neutral point as already explained, and I_{xx} is the moment of inertia of the spar. The moment of inertia depends on the geometry of the spar cross section and it is calculated according to Equation (8.12). t_w is the thickness of the web plate, h_w is the height of the web plate, l_f is the length of the flange, and t_f is the thickness of the flange. The moment of inertia is iterated such that the maximum stress is as close as possible to the ultimate compressive stress of the material when the ultimate lift load is considered.

[1] URL `http://ocw.mit.edu/courses/aeronautics-and-astronautics/16-01-unified-engineering-i-ii-iii-iv-fall-2005-spring-2006/systems-labs-06/spl10.pdf` [Cited on 13/06/2016]

The height of the web plate is not changed, because the spar is attached to the wing skin.

The dimensions of the spar for the non-tapered wing are determined for the largest stress location. Once the dimensions for the spars are determined these will be used for the complete spar.

The dimensions for the tapered wing vary along the span due to the taper. This means that the web plate height also changes along the span. Because the web already changes along the spar and the spar cannot be extruded for this reason, it is also chosen to have a varying flange length. The variation is linear like the variation of the chord of the wing.

Once the moment of inertia of the spar along the span in determined, the maximum stresses are also determined. These maximum stresses can be used for the calculations of the buckling of the skin. The assumption for the determination of buckling in the skin is that the skin has the same deformation as the flange. The deformation of the flange is determined according to Equation (8.13). After the deformations along the span are known the stresses in the skin can be determined by using Equation (8.14).[28]

$$\sigma_{max,spar}(y) = E_{al} \cdot \varepsilon_{flange} \qquad (8.13) \qquad \sigma_{max,skin}(y) = E_{pl} \cdot \varepsilon_{flange} \qquad (8.14)$$

E in these equations is the Young's modulus of the material and ε is the strain in the material due to the stresses. Using this method only the stresses in the skin at the front and rear spar are known. For simplicity at this stage only the stresses of the skin at the front spar are considered, which is conservative. To calculate the stress at which the skin starts to buckle Equation (8.15) is used [29].

$$\sigma_{cr}(y) = \frac{\pi^2 E_{pl} k_c}{12(1-\nu^2)} \left(\frac{t_{skin}(y)}{b(y)} \right)^2 \qquad (8.15)$$

Where k_c is the buckling constant for buckling due to compression. This constant depends on the way the skin is attached at the boundaries and the dimensions of the skin between the boundaries. The skin is assumed to be simply supported at the boundaries and together with the dimensions of the skin between the boundaries, the value of k_c is determined to be 4.0.

With all the equations and method discussed so far the concepts of the non-tapered, half tapered, and tapered wing are examined. The results of the concept examination are shown in Tables 8.5 to 8.8.

Table 8.5: Materials of the components.

Concept	Non-tapered			Partially tapered			Tapered		
Spar	6061-T6	6061-T6	7075-T6	6061-T6	7075-T6	6061-T6	6061-T6	6061-T6	7075-T6
Stiffener	6061-T6	6061-T6	7075-T6	6061-T6	7075-T6	6061-T6	6061-T6	6061-T6	7075-T6
Rib	6061-T6	6061-T6	7075-T6	6061-T6	7075-T6	6061-T6	6061-T6	6061-T6	7075-T6
Skin	PCT	5182-H19	5182-H19	PCT	5182-H19	5182-H19	PCT	5182-H19	5182-H19

Table 8.6: Estimated number of the components of the I-beam concepts.

	Non-tapered			Partially tapered			Tapered		
Spars	4	4	4	8	8	8	4	4	4
Stiffeners	28	22	28	26	24	32	44	32	40
Skin panels	8	8	8	8	8	8	8	8	8
Ribs	6	6	6	6	6	6	6	6	6
Total nr. of components	46	40	46	48	46	54	62	50	58

For the total mass of the wing a contingency factor of 25% is used to account for actuators, lights, etc. The wing also has to be modular and this results in a higher mass. Therefore, the contingency factor is taken more conservative. Then the mass is rounded off till the nearest integer.

Table 8.7: Estimated mass of the components of the I-beam concepts in kg.

	Non-tapered			Partially tapered			Tapered		
Spars	25.2	25.8	21.0	25.9	19.4	16.7	18.0	17.8	16.0
Stiffeners	2.2	1.7	2.2	2.0	1.9	2.5	3.4	2.5	3.2
Skin panels	56.0	52.0	54.0	54.0	48.0	50.0	52.0	44.0	46.0
Ribs	1.8	1.8	1.8	1.5	1.5	1.5	1.3	1.3	1.3
Contingency factor	1.25	1.25	1.25	1.25	1.25	1.25	1.25	1.25	1.25
Total mass	107	101	99	105	89	89	93	82	83

Now the concepts are worked out and the masses of the parts are determined, it is possible to estimate the cost of the wing. First, the mass of the components of the wing are multiplied by the price per kg of the used material. To determine the cost of a component the production method has to be known. Once that is known a multiplication factor can be used to estimate the price more accurately.

Table 8.8: Estimated cost of the components of the I-beam concepts in €.

	Non-tapered			Partially tapered			Tapered			Production cost multiplication factor
Spars	60	61	97	61	46	77	42	42	74	3.7, 13.0
Stiffeners	5	4	10	5	5	12	8	6	15	11.9
Skin panels	358	122	249	346	113	230	333	104	212	5.6
Ribs	4	4	8	4	4	7	3	3	6	5.6
Total material cost	427	191	360	415	168	323	386	155	304	
Total cost of components	2310	979	1217	2813	1313	2471	2523	1217	2361	

The multiplication factors are determined from the prices of several manufacturers. The price and mass of the component is calculated and subsequently the price per mass in €/kg for the component is determined. The specific cost of the component is then divided by the specific cost of the materials and this yields the production cost multiplication factor. This is done for multiple companies and from these factors the average is calculated. The spars for the partially tapered and tapered wing planforms have to be manufactured differently. The method which is used in aerospace engineering to make spars with variable web dimensions is to use angle beams to connect the web to the flange of the spar. This would require extra labor hours and therefore a larger cost per component. For this reason a multiplication factor of 13.0 is used to estimate the cost of the spars which cannot be extruded.

Box-beam spar concepts

The method to examine the box-beam spar concepts is the same as used for the examination of the I-beam spar concept. The difference now is that the spar forces are not divided over two spars. The results can be seen in Tables 8.9 to 8.11.

The results shown that the box-beam concepts need more components. This is a logical consequence of the fact that only one spar constraints the skin. Therefore, more stiffeners are needed to prevent the skin from buckling. Furthermore, these concepts are also a bit more expensive. This is also a consequence of the larger number of stiffeners.

Sandwich structure concept

This concept relies on the sandwich structure used in the aerospace industry with composites, but to keep it cheaper, the carbon fiber used as a skin is replaced by aluminum or reinforced plastics with short fibers ($<5\ \mu m$). The concept will make use of Al 6061 T6 and the inside of the airfoil is filled up with foam. From the sandwich theory, it can be assumed that the core only carries the shear forces, while the

Table 8.9: Estimated number of the components of the box-beam concepts.

	Non-tapered			Partially tapered			Tapered		
Spars	2	2	2	4	4	4	2	2	2
Stiffeners	81	64	84	110	74	104	138	98	108
Skin panels	8	8	8	8	8	8	8	8	8
Ribs	6	6	6	6	6	6	6	6	6
Total nr. of components	97	80	100	128	92	122	154	114	124

Table 8.10: Estimated mass of the components of the box-beam concepts in kg.

	Non-tapered			Partially tapered			Tapered		
Spars	21.7	21.9	18.5	18.3	18.5	16.0	15.2	15.4	15.3
Stiffeners	6.4	5.0	6.9	8.6	5.8	8.5	10.8	7.6	8.9
Skin panels	56.0	52.0	54.0	54.0	48.0	50.0	52.0	44.0	46.0
Ribs	1.8	1.8	1.8	1.5	1.5	1.5	1.3	1.3	1.3
Contingency factor	1.25	1.25	1.25	1.25	1.25	1.25	1.25	1.25	1.25
Total mass	108	101	101	102	92	95	99	85	90

Table 8.11: Estimated cost of the components of the box-beam concepts in €.

	Non-tapered			Partially tapered			Tapered			Production cost multiplication factor
Spars	51	51	85	43	43	74	36	36	70	3.2, 13.0
Stiffeners	15	12	32	20	14	36	25	18	41	11.9
Skin panels	358	122	249	346	113	230	333	104	212	5.6
Ribs	4	4	8	4	4	7	3	3	6	5.6
Total material cost	428	189	374	413	174	347	397	161	329	
Total cost of components	2369	1012	2092	2757	1381	2718	2647	1281	2619	

skin carries all the normal stresses. Therefore the concept is decoupled in two problems, one being only the shear force along the core, and the other the bending of the outer skin.

The normal stresses in the skin can be computed by means of the general bending equation, given in Equation (8.16), where the moment of inertia, I_{xx}, is calculated for an airfoil by means of Equation (8.17). Z_u and Z_l are the upper and lower coordinates of the airfoil along the chord, and c is the chord at the location of the bending moment. It is taken as the the outer shape inertia, minus the inertia of an airfoil with twice the skin thickness as a chord.

$$\sigma = \frac{Mz}{I_{xx}} \tag{8.16}$$

$$I_{xx} = \int_0^c \frac{1}{3}[(Z_u - \bar{z})^3 - (Z_l - \bar{z})^3]dx \tag{8.17}$$

The centroid, $\bar{z}$, and the area are computed by means of Equations (8.18) and (8.19)[2]. All the integrals have been evaluated using the Simpson's rule.

$$A = \int_0^c (Z_u - Z_l)dx \tag{8.18}$$

$$\bar{z} = \frac{1}{A}\int_0^c \frac{1}{2}(Z_u^2 - Z_l^2)dx \tag{8.19}$$

[2]URL http://ocw.mit.edu/courses/aeronautics-and-astronautics/16-01-unified-engineering-i-ii-iii-iv-fall-2005-spring-2006/systems-labs-06/spl10b.pdf [Cited on 09/06/2016]

The shear stress in the core is computed by means of Equation (8.20), where V is the shear force at a given location, and Q is the area above the location where the shear stress is computed times the centroid of that area to the shear location. For all the planform concepts, the maximum shear stress will occur at the root, on the airfoil centroid.

$$\tau = \frac{QV}{I_{xx}t} \tag{8.20}$$

Once the maximum shear stress is computed, a foam is selected which can handle those stresses, Indeed, the geometry of the airfoil cannot be changed, therefore these stress levels are the lower limit. However, a foam with a higher shear strength is selected, for several reasons. First, the lower strength ones are too expensive when bought as slabs, and the expandable ones are not suggested for casting. On the other hand, some inserts will be needed for connections, leading to higher local shear stresses.

An overview of the required of the structure's main parameter is given in Table 8.12 and Table 8.13. The plastic skin thickness is 2 mm for all the concepts, since sheet thicknesses for plastic can not be manufactured with a lower thickness.

Table 8.12: Plastic skin concept overview.

	Fully tapered	Half tapered	Non tapered
τ_{max} (MPa)	0.11	0.17	0.17
m_{core} (kg)	44	51	49
t_{skin} (mm)	2.0	2.0	2.0
m_{skin} (kg)	55	59	60
Contingency factor	1.25	1.25	1.25
Total mass (kg)	124	138	136

Table 8.13: Aluminum skin concept overview.

	Fully tapered	Half tapered	Non tapered
τ_{max} (MPa)	0.11	0.17	0.17
m_{core} (kg)	44	51	49
t_{skin} (mm)	0.51	0.61	0.71
m_{skin} (kg)	25	32	42
Contingency factor	1.25	1.25	1.25
Total mass (kg)	85	103	114

After the initial sizing, a price estimation of the material and production is performed. The same production factor as for the skin in the I beam concept is used for the skin, being 5.6. For the foam a production factor of 3 is applied. To obtain this factor it was assumed that the production factor of the skin is composed of two parts, having an equal weight in the total factor: the cost of the molds and the press itself. For the foam, the molds will be about the same as the one produced for the skin, hence this will be a factor of 2.8. On top of this, a factor of 0.5 is added for the required material for the mixing. This results in a production factor of 3.3.

The different price estimations for each component and the complete wing are displayed in Table 8.14 and Table 8.15. The first two lines are always the cost of the raw material, whereas the last two ones are the price for the production.

Wing structure concept trade-off

Now all concepts are examined, a trade-off for the structural design can be performed. The criteria of the trade-off are the mass of the wing, the estimated component cost, the amount of parts, the ease of assembly, the man hours, amount of different materials and the readiness of technology.

Table 8.14: Price estimation with a plastic skin, in €.

	Fully tapered	Half tapered	Non tapered
Foam cost	100	117	112
Plastic cost	355	380	383
Core production cost	331	386	369
Skin production cost	1986	2128	2142
Total cost	2772	3011	3006

Table 8.15: Price estimation with a aluminum skin, in €.

	Fully tapered	Half tapered	Non tapered
Foam cost	100	117	112
Aluminum cost	59	76	101
Core production cost	331	386	369
Skin production cost	331	424	567
Total cost	822	1003	1149

The mass, cost, and amount of parts are determined in the previous sections. The mass of the wing is very important. From the results of the concepts it becomes clear that the mass budget of the wing cannot be met, so it is important that the mass of the wing is as low as possible. However, it is not as important as the cost, so a weight factor of 4 is used. Furthermore, the cost of the wing should still be as low as possible to meet the cost requirement of the UAV, so the weight factor of this criterion is also 5. The amount of parts influences the amount of man hours and therefore also the cost. However, having more of the same parts is more cost effective. Consequently, a weight factor of 3 has been assigned as it has positive and negative consequences for the cost.

The ease of assembly is reasoned from the methods to fit all components together. The spar structures are not complicated to assemble, but these concepts will take a lot of man hours. The foam core concepts is harder to assemble, because adhesives are needed. The ease of assembly affects the required skills of the laborers and this influences the cost. As it is a fraction of the cost, it will be given a weight factor of 4.

As mentioned, spar structures are less efficient when it comes to man hours, because all components have to be connected by rivets. The foam core structure do not have as many components as the spar structures, so less man hours are needed for assembly. The man hours affect the cost by a large amount, because manual labor hours are expensive. Therefore, this criterion is given a weight factor of 4.

The amount of different materials has influence on the certification of the wing, so a low amount of different materials is preferred. As the certification is not as important as the mass and the cost for the design of the wing, the weight factor is 3.

The readiness of the used technology in the concepts also is included in the trade-off. Both techniques are used in aerospace design, however the foam construction is not used for large aircraft, so the readiness of this technology is a bit lower. Because both constructions are possible, the weight factor for the readiness of technology is set to be 2.

The trade-off of the wing structural concepts is shown in Tables 8.16 to 8.18.
From the trade-off with the current values for the criteria comes clear that the tapered foam wing with an aluminium 5182-H19 skin is the best option for the wing concept from a structural perspective.

Trade-off sensitivity analysis

For the trade-off sensitivity analysis different possible scenarios are determined which influence the weights of the trade-off criteria. The results for the different scenarios are shown in Figure 8.4. The sensitivity analysis is done for the five concepts which have the highest total score for the initial trade-off.

Table 8.16: First trade-off table with non-tapered concepts.

	Weight	I-beam			Box-beam			Foam core	
		PCT	6061-T6	7075-T6	PCT	6061-T6	7075-T6	PCT	6061-T6
Mass	4	3	3	4	3	3	3	1	2
Component cost	5	3	5	4	3	4	3	1	4
Amount of parts	3	4	4	4	3	3	2	5	5
Ease of assembly	4	1	2	2	1	2	2	3	3
Man hours	4	2	2	2	2	2	2	4	4
Amount of different materials	3	3	4	4	3	4	4	2	2
Readiness of technology	2	3	5	5	3	5	5	2	2
		66	87	86	63	79	71	62	81

Table 8.17: Second trade-off table with partially tapered concepts.

	Weight	I-beam			Box-beam			Foam core	
		PCT	6061-T7	7075-T7	PCT	6061-T7	7075-T7	PCT	6061-T6
Mass	4	3	5	5	3	4	4	1	3
Component cost	5	2	4	3	2	4	2	1	5
Amount of parts	3	4	4	4	1	3	1	5	5
Ease of assembly	4	1	2	2	1	2	2	3	3
Man hours	4	2	2	2	2	2	2	4	4
Amount of different materials	3	3	4	4	3	4	4	2	2
Readiness of technology	2	3	5	5	3	5	5	2	2
		61	90	85	52	83	67	62	90

Table 8.18: Third trade-off table with tapered concepts.

	Weight	I-beam			Box-beam			Foam core	
		PCT	6061-T8	7075-T8	PCT	6061-T8	7075-T8	PCT	6061-T6
Mass	4	4	5	5	4	5	5	2	5
Component cost	5	2	4	3	2	4	2	2	5
Amount of parts	3	3	4	4	1	2	1	5	5
Ease of assembly	4	1	2	2	1	2	2	3	3
Man hours	4	2	2	2	2	2	2	4	4
Amount of different materials	3	3	4	4	3	4	4	2	2
Readiness of technology	2	3	5	5	3	5	5	2	2
		62	90	85	56	84	71	71	98

The first scenario is a more driving mass requirement and the importance of the lowest mass is more important than the cost. This means that the mass and the amount of parts get an weight factor of 5. Furthermore, the cost and man hours have been given a weight of 3.

The second scenario states that the man hours are going to be more expensive and the manual labor time of the concept is preferred to be as low as possible. The weight factor of the man hour criterion is therefore set to 5. The resulting total score of the concepts for this scenario is shown by the third bar in

each column graph.

In the third scenario a situation occurs where a lot of drones need to be build in a short period and therefore the assembly time should be low. This results in a weight factor of 5 for the amount of part, ease of assembly, and the man hours. Furthermore, the cost and mass is considered less important and is given a weight of 3.

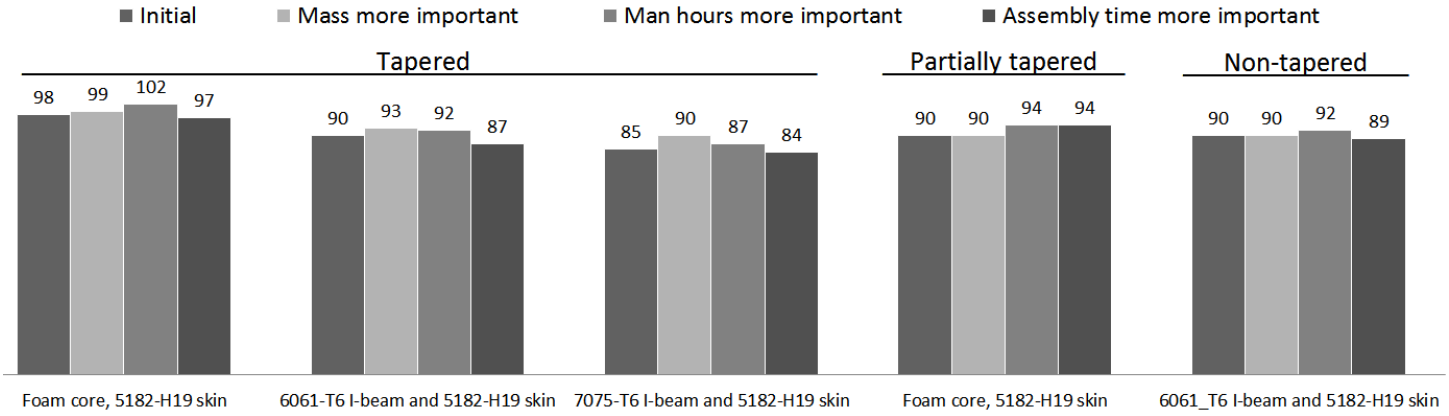

Figure 8.4: Concept total score for different trade-off weight scenarios.

From this sensitivity analysis can be concluded that the tapered wing with a foam core and aluminium 5182-H19 skin has the highest score at all scenarios.

Wing structure preliminary design

From both the aerodynamic performance (see Section 5.2) and the structural point of view, the taper sandwich concept was the most optimal choice for the wing planform design. Once this decision was made, the structure could be worked out more in detail and optimized for both weight and manufacturing. The first step was to include cut outs in the planform, at the location of the flaps and ailerons, according to the dimensions required from Section 7.2.

Afterwards, a more detailed look is taken at the complete load carrying structure, since the calculations done for the trade-off were just the basics. In the following sections, the stress levels in the skin are analyzed closer to the inserts, the core will be looked more in depth at, whilst trying to make it lighter.

The nomenclature used for each part in the further design of the wing is shown in Figure 8.5.

Design loads

Beside the ultimate positive load factor load case, many more load are applied to the wing during its lifetime. Several were already explained in Section 8.3, but some more do apply. The most important one used in this preliminary design was obtained from the regulations CS-VLA 572 [12]. This states that all primary structure must have strength capabilities to achieve adequate safe-life. From AMC VLA 572(b), showed in Figure 8.6, the maximum stress in the skin for the Al 5182 H19 alloy can therefore not exceed 210 MPa at limit load factor.

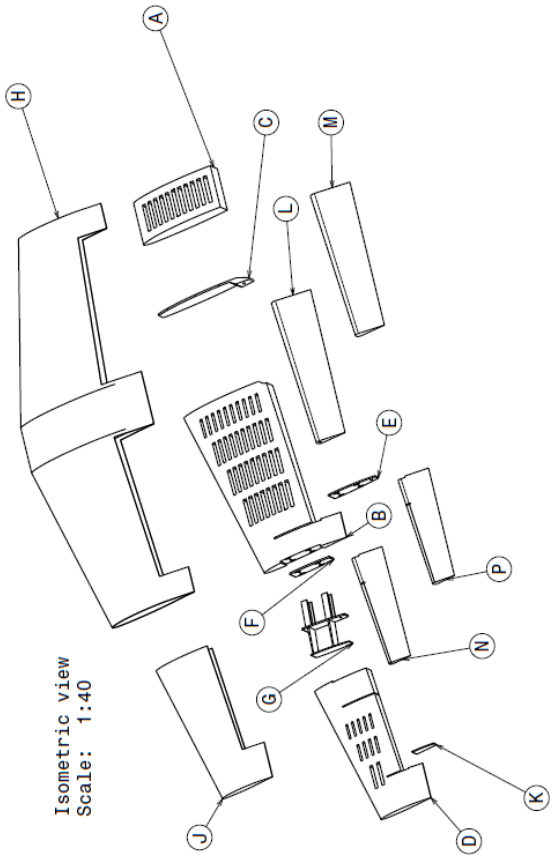

Figure 8.5: Wing part nomenclature.

Table 8.19: Wing part nomenclature.

Bill of Material: Wing	
Number	Part Name
A	Wing_core_fuselage
B	Wing_core_inboard
C	Wing_insert_fuselage
D	Wing_core_outboard
E	Wing_insert_flap
F	Wing_insert_edge
G	Wing_insert_modularity
H	Wing_skin_inboard
J	Wing_skin_outboard
K	Wing_insert_aileron
Bill of Material: Flap	
Number	Part Name
L	Flap_core
M	Flap_skin
Bill of Material: Aileron	
Number	Part Name
N	Aileron_core
P	Aileron_skin

AMC VLA 572 (b)
Parts of Structure Critical to Safety (Interpretative Material and Acceptable Means of Compliance)

1 The use of the following stress levels may be taken as sufficient evidence, in conjunction with good design practices to eliminate stress concentrations, that structural items have adequate safe lives:

Material used	Allowable normal stress level of maximum limit load
– Glass rovings in epoxy resin	25 daN/mm^2
– Carbon fibre rovings in epoxy resin	40 daN/mm^2
– Wood	According to ANC-18*
– Aluminium Alloy	Half of rupture tensile strength
– Steel Alloy	Half of rupture tensile strength

Figure 8.6: Acceptable means of compliance for fatigue.

However, since the UAVs will be flying non stop during the duration of the mission, the amount of cycles may be reached at a certain point. This is why a more detailed analysis can be performed, or a maximum amount of flight hours can be set as a limit for the wing. At this stage, the wing should be changed, which is an easy operation due to presence of the modularity, and the old wing can be checked for any damage. If the later one is still found to be safe and within specifications, it can be reused on another aircraft. This way of designing for the stress level makes it easier and a lighter structure. Additionally, if a UAV is found to be defective, the unit price of a wing is low, in such a way that the cost engendered by fixing the wing remains at an overall low. Moreover, the stress levels for which the wing skin is designed is at limit gust load, meaning this is a flight condition the UAV will only experience a few times during its lifetime. A load case where fatigue is easier to design for, is landing. When the UAV hits the ground the wings experience a stress change of 1g upward, up to 2.5g downward, due to the impact.

Since the maneuver and gust envelope almost overlay each other at this stage, one can think that the limit load factor could be easily reached with maneuvers. Nonetheless, as the UAV is fully automated, this means an internal mechanism can be programmed into it, setting range control on the inputs it can give. This is the same principle as giving a pilot restriction on which commands may be used simultaneous, but yet the UAV will always obey those rules, making it more predictable and safe.

From [3], an initial lift distribution assumption can be taken to be linear between the tip and the root. This was modeled in the FEM analysis by applying a constant pressure over the wing surface, whose magnitude equals $n_{lim}mg/S$ for the limit load, and $n_{ult}mg/S$ for the ultimate load. Since the wing is tapered, this will approximate the linear lift distribution. The root stresses were verified and validated afterwards by applying a concentrated tip load, producing the same root moment.

Skin

Before further designing the skin, the skin thickness obtained from the trade-off was verified and validated by means of a FEM analysis. From there on, the skin was further designed.

This means the skin thickness had to be adapted to meet this requirement. Using FEM analysis, this was found to be 0.6 *mm* Al 5182 H19 skin for the inboard section, and 0.3 *mm* for the outboard section. The outboard section is still over designed, but it was judged that any thickness below this will make it much harder to handle. An overview of the skin stress distribution at limit load along the wingspan is displayed in Figure 8.7.

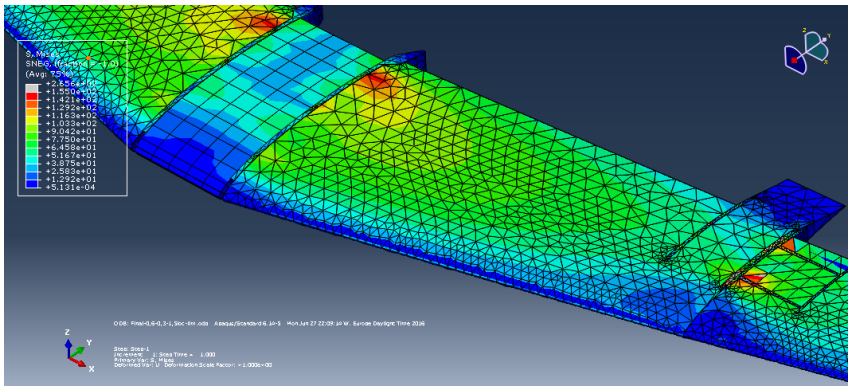

Figure 8.7: FEM analysis of the wing's skin at limit load.

Inserts

During the design of the inserts, two important aspects are taken into account. First, the inserts should be strong and stiff enough to handle the local forces which are introduced into the structure. Moreover it should also have good shear properties and a large contact patch with the core material, to reduce the shear stresses in both the insert and the core. There are 4 locations for the inserts: the connection of the wing to the fuselage, the flap attachment, the aileron attachment and lastly the modularity insert.

The first insert, at the fuselage, serves two purposes: the first one being to connect the complete wing to the fuselage, but also to connect the flap to the wing. The insert is located just inboard of the fuselage's width, with the 3 pin holes centered above their attachment on the fuselage. The utility of this insert is mainly to transfer the shear loads of the lift to the fuselage, without introducing the normal forces or the bending moment, which are transferred through the skin to the other fuselage insert.

The second important insert group is linked to the flap. As already explained in the previous paragraph, the flap will be hinged to the wing on the inboard side by means of the fuselage insert. However, a second insert was placed at the outboard location of the flap, to support it at both ends, and therefore reduce the bending force along the hinge line of the flap. If this moment were to become to big in the detailed design of the flap, an extra insert can be added in the middle of the flap, as is explained for the aileron. This outboard insert is also the second connecting point for the outboard modularity, as the

[3]URL `http://ocw.mit.edu/courses/aeronautics-and-astronautics/16-01-unified-engineering-i-ii-iii-iv-fall-2005-spring-2006/systems-labs-06/spl10.pdf` [Cited on 13/06/2016]

modular insert slides and locks into place at this place.

The next insert group is the biggest part of the inserts, and concerns the outboard wing modularity. The concept can be seen in Figure 8.8. The edge and flap outboard insert are in place in the inboard core, and the modularity insert is glued in place in the outboard core. The outboard core is then slid in the inboard core. In both cores, 2 inserts are present running along the chord, to be able to transfer the outboard lift as two shear forces, instead of a moment.

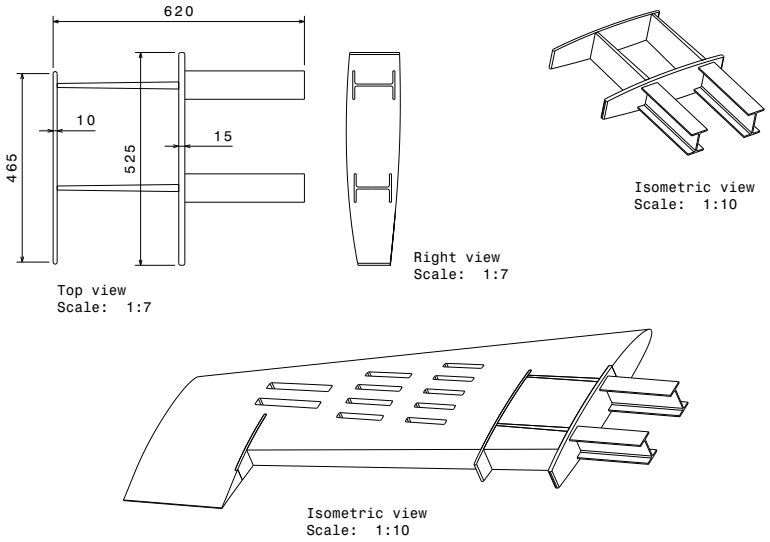

Figure 8.8: Technical drawing of the modular insert.

The last insert group is related to the aileron connection. As for the flap, 2 inserts were used on either side of the aileron, with an additional one in between. The inboard insert is integrated into the modularity inserts which assigns two tasks to that insert and therefore reduces weight and cost.

Afterwards, the modularity inserts were looked at in more detail. Two important aspects are the strength of the insert, and the connection to the core and skin. To make the lightest inserts, the modularity is placed closest to the flap. This allows to use the flap insert as part for the modularity insert. The inserts will be made with PP plastic, which has the lowest density, while still being strong and and easily injection moulded.

Core

To lighten the complete internal structure, several leads were taken. First, a different density foam can be used at different locations. The shear stresses in the removable outboard section is much lower than those encountered at the root of the wing, therefore they need less strength. This allows the use of less stronger foam, which is also less dense. Another way of lightening the structure, is by removing material, hence making some lightening holes. Those holes, if placed and sized correctly, will not change the maximum load bearing capabilities of the wing. Two important elements need to be taken into account: on one side, there must remain enough material to handle the shear load, whilst not producing stress concentration. On the other hand, the foam helps to prevent skin buckling, this is the main reason not to have stiffeners. Therefore the hole's geometry should be in such a way that it does not contribute to buckling.

First the holes are sized according to buckling, by means of Equation (8.21). This gives the maximum compressive stress allowed in the skin before it buckles. The critical stress should be higher than the maximum compressive stress at the location of the hole, when the ultimate loading is applied. The value of k_c depends on both the aspect ratio of the hole, and the type of clamping along the edges. Since the skin is glue to the core, and the distance between two holes is assumed to be at least the hole's width, then all our edges can be assumed to be clamped. The value of k_c can be read of the graph shown in Figure 8.9[29], following the top dashed line.

In order to decrease the stress concentration, and the validity of clamped condition, it was assumed to keep a constant span wise distance between the holes of 100 mm, and 125 mm from inserts. For the chord wise distribution, at least 1.5 the hole size is left between the holes. The holes are always 150 mm separated from the leading edge, to allow for both a good impact resistant leading edge and shape integrity. Indeed, the first one is helped by the foam being able to absorb a relatively large amount of energy in case of impact, therefore giving less chance of failure. The second advantage is for performance: having core allows the skin to retain its form more easily, which is important for aerodynamic purpose.

$$\sigma_{critical} = \frac{\pi^2 E k_c}{12(1-\nu^2)} \left(\frac{t}{b}\right)^2 \tag{8.21}$$

The holes' geometry was calculated in such a way that they cover the biggest area, in order to remove more material, whilst still meeting the buckling requirement. The holes sizes are displayed in Table 8.20. The row are counted from the the centerline outwards.

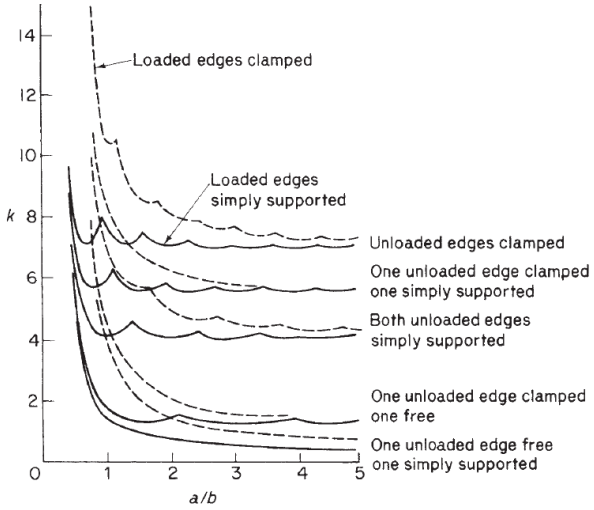

Figure 8.9: Buckling coefficient k_c for thin plates in compression.

Table 8.20: Lightening hole sizes.

	row	Highest stress (MPa)	a (mm)	b (mm)
Inboard	1st	220	28	210
	2nd	140	35	262
	3rd	120	38	285
	4th	105	41	307
Outboard	1st	90	22	165
	2nd	70	25	187
	3rd	35	35	262

The torque produced by the wing can be superimposed. But as the complete skin forms an enclosed area, it is assumed that foam core does not take any load, and that all shear is taken up by the skin. Equation (8.22) can be used to find the shear flow in the skin. The maximum torque at the root is the sum of all the torque produced along the span, given by Equation (8.23).

$$T = 2Aq \tag{8.22}$$

$$T = \frac{1}{2}\rho V^2 S C_M \bar{c} \tag{8.23}$$

Since the airfoil is the same for the complete wing, the torque can simply be computed by using the MAC and half the area. The worst case were the torque is produced is at limit load, therefore at cruise speed. Taking C_M to be the greatest magnitude, being -0.11, the total root torque is equal to 6136 Nm. This produces a shear stress of 31 MPa, and inserting it in the Von Mises' criterion with the highest tensile stresses of 190 MPa due to bending, only result in an increase of 0.85 MPa of the yield stress. Even thought the torsion due to the lift being applied in an other location than the shear center is not taken into account, the magnitude of these stresses is neglectable. This shows that torsion of the wing is not a problem, and was a valid assumption to exclude it from the trade-off load case.

Finally, the drag is added up in the same manner, with all the reaction forces taken by the skin, both shear and normal stresses. This is because the drag acts along the strongest axis of the airfoil.

An overview of the inboard core structure is displayed in Figure 8.11, and a FEM analysis of the holes is shown in Figure 8.10.
The stress legend displayed in Figure 8.10 is the maximum allowable shear stresses, and the lighter colored area shows the inserts.

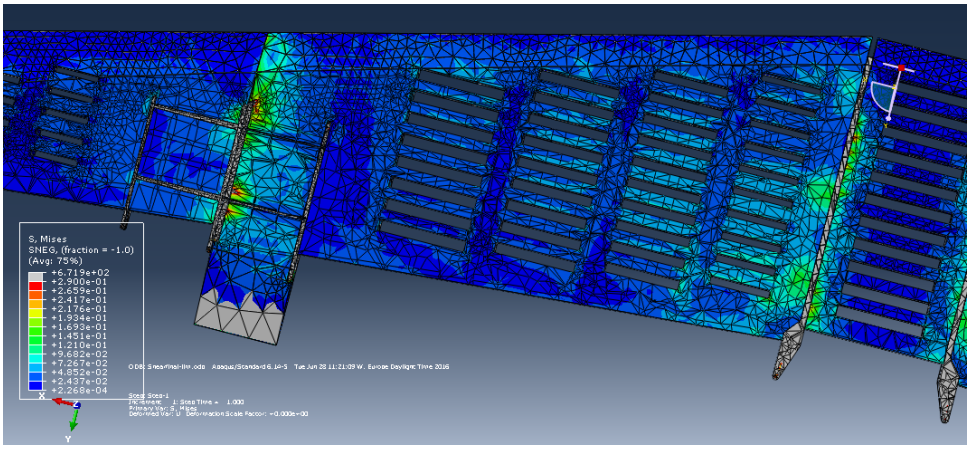

Figure 8.10: Technical drawing of the outer section of the wing.

control surfaces design

The ailerons and flaps of the wing also need a structure to maintain their shape when deflected. It could be done by injection molded skin panels with integrated stiffeners. However, due to the possible high temperatures at the ground stations, it is possible that the plastic will become soft. This would limit the operation of the UAV. Therefore, it is decided to use the same construction method as had been used for the construction of the wing. The skin will be made from aluminium 5182-H19 and the core from expandable foam.

The location of the servo for the flaps is in the fuselage section of the wing. The servo can transfer the rotation through a belt to a tube which is connected to both the flaps. Two servos will be used for the control of the flaps. consequently, if one servo fails it is still possible to operate both flaps, however the response will be slower. Furthermore, ailerons will be operated by one servo each. The ailerons will have a tube inserted in the foam. A belt which is attached to the servo is attached to this tube to rotate the aileron. For this a cut-out will be made in the leading edge of the elevator. The servo will be attached to the modularity insert of the outer section of the wing. For a better understanding of the locations of the servos, refer to Figure 8.11.

Final design values

During the design of the wing, the cost and mass of each component was estimated. The estimation of the mass and cost is shown in Table 8.21. The cost estimation only includes the price of the raw material and the man hours required, since the price of molds were not to be included [5]. What each column represents is shown in the first row of the table. The raw material cost is estimated by multiplying the mass of each part times the instances and the material cost. The used material cost for the inserts and skin is found in CES Edupack [24]. Furthermore, the material cost of the foam is found on the website of US Composites[4]. For the machine cost a multiplication factor is implemented. For the foam a multiplication factor of 1 used. The inserts are injection molded and therefore a factor of 2 is used. Finally, the forming of the skin sheets is an expensive process, so a multiplication factor of 4 is chosen. For each product the production time is estimated and this time is multiplied by €40/hr to determine the production cost. The total cost of each component is multiplied by the instances of each component is shown in the last column. For each type of component the total cost is determined and these values are summed together with extra assembly cost and cost for the adhesives in Table 8.23.

The final mass of the wing is shown in Table 8.22. The total mass of all component types are summed and extra mass is added for, for example, the adhesive to connect the skin and inserts to the foam.

Modularity

The wing is divided in three parts; A center part and two outer parts. To attach the central wing section to the fuselage six pins will be inserted through the wing into the fuselage. These will be put in from the top of the wing, and screwed into nuts which are already present in the structure of the fuselage.

[4] http://www.uscomposites.com/foam.html

Table 8.21: Wing component breakdown.

	Mass [kg]	Amount of parts [-]	Raw material cost [€]	Machine cost [€]	Production time [hr]	Labor cost [€]	Total cost [€]
Inboard core	10.2	2	144	144	2.0	80	368
Fuselage core	3.0	1	21	21	1.0	40	81
Outboard core	4.1	2	58	58	2.0	80	195
					Total foam cost [€]		645
Fuselage insert	4.0	2	8	16	1.0	40	64
Outboard flap insert	0.9	2	2	4	1.0	40	45
Edge insert	0.9	2	2	4	1.0	40	45
Modularity insert	2.8	2	6	11	1.0	40	57
Aileron insert	0.2	2	1	2	1.0	40	43
					Total insert cost [€]		254
Inboard skin	15.8	1	60	240	2.0	80	380
Outboard skin	1.7	2	13	53	2.0	80	146
					Total skin cost [€]		526
Flap core	1.9	2	27	27	1.5	60	113
Flap skin	1.6	2	12	49	1.5	60	121
Aileron core	0.8	2	12	12	1.0	40	63
Aileron skin	1	2	8	30	1.0	40	78
					Total control surfaces cost [€]		375

Table 8.22: Wing mass build up.

Component	Mass [kg]
Core	31.5
Inserts	17.8
Skin	19.3
Ailerons	3.6
Flaps	6.8
Extra	8
Total wing mass	87

Table 8.23: Wing cost build up.

Stage	Cost [€]
Assembly	400
Core production	645
Insert production	254
Skin production	380
Control surface production	375
Adhesive	250
Extra	230
Total wing cost	2535

Alternatively, a clamp could be used to be closed on top of the wing, in order to secure it to the fuselage. Despite making the cover slightly less aerodynamic, this reduces the stress and therefore the mass of the wing.

The outer wing parts are made modular, because these parts will probably be the first parts of the wing which get damaged. If a wing gets damaged at the outer part it is not necessary to remove one half of the wing or the complete wing, but just the outer part. The two spars which stick out of the outer section, see Figure 8.8, are inserted in the center wing section and secured by a pin. This pin will be inserted from the leading edge of the wing through the two I-beams.

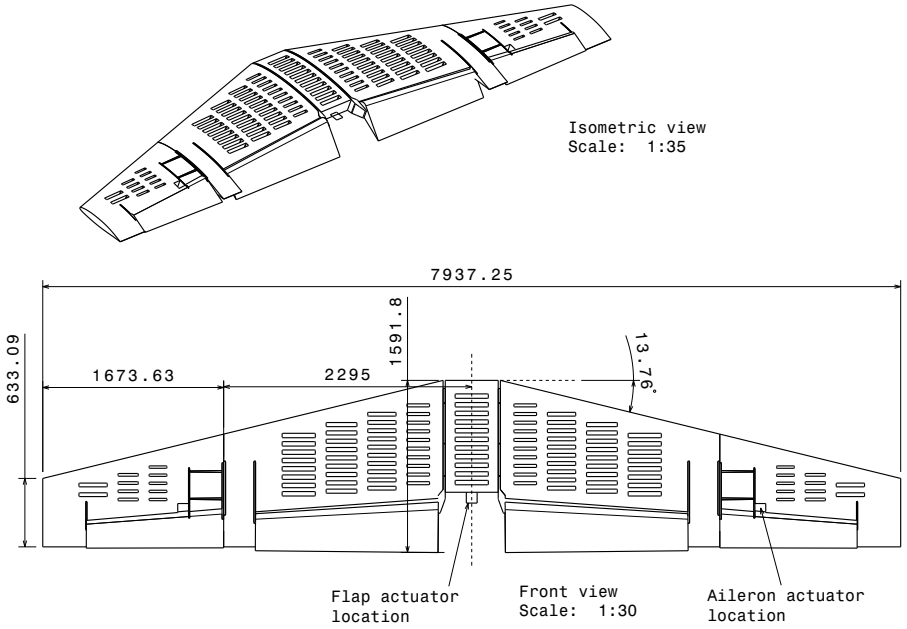

Figure 8.11: Final wing planform layout.

Manufacturing

During the wing design process, it was kept in mind that it should first of all be able to be produced, but at the same time, have a low cost. This meant that CNC'ed parts were not an option. There are three major components which need to be produced for the wing, being the foam core, the aluminum skin and the plastic inserts.

The aluminum skin will be formed by means of a press, which will press the skin into the right shape. The skin will be made out of a separate top and bottom cover, and will then be bonded by means of adhesive to the core and inserts. However, the skin should also be bonded to itself, to increase torsional rigidity and strength. Indeed, only if the skin forms a closed loop can the assumption be used of Equation (8.22). This will not be a problem at the the trailing edge, as both skins are on top of one another. To solve this continues connecting at the leading edge, a small aluminum plate should be place in between the skin and the core, onto which both skins will be bonded. This little piece of aluminum will allow to transfer the shear. However, bonding the skins at the nose of the airfoil is not desirable from an aerodynamic point of view, as it introduces imperfection, and therefore disrupts the boundary layer. For this reason, the seam line should be smoothen after bonding, and a layer of paint should be applied. The bonding could be done with an expanding epoxy, despite usually needing curing at temperate, to fill up any gap left due to the the imperfection of manufacturing. But if curing is required, this would discard most plastics as inserts, and would raise the cost.

The pressing of the skin will introduce strains, but this can be used as an advantage on the compressive side. Indeed, the strain introduces pre-tension, which reduces the magnitude of the compressive stress of the skin. In a further stage, this could be used to lighten the structure even further, by increasing the size of the holes in the core. This needs however more detailed analysis. On the other hand, the holes can be left untouched, by which an extra margin is taken against buckling.

For the production of the core, two options are possible: CNC already formed foam slabs, or using expandable foam. The first option is not feasible for this project for several reasons. First, as stated earlier, CNC'ing complex shapes is not a solution, as this will be over the cost budget by a big margin, especially for such big pieces. Secondly, the slab sizes manufacturing can provide are not big enough to allow the core to be CNC'ed out of one slab. Dimensions of slabs are usually around 1250x2500, with a maximum thickness of 100 mm . This means at least 6 slabs should first be connect by means of adhesive, which lengthens the production process , making it more costly, but also adds weight in the

form of the adhesive. Lastly, CNC'ing removes at lot of material, which is not Cradle-to-Cradle, but also makes the customer pay for more material than what is actually needed, hence increasing cost.

The second option is to expand foam in molds which have the required shape. Additionally, in these molds could already be all the lightening and inserts holes. From information gathered from manufactures, this is a feasible production method. The expanded foam should have uniform properties within a given range all across the foam. To control the process even better, and get better properties, a mixing machine can be added to mix both components of the foam. This method of production will be cheaper, if the price of the molds are not considered, as stated in the project reader. But some thinking about decreasing the molds' price was also done during the structural design of the wing. First of all, all the lightening holes on a given line along the chord can have the same dimensions. Furthermore, when CNC'ing the outer shape, the holes should only be made on the edge, after which the extrusions of the holes can be placed in between the two molds.

Lastly, the production of the insert can be done with injection molding, where both VanBerlo has experience, and complex shapes can be made relatively easy. Indeed, the total mass taken up by the inserts is a relative big part of the wing and some mass can be shaved off during the detailed design, by optimizing the load paths and shape of the inserts.

8.4 Landing gear structure

Preliminary gear sizing

The UAV has a tricycle landing gear configuration with a fixed gear. The reasoning for the selected landing gear configuration was already given in Section 4.2. The first step in landing gear sizing was determining the height and wheel track of the main landing gear. Being a small aircraft, the UAV will have two main landing gear wheels and a single nose wheel.

The main gear positioning will be at 2.10 m from the nose, which is at 13.9 cm behind the most after center of gravity location. Due to the minimal propeller clearance required, the landing gear height is large relative to the main fuselage dimensions. The main considerations for this placement were the division of the load between the main gear and the nose gear, and the available rotation during take-off.

The nose gear will be attached at the beginning of the main fuselage section. However the strut will angle the nose wheel forward at 20° so that the location of the wheel and thus of the load application point lies at 0.41 m from the nose. Due to this location the loads on the nose gear will have a short load path into the main fuselage structure, and due to the angle of the strut will be better suited to take-off and landing of rough terrain.

In this configuration the nose gear will take up 12.7% of the static load on the ground. Usually you would want at least 8 - 20% of the load on the nose gear for steering [6], however as the UAV will be maneuvered by personnel on the ground the main concern is that the nose gear will dig in or get stuck on uneven ground. With a limited load on the nose it is free to move over irregularities, whilst keeping most of the load on the main gear.

The height of the landing gear is sized on two things: the required propeller clearance and the required pitch clearance of both the horizontal tail and the aft fuselage edge. The required propeller clearance is at least 180 mm [12]. Using the fuselage height and the propeller diameter Equation (8.24) is used to compute the required landing gear height.

$$h_{lg} = \frac{1}{2} \cdot (L_f + d_{prop}) + h_{clearance} \tag{8.24}$$

$$h_{lg} = (L_f - x_{ml}) \cdot tan(\theta) \tag{8.25}$$

The other requirement for the height is that it must provide sufficient clearance for all parts of the fuselage during take-off rotation. The critical parts of the aircraft in this case are the horizontal tail, and the most aft part of the fuselage. The pitch angle at the end of rotation is required to be at 90% of $C_{L_{max}}$, and is equal to 15.26°. An additional 3° is added as a margin. With the dimensions of the fuselage the required landing gear height can be determined from Equation (8.25), where θ already includes the margin. The horizontal tail is located at the top of the fuselage, therefore in that case the fuselage height must be subtracted.

Finally a maximum landing gear height can be determined from the fact that the UAV will have to fit in a 20 ft container while still on its wheels. Therefore it must be checked whether the UAV height fits

in the container. A summary of the required minimal fuselage heights can be found in Table 8.24.

Table 8.24: Landing gear height constraint results.

Constraint	Landing gear height (m)
Propeller clearance	0.51
Fuselage clearance	0.42
Tail Clearance	0.36

As can be seen the propeller clearance is the critical parameter in this case. With a fuselage height of 0.51 m.

Next the wheel track of the main landing gear was determined. This is based on tip over constraints, and is usually sized for ground stability with a side wind load case and a steering constraint [6]. In our case the steering constraint is not applicable as the drone will not taxi automatically. Therefore the wheel base is only checked for side wind conditions. The wheel track is also the main element which sizes the length of the landing gear struts, and as can be seen in Section 8.4 is essential to determining the stroke of the solid spring landing gear. An increased strut length increases the stroke, which decreases the landing loads on touchdown. The wheel track needed for ground stability can be determined from Equation (8.26).

$$T = \frac{c_{d_{side}} \cdot \rho \cdot V_{wind}^2 \cdot S_{side} \cdot H_{cg} + 0.06 \cdot L_{tail}}{gM} \tag{8.26}$$

Equation (8.26) provides a minimal wheel track requirement of 0.31 m. From the container width and knowing that two fuselages must fit side by side, we can determine that the maximum for the wheel track is 1.84 m. This value is way higher than the required value but as it is beneficial for landing loads the upper value is used. Another benefit of having the landing gear pre-mounted inside the container is that it greatly eases ground assembly operations. A summary of the main landing gear dimensions is given in Table 8.25.

Table 8.25: Initial sizing results.

Constraint	Landing gear height (m)
Landing gear height	0.51
Main gear wheel track	1.84
Main gear longitudinal position (from nose)	1.57
Nose gear longitudinal position (from nose)	0.27

Gear loads

The landing gear will need to be sized to take up all the energy during landing. The maximum expected vertical velocity during landing is set for in regulations [12] and can be determined with Equation (8.27), giving 2.25 m/s on touchdown.

$$V_{vert} = 0.51 \cdot \left(\frac{W}{S}\right)^{0.25} \tag{8.27}$$

$$KE_{vert} = 0.5 \cdot MTOW \cdot V_{vert}^2 \tag{8.28}$$

For a solid spring landing gear the stroke is equal to the deflection of the strut. Using an energy method it can be determined how much this must be. The total energy on touchdown can be calculated from the vertical velocity and the mass as explained in Equation (8.28). The mass in this case is the maximum take-off weight, in case something goes wrong just after take-off. Equation (8.29) helps determine the energy absorbed both by the tire and the strut of the landing gear, where F is the average total load on the shock absorber, and η is the absorber efficiency. For tires $\eta_T \approx 0.5$, and for a solid spring $\eta \approx 0.6$ [6]. Equations (8.28) and (8.29) can be rewritten with the required load factor to find an expression for the required stroke of the main landing gear, Equation (8.30). For landing $N_{gear} = 3$.

$$KE_{abs} = \eta FS \tag{8.29}$$

$$S = \frac{V_{vert}^2}{2g\eta N_{gear}} - \frac{\eta_T}{\eta} S_T \tag{8.30}$$

The stroke of the tires was calculated based on the chosen tires, the dimensions of which can be found in Table 8.26. The tires chosen are slightly larger than conventional tires, which will increase their shock absorption and therefore aircraft performance on rough terrain. The advised maximum tire pressure is 210-310 *kPa* for wet grass on soft soil, and 275-415 *kPa* for dry grass on hard soil or hard packed sand. 300 *kPa* was chosen for versatility, but can be adjusted on a case by case basis anywhere between 210-410 *kPa* as required. This brings the required stroke of the main landing gear to 7.9 *cm*.

Table 8.26: Wheel dimensions.

Dimension	Value	Unit
Main wheel diameter	0.381	*m*
Main wheel width	0.152	*m*
Main wheel rolling radius	0.155	*m*
Nose wheel diameter	0.254	*m*
Nose wheel width	0.102	*m*
Nose wheel rolling radius	0.122	*m*
Inflation pressure	300	*kPa*

Landing gear strut design

The dimensions of the main gear strut can be seen in Figure 8.12. In designing the main landing gear strut the regulations from CS-VLA [12] dictate that three load cases must be taken into account: A three point landing, a two point landing, and side load condition. Of the three the two point landing is the most critical, with the main gear taking all of the weight of the UAV, but the strut is checked for all three cases. The two point landing load is combined with a braking force to find the most critical load case. The stresses are analysed at the root of the strut, where the moment from the applied force is at its greatest. As the gear must be strong enough to withstand the generated stresses, but still deflect sufficiently to act as a shock absorber. Near the wheel the bending stress are much lower, therefore the strut tapers towards the bottom. The cross sectional area is smallest at the tip, therefore the axial stresses will be the greatest there.

Table 8.27 gives the maximum stresses in a single strut of the main landing gear. As can be seen the two point landing is indeed critical. Because of the requirements on gear stroke quite a high deflection is needed. In order to be able to easily manufacture the tapered main beam strut, the part will be die cast. This boasts lower mechanic properties but makes the part cheap and rapidly producible. Therefore casting aluminium B390 was chosen for the main landing gear struts. A sensitivity analysis has also been carried out, to see what kind of tolerances have to be placed on the manufacturing of the strut. These can also be seen in Table 8.27. 5% of the length has been subtracted from first the height and then the width of the root cross section and then the strut was re-analyzed. The axial stresses are so far below the buckling stress that they have not been revaluated.

For the nose gear the same procedure was followed as for the main gear. The regulations specify three different load cases on the nose gear: an aft load, a forward load and a side load. The maximum static load on the nose gear is taken as the force on the nose with the center of gravity at the most forward position. The nose gear strut is a thin walled tube, as can be seen in Figure 8.13 together with the dimensions. The maximum axial stresses were found to be at most 0.9% of the critical buckling load, and thus they were not taking into consideration when checking the sensitivity of the design.

Finally a cost estimation is made of the landing gear, as seen in Table 8.29. The main wheels are relatively expensive because they include the braking system. The cost estimation of the struts was based on a casting cost estimate, with a margin included for personnel and overhead.[5]

[5]URL `http://www.custompartnet.com/estimate/`[Cited on 27/06/2016]

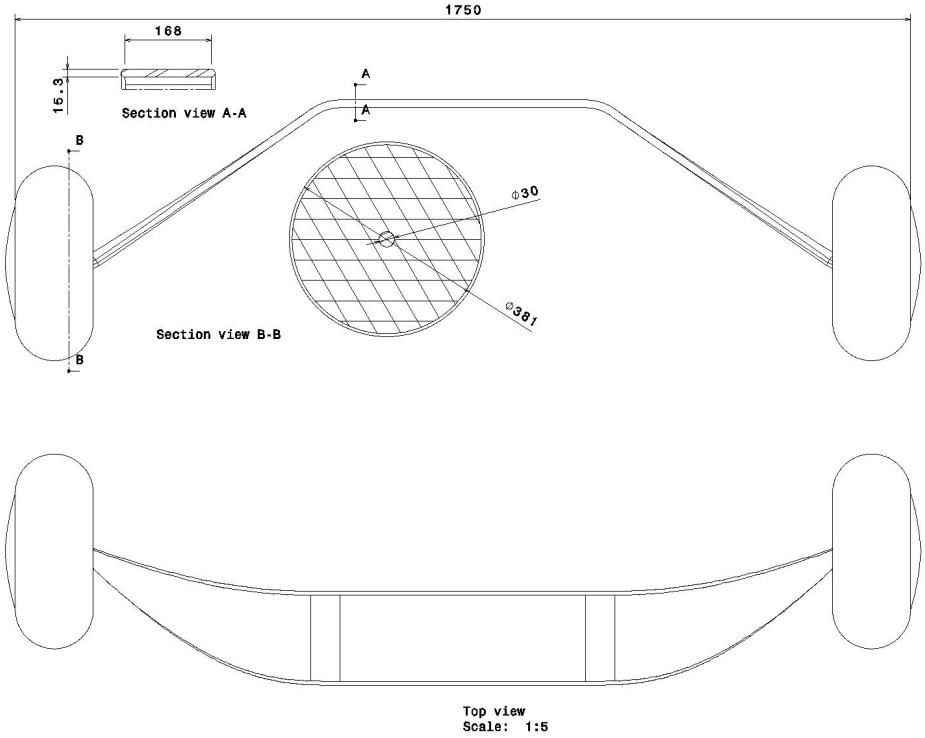

Figure 8.12: Main landing gear view.

Table 8.27: Main gear strut stresses and deflections.

Dimension	Value	Value -3% width	Value -3% thickness	[Unit]
Aluminium B390 yield stress	250	-	-	*MPa*
Critical buckling stress	324.6	-	-	*MPa*
2 point landing: Main gear maximum bending stress	234.7	241.6	249.8	*MPa*
2 point landing: Main gear maximum normal stress	6.5	-	-	*MPa*
Side load : Main gear maximum bending stress	115.0	118.3	122.4	*MPa*
Side load : Main strut maximum normal stress	4.9	-	-	*MPa*
Deflection at maximum load	5.1	5.3	5.6	*cm*

Table 8.28: Nose gear strut stresses and deflections.

Dimension	Value	Value -3% width	Value -3% thickness	[Unit]
Aluminium B390 yield stress	250	-	-	*MPa*
Aft load max bending stress	2.9	3.2	3.0	*MPa*
Forward load maximum bending stress	117.5	130.2	123.7	*MPa*
Side load maximum bending stress	106.4	117.9	112.0	*MPa*

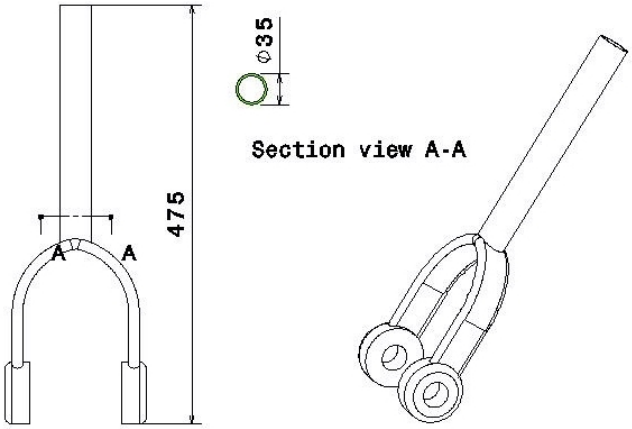

Figure 8.13: Nose landing gear view.

Table 8.29: Landing gear mass and cost summary.

Parameter	Mass [kg]	Cost [€]
Main gear strut	12.48	126
Main gear wheel and brakes	2.95	395
Nose gear strut	1.10	21
Nose gear wheel	2.00	91
Total	**18.53 kg**	**€633**

8.5 Tail structure

Loads on tail control surfaces

The loads on the tail surfaces are determined according to regulations. To determine the loads on the horizontal tail CS-VLA 423 and Figure B2 of Appendix B of the CS-VLA are used. From this table is found that the limit maneuver load increment is 690 N. The maximum static control load during cruise is 244 N. Furthermore, the force on the horizontal tail due to a limit maneuver is 625 N. Therefore, the limit total force on the tail can be up to 1560 N.

Tail structural concepts

For the connection of the tail to the fuselage three possible structural concepts have been proposed. To keep the cost down, the structure should be as simple as possible. The more complex parts, the more man hours hence more production cost. The concepts are sketched in Figure 8.14.
The first concept consists of a simple circular beam connecting the tail with the fuselage. These concepts has been proven by a lot of UAVs such as the Raven UAV. This concept is very simple and therefore popular in UAV design. However, for heavier UAVs with the size of a utility plane it is much less common. The beam will have a constant thickness and cross-section when produced by extrusion and therefore becomes less efficient in terms of weight as the loads at the neighbourhood of the fuselage are much higher due to the moment arm.

Connecting struts from the bottom of the fuselage to the main beam can reduce the weight of main beam by carrying part of the bending loads. The decision was made to load from the back, so the struts should be removable from the main beam to ease loading. The struts can be connected by hinges to the fuselage so that the struts rotate to the ground and the payload can be loaded.

The last concept consists of a complete truss structure. This concept is applied in a lot of structures for its simplicity. It can also be more optimized for weight as the thickness of the struts can be varied over the beam length. Furthermore it can take bending loads much easier as the structural weight is present at a much further location from the center of area (of the cross-section) compared to a single beam.

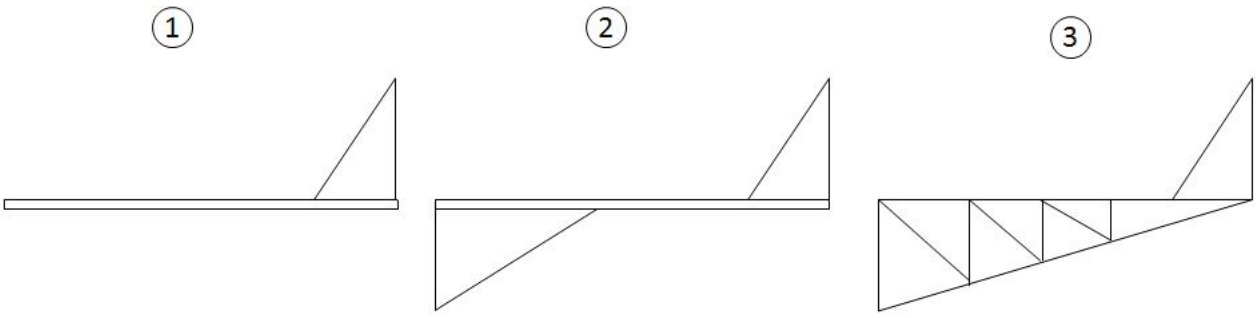

Figure 8.14: Tail structural concepts.

However the structure needs to be welded which is a rather expensive process for aluminium. Steel would be a better solution for a welded structure, but will make the structure heavier. Furthermore welding is a time consuming process and is difficult to automate for large production series. Besides the whole structure would need to be hinged or removable to be able to load from the back.

A summary of advantages and disadvantages of the three concepts is given in Table 8.30.

Table 8.30: Trade-off concepts for tail structure.

	Advantages	**Disadvantages**
Single beam	Very simple structure Low production cost	High structural weight More difficult to integrate in fuselage
Supported beam	Lower structural weight	More difficult handling Struts in compression
Truss structure	Easier integration with fuselage Lowest structural weight	More difficult handling Needs hingest at highest load location High production cost and complexity

From Table 8.30 it can be concluded that both cost and handling aspects make the third concept unattractive for the current design and therefore excluded from the possible concepts. The decision between the two other concepts will be determined by whether the supporting beam can have a weight advantage and if this advantage outweighs the extra complexity and cost. This section will proceed with a structural analysis to determine the weight of both concepts.

Concept analysis

Loads from the tail need to be introduced into the fuselage. These loads cause shear, bending and torsion into the fuselage. The drag on the tail causing tension in the beam is neglected for the reason that the drag force is considerably lower than the lift produced by the tail surfaces and tension loads can be carried easy by the beam. Also the aerodynamic moments of the tail surfaces are neglected since the tail have symmetric airfoils.

The loads on the tail surfaces are determined by CS-VLA and calculated in Section 8.5. The loads on horizontal tail are 1560 N and on the vertical tail 500 N. The length of the beam is determined by distance between the aerodynamic center of the tail and the location where the beam is attached to the fuselage. This length can be calculated by Equation (8.31). Since both horizontal and vertical tail have the same plan form, both tail arms are the same. The input values of Equation (8.31) where determined using the design parameters.

$$L_t = x_{LE_{tail}} - (x_{fuselage} + L_{fuselage}) + xlead_{MAC_{tail}} + 0.25 \cdot MAC = 2.5m \tag{8.31}$$

The loads on the cross-section of the beam at the location of the fuselage are given in Figure 8.16. The worst case scenario is that both horizontal and vertical tails produce their maximum loads according to certification specification.

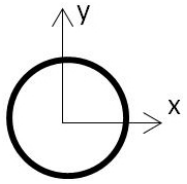

Figure 8.15: Tail beam reference system.

Figure 8.16: Loads on tail structure.

F_x	1.560 kN
F_y	0.5 kN
M_y	3.9 kNm
M_x	1.25 kNm
T	0.323 kNm

In concept 2 the single beam is be supported by struts connected to the bottom of the fuselage. This can be either one strut in the middle of the fuselage, or two struts to both ends of the fuselage. There are two reasons to go for only one strut. The width of the fuselage is rather small compared to the height, implying that the arm of the supporting strut is small and hence the loads will be higher to counteract a certain moment. Besides the loads on vertical tail are much lower and hence the moment is also lower. When designing for the horizontal loads even with a supported strut the beam would be able to handle loads from the vertical tail as the thickness of the beam is homogeneous. Therefore the extra structural material would be ineffective for counteracting loads from the vertical tail.

A FBD of the supported strut is given in Figure 8.17. The main beam will be clamped to the fuselage and will be able to react to the moments. The strut has to be hinged as it needs to be removed during loading. The connection point to the main beam will have to be made detachable. The strut will only take loads in the direction of its axis. To be able to solve for the force of the strut, it is assumed that the structure is designed such that the reaction moment equals $F \cdot Le$. The idea is that the beam can be sized for the loads as if the moment arm of the tail is Le. Now the force in the strut can be calculated using moment and force equilibrium.

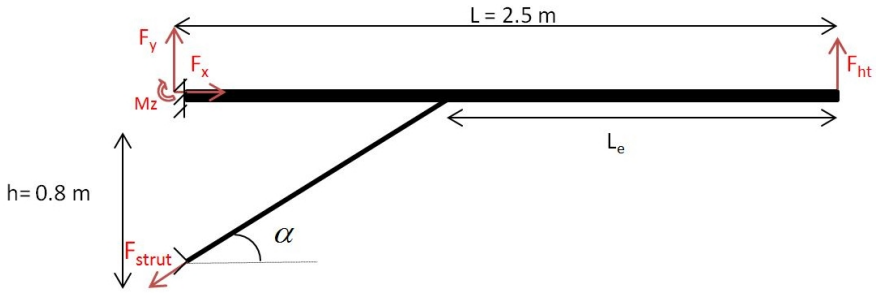

Figure 8.17: Free body diagram of the supported beam.

Weight comparison

A weight comparison has been made between a single beam and a supported beam. This was done using the load from only the horizontal tail as load case. The two structures are designed taking into account bending, shear, normal stresses and buckling in the strut. In Figure 8.17 the force acts in an upward direction, but acts in a downward direction in certain flight phases. This will cause compression, and hence the possibility of buckling of the strut. In this analysis, the yield stress, modulus of elasticity and density is taken to be 250 MPa, 68 GPa and 2700 kg/m^3 (general aluminium alloys). Also the limit for extrusion is taken into account. The thickness of the tube cannot be lower than 1 mm. The angle α (see Figure 8.17) has been optimized for a certain strut diameter and load case. The strut diameter has been chosen such that the angle α coincidence with the upsweep angle of the UAV and the strut has the possibility to be integrated into the tail cover. The result is summarized in Table 8.32.

Conclusion on tail structure concept

It was calculated that the supporting structure reduce the weight by 34%. The weight savings are not considered high enough to go for a more complex structure which would require a higher cost. Therefore the concept with only one beam (concept 1) is chosen.

Table 8.32: Weight comparison single beam to supported beam.

	Single beam	Supported beam
Diameter main beam (mm)	80	80
Thickness main beam (mm)	2.5	1
Mass main beam (kg)	3.8	1.7
Diameter strut (mm)	/	45
Thickness strut (mm)	/	1
Mass strut (kg)	/	
Total mass (kg)	3.8	2.5

Mass and cost tail structure

Extruded aluminium tubes can be bought off-the-shelf and are therefore the most attractive solution. Extruded profiles can be easily provided by a lot of metal companies. An example beam is given in Table 8.33[6]. The price of manufacturing the tube to be connected to the fuselage is not included in the price. Aluminium tubes of 80x2.5mm have been found but without price. It is assumed that a tube of 80x2.5mm has the same price.

Table 8.33: Off the shelf aluminium beam.

Diameter	80 mm
Thickness	2 mm
Material	Aluminium
Mass	3.4 kg
Cost	€31.2
Manufacturer	Pext

Verification and Validation

A single aluminium beam of 80x2.5 mm as tail structure was analyzed together with the fuselage structure using FEM (see Section 8.2) and did not fail under ultimate loads. To validate the results it is recommended to do an ultimate load test with the tail beam.

8.6 Empennage structure

The inner structure of the tail wings is also made from foam and inserts. The limit load in the horizontal and vertical tail surfaces are determined in Section 8.5. Furthermore, for a safe-life approach of the tail for regulations, the stresses at limit load should not exceed half the ultimate strength of the load bearing materials. The skin of the tail surfaces will also be made from aluminium 5182-H19 for the reasons as explained in Section 8.1.

Empennage wing design

For more effective manufacturing the vertical and horizontal tail surfaces are the same. This will have the consequence that one of the two surfaces will be over-designed, however the manufacturing can be more cost effective. From the loads which act on the tail wing surfaces can already be seen that the loads on the horizontal tail are more demanding for the structure than the loads on the vertical tail, so the vertical tail will have the same design as the horizontal tail.

The skin thickness should be 0.4 mm at the root to achieve the regulation requirement of the stresses. This is validated by using FEM analysis. Furthermore, the foam core fills up the complete wing to maintain the shape of the wing during flight. There are two inserts per wing. These inserts are used to

[6]URL `http://www.pext.nl/aluminium-ronde-buis-80x2` [Cited on 19/06/2016]

transport and carry the loads which act on the elevator or rudder. The actuator of the elevator can be placed in the root insert and therefore no wires of other components have to be placed into the foam core.

Elevator design

The elevator design will also be made from an aluminium skin and foam core. This has the same reasoning as the aileron and flap design. The heat of some of the operating environment can soften plastic parts and make them too soft for operation. This would limit the operation and therefore it is not used.

Final empennage weight and cost

The weight and cost of the empennage are shown in Table 8.34.

Table 8.34: Mass and estimated cost of empennage

Component	instances	mass (kg)	Material Cost (€)	Production cost (€)	Assembly cost (€)
Skin	3	3.4	10.2	60	60
Core	3	4.8	34.1	120	60
Root insert	3	5.0	31.5	30	30
Tip insert	3	0.2	1.3	15	30
Elevator skin	3	2.2	5.1	30	60
Elevator core	3	1.8	12.8	45	60
tail connector	1	1.9	4.5	30	0
tail connector cover	1	0.5	3.2	40	0
Total	20	19.8	100	370	300
Total mass	19.8	[-5%,+10%]	**Total cost**	770	[-10%, +30%]

The material cost of the aluminium, plastic and foam is explained in Table 8.1. The skin of the empennage can be made by stretch forming. When this method is used, the skin can be produced from one sheet. The cost per skin is assumed to be €20, this includes the time to put the sheets into the machine, the production time of the machine itself. The core production cost are assumed to be €40 per core. This includes the time to fill the mold with expandable foam and finishing the core after removing it from the mold. The production cost of the root inserts contain the manufacturing time. The cost for the elevator skin and core, and the tip insert are determined in the same way as the skin, core and root insert of the wing. Furthermore, the tail connector can be made by casting. This production cost include the setup time of the casting mold and the finishing of the parts after casting. The production cost of the tail connector is assumed to be €30. Finally the aerodynamic cover of the tail connector has an estimated production cost of €40. The production will be done by injection molding and the cost contains the production time. For the assembly costs an assembly time per part is assumed and multiplied by €40/hr.

8.7 Nose and tail cover

It was assumed in the structural analysis that the nose and tail covers are non-load bearing. Therefore these can be made either out of thin aluminium plates or plastic.

Nose cover

For the nose cover aluminium is the chosen material due to plastic not being a safe possibility with the heat generated by the engine. Furthermore the nose cone needs to cope with impact and vibrations loads of the engine. Aluminium plates can be manufactured to the right shape by forming the sheets. Either press forming or rubber forming could be used to form the aluminium sheets. The advantage of rubber forming would be that there is only one product related tool required and therefore no matching tools are required, reducing the cost. The disadvantage is that a large press force is required and these

are expensive. Furthermore the cycle time is rather high, making the process cost effective for only low production series (100-2500 parts).

The cost estimation is started with an off-the-shelf 1 *mm* aluminium treated sheet with a price of €12/m^2[27] and a nose cover area of 1.23 m^2 resulting in a material cost of €14.76 per nose cover half. Then this sheet is cut to the right shape which takes roughly 15 minutes at €40 per hour labour cost and pressed in a rubber forming machine, which takes another 15 minutes. Furthermore it is assumed that the rubber press costs €50 per use, which results in a nose cover half price of €64.8. The rubber press costs are higher here than for the fuselage parts as this part requires more complex curvatures and needs to be pressed deeper, requiring a larger machine. This price is doubled to account for the second half of the nose cover and then another 30 minutes labour is taken into account for trimming and assembly, resulting in a total price of €170.

Tail cover

Plastic shapes can be manufactured using injection moulding or vacuum forming. The equipment and mould cost for this process are rather high. However it has a low cycle time, making the process attractable for high product series. A simple bending test simulating actual flight loads should be performed on the beam to validate the results. For the price estimate long plastic storage boxes were looked at due to their shape and thickness similarity to each of the tail cone halves. The average of two of these boxes is used as the base for the cost estimation. The first one is a 100 *cm* long, 40 *cm* wide and 18 *cm* high and costs €9.09 per box (excluding tax and shipping) when ordered in a quantity of 90 or more[8]. The second box is slightly longer at 101.6 *cm*, wider at 51.8 *cm* and slightly less high at 17.8 *cm*. This box costs €26.88 per box (excluding tax and shipping) when 40 or more boxes are ordered[9].

A factor of 3 is applied to the average of €18.00 to account for the larger size of the tail cone at 171 *cm* length, 70 *cm* width and 24 *cm* height and then the results is doubled to account for both halves of the tail cone, which results in a cost of €108. On top of this price four hinges is added at €3 each[10] and one latch costing €4.70[11]. These hinges and latches are mass produced and not designed specifically for aerospace usage, so are not the lightest possible design however are very cheap. Finally one hour of assembly time is taken using a cost of €40 per hour for drilling and attaching the hinges and latch. This brings the total of the tail cone to €165.

After contacting several companies asking for a quote, it seems that the long length of the tail cone forms a problem for most injection moulding companies. If no company can be found in the future with the capability to create a plastic shape with the required length, then each side of the tail cone will need to be split in half. Using the average price of the storage boxes, €18.00, for each quarter of the tail cone results in a cost of €72. Then the four hinges, latch and 1.5 hours of labour are added, resulting in €149.7. Then each front and back cover are attached at the top, bottom and twice on the side with small metal plates, costing €1 each, and then to keep the transition between the front and back cover on each side aerodynamic, the seam is covered with speed tape with a cost of €2[12]. Furthermore the type of fastener for the mounting plates requires careful attention as it will attach two different materials together. For this screw rivets are chosen as they have flat heads which is beneficial for drag and can be screwed into place with the ideal torsional level to not damage the plastic. Then the inside of the screw is closed with a nut to prevent the screw rivet from coming loose over time. This also allows for modularity of the tailcone parts. If the nut and screw rivet do start coming loose over time, then the crew rivet or nut could be welded to the metal plate. €1 is added to the price to account for these screw rivets[13], which brings the total for the tail cone built up out of four sections to €160. This is cheaper than the double part tail cone, as the plastic parts are easier to manufacture, however the tail as a whole

[7] URL https://www.aluminiumopmaat.nl/vlakke-aluminium-plaat.html [Cited on 27/06/2016]

[8] URL http://www.plasticboxshop.co.uk/home-storage-c1/bedroom-and-bathroom-organisation-c16/underbed-storage-boxes-c42/55lt-shallow-and-long-under-bed-box-with-lid-plastic-box-shop-pallet-deal-90-p1729 [Cited on 27/06/2016]

[9] URL http://www.justplasticboxes.com/Sterilite-Underbed-Storage-with-Wheels [Cited on 27/06/2016]

[10] URL https://www.alibaba.com/product-detail/Factory-Price-Bulk-Door-Hinges_60421008747.html?spm=a2700.7724857.29.3.NB5Ezp&s=p [Cited on 27/06/2016]

[11] URL https://www.alibaba.com/product-detail/Industrial-Equipment-twist-draw-latch_60425257824.html?spm=a2700.7724838.0.0.JsT97Q&s=p [Cited on 27/06/2016]

[12] URL http://www.aircraftspruce.com/catalog/cspages/3mproptape.php [Cited on 27/06/2016]

[13] URL https://www.alibaba.com/product-detail/ROHS-blue-zinc-plated-carbon-steel_60146075449.html?spm=a2700.7906341.35.1.wn3HrC&s=p [Cited on 27/06/2016]

is significantly less strong and less stiff and has more parts that could fail. Furthermore it will be more heavy.

Chapter 9

Payload and dropping mechanism

The mission of the UAV is to deliver a package of 20 kg to people in need with an accuracy of 25 by 25 m. To achieve this accuracy a specific drop procedure is required. This procedure is explained in Section 9.2. The drop mechanism design is explained as well in Section 9.1.

9.1 Drop mechanism design

The packages will be loaded at once by inserting a rack containing the packages in the UAV. As a consequence the dropping mechanism has to be in the rack. The rack should therefore have a electrical connection to the flight computer in order to activate the dropping mechanism during flight. Although the dropping mechanism itself is designed by VanBerlo the system around the dropping mechanism should be designed. The packages are stacked longitudinally with a fuel tank in between the third and fourth package above the landing gear. The dropping mechanism should be right on top of the center of the packages in order to drop the packages vertically, otherwise the packages can sit askew and as a result get stuck. Underneath the packages there will be doors which closes the bottom of the fuselage. There will be two doors in front of the main landing gear and two doors behind it. This is done because an open bottom results in vortices which increase the drag of the UAV. The doors will not be load bearing and are just simply plates with a spring which open because of the weight of the packages and close automatically when the package has left the fuselage.

9.2 Drop maneuver

For the dropping procedure two different situations have to be taken into account. Dropping in a warzone and dropping in regular disaster areas. In the first situation the UAV is cruising at an altitude of 1000 m to stay outside the range of small arms fire while in the second situation the UAV is cruising at an altitude of 150 m. In this section the two related dropping procedures are explained. A software programme is written to be able to calculate load factors and power loading and to visualize the drop procedure. This programme was developed based on the theory explained in Elements of airplane performance by Ger J.J. Ruijgrok [19]. All calculations are performed at the service ceiling of 3000 m. This is considered to be a conservative assumption as many maneuvers such as the climb maneuvers will be performed at a lower altitude.

Warzone drop

The scenario of a besieged city is assumed for a warzone drop. Dropping aid in a besieged city is a realistic scenario nowadays. For example, the city of Deir-ez-zor in Syria was besieged by ISIS in June 2016[1] and the Red Cross performed food droppings in the area.

Fly-in and first loiter

The drop maneuver starts with a fly-in and a loiter phase with a radius of 1100 m. During this loiter phase the go/no-go signal is received. For safety reasons this loiter phase is performed at cruise altitude as the small arms fire can not harm the UAV at this altitude. It might be that the besieged city is taken over by hostile groups which would mean that the UAV should not drop the supplies. In Figure 9.1 the fly-in and loiter phase are shown.

First descend

The first descent is a descent towards 150 meters while spiraling. In Figure 9.2 the descent motion is presented.

Second loiter

The next phase is the second loiter at 150 m altitude. During this loiter (radius is 1100 m) the wind direction is measured using GNSS, pitot tube and magnetometer. AvioniCS stated that using these instruments the wind direction can be determined. This is necessary because the UAV may not have

[1] URL `http://nos.nl/artikel/2108691-voedseldroppings-syrie-zijn-laatste-redmiddel-voor-rode-kruis.html` [Cited on 06/06/2016]

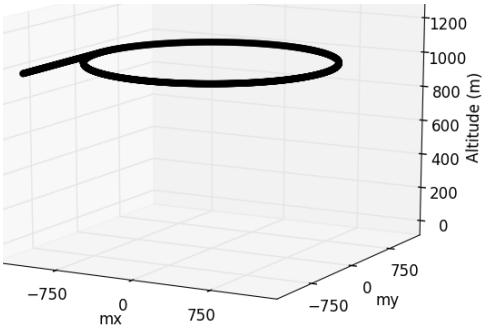

Figure 9.1: Fly-in and first loiter. V= 43 m/s, N=1.014, R=1100 m.

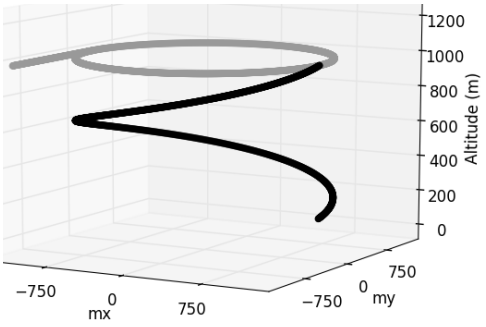

Figure 9.2: First descent. V= 43 m/s, N=1.017, R=1100 m, RD=5.2 m/s.

any backwind while dropping as the groundspeed will be too high. This wind direction determination is not required to be very accurate as a rough estimation is enough. In Figure 9.3 the second loiter phase is presented.

Turn towards approach heading

When the approach heading is determined based on the wind direction the UAV performs a turn with a constant radius of 410 meters. To be able to maintain the constant radius while turning the UAV flies in a straight line, tangent to the loiter circle at the point where the UAV leaves this circle. This is done for the sake of easy computation and analysing. It is a conservative maneuver and other maneuvers are very well possible. In Figure 9.4 the flight path of the drone during the turn is presented.

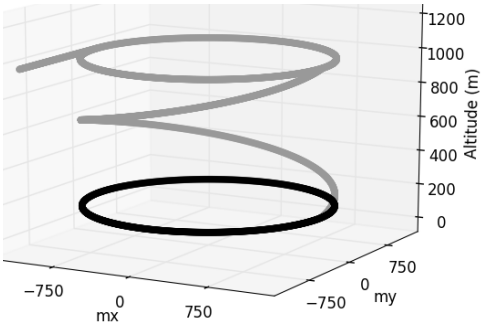

Figure 9.3: Second loiter. V= 43 m/s, N=1.017, R=1100 m.

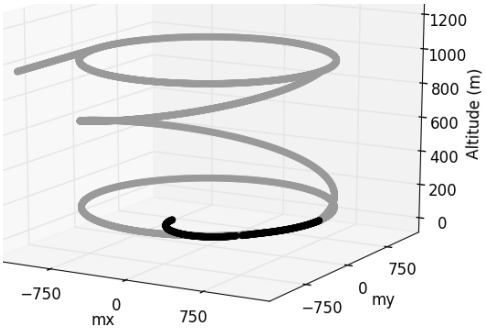

Figure 9.4: First turn. V= 30 m/s, N=1.02, R=410 m.

Final descent, dropping maneuver and climb

When the UAV is headed towards the dropzone the final descend commences. The UAV descends with a rate of 6 m/s while slowing down linearly to 23.7 m/s flight velocity which is 1.1^2 the stall speed at 3000 m. The UAV is at 15 meters when the fly-in zone is reached. After the drop the UAV climbs back to 150 m altitude with a maximum, constant rate of climb of 4.25 m/s with a flight velocity of 25 m/s. It is important for safety reasons that the UAV climbs as fast as possible which is the reason why the highest rate of climb procedure is chosen. In Figure 9.5 the flight path is presented.
Drop accuracy requirements lead to the decision of performing a ballistic drop of the packages while making use of a guiding parachute to ensure the preferred orientation of the package when falling towards the ground. Inaccuracies in position determination and altitude determination, wind deviation and velocity inaccuracies induce a limited range in which the UAV can still drop the package. This can be seen in Figure 9.6. The bigger green circle represents the area in which the UAV has to fly to be allowed to send the signal for dropping assumed it is headed towards the center of the dropzone. The maximum distance from the center of the dropzone (blue, smaller area) is 51.2 m while the minimum distance is 42.1 m. In the calculation it is included that the delay between the signal of the release system and the actual start of the ballistic drop is 0.4 s. This value should be determined experimentally when the first prototype of the UAV is operational as it is very difficult to model these properties beforehand.

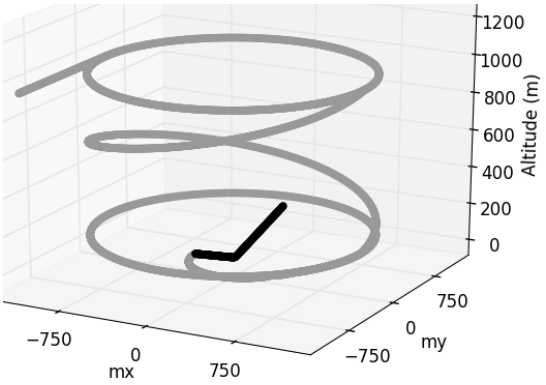

Figure 9.5: Final descent and climb. V= 25.02 m/s RD= 6 m/s. RC=4.2 m/s.

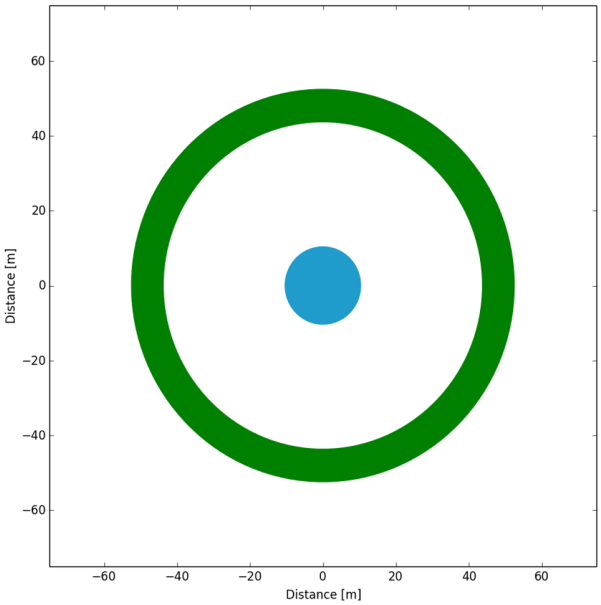

Figure 9.6: Drop margin including uncertainties and deviations.

The final velocity of the package is 18.3 m/s in the horizontal plane and 17.6 m/s in the vertical plane. The assumptions made are listed in Table 9.1.

Table 9.1: Assumptions and deviations of drop maneuver.

Type of deviation	**Magnitude of deviation**
Mass package + parachute	22.0 kg
C_d package+parachute	1.05
Reference area of package	0.23 $m2$
v-horizontal uncertainty	0.22 m/s
Altitude uncertainty	1.4 m
Drop delay	0.4 s
Wind deviation	2.15 m

The mass of the package is the prescribed mass of the supplies including the packaging material. As stated in Table 9.1 a guidance parachute mass is included as well. The C_d of the package including parachute is obtained from [30]. The uncertainties in altitude and position are retrieved from experts from the company AvioniCS. The wind deviation is determined through a self developed programme. The wind velocities induced by the Bell Huey flight conditions requirement impose a small deviation of 2.15 m but is quite significant considering the small falling time of the package (ca. 1.8 s).

Second turn and final climb

After the UAV has climbed to 150 m it will perform a horizontal turn towards the original loiter circle. After this turn a climb towards 1000 m at the maximum climb rate of 4.2 m/s is performed after which the UAV flies off to its new location. Also during this maneuver it is important for safety reasons that the UAV climbs as fast as possible. The sooner it is at a higher altitude the sooner the parachute can be deployed if required and the sooner the UAV is beyond the range of small arms fire. Due to the climbing while turning the maximum climb rate is lower than the normal maximum climbrate. The theory used for this computation can be found in Ruijgrok [19]. The maneuvers are shown in Figure 9.7. It should be noted that the radius of the upward spiraling climb is larger than the descending one presented in Figure 9.2. This is decided to make sure that the UAVs are less likely to crash into each other.
The total time of this maneuver without fly-in and fly-out is 13.8 minutes. This means that for the war

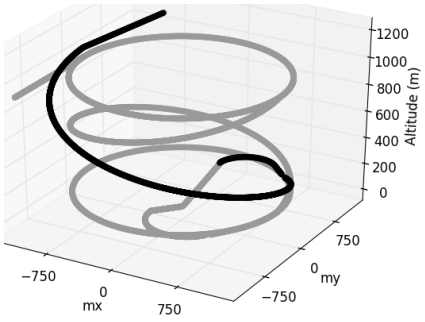

Figure 9.7: Turn, second climb and fly-away. V_{turn}= 30 m/s. R_{turn}=451.1 m, N=1.02, V_{climb}= 25.0 m/s, CR=4.2 m/s.

zone operations five times 13.8 minutes should be taken into account for the dropping procedures.

Normal drop procedure

The normal dropping procedure start off at an altitude of 150 m. It will start with a fly-in followed by a loiter phase in which a go/no-go signal will be received and the wind direction will be determined. This is presented in Figure 9.8.

Final descent, drop approach and fly-out

The final descent and drop approach is exactly the same compared to the war-zone procedure and is therefore already explained in Section 9.2. The maneuver is shown in Figure 9.9.

Also the last phase of the procedure is very similar to the phase described in Figure 9.9 except that in the normal case a climb to 1000 m is not required as 150 m is already the cruise altitude of the UAV. The extra turn is not necessary as well.

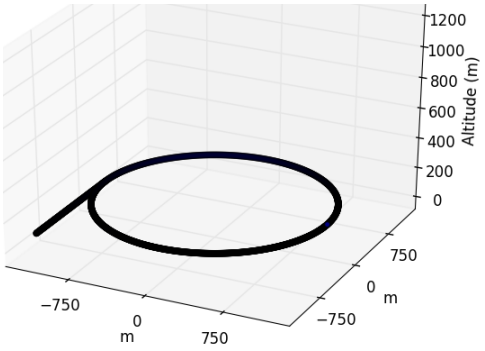

Figure 9.8: Fly-in/loiter period.

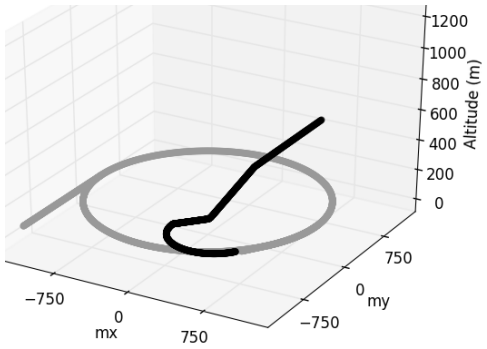

Figure 9.9: Final descent and climb. V_{turn}= 30 m/s, N=1.02, R=410 m, V_{climb}= 25.0 m/s, CR=4.2.

The total duration of this maneuver without fly-in and fly-out is 4.5 minutes. This means that for the normal operations five times 4.5 minutes should be taken into account for the dropping procedures.

9.3 Functional flow of dropping

In Figure 9.10 the flow diagram of the dropping maneuver is given. In the top level all the general functions are given. The other general functions are stated in different sections. The assemble UAV, load and prepare UAV, Landing & turnaround and ending mission are stated in Section 11.7 because they are mostly affected by the ground operations. The take-off function is stated in Section 6.4 as it is most dependent on the performance of the UAV.

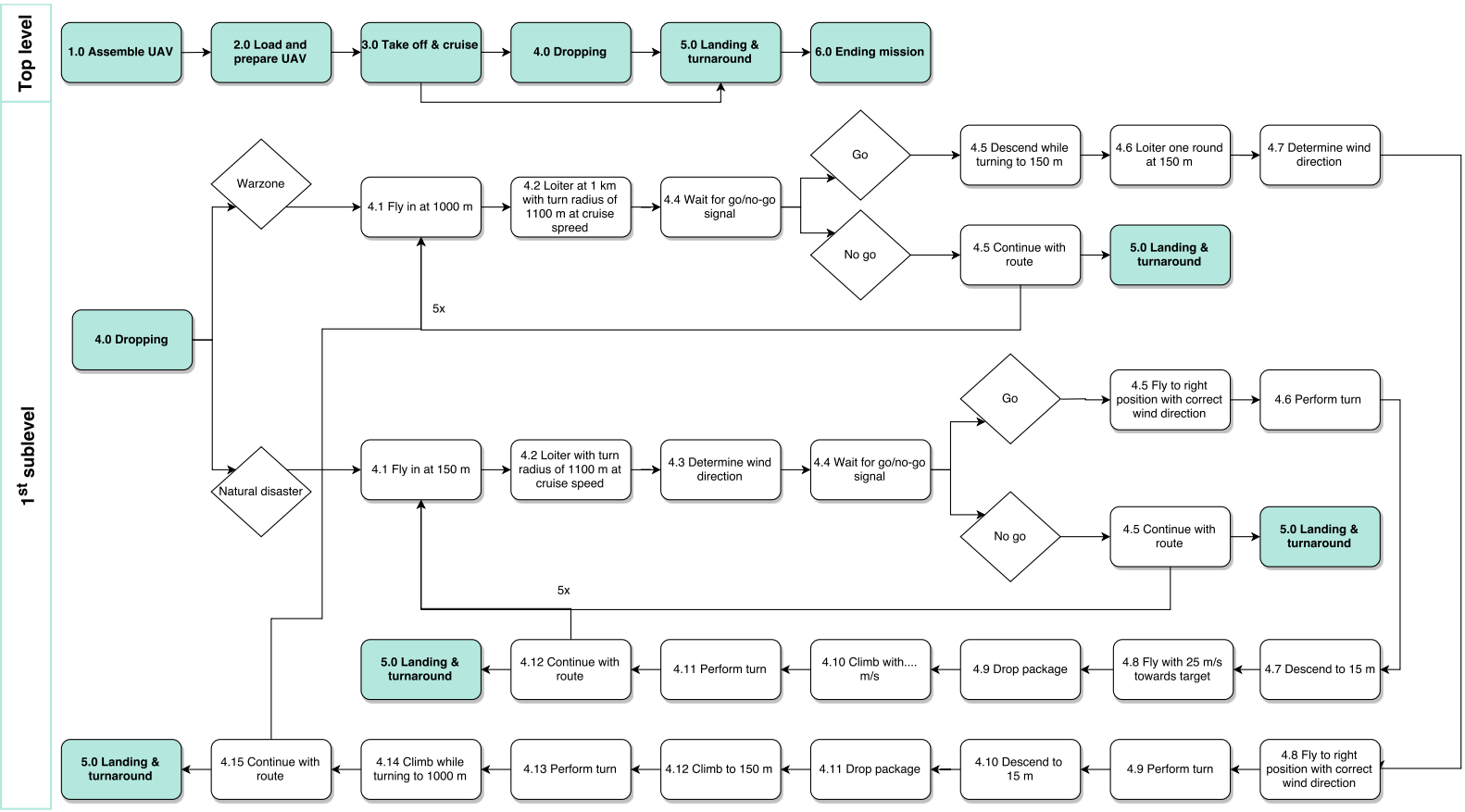

Figure 9.10: Flowchart of the dropping maneuver.

9.4 Verification and validation

The software written to analyse the dropping procedure is checked to make sure that no errors are made. A critical look was taken at all the climb rates that were computed. An example of an errors that was discovered by this critical look was the fact that the climb rate during turn turned out to be higher than the climb rate during normal climb. This is of course not possible which is why thorough debugging of the code is performed after which the code was adapted. The results of the code was visualised and the visualisations are a good way of checking the code. The requirement of the 25 by 25 meter drop accuracy is hereby met. The assumptions made are listed in Table 9.1. These are based on values obtained from AvioniCS and other experts. When the package is released in the green zone as showed in Figure 9.6 the package will with a great likelihood land in the dropzone. Validation of this requirement should be done experimentally when the first dropping mechanism or prototype is ready. The signal delay should be determined experimentally as well.

Chapter 10

Auxiliary UAV systems

In this chapter the auxiliary systems are explained, starting with the fuel system in Section 10.1. This is then followed by the exhaust gas temperature probe in Section 10.2, the wheels and braking systems in Section 10.3, the anti-icing systems in Section 10.4, the firewall in Section 10.5, the avionics in Section 10.6, the communication and navigation systems in Section 10.7, the collision avoidance in Section 10.8, the lighting in Section 10.9, the emergency systems in Section 10.10, the electrical systems in Section 10.11, the hardware and software interfaces in Section 10.12 and finally the communication within the system in Section 10.7.

10.1 Fuel system

In order to fulfill both the ferry ranges stated in Section 6.3 two fuel tanks are sized for the UAV. One for the normal operations and the other one for transporting the UAV over a large distance. The fuel tank for normal operation is stationed above the main landing gear because it is not possible to drop the packages at that location. It is chosen to take the same frontal area of the fuel tank as for the packages, with a required volume of 41.8 dm^3 this results in a fuel tank length of 19.0 cm. The regulation state that there should be room for a 2% expansion of the tank [12]. This results in a required space of 19.4 cm lengthwise. The large tank required for a large ferry range is located in front of the normal tank. To avoid sloshing in the tank the height of the fuel tank is chosen to be large and in order not to loose space a tank with the same frontal area of the other fuel tank and packages is chosen. This results in a fuel tank length of 72 cm. The required additional space because of the expansion rate will be 1.4 cm which results in a required space of 73.4 cm. When looking at off the shelf fuel tanks there are no fuel tanks which have a suitable price and dimensions for the UAV. Therefore it is chosen to have custom build fuel tanks, because of the minimum order size of 500 UAVs this should be possible for a reasonable price. Looking at the fuel tanks for ferry range the price will be around €450,- for a polyethylene tank and for the normal tank around €108,-. However the cost of the fuel tank for ferrying will be included in the operational cost because it is portable and can be used by other UAVs, the normal tank is included in the unit cost of the UAV. The flight envelope in Section 6.1 shows that there are also negative g-forces. In CS-VLA 943 [12] it is stated that the engine cannot malfunction under short negative accelerations like gusts. In order to avoid this malfunctioning there should be a non-return valves in the fuel hoses to avoid flowing back of fuel to the tank. The fuel hoses from the tank to the engine will have a length of 3.5 m and it is assumed that it has a diameter of 0.5 cm, this gives a volume of 0.068 l. The maximum fuel flow of the engine is 0.0046 l/s, this results in enough fuel for 15 s which is more than enough for a gust. The fuel hose length of 3.5 m comes from the fact that the fuel connection will be placed at the end of the fuselage in order to make it more accessible when loading the rack.

A fuel pump is already included in the engine and it is a Mikuni single exit fuel pump with a capacity of 14 l/h. No redundant fuel pump is included with the engine and will also not be added to the design to try to meet the cost budget. For safety and reliability, however, it is recommended to be included. A second, identical fuel pump will add roughly €20 to the price[1]. Furthermore a gascolator is included to the bottom of the tank to remove water, which is essential to prevent condensed water from entering the engine. A gascolator from the company ACS is chosen due to their reputation and low price at €65[2]. For contaminants other than water a fuel filter is used to prevent them from entering the engine. Here a Bosch fine fuel filter is chosen, again because the component is cheap at €5[3] and the company has a good reputation. Each Bosch fine fuel filter can remove 15 g of contaminants in total before replacement.

Finally for extra safety a pressure release valve will be included in the fuel tank to prevent pressure build up and so possible explosions if the fuel tank gets heated by for example the sun or an engine fire.

10.2 Exhaust gas temperature probe

An exhaust gas temperature probe measures the exhaust gas temperature which gives an indication of the engine health. This allows for engine failures to be predicted for less UAV in flight failures and

[1] URL `https://www.amazon.com/Mikuni-Fuel-Pump-Rectangular-DF44-227/dp/B000HS8RRI` [Cited on 18/06/2016]
[2] URL `http://www.rotaxservice.com/rotax_engines/rotax_582UL.htm` [Cited on 15/06/2016]
[3] See Footnote 2

longer times between maintenance. The Victor 1 Super operators manual[4] states that the exhaust gas temperature should never exceed 580°C during cruise and 600°C at maximum velocity. Furthermore the exhaust gas temperature is also used to calibrate the carburetters.

The chosen probe is a €91 Alcor probe[5] which is FAA and PMA certified and comes with a five year warranty. Simonini also provide an exhaust gas temperature probe as an option, which costs €113. As this can be shipped with the engine components, it does have a shipping cost advantage over the Alcor probe. However in this report the shipping costs are not taken into account, so the Alcor probe is used.

10.3 Wheels and braking systems

For the main wheels and brakes an ultralight brake kit is found that includes the wheels, rims and brakes for €395 [6]. This is an hydraulic system intended for use by a pilot with a lever and so will need modification for use with an electric servo. Unfortunately electric brakes are only used in heavy applications and are not available off-the-shelf in the required size for the UAV. For the nose wheel again an ultralight kit is used. This is the Hegar wheel kit costing €79 [7] and still requires a tire, which will cost €12 [8].

10.4 Anti-icing systems

In certain conditions there is a danger of ice growth, particularly in airflow stagnation areas such as on the leading edge of the wing and tail surfaces, and on the leading edge of the propeller [31]. This can affect the aerodynamic performance of the UAV, increasing drag and impeding control surface movement. In large quantities it can prevent the UAV being able to maintain altitude and so likely causing a crash.

Icing conditions are most prevalent at temperatures below freezing point, between -20 and 0 °C [32]. Since the UAV will be flying between 1000 m and 1500 m in height, the expected temperature obtained from the International Standard Atmosphere will be around 5 to 10 °C. Therefore icing is not expected to be an issue in the majority of the missions. However it does constrain the possible operations in cold areas, such as close to the poles or in mountainous regions such as Nepal. Although most of Nepal will still be accessible except on the coldest winter days as the capital Kathmandu has an average temperature of 9 degrees in its coldest month, January. To allow for operations in these area full de-icing systems could be integrated into the UAV with significant cost penalties. A certified de-icing system costs at least €15,000[9], so is well out of the price range and will not be used. An additional issue is that the cheapest systems use a foil wrap over the leading edge to then run electricity through it. This requires more power than the standard engine alternator provides and it will heat the surface preventing the use of the cheaper plastics.

Another cheap system is to integrate a system which leaks glycol or another anti-ice fluid out of the leading edges. This system will add roughly 30 kg to the aircraft, which is significant on out MTOW of 330 kg, and costs at least €20,000[10]. Another consideration is that anti-icing fluids are very toxic to the environment as they will remove oxygen from the ecosystem.

Another possibility is to apply anti-ice coating to prevent ice from being able to adhere to the UAV. The NEI Corperation anti-ice coating called NANOMYTE SuperAi will cost €24 and weigh 0.1 kg per UAV assuming a coverage area of 5 m^2 [11]. The coverage area is obtained using 50 cm coverage along the main wing span, 30 cm along the empennage surfaces and 5 cm along the propeller blades. This coating will reduce the ice adhesion strength by 40 - 50%[12] and so increase the possible operating conditions without using de-icing systems. However no references of such a coating being used on an aircraft were found, so it should be thoroughly tested before flying in sub zero conditions. For now, so before this coating has proven itself, the UAV will be limited to operational areas where the temperature is above

[4] URL http://www.flyproducts.it/manuali/manualieng/VICTOR1ENG.pdf [Cited on 14/06/2016]
[5] URL http://www.aircraftspruce.com/catalog/inpages/alcoregttit6.php?clickkey=14225 [Cited on 14/06/16]
[6] URL http://store.freebirdinnovations.com/product-p/bx44708.htm [Cited on 20/06/2016]
[7] URL http://www.aircraftspruce.com/pages/lg/nosewheels_hegar/hegarwbkits.php [Cited on 20/06/2016]
[8] URL http://www.aircraftspruce.com/catalog/lgpages/13-400-6.php [Cited on 20/06/2016]
[9] URL http://www.aero-news.net/index.cfm?do=main.textpost&id=4249a78c-f86e-456c-8209-822a12fa644a [Cited on 07/06/2016]
[10] URL http://www.flyingmag.com/safety/weather/madness-icing [Cited on 16/06/2016]
[11] Cost and weight information from email correspondence
[12] URL http://www.neicorporation.com/products/coatings/anti-ice-coatings/ [Cited on 07/06/2016]

the freezing point. Based on the International Standard Atmosphere model of the atmosphere, when the temperature on the ground (sea level altitude) is below 6.5 °C then our normal operations will start to be affected as the temperature at our optimal cruise altitude will be too close to 0 °C to fly safely. We will still be able to continue operations, albeit with a smaller range, until the ground temperature drops below 0.5 °C by lowering the cruise altitude. This is assuming that a 10 °C lower temperature at sea level will result in a 10 °C lower temperature at the cruise altitude, which is not a very accurate assumption for the higher cruise altitudes, however is suitable to get a feeling for the new allowable operating conditions. The client, Wings for Aid, has agreed to these restrictions in operating conditions in order to still try and meet the cost budget.

Other than the various leading edges across the UAV, some other systems need to be kept warm to prevent icing if in the future a Wings for Aid UAV is developed that can fly in sub-zero temperatures. These are the pitot tube, the engine air intake to prevent carburettor icing and a possible collision avoidance system to prevent ice from blocking the view of the sensors. Additionally the battery should be kept above 0 °C, because in sub zero conditions it will not charge any more. When the battery reaches -15 °C, then it will not be able to discharge either. Furthermore no ice should develop in areas which would hinder the dropping of the packages for the movement of the control surfaces.

10.5 Firewall

Behind the engine a firewall is required by CS-VLA regulations [12] to prevent a fire quickly spreading from the engine to the rest of the UAV. These regulations accept a stainless steel sheet with a thickness of 0.38 mm by default as a suitable firewall material. Using the fuselage dimensions of 58 by 75 cm results in a firewall weight of 1.28 kg. Furthermore it will cost roughly €30 [13].

Other considerations are that the fittings for the electrical wire and pipes that pass through the firewall must be fire and corrosion resistant. Furthermore the fuel tank must be at least 13 mm behind the firewall. This spacing is taken into account when designing the layout of the fuselage, so this regulation will be met. For extra safety a pressure release valve will be included in the fuel tank to prevent pressure build up to dangerous levels. Additionally when the surface of the firewall adjacent to the fire is heated to 1100 °C for five minutes the electrical system must be able to continue safe operation and not create any additional fire hazard. This will be obtained by ensuring that the electrical system is correctly grounded on both sides of the firewall, that the electrical system behind the firewall can operate safely without the alternator working, that the battery is placed away from the firewall and that the battery has enough energy stored at all times to continue operations for at least five minutes. Other materials in close proximity to the firewall must not ignite when the firewall is heated to 1100 °C for fifteen minutes, or must be able to self-extinguish. This will be achieved by only using metals for the surrounding structure, currently aluminium is used for the main structure of the fuselage. As aluminium has a melting point of 660 °C, this should be tested that the structure keeps structural integrity until the UAV has landed by emergency landing or by using the parachute. This parachute should additionally not be easily flammable and the attachment of the parachute to the core structure should be at a safe distance away from the heat.

10.6 Avionics

The avionics for the Wings for Aid UAV will be provided by Avionics Control Systems, or AvioniCS. The UAV has been designed while in contact with AvioniCS to ensure that all the required parts will have the power and space required and are in a suitable location. Furthermore the weights of the parts were taken into account for the UAV design. The following components will be provided by AvioniCS.

- Flight computer
- Inertia measurement unit (IMU)
- ADS-B receiver, transmitter and antenna
- GNSS receiver
- Electronic speed control (ESC) units
- Servos
- Battery
- Magnetometer
- Pitot tube
- Radio altimeter

[13] URL `https://www.metalsdepot.com/products/stainless2.phtml?page=sheet` [Cited on 10/06/2016]

- Electrical components such as wiring, fuses, grounding points and voltage converters
- Data cabling and other cabling needed for the systems to communicate

The flight control box will contain the autopilot computer and the IMU. AvioniCS recommended using a cast aluminium box such as the 546-1590BB box from Hammond Manufacturing[14]. This box weighs 222 g, costs €6 and has the dimensions 120 by 94 by 30 mm. This box is currently significantly oversized, which is to account for future black box components such as an emergency locator transmitter or an underwater locator beacon. These components will most likely be required by the EASA CS-LUAS regulations when released and so will be needed for the certification of the UAV.

AvioniCS have given a rough estimation of the price of all of these systems at €3000. To get an estimate if this budget is realistic the prices of each component were estimated through some market research in Section 10.7 for the Communication and navigation systems and Section 10.11 for the battery. The results can be found in Table 10.1.

Table 10.1: AvioniCS component price estimation.

AvioniCS component	**Price [€]**	**Price range [min,max]**
Flight computer	150	[-50%,+50%]
IMU[15]	1,500	[-20%,+10%]
ADS-B transeiver with GNSS and antenna	700	[-10%,+20%]
7 ESCs	140	[-40%,+10%][16]
7 Servos	140	[-10%,+40%][17]
Magnetometer[18]	200	[-10%, +5%][19]
Pitot tube[20]	300	[-10%, +5%][21]
Radar altimeter	500	[-20%,+40%][22]
Cabling	50	[-50%,+50%]
Battery	30	[-20%, +0%]
Total	**€3,660**	**[€2939,€4320]**

This shows that the AvioniCS budget is very tight, possibly too tight. To account for possible price increases in the future the prediced value of €3,660 is used for the rest o fthe cost estimates. The €3,000, may be feasible if some corners are cut, such as using a GNSS receiver with a very poor accuracy in the order of 5 m horizontally and 50 m vertically. Additionally electronics generally have bulk discounts which will help AvioniCS make the budget. The software and development costs are neglected from the unit price as per instructions from the client, Wings for Aid.

AvioniCS have also given an estimate on the amount ot power required for the avionics systems. This is 15 to 20 W and it will be shown in Section 10.11 that this is not a problem.

10.7 Communication and navigation systems

In order to be able to operate the UAV in certified airspace it must meet the regulators requirements. The two main challenges regarding the integration of unmanned vehicles into regulated airspace are the lack of on-board sense and avoid capability, and the vulnerability of the communications link to the

[14]URL `http://nl.mouser.com/ProductDetail/Hammond-Manufacturing/1590BB/?qs=sGAEpiMZZMsrGrAVj6eTvetfgLuTxoBa7awfOHMxXV0%3d` [Cited on 19/06/2016]

[15]Estimation based on communications with AvioniCS

[16]The high minimum is due to this being a pure electrical component so should have discounts in bulk.

[17]The high maximum here is due to the possibility that the cheap servos are not reliable enough.

[18]Based on URL `http://www.aircraftspruce.com/catalog/inpages/mglsp6.php?clickkey=50782` [Cited on 19/06/2016]

[19]The -10% is for the possibility of a bulk discount and the +5% is for if the chosen manufactorer can not produce enough units and another maunfactorer is needed.

[20]Based on URL `http://www.aircraftspruce.com/catalog/inpages/rvnjetpitot.php?clickkey=5714` [Cited on 19/06/2016]

[21]See Footnote 19

[22]No radar altimeters are readily available for ultralights and certified altimeters rapidly become very expensive, resulting in a large uncertainty.

ground [33].

The first step in airspace safety is making the UAV visible to other airspace users. This will be done by integrating an ADS-B OUT system in the UAV, which will broadcast information such as identification, locations, altitude and velocity. The information will be obtained from the UAV's navigation system. This information will allow other aircraft and ATC to determine the UAV's trajectory and notify it of possible collision.

The next step is that the UAV must be able to actively avoid collision itself. It will do this based on an Airborne-based Sense and Avoid (ABSAA) system which operates based on information received from cooperative aircraft. This means that the other aircraft must be actively broadcasting their position and velocity information. Already a large percentage of the worldwide fleet is equipped with ADS-B, and all commercial aircraft will be required to be equipped with ADS-B by 2020 [34]. This system will likely be integrable within the next 4 years [33]. Therefore the ABSAA system will be based on ADS-B information, and will allow the UAV to communicate automatically with surrounding aircraft. The autopilot will designate a hazard zone in which another aircraft becomes a threat to the UAV, and will take corrective action to avoid a collision, before returning to its original path towards the waypoint.

The navigation and communication system will be designed by AvioniCS, one of the partner companies of the Wings for Aid consortium, however to get a gauge on the power and weight of these systems a market research is done. It is found that the cheapest available complete ADS-B system is provided by uAvionix and costs €1780[23]. It is built up of a ADS-B transceiver[24], which is a combined transmitter and receiver, and a navigation source[25], which combines the functions of a GNSS receiver and a pressure altimeter with an accuracy of 10 cm. Furthermore they are fully certified, have a combined weight of 50 g and average power use of 0.5 W at 6 V for the transceiver and 0.5 W at 5 V for the navigation source. The transceiver uses 30 W at peak power for 400 μs whenever it transmits. This set up does still require an antenna which will weight 20 to 30 g and cost roughly €25[26]. Overall the weight and power are not a problem within the mass and power budgets, however the price is quite high as it is over half of what AvioniCS estimated that they would need for the complete avionics system. We expect that AvioniCS can build this system much cheaper by not certifying the system and by using bulk discounts which are significant for electronics. Additionally not all of the features in the uAvionix system are required in the Wings for Aid system, such as the backup battery, high sensitivities and large operating temperature range.

10.8 Collision avoidance

With the communication system preventing collisions between UAVs and other aviation vehicles in the airspace another collision avoidance system is required to detect objects near the UAV and prevent it crashing into objects without a transponder such as buildings, poles, mountains and other tall objects. It will also help prevent accidents if a transponder fails. For the obstacle avoidance various options are possible. These are radar, optical, and LiDAR, or Light Detection And Ranging. Radar has the largest sensing range and is the least affected by weather, however requires a large sensor, which increases weight and drag [35]. Optical sensors are the cheapest and smallest sensors, however it requires daylight, descent weather conditions and large amounts of computing power [35]. The final option, LiDAR, provides a middle road in terms of size, costs and weather conditions. However the cheap units do have a short range and small field of view. The cheapest unit is the LiDAR-Lite v2 which costs €132[27], has a range of 40 m, an accuracy of +/- 0.025 m, an acquisition time of 0.02 and consumes 0.5 W[28]. The range of 40 m can be problematic as it will provide 0.9 seconds of warning before impact at the cruise speed of 43 m/s and 2.2 s at the stall speed of 18.2 m/s at 1500 m. Another issue with this system is that it is not a full LiDAR system as the laser does not scan, but is static. Therefore it will only be able to detect large obstacles directly in front of the UAV such as a building or the ground, making this device very useful for landing. A scanning LiDAR system would cost at least €1000, not including software, making it unfeasible.

To prevent collision with the ground a radar altimeter system will be included as a ground proximity warning system. This will additionally help to accurately determine the altitude of the UAV during

[23] URL `https://www.unmannedsystemssource.com/product-category/atc-devices/` [Cited on 16/06/2016]
[24] URL `http://www.uavionix.com/products/ping2020/` [Cited on 16/06/2016]
[25] URL `http://www.uavionix.com/products/pingnav/` [Cited on 16/06/2016]
[26] URL `http://www.aircraftspruce.com/catalog/avpages/monopole11-13561.php` [Cited on 16/06/2016]
[27] URL `http://www.robotshop.com/en/lidar-lite-2-laser-rangefinder-pulsedlight.html` [Cited on 07/06/2016]
[28] URL `https://www.sparkfun.com/products/retired/13680` [Cited on 07/06/2016]

landing and greatly reduce the height over which the UAV can pass the screen height during landing approach and so reducing the landing distance. Another option was to use the barometer to determine the altitude a low altitudes. Cheap barometers can have accuracies of 0.3 m[29], however are relative and so need to calibrated with the pressure on the ground to be accurate in the absolute sense. This calibration can be done easily with someone on the ground who also has a barometer, however this requires a barometer to be present at every drop site which is a logistic challenge and additionally if the barometer at one of the drop sites fails, then no more packages can be dropped to that area. Additionally this could create issues when flying at the non-warzone cruise altitude of 150 m away from the areas when the on ground barometers are, as local drops in pressure would cause the UAV to think that it is flying higher than it actually is an so create the danger of flying into tall obstacles such as flats and hills.

10.9 Lighting

Another important way to avoid collisions is to be visually seen by other aircraft by using lighting. The EASA regulations for CS-VLA refer to the lighting requirements of the CS-23 [12] which specifies the required lighting set up.

Firstly navigation lights are required on each wingtip and on the top of the tail. On the right wingtip a green light must be mounted which shines forward and to the side with an angle of 110°. The left wing tip must have a similar light, but colored red and these lights must be placed laterally as far apart as practically possible. The tail must have a white navigation light mounted as far aft as practicably possible and point in the rearward direction. Additionally strobe lights, also called anti-collision lights, are required. These lights must have a full 360° spherical coverage around the aircraft, which is done by placing a strobe light on each wingtip, a strobe light on the top and bottom of the fuselage and one last one on the vertical tail. This results in a total of three navigation lights and five strobe lights. For these lights it is chosen to use LED's due to their high reliability, low cost and low power usage. The chosen light is the NavStrobe Aircraft Wingtip Nav Light 5W-A-1512, which is a €30, 5 W, 9 g, non-FAA/PMA approved LED light[30]. This light has a continuous and strobe setting, meaning that it is possible to use this light for both the navigation and strobe lights, which makes maintenance and repairs significantly easier and allows for a reduced amount of light required to be available as spares. Furthermore this light is shaped as a tower with 23 LED's around the sides of the cylinder and four on the top, providing a half spherical area of illumination. Eight of these LED towers cost €240 and weigh 72 g. Another consideration is that they provide a luminous Flux of 3060 lumen at 0° and 745 lumen at 90°, which is a little above the requirement of CS-23. Therefore the reason that these lights are not certified is likely due to the parts, materials, employees, organisation and methods have not gone through the certification process.

The green an red color for the wingtip navigation lights will be obtained by using a colored plastic dome over the light. The other lights also will need covering to protect the electronics, which will be done by using a similar plastic dome, but clear. Assuming that the dome and corresponding gasket cost €10, this bring the total for the lights to €320. Other considerations are that these covers must, according to regulations be flame resistant, not change colour or shape or lose any appreciable light transmission during normal use.

Other lights such as landing lights and taxi lights are also required by CS-23, however are not used in the Wings for Aid design as there are no pilots and no optical sensors in use.

10.10 Emergency systems

To avoid danger to bystanders on the ground the UAV will be equipped with a large parachute for emergencies. The parachute will be located at the top of the fuselage just in front of the wing so that the UAV will fall landing gear first. This has as benefits that the UAV will have a lower terminal velocity due to having more drag and it gives a chance that some parts of the UAV will not be damaged and so can be reused. The parachute chosen is the 'Rescue parachute Smart' by Independence paragliding[31]. This parachute costs €540 ex. tax and shipping and weighs 1.8 kg. Additionally it has a sink rate of 6.3 m/s at 120 kg weight. This corresponds with a parachute $\frac{1}{2} \cdot \rho \cdot S \cdot C_D$ value of 29.66, which can be used with the UAV MTOW to obtain the maximum sink rate of 10.5 m/s for the UAV. This gives people on the ground 9.5 s to get out of the way if they hear the UAV crashing when it is at an altitude

[29] URL `http://www.microtim.com/` [Cited on 19/06/2016]
[30] URL `http://www.aircraftspruce.com/pages/el/winglights/navstrobe11374.php#review_tab` [Cited on 15/06/2016]
[31] URL `http://shop.independence.aero/english/rescue/rescue-parachutes-paragliding-and-hang-gliding/smart.html` [Cited on 19/06/2016]

of 100 m. This parachute does have a maximum rated weight of 120 kg and so will need modification to prevent ripping if deployed with MTOW. For the project it is assumed for simplicity that the cost of modifications is equal to the bulk discount from purchasing 500 units. Finally the method of parachute deployment will be a hatch which is spring loaded by some small springs. This hatch will be attached to the parachute, so when the hatch is released it will be blown away by the free stream and will pull the parachute out with it. The hatch will have rounded edges to prevent it damaging the parachute after deployment.

Furthermore a loud siren is added to the emergency system to warn people and animals on the ground to get out of the way. The UAV will be falling at 38 km/h it weighs 350 kg and so will cause major harm to whatever it hits. The siren chosen is a 12 V 120 dB Piezo buzzer and costs roughly €5[32]. It runs on 12 V which is the same voltage as the main battery, however as this is an emergency system it is required to run even when the main batteries have failed. Therefore four 3V batteries are lined up in series to guarantee that the siren will have the required power. The batteries used are coin cell batteries due to their low weight, small size and only cost about €0.50 each when ordered in bulk[33]. They provide roughly 90 mAh each[34], which means that, as the siren uses 350 mA, the four batteries will be able to power the siren for roughly 60 minutes under ideal conditions. This allows for plenty of battery charge degradation over time and due to cold temperatures as the UAV will need a maximum of five minutes of siren turned on time when falling from its service ceiling of 3 km with the parachute deployed.

10.11 Electrical systems

The electrical power required for all of these systems will be generated by a 200 W 12V alternator in the engine and converted from AC, alternating current, to DC, direct current, by a 12 V Ducati rectifier provided with the engine by Simonini. During cruise the engine RPM is roughly half the maximum RPM, so the alternator will providing a continuous 100 W. This is still enough to power all systems. The average power usage is summarized in Table 10.2. The 20 W is the high end of the power estimation from AvioniCS and the 40 W from the lights is from using eight 5 W lights.

Table 10.2: Summary of the power use in the UAV.

System	**Average power [W]**
AvioniCS	20
Navigation and strobe lights	40
Total	**60 W**

As this is an average power required a battery is required to provide the energy required during peak loads. Additionally the battery averages the power produced by the alternator as this varies throughout flight and if the engine or alternator fails then the battery will still be able to power the UAV for a limited amount of time to perhaps get to safety or perform a maneuver to deploy the emergency parachute in a more safe fashion.

For the type of battery chosen, a lead battery is chosen for it's low cost and good reliability. The reliability is especially important as there will not be a redundant battery due to the extreme cost saving measures. The selected battery is the Ultracell UL7-12, which is a 12 V VRLA, valve-regulated lead acid, battery with a capacity of 6 Ah at 1.20 A and a maximum discharge current of 105 A (1260 W) for 5 s[35]. Furthermore this battery has a price of €28 and weighs 2.05 kg [36]. Added benefits of having a VLRA battery is that is requires very little maintenance and can be mounted in any orientation, which is important for functioning in negative g's and side loads.

The most important parts of the electrical system are laid out in Figure 10.1.

[32]URL http://www.amazon.com/Continuous-Sound-Decibel-Buzzer-Speaker/dp/B00HR6P9QU/ref=sr_1_3?ie=UTF8&qid=1464949818&sr=8-3&keywords=piezo+siren [Cited on 07/06/2016]

[33]URL http://batterijenland.nl/knoopcellen/lithium-3v-knoopcel/cr2016/knoopcel-batterij-cr2016/art_c651_a4431 [Cited on 07/06/2016]

[34]URL https://en.wikipedia.org/wiki/List_of_battery_sizes [Cited on 07/06/2016]

[35]URL https://www.123accu.nl/pdf/ANB00546.pdf [Cited on 15/06/2016]

[36]URL https://www.123accu.nl/Ultracell-UL7-12-VRLA-loodaccu-12V-7000-mAh-i25434.html?gclid=Cj0KEQjw-YO7BRDwi6Stp7T296ABEiQAD6iWMb_CXqyfV9r_Y3B2fsdZq7xXSjg8WBzjfJUbT6m6ejMaAiIa8P8HAQ [Cited on 15/06/2016]

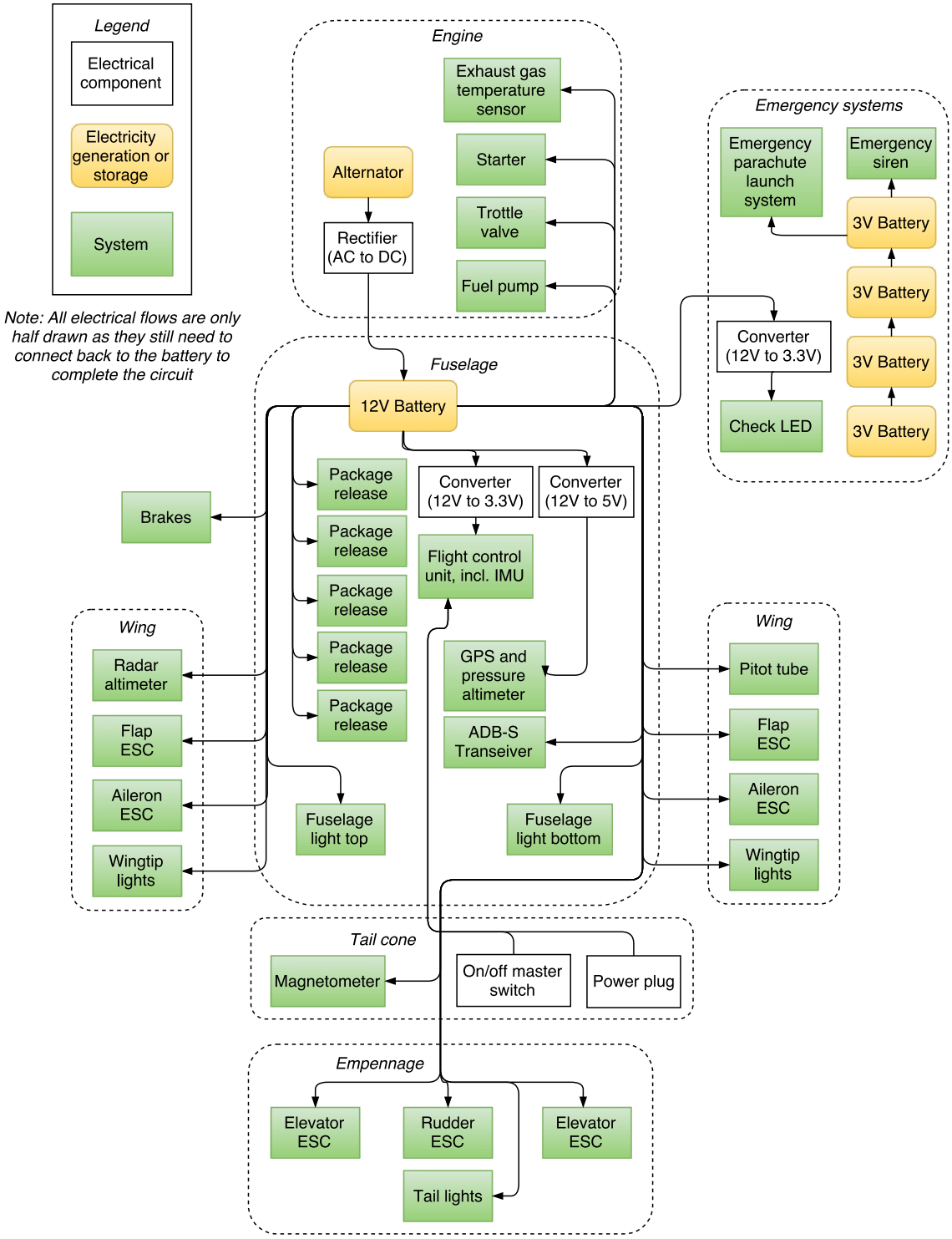

Figure 10.1: Electrical system layout.

The converters shown are DC converters, which are very energy inefficient as they turn the excess voltage into heat. So if the voltage is halved, then double the required wattage is needed as input to the converter to power the component. However they are very cheap and the parts powered by the low voltages do not use much current, so the loss is not much in total. Additionally the electrical system will need grounding points and fuses for safety.

10.12 Hardware and software

Finally, the relations between the hardware and software can be found in this section. To keep the figures simple the hardware-software diagrams have been split into different subsystems. Starting with the engine block diagram in Figure 10.2 and the communications and navigation system in Figure 10.3.

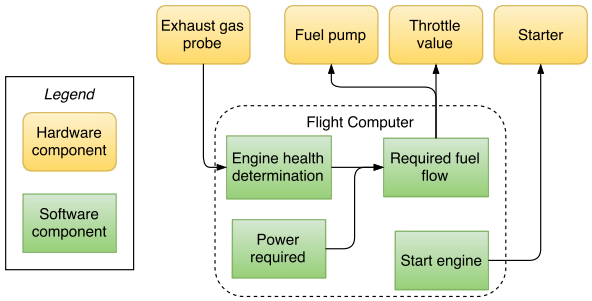

Figure 10.2: Hardware-software diagram for the engine.

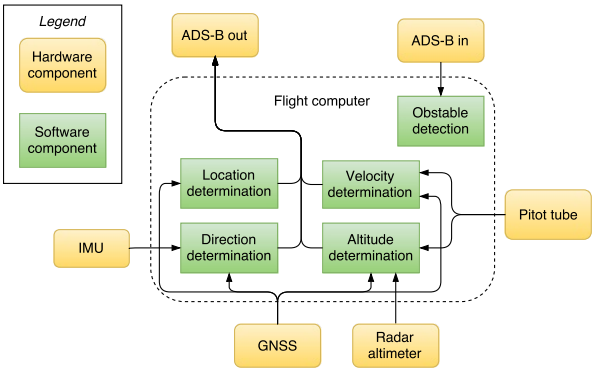

Figure 10.3: Hardware-software diagram for the communications and navigation system.

The hardware-software interface of the control surfaces can be found in Figure 10.4.

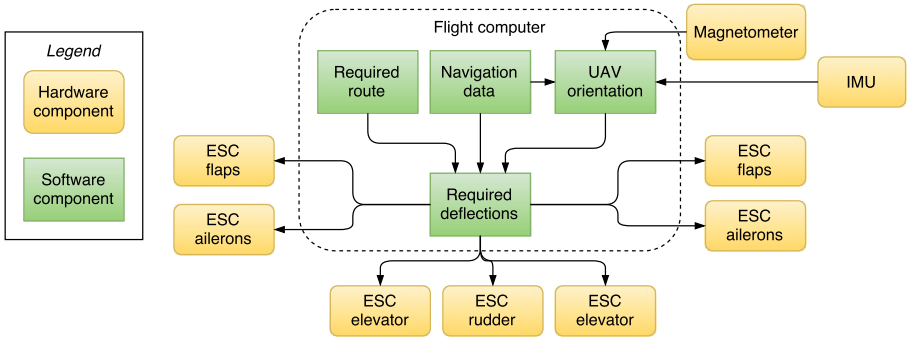

Figure 10.4: Hardware-software diagram for the control surfaces.

For dropping the packages the hardware-software diagram can be found in Figure 10.5, while Figure 10.6 shows the final diagram, the emergency system.

10.13 Communication within system

Since the UAV needs to be able to, for example, determine its position it is important that it can communicate with navigation satellites. To get an overview of the needed infrastructure of the communication system, some communication flow diagrams are made. These flow diagrams can be seen in Figures 10.7 and 10.8. Next to the communication with navigation satellites, the communication system is also of importance for receiving coordinates of the drop locations and receiving the go/no-go drop signal at the drop locations. Also for remote sensing of objects in the path of the UAV, like a tree or high building, which triggers an avoidance signal and to receive Inter Drone Communication (IDC) signals to make sure UAVs do not collide with each other.

The navigation, Bluetooth, USB, avoidance and IDC signals initially all follow the same path in the communication system, which can be seen in Figure 10.7. The signal is first received by a signal receiver, after which the analog signal is sent to a demodulator to separate the useful signal from the carrier wave. This demodulated signal is then converted from analog to digital by the analog to digital converter. The final step is then to decode the signal, after which it will be sent to the "User".

What the "User" will be depends on the signal received. If it is a Sat-NAV signal, the decoded signal will be sent to the on-board flight computer which will determine the position of the UAV based on this

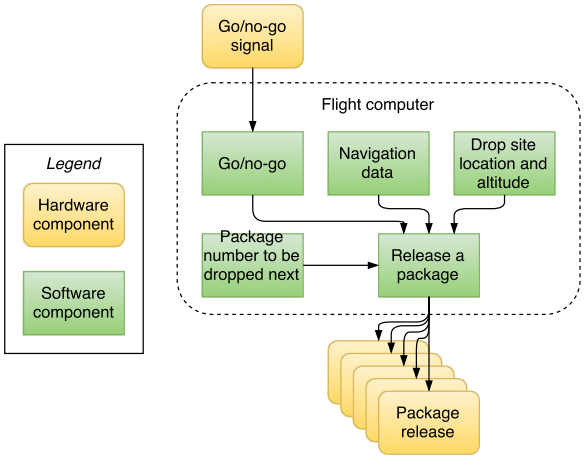

Figure 10.5: Hardware-software diagram for the package drop system.

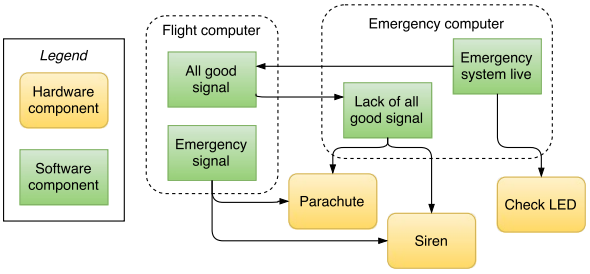

Figure 10.6: Hardware-software diagram for the emergency system.

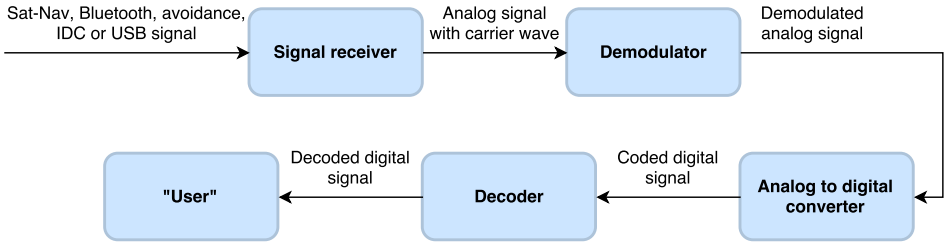

Figure 10.7: Shared communication flow diagram.

decoded signal, as seen in Figure 10.8. The position is then sent to both the autopilot and a coder. The autopilot will sent out control signals to the control surfaces and engine based on the received position signal to keep the UAV in position and on track. The control surfaces and engine send a feedback signal back to the autopilot to make sure they are in the correct position, if not, additional control signals are sent. The position signal sent to the coder will be coded and then sent to the digital to analog converter. Then the coded analog position signal will be modulated onto a carrier wave, after which it is sent to an amplifier. This amplifier amplifies the analog signal to make sure it will be received by the ground station. The amplified signal is sent to the antenna, where it will be broadcasted. For the USB, Bluetooth and Collision Avoidance communications see [5].

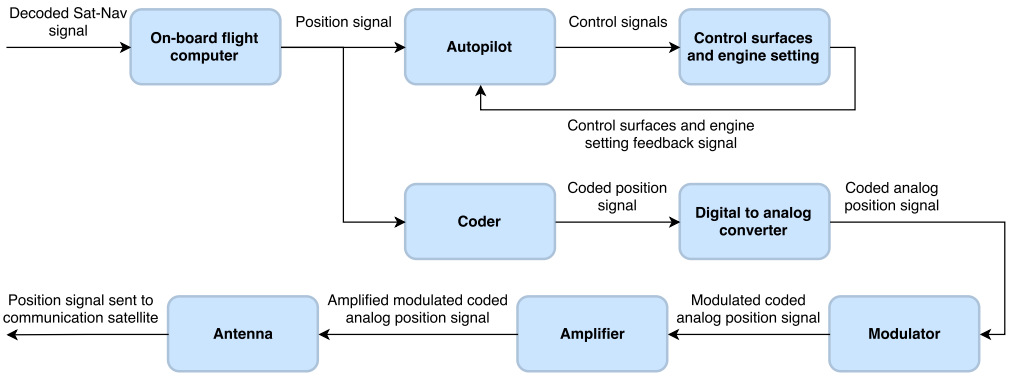

Figure 10.8: GPS signal communication flow diagram.

Chapter 11

Operations and logistics concept

The operations and logistics of the Wings for Aid programme determine for a great part the success of the concept. The UAVs have to compete with the traditional ways of aid supply such as trucks, aircraft and ships. Transportation by railroad could be an option but it is considered not flexible enough which is the reason why it is not considered. In this chapter the whole operation from start to end is described and analysed. A comparison is made between the conventional ways of aid supply and the Wings for Aid is compared with them as well. In the end two different scenarios are sketched and analysed. After this the capacity requirement is validated.

11.1 Global logistics

Efficient aid supply on a large scale requires an efficient organisation. Especially from a logistical standpoint it is therefore necessary that the UAVs are positioned on strategic locations all around the world. From these locations the UAVs have to be transported to the inflicted areas. Both the choice for locations and the different ways of transport will be explained and analysed in this section.

Choice of logistical hub location

The following locations are chosen:

- Panama City, Panama
- Libreville, Gabon
- Reggio Callabria, Italy
- Dubai, United Arab Emirates
- Kuala Lumpur, Malaysia

As can be seen in Figure 11.1 all hub locations are at the coast. This is an important criterium for a large logistical hub in general as access to the sea is extremely important.

The Caribbeans are often affected by hurricanes which make it a vulnerable area. A logistical hub for Wings for Aid UAVs close to this area is therefore a need. Panama City is chosen as it is already a distributional hub of the Red Cross. There are already people with experience available due to this distribution center and the port is familiar with the shipments involved. Another advantage is that the pacific ocean can easily be reached by making use of the Panama locks. Other notorious disaster areas like Chile and Columbia can then be supplied as well.

Nowadays there are many African countries affected by drought or affected by war[1] [2]. This means that there is a significant need for precise aid delivery as offered by the Wings for Aid programme. Locating a logistical hub in Africa comes with difficulties as many countries are unstable, especially in central Africa[3]. Also corruption plays a big role throughout the African continent which makes it a difficult continent to place a hub in[4]. The choice for Libreville, Gabon is based on the stable political situation that has been there for 42 years now already and the presence of a large harbor in the city[5].

North Africa and the Middle East are affected by conflicts especially since the Arab Spring which started in December 2010[6]. Conflicts imply humanitarian aid and together with the recurring droughts in the Horn of Africa a close by logistical hub is needed[7]. The choice of having a logistical hub in Reggio Callabria, Italy is easily made. Italy is a stable country and all the above mentioned areas can be reached

[1] URL http://www.rodekruis.nl/hulp-wereldwijd/noodhulp/droogte-in-afrika?gclid=Cj0KEQjw1v66BRCV-6rh6s-Biu8BEiQAelpui0PKQCRWODhXSo855QFKsiFgN49-5Zw5QyP9ReUqHBgaArLb8P8HAQ [Cited on 14/06/2016]

[2] URL http://www.globalsecurity.org/military/world/war/[Cited on 14/06/2016]

[3] URL http://afkinsider.com/47108/unstable-countries-africa/[Cited on 15/06/2016]

[4] URL http://www.inquisitr.com/2744866/top-10-most-corrupt-countries-2015/ [Cited on 15/06/2016]

[5] URL http://www.bbc.com/news/world-africa-13376333 [Cited on 15/06/2016]

[6] URL http://www.bbc.com/news/world-12482315 [Cited on 15/06/2016]

[7] URLhttp://www.theguardian.com/global-development/poverty-matters/2011/aug/11/horn-of-africa-drought-resilience [Cited on 15/06/2016]

easily from this city. Reggio Callabria possesses a large harbor and on top of this the World Food Programme is also stationed in Italy which will have a benefit for the organisational aspect of the whole operation according to Eelko Brouwer, Humanitarion Coordinator for the Red Cross.

Dubai is growing rapidly as biggest humanitarian hub of the world[8]. From this strategic location two third of the world population can be reached within eight hours[9]. Close to countries like Afghanistan and Pakistan that were even recently infested by earthquakes, the Wings for Aid programme would provide a fitting solution to the need of fast aid supply when the UAVs are stationed in Dubai[10]. Next to its strategic location Dubai is also known for its vast experience with aid supply and according to Eelko Brouwer, Humanitarion Coordinator for the Red Cross, it is expected that this will help the organisational part of the Wings for Aid programme significantly.

South-East Asia is known for its severe natural disasters. In the last three decades over 900.000 people have died due to cyclones and tsunamis[11]. The need for a Wings for Aid logistical hub is therefore evident. The Red Cross already has a large distributional center in Kuala Lumpur, Malaysia and this center is the main hub for all humanitarian aid in the region. The strategic location and the available experience makes Kuala Lumpur the perfect location in the South East Asia region.

Transportation of UAVs

Four ways of transporting the UAVs to disaster areas are considered: truck, ship, cargo aircraft and self flight of the UAVs. The latter means that the UAVs will take-off from the logistical hub and will ferry to the prepared ground station in the disaster area. These four ways of transportation are analysed and explained in this section. For this analysis a distinction should be made between a fast response and a slower response. This has a large influence on the to be chosen way of transportation.

Analysis of transportation methods

Three criteria are considered when analysing the different ways of transportation of the UAV.

- **Time:** the sooner the UAVs are in the disaster area the better. Especially in cases of natural disasters such as tsunamis the first days are critical which means that time is a very important criterium.
- **Ease of use:** loading and unloading the vehicles cost time that would preferably be diminished. The transportation methods are therefore evaluated on this aspect as well. Besides, aid operations are prone to legal complications and avoiding any of this as much as possible is preferred as well.
- **Costs of operation:** cost of operation is an obvious criterium as funds are often limited. Costs are to be expressed in costs per UAV per kilometer as this will include the capacity of the transportation method.

Trucks are limited by the fact that they need an accessible road to drive on to deliver the UAVs to the disaster areas. Trucks are not fast, especially when the roads are in a bad state and they are furthermore prone to the political situations that are present in the areas through which the trucks have to travel. Trucks are easy to handle in terms of loading/unloading. They are used all over the world and can be repaired in a relatively simple manner, even in remote areas. During long trips however convoys might get into trouble with border police. This makes the trucks vulnerable for delays and might give legal complications. On the other hand trucks are very cheap in operation. They cost, based on the market analysis presented in [36], €0.90 per km (assuming that a container can contain ten tonnes of goods and that one container fits on one truck). In Table 11.1 the average truck velocities are presented. The values presented in this table are based on truck convoys from the Red Cross.
From the values in Table 11.1 it can be concluded that the range and speed of trucks is very limited. This means remote areas will be hard to reach with a truck.

Ships are limited by the fact that they need water and a well equipped harbor to be able to deliver the UAVS to the disaster areas. Ships are not fast. Nowadays the bigger container ships sail with a

[8] URL http://www.ifrc.org/en/news-and-media/news-stories/middle-east-and-north-africa/united-arab-emirates/delivering-relief-from-the-worlds-largest-humanitarian-hub-in-dubai-65303/ [Cited on 15/06/2016]

[9] URL http://www.ifrc.org/en/news-and-media/news-stories/middle-east-and-north-africa/united-arab-emirates/delivering-relief-from-the-worlds-largest-humanitarian-hub-in-dubai-65303/ [Cited on 15/06/2016]

[10] URL http://www.volkskrant.nl/buitenland/aardbeving-in-grensgebied-tussen-afghanistan-en-pakistan~a4279347/ [Cited on 15/06/2016]

[11] URL http://www.alletop10lijstjes.nl/top-10-grootste-natuurrampen-van-de-laatste-eeuw/ [Cited on 15/06/2016]

Table 11.1: Average truck velocities in different regions.

Region	Average truck velocity km/hr	Average covered distance in 24 hours
Europe	70	1680
Middle-East	60	1440
South America	40	960
South East Asia	30	720
Africa	30	720

velocity of about 30 km/hr[12]. In Figure 11.1 the range of ships achieved in 72 hours is presented and is approximately 2160 km.

Figure 11.1: Ship range (2160 km) in 72 hours assuming an average velocity of 30 km/hr.

On top of the limited distance travelled in 72 hours the handling time of ships is very large. Experience from the Red Cross states that arranging a ship and payload, including all the related harbor dues and permits, will take one to two weeks. Another disadvantage is that there is almost always another mode of transportation required that will transport the UAVs from the harbor to the airstrip. This will add a significant transportation time to the operation depending on the distance to be travelled over land. In conclusion, one can state that a ship is not a good option for quick response aid supply. The logistics concerning ships is complex. Well equipped harbors are required to load and unload the ships and the legal aspect can be complex. A rough estimation on the cost of a container per km is made based on data from the Hofstra university in New York[13]. With these data an average operational costs of €0.24 per km is computed. This value includes port charges.

Cargo aircraft have the advantage of being fast and having a large range. A worldwide used cargoplane is the C-130 Hercules which has a range of around 4000 km and it can fly this distance in circa eight hours. This range is shown in Figure 11.2.
In Figure 11.2 it can be seen that almost every notorious disaster area can be reached from the hubs within eight hours. This means that this transportation method is very well applicable for quick response emergency. However the amount of UAVs that can be carried by a C-130 is limited to six due to the relatively small cargo floor of 3.1x12.4 m[14]. With the right crew the C-130 the loading time is reasonably quick. Furthermore, according to Eelko Brouwer, humanitarian coordinator of the Red Cross, the first aircraft with UAVs can be in the air within 24 hours after a natural disaster has happened. This

[12] URL `http://www.lowtechmagazine.be/2010/02/moderne-containerschepen-trager-dan-oude-zeilschepen.html` [Cited on 15/06/2016]
[13] URL `https://people.hofstra.edu/geotrans/eng/ch7en/conc7en/daily_operating_costs_teu.html` [Cited on 15/06/2016]
[14] URL `http://www.globalsecurity.org/military/systems/aircraft/c-130-specs.htm` [Cited on 15/06/2016]

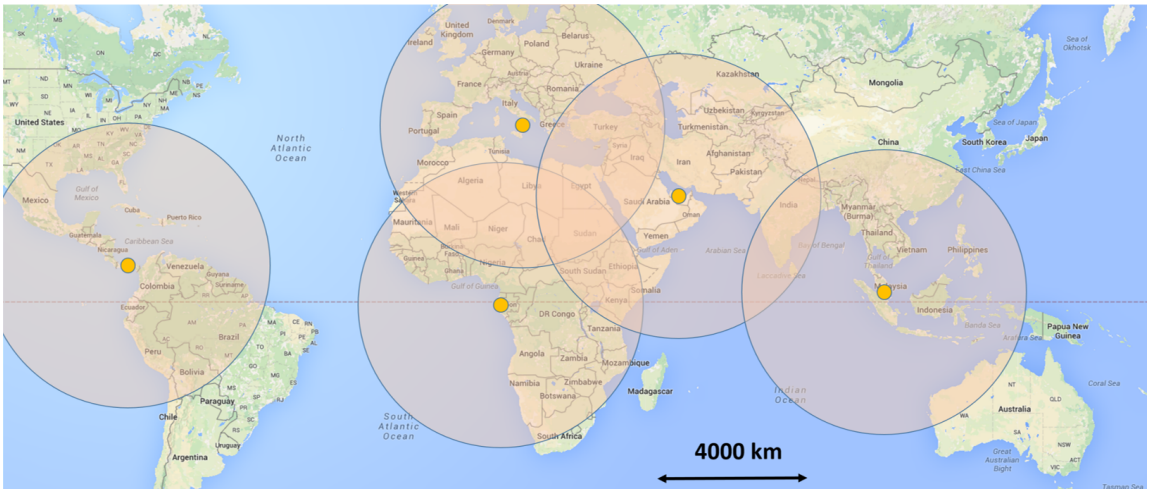

Figure 11.2: Range of the C-130 Hercules cargo aircraft.

makes it very suitable for fast response aid. When the airstrip from which the UAVs will operate is not long enough the C-130 is not able to land directly at this airstrip. This means that it has to deliver the UAVs to a nearby airport from which the UAVs will be transported by truck to the airstrip itself. This is a drawback as the handling time will increase significantly. The C-130 comes with an operational cost of $18,507 per flight hour[15] which is €5.03 per UAV per km assuming again a cruise speed of 500 km/hr. In conclusion, it can be stated that transporting UAVs with a C-130 Hercules is a great solution to deliver the UAVs quickly to the disaster area. It comes with high operational costs however.

The UAVs can achieve a ferry range (range of the aircraft without payload) of 820 km. This extended range can be made use of by letting the UAVs fly to the disaster area themselves. If the airstrip from which the UAVs will operate is prepared so that the UAVs can land on it they can fly directly to their destination avoiding any other means of transportation. When the regular payload is replaced by a fuel tank the range can even be extended to 2550 km which will increase the employability of this concept significantly. In Figure 11.3 the two different ranges that can be achieved with no extra fuel tank and including extra fuel-tank are depicted in pink and green (or smaller and larger circle) respectively.

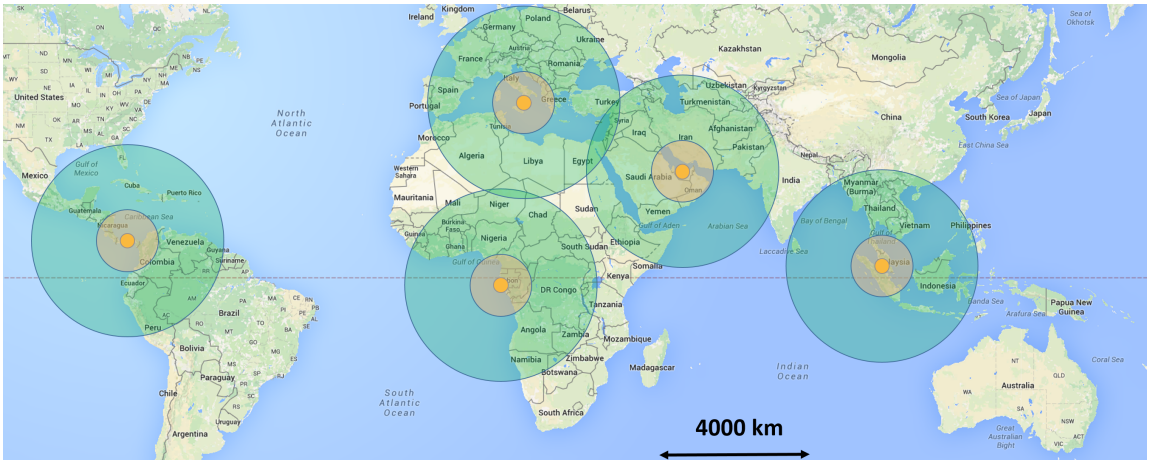

Figure 11.3: Ranges without extra fuel tank (pink, small circle) and including extra fuel tank (green, largest circle).

As can be seen in Figure 11.3 the extended ferry range is around 2550 km while the travel time will be around 16.5 hours assuming an average velocity of 43 m/s. The biggest advantage from a logistical point of view is that there are no containers required to transport the UAV in. This means that there is no

[15]URL *http://nation.time.com/2013/04/02/costly-flight-hours/* [Cited 28 April 2016]

time wasted on loading of containers and other vehicles. The UAVs are assembled and can take-off one after the other rapidly if the operation is carefully prepared. During the ferry phase the UAVs are not hindered by any reduced accessibility on the ground caused by the disaster or political situation and are able to land directly at the airstrip of destination. This means that there is no follow-up transportation phase required which reduces the handling time significantly. It also means that the UAVs are already assembled which reduces the handling time even more. Due to the possibility of sending a significant amount of UAVs shortly after the emergency operation is initiated, the aid supply can already start at a large capacity if the other required resources are available as well. The operational costs of the ferry method are the same as the operational costs of the UAV in normal operation, however some costs may be added due to the fact that a guiding aircraft has to fly along the UAVs. However the operational costs of this guiding aircraft can be divided among many UAVs as the aircraft can probably guide dozens of UAVs at the same time. Operating costs of €0.17 per *km* are estimated based on the engine maintenance costs and fuel use. It is expected that other systems or guidance aircraft might have to be added to the operation which will increase the transportation costs. As a conclusion it can be said that this way of transporting UAVs can be applied in the early stages of the emergency operation as well as in a later stage while it is still relatively cheap. The ferry concept requires a thorough analysis as it is an unproven concept. This extensive analysis is beyond the scope of this project but some recommendations for further research will be given in the next paragraph.

Recommendations ferry concept The ferry concept requires the UAV to sustain automated flight for around 2550 *km*. Before this concept can be applied in the wings for aid programme some issues have to be overcome. One of the issues that arise are the problems with communication. As the UAV will ultimately be equipped with a radio system with a range of 500 *km*. This means that either several ground stations have to be available along the flight route or a guiding aircraft has to fly along as a mobile command center to guide the UAVs to their destination. Besides these two options a satellite communication based system can be integrated into the UAV to guarantee control during flight. All these options have to be carefully looked at in future studies. The second issue is related to airspace control and authorities. It is expected that it will be legally difficult to let dozens of UAVs fly through controlled airspace and over populated countries that are not directly involved in the disaster. For the sake of safety the UAVs could fly over sea and ocean as much as possible but this will not always be possible. Furthermore it is expected that the UAV needs to be fully certified to be allowed to perform this mission. It is recommended that this issue is carefully investigated in the future. Due to the lack of redundancies the UAV has a significant chance of crashing during the ferry phase. Besides the risks for the people on the ground the loss of a UAV will also add to the costs of the total mission. It is recommended that these risks are carefully investigated in the future.

Conclusions on transporting methods.

The analysis on the transporting methods showed that every method has its advantages and disadvantages. Based on this analysis it is recommended that for the Wings for Aid programme all different ways of transport are considered when planning a mission. It is expected that multiple or possibly all methods will be used during an emergency aid delivery mission as the needs in a disaster area change over time and the total costs keeps increasing. As a summary Table 11.2 is constructed.

Table 11.2: Summary of transportation methods

Method of transportation	**Truck**	**Ship**	**Cargo Aircraft**	**Ferry method**
Initiation time	within 24 hrs	within 2 weeks	within 24 hours	within 72 hours
Travel speed *km/hr*	30-70	30	500	150
Additional transport required?	No	Yes	Yes	No
Operational costs €per UAV per km	0.45	0.12	5.00	0.15

With the use of this table the best transportation method can be chosen depending on the type of mission.

11.2 Local logistics

In order to be able to bring in the ferrying UAVs, a ground site is set up. To set up the ground site first some operational equipment and personnel have to be transported to the ground site. The equipment and personnel which can be found locally is transported with trucks to the ground site. Equipment and personnel which have to come from other places are transported by aircraft to a nearby airport in order to start the operation as fast as possible. From the airport the equipment and personnel are transported to the ground site by trucks. The moment the equipment and personnel have arrived at the ground site the site is secured and a fence is built around it. When the ground site is secured, a warehouse and personnel tent is set up where all the equipment and personnel can be stored. After that an electricity system is set up and the other required tents are set up. For safe handling of fuel a separate part of the ground site is closed and locked so everyone without clearance is not able to get access. In the meantime an ATC tower is built up, a runway is prepared and some primitive sanitation is created to ensure proper hygiene for the personnel. After the ground site is finished the packages can be stored and the personnel can be divided amongst different stations and can be trained in the different tasks available. When everything is ready the ground site is able to receive the first UAVs. The first UAVs should be able to use the ground site within three days, then there are runways and handling tents and also trained and professional personnel at the ground site which can process the UAVs. The whole ground site can be set up within 72 *hr* if the local aid organisations are prepared for disasters according to Eelko Brouwer, humanitarian coordinator of the Red Cross. However the capacity will be limited at that moment. The following days more equipment and personnel will be available and more UAVs can be flown in/transported from the main hub.

11.3 Ground operations

In Figure 11.4 the general layout for the ground site can be found. The large arrow represents the general wind direction in the area. The dark blue (R) surfaces are the two available runways which are placed parallel to the wind direction in order to make landing and take-off more efficient. In the optimum case there are two runways (dark blue, R) available, one for landing and one for take-off. After the landing of the UAV the ground operations start and will end again when the UAV takes off. When the UAV has landed the engine will be shut-off and at the moment the propeller has stopped spinning two people will push the UAV to the pink (T) depicted area. In this area the testing tent is stationed. In this tent it is checked if there are any damages on the UAV as a result of the mission. This is done electronically by the available sensors in the UAV and visually by a mechanic. The outside of the UAV is checked visually for cracks or major damages, also the tires and brakes are checked visually by looking at the profile of the tires and disk pads on the brakes. The avionics including sensors, actuators and cabling are checked electronically on damages. Furthermore the package rack is unloaded and positioned on a cart and the new mission coordinates are uploaded to the UAV flight computer. If there are damages found the UAV will be transported to the green area (M). In this tent maintenance is performed on the UAV. The damage is fixed by replacing the whole broken section of the UAV, if it is not possible to fix the UAV easily it will be sent back to the main hub to get fixed. After the maintenance is performed or in the case there is no damage found, the UAV is sent to the lilac areas (L). At this station a new rack with fuel and packages are loaded from the cart to the UAV and the rack is electronically connected to the UAV. These racks are already loaded beforehand in the warehouses (light blue, W) and in the fuel storage area (red, F) to ensure fast handling. After that the fuel connection between the engine and tank is checked. Then the UAV is transported to the purple area (G) where it waits for take-off. When the team receives a go-signal the UAV is pushed towards the runway (dark blue, R). If the UAV will receive another go from ATC the engine will be started using the button on the tail of the UAV and it will take off. Besides the ground operation stations there are several other locations which are not influencing the ground operations on the ground site but have an important role in the supply for the ground operations. There is a place where the fuel is stored (red, F). At this location the fuel barrels are stored safely and at a safe distance from the other locations. Also there are various warehouses where equipment, spare parts and bulk products of food and water are stored (light blue, W). Furthermore there are tents where the personnel have sanitation and sleeping places (beige, P). Finally there is an ATC tower present to give go/no-go's to the UAVs for take-off (light green, A) and to keep track of all ground operations.

In the different tents different kind of personnel is deployed. There are three types of personnel available which are local personnel, specialists and volunteers. In the testing tent (pink, T) two specialist and four locals are always available who test the UAV on damage and unload the rack. The specialist

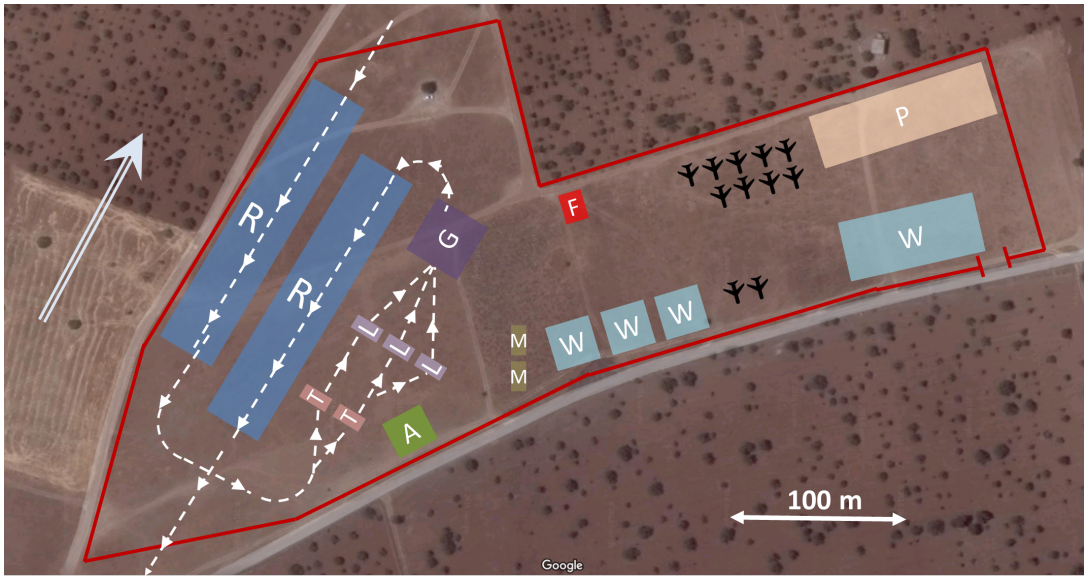

Figure 11.4: Typical ground site layout.

will overview and checks the work of the locals. In the maintenance tent (dark green, M) there are also two specialists and four locals available who perform together the maintenance on the damaged UAVs. In this case the specialist also checks the work done by the locals. Loading the racks in the loading tent (lilac, L) will be done by six locals and the fuel tank is connected by volunteers. The ATC will be manned by two specialists. Furthermore there are four locals pushing the UAVs to the tents from the runway and to the runway after reloading. There are also ten additional locals which provide food, supplies and cleaning. Eight locals are also used to assemble the packages in the warehouses. Lastly there are ten additional volunteers that keep track of the logistics in the different tents.

As previously said the ground logistics are divided in different stations. The amount of minutes the UAVs are on different stations in the ground logistics can be seen in Figure 11.5. When adding up the times the UAVs will have a total ground operation time of 29 *min*. However the ground operations are ordered in separate stations, where every station takes a certain amount of time and after that the whole line is shifted forward. The most limiting case in the ground operations are the 6 *min* of the test tent (pink, T). So the total time will be 29 *min* but the time a next UAV will take-off will be less than 6 *min* which means the requirement of matching the capacity of the C130 Hercules can be met.

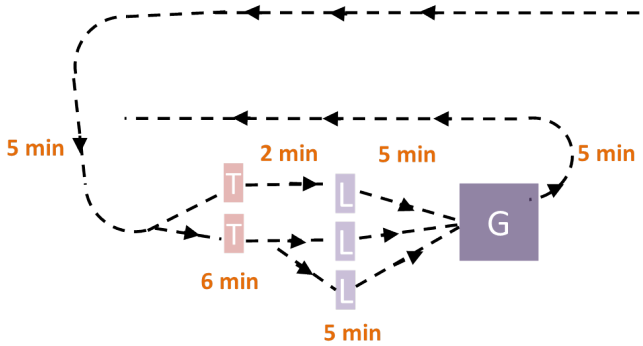

Figure 11.5: The amount of time different stages of the ground operation take.

11.4 Operational cost estimate

The operational cost of the mission can be divided in several parts. The largest contributions are the goods that are continuously required during the mission, such as fuel, oil, personnel and food. The smaller parts of the operational cost are the things which have already been bought and only have to be

deployed to the ground site once such as tents, sanitation and fences. The latter costs are very small and will be neglected. The cost of the aid is not taken into account as operational cost. The operational cost for a warzone mission and natural disaster will be different, this is because the cruise altitude during the warzone is much higher than in mission for a natural disaster as explained in Section 6.2. The result is that the drag will be higher in the case of a normal mission and therefore the fuel consumption is higher. However the loiter time will also be much lower because of the lower altitude as explained in Section 9.2. When combined the fuel use is higher in the warzone mission. For the warzone it is calculated that the cost of the fuel, oil and the engine maintenance is then 84.12 €/mission, for the natural disaster mission the cost will be 68.30 €/mission. The cost of the personnel will be the same for both missions and is divided by the three different groups of personnel, the first group are the specialist, the second group the locals and the volunteer group is the third group, however the volunteers do not get paid. In total there are six specialists who get paid 40 €/*hr* and 38 locals which get 3 €/*hr*. Normalizing it per mission the operational cost for personnel will be 32.60 €/mission. According to USDA (United States Department of Agriculture) the price of a moderate meal is 61.85 €/person/week[16]. For the whole work force this results in a weekly price of around €3,200. Normalizing this to price per mission gives 1.7 €/mission. The total operational cost for the mission will then be 118 €/mission for a warzone operation and 103 €/mission for a normal operation. When looking at how many food a person requires a day it can be estimated how expensive the operation will be per day per person. It is assumed that a person needs 0.5 *kg* a day of food, this gives 0.61 €/day/person for a warzone and 0.53 €/day/person for a normal mission. The total operational cost can be seen in Appendix A.

11.5 Wings for Aid deployability

The Wings for Aid concept can be deployed in many areas. In this section the areas in which the Wings for Aid concept excels compared to more traditional aid supply methods are analysed and explained. This will be done for both the warzone mission and normal mission.

Deployability in warzone missions

For the warzone mission only the cargo aircraft and helicopter can compete with the Wings for Aid concept as the other means of transportation are not applicable considering the situation on the ground. The Wings for Aid UAV is superior to the cargo aircraft in terms of costs, accuracy and flexibility. Compared to the UH-1 helicopter the UAV is cheaper but comparable with respect to drop accuracy and flexibility of operation. The flexibility of operation takes into account required runway distances and runway conditions, ease of loading, ease of transporting and ease of maintainability. In Table 11.3 the options are given.

Deployability in regular missions

For the regular mission the same means of transportation can be used but now the truck is also a valid option. Assuming the worst case situation in which the truck can only drive 30 *km*/*hr* the truck will need to drive for 17 hours. The flexibility of operations is extremely low as the truck is strongly dependent on the conditions of the road. This is why it will often not even be a competitor of the Wings for Aid concept. In Table 11.3 the truck is summarized as well.

Table 11.3: Comparison between different modes of transport.

Type of mission	Wings for Aid UAV	C-130 Hercules	UH-1 Bell Huey	Truck
Time to deliver 22,500 *kg* at 500 *km*	24 *hr*	24 *hr*	40 *hr*	17 *hr*
Costs per 22,500 *kg*	€27,423	€32,678	€897,000	€1,012
Drop accuracy	25 by 25 *m*	400 by 400 *m*	<25 by <25 *m*	n/a
Flexibility of operation	High	Low	High	Very low

11.6 Scenarios

In order to find the difficulties in the operation and to create a clear picture of the operation two different missions are worked out. One mission will be in a warzone and one in a natural disaster because of the different flight procedures as explained in Section 6.2. The warzone consist of a mission in Syria coordinated from Turkey and the natural disaster will be the tsunami from 2004 in Southeast Asia.

[16]URL`http://www.cnpp.usda.gov/sites/default/files/CostofFoodApr2016.pdf` [Cited on 17/06/2016]

Mission in warzone

In the Syrian civil war several cities are under siege by different fighting parties[17]. To deliver aid to different cities in Syria a ground site is built in Turkey in the North of the city of Şanliurfa. Using the method explained in Section 11.2 the UAVs ferry from the closest main hub to the ground site. In the case of Şanliurfa the closest main hub is Reggio Callabria in Italy. When looking at Figure 11.6 the distance between these two locations when flying over water is around 2300 *km*. Which is shorter than the maximum ferry range of 2550 *km* and therefore the UAV is able to fly to Şanliurfa in one go. When the ground site is built the layout is the same as in Figure 11.4 because the ground site in Figure 11.4 is based on the location in Şanliurfa.

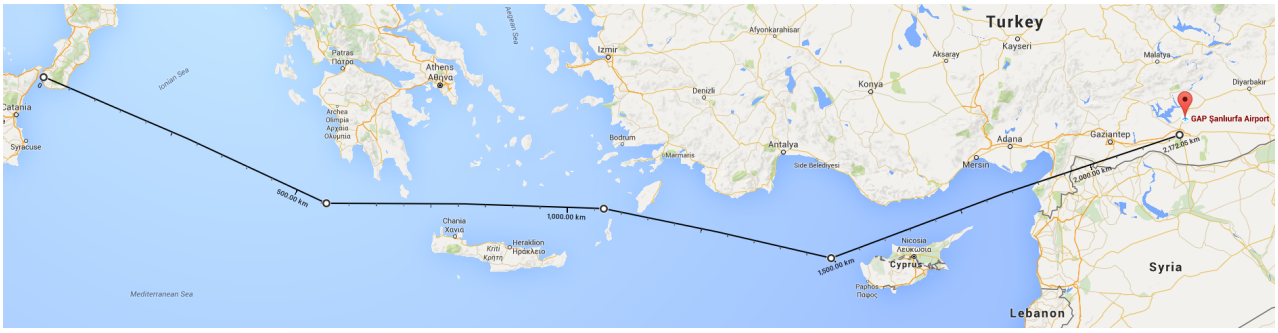

Figure 11.6: Ferrying from Reggio Callabria to Şanliurfa.

When the groundstation is operational the UAVs start flying the mission. In Figure 11.7 the maximum range of the UAV can be seen including one possible mission. This particular mission consists of flying 250 *km* to Deir-ez-zor and dropping the packages. After that the UAV will fly back according to the type 1 mission profile in Figure 6.2. The reason to choice for this type of mission is because there is no suitable airstrip on a distance of 500 *km*. The example mission is dropping all the packages in one besieged city, in this case Deir-ez-zor because this mission has been performed with normal aid delivery very recently[18]. In Figure 11.8 the light blue blocks represent the different possible dropping locations spread out over the city.

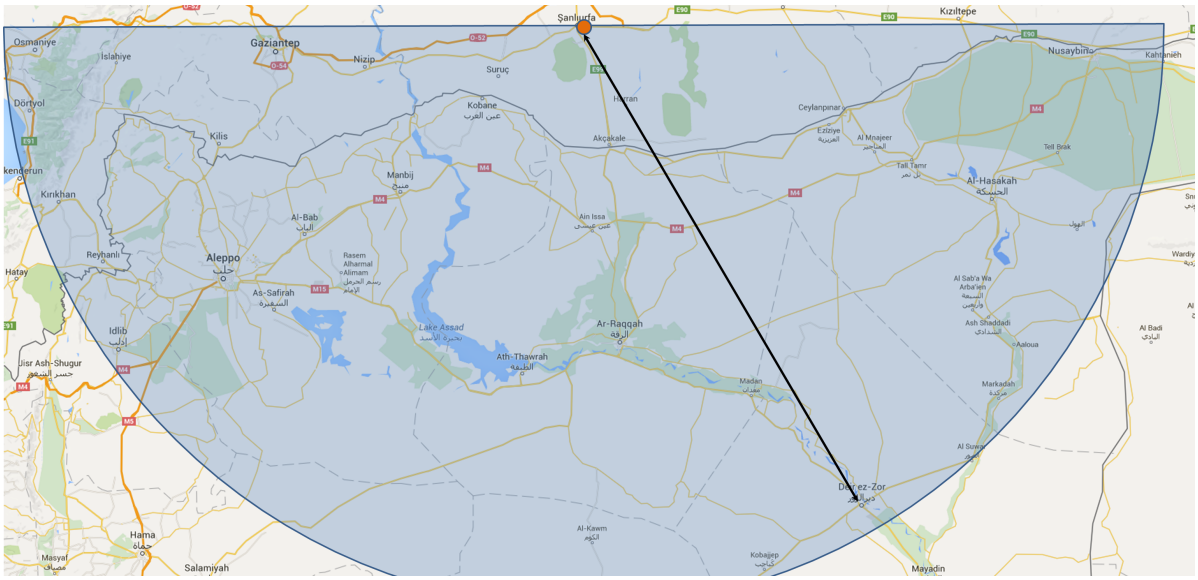

Figure 11.7: Maximum range of one UAV.

The operational costs of the mission highly depends on the duration of the mission. During a siege like this the mission can easily takes months or even years. For now a cost estimate is built on the estimate

[17]URL `http://syriainstitute.org/siege-watch/` [Cited on 15/06/2016]
[18]URL `http://syriainstitute.org/siege-watch/` [Cited on 15/06/2016]

Figure 11.8: Possible dropping locations in Deir-ez-zor.

of three months of deployment. The operational cost of the total mission is 118 €/mission and during the three months the UAVs will fly a total of 23,400 times. A total cost for operation in the three months will then be €2,771,000,-. During this three months the UAV will drop 22,500 *kg* of aid per day which gives a total of 2,025,000 *kg* or 2,025 *tonne* of aid. The UAVs will eventually fly a distance of 11,700,000 *km*.

Mission in natural disaster

The second mission will be a natural disaster, it is chosen to show a mission for the tsunami of 2004 in Southeast Asia because this mission showed very well the problems of transporting the aid supplies with trucks via roads[19]. The area which was affected the heaviest by the tsunami was the island of Sumatra and especially the region of Aceh. For the sake of the example two ground sites are built on this island to send the aid to the villages. The reason for two ground sites is because of the mountainous region between the affected region and the ground site which has the consequence that there is no direct flying possible. The UAVs will in this case also ferry in from a main hub. The main hub which is the closest to both of the ground sites is the hub in Kuala Lumpur. In Figure 11.9 the route that the UAVs have to fly from Kuala Lumpur to the ground sites can be seen. The distance is 324 *km* from Kuala Lumpur to Medan where the first ground site is stationed and 540 *km* to Lkoseumawe where the second ground site will be. When looking at the distances it can be noticed that both of the missions can be flown without the extra fuel tank installed because the distance is shorter than the 750 *km*. Furthermore the distance to Medan is shorter than 500 *km* and therefore the UAVs are able to transport equipment to the ground site.

In Figure 11.10 the maximum range of the UAVs is shown together with five possible routes the UAVs can fly to deliver aid to the largest villages and cities on the coast. The dots in Figure 11.10 represent the drop locations and the arrows show the flight direction of the UAVs. The kinks in the flight paths are due to the mountains that are located in between the ground sites and dropping locations. For this mission there are no exact dropping locations assigned. This is because of the destructing effects of a tsunami which make it pointless to assign dropping locations at this moment. However it is expected that there are, partly because of the destruction, locations to drop the aid.

As said in Section 11.4 the operational cost will only differ because of the difference in fuel use between the missions. The cost of a three month mission will be €2,401,000,- which is €370,000,- less than the mission in a warzone. Furthermore the same amount of aid and distance is dropped and flown.

11.7 Operational flow diagram

In Figure 11.11 the functional flow diagram for the operations can be seen. At the top level all the blocks the UAV has to perform are stated. From the toplevel, assemble UAV, load and prepare UAV, Landing & turnaround and ending mission are affected by the ground operation and are stated in Figure 11.11.

[19] URL`http://reliefweb.int/report/indonesia/humanitarian-and-human-rights-situation-aceh-forum-asia-background-briefing-paper` [Cited on 17/06/2016]

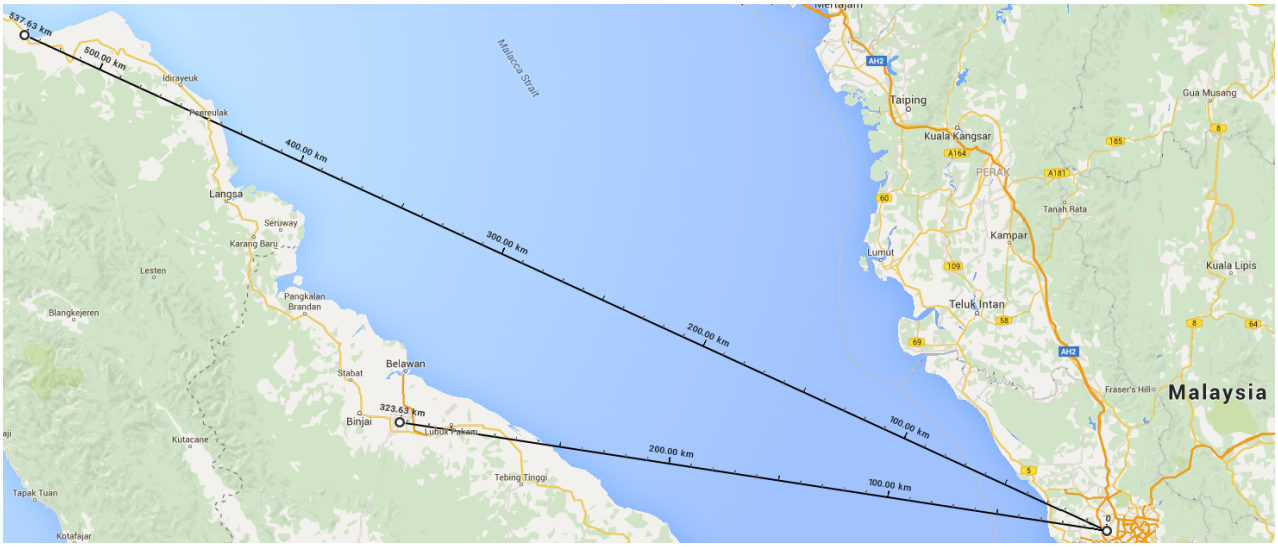

Figure 11.9: Ferrying from Kuala Lumpur to the ground sites on Sumatra.

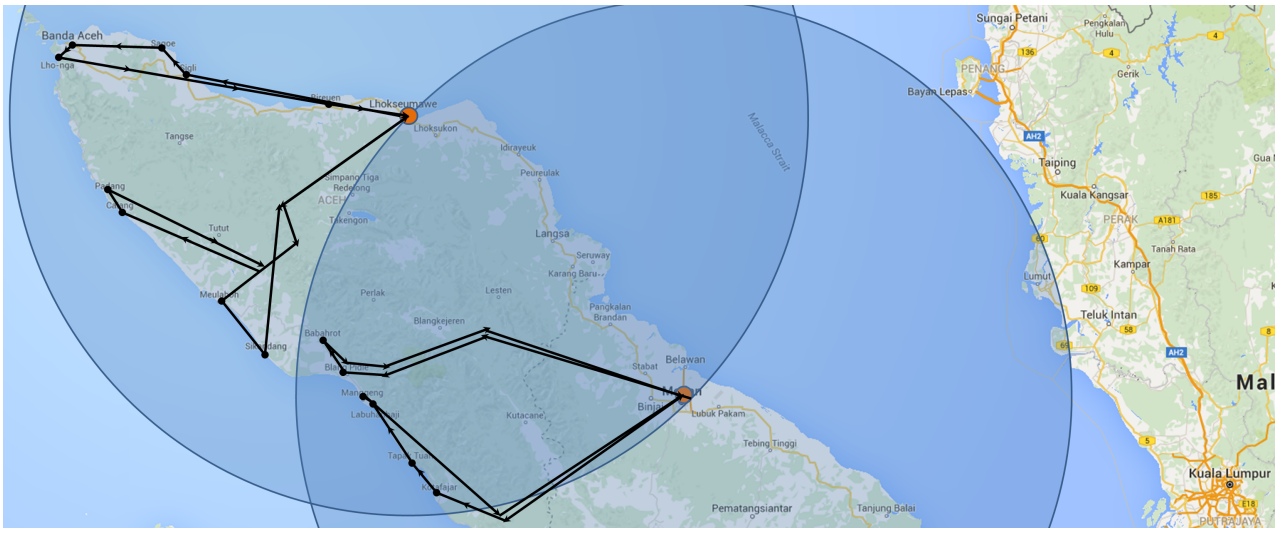

Figure 11.10: Maximum distance UAVs could fly including example routes.

Take-off & cruise and dropping are stated respectively in Section 6.4 and Section 9.3.

11.8 Verification and validation

Using the computed turnaround time of 6.4 *min* in Section 11.3 the capacity of the mission can be calculated. Using this turnaround time the capacity is 22,500 *kg* per 24 *hr*. For the warzone missions this means that a minimum of 50 UAVs are required to reach this capacity using the mission duration of 4.75 *hr* as computed in Section 6.6. For the normal mission an amount of 45 UAVs is required to reach the capacity. This means that the requirement of 22,500 *kg* per 24 *hr* is met.

The capacity depends extensively on the turnaround time of the UAV during operation. An estimation is made on this turnaround time, however it is very difficult to verify this data as similar operations are scarce. Validation should be done when the UAVs are produced and operable. However due to the station wise approach the turnaround operations are flexible so the turnaround time can be reduced if more stations are added.

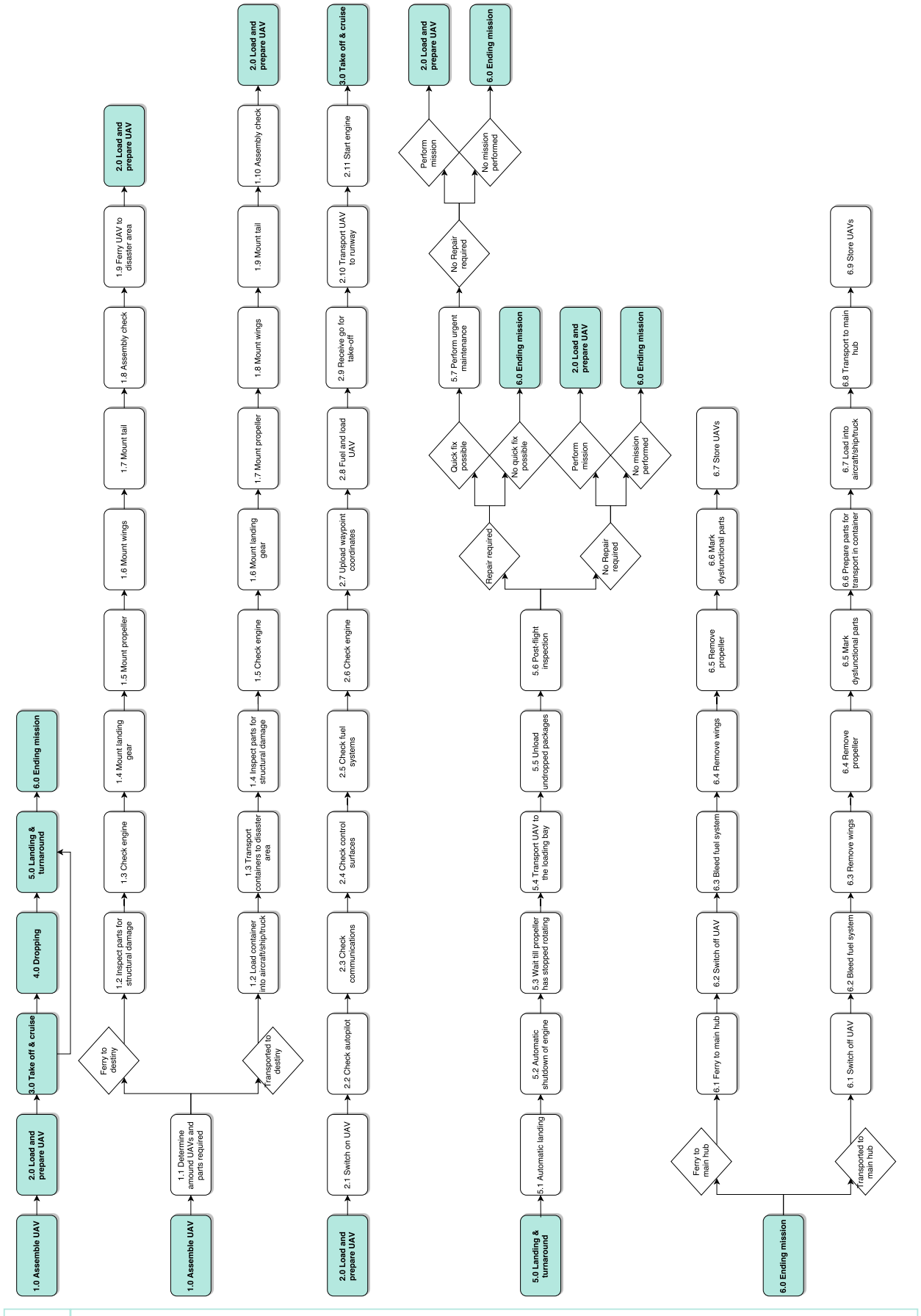

Figure 11.11: Flowchart of the operation logistics.

Chapter 12

Final design evaluation

In this chapter a evaluation of the design will be made in terms of resources and requirement compliance. Furthermore the risk, reliability, maintainability and safety of the project will be analysed.

12.1 Cost budget

First the costs of all non-structural parts of the UAV are listed in Table 12.1 and the price estimates of all structural parts can be found in Table 12.2. All prices are excluding tax and shipping costs. Furthermore the options found in Table 12.3 could be made available for a customer to choose.

Table 12.1: Cost of all non-structural parts.

Part	Price [€]	Price range [min,max]
Engine	4,140	[-0%, +2%][1]
Two propeller blades	340	[-0%, +0%]
Propeller hub	201	[-0%, +0%]
New reduction pulley and belt	77	[-100%,+0%][2]
Radiator	65	[-0%, +0%]
Reservoir	56	[-0%, +0%]
Exhaust gas temperature probe	91	[€82,€113][3]
Fuel tank	120	[-10%,+10%]
Fuel filter	5	[-5%, +5%]
Gascolator	65	[-5%, +5%]
Emergency parachute	540	[-10%,+30%][4]
Emergency Siren	5	[-10%, +5%]
Four Emergency 3V batteries	2	[-10%, +5%]
AvioniCS	3,660	[€2939,€4320]
Eight lights	320	[-10%, +5%]
Main wheels and brake system	395	[-50%,+50%]
Nose wheel	91	[-10%, +5%]
De-icing coating	24	[-0%, +0%]
Total	**€10,197**	**[€9,316,€11,180]**

Table 12.2: Cost of all structural components.

Part	Price [€]	Price range [min,max]
Fuselage and engine mount	775	[-10%, +10%]
Wing	2,535	[-20%,+20%]
Empennage	770	[-10%,+30%]
Tail boom	31	[-10%, +0%]
Tail cone	165	[-20%,+20%]
Nose cone	170	[-20%,+20%]
Landing gear struts	147	[-10%,+10%]
Total	**€4,593**	**[€3,847,€5,490]**

Table 12.3: Optional extra price list.

Part	Price [€]
Nose gear brakes	190
Extra fuel pump	65
Long wave radio	2,000
Redundant GNSS	100
Redundant IMU	1,500
Redundant servos and ESC	280
De-icing system	15,000
Underwater beacon	500
Emergency transmitter	150
Total	**€19,785**

So in total the unit cost is €14,790, with a margin of [€13,163,€16,670], excluding tax and shipping of all the separate parts. This is also excluding mould costs and development costs as per the DSE assignment.

[1] The €100 extra for the engine is from possibly having to pay for the exhaust modifications required to make the exhaust fit in the nose cone. This cost has not been taken into account in the rest of the report the modification does not require any new parts, only a different orientation of the existing parts before welding.

[2] It may be possible to obtain this component with no extra charge if it is possible to save the same amount by not buying the old pulley and belt from Simonini if possible.

[3] The minimum here is the price of the Alcor probe with a 10% bulk discount and the €113 is the Simonini probe.

[4] The large maximum here is for if the modifications turn out to be more expensive than expensive.

Of the options Table 12.3 the first two, the nose gear brakes and fuel pump, are recommended. The landing requirement is still met without the nose brakes, however then there is no redundancy for the braking system. The long wave radio is needed to control the UAV from a distance in case of an emergency. The other options mostly increase reliability and so safety by adding redundancy, with the exception of the de-icing and locator beacons. The de-icing is advised as an option for UAV intended to be used in cold environments. the locator beacons help find the UAV after a crash and to help determine the cause of the accident and the prevent future crashes.

12.2 Weight budget

For the weight first the weight of all parts are listed in Tables 12.4 to 12.6, the weight of the structural components in Table 12.7 and the weight of the components in the rack in Table 12.8.

Table 12.4: Weight of propulsion system.

Part	Weight [kg]	Weight range [min,max]
Engine	32	[-0%,+10%]
Propeller	2.74	[-2%,+2%]
Radiator	1.1	[-5%,+5%]
Reservoir	0.01	[-20%,+20%]
Rectifier	0.1	[-20%,+10%]
Fuel piping	0.05	[-20%,+20%]
Total	**39.34 kg**	[38.53,43.02]

Table 12.5: Weight of other Systems.

Part	Weight [kg]	Weight range [min,max]
Emergency parachute	1.8	[-0%,+10%]
Emergency Siren	0.06	[-0%,+10%]
12V battery	2.05	[-5%, +5%]
Flight control unit	0.72	[-10%,+20%]
ADS-B in/out with GNSS	0.1	[-5%, +5%]
Eight lights	0.08	[-5%,+10%]
Fuel tank	3.5	[-5%, +5%]
Nose wheel	2	[-5%, +5%]
Main wheel with brake system	2.95	[-5%, +5%]
Pitot tube	0.1	[-20%,+20%]
Radio altimeter	0.5	[-20%,+20%]
De-icing coating	0.1	[-0%, +2%]
Magnetometer	0.18	[-5%, +5%]
Total	**9.34 kg**	**[8.85 kg,9.44 kg]**

Table 12.6: Weight of fuel system.

Part	Weight [kg]	Weight range [min,max]
Fuel tank	3.5	[-5%,+5%]
Fuel piping	0.05	[-20%,+20%]
Total	**3.55 kg**	**[3.37 kg,3.74 kg]**

Table 12.7: Weight of all structural components.

Part	Weight [kg]	Weight range [min,max]
Fuselage and engine mount	12.28	[-5%,+5%]
Wing	87.14	[-5%,+5%]
Empennage and tail boom	23.2	[-5%,+5%]
Landing gear struts	27	[-5%,+5%]
Tail cone	6.11	[-7%,+7%]
Nose cone	2.233	[-25%,+25%]
Wing connection	1.5	[-0%,+30%]
Total	**159.4 kg**	**[152.1 kg,171.9 kg]**

Table 12.8: Weight of the rack components.

Part	Weight [kg]	Weight range [min,max]
Payload	100	[-0%,+0%]
Payload rack	7.6	[-5%,+5%]
Total	**107.6 kg**	**[107.2 kg,108.0 kg]**

Adding up all the components give a total OEW of 211.6 *kg* and then including the 107.6 *kg* payload

and 31.2 kg fuel results in a MTOW of 350.4 kg. This is done to account for the components neglected in Table 12.5 such as the emergency 3V batteries, all electrical and data cabling, the gascolator, air filter, fuel filter, fuel pump and the ESCs and servos. These systems are all light weight, however their weight adds up when added to the UAV.

12.3 Requirement compliance analysis

The design is checked primarily with all the main stakeholder requirements in Table 12.9. As you can see almost all the stakeholder requirements are met, however some of them only partially met. There are still some limits to the operational conditions of the UAV which may limit the 24/7 operation and take-off and landing conditions. As already explained in the stability section the UAV is not quite as stable as a Cessna 172.

Table 12.9: Stakeholder requirement compliance check.

Requirement	Achieved
The UAV shall be able to perform take-off and landing in conditions as harsh as possibly encountered during an aid mission.	Partially
The unit cost of the UAV shall be less than €15,000 based on the bill of materials and unit production cost.	Yes
Operational cost shall be less than that of a UH-1 helicopter.	Yes
The round trip distance shall be higher or equal than 500 km with 100 kg payload.	Yes
The UAV shall have swarm operating capabilities.	Yes
The UAV shall be able to use either gasoline or diesel of poor quality as propellant.	Yes
The UAV shall be able to drop packages from a minimum of 15m altitude in the fly-in zone.	Yes
The UAV shall operate autonomously between take-off and landing.	Yes
The UAV shall fit in a 20 ft container.	Yes
The UAV shall be designed for replacement of broken parts.	Yes
The UAV shall be able to take-off and land in a 100 m visibility radius.	Yes
The UAV shall be equally or more stable than a Cessna 172.	Partially
The UAV shall be able to operate 24/7.	Yes
The maximum payload mass shall be 100 kg per flight.	Yes
The payload shall be dropped in 5 different packages of 20 kg each.	Yes
The packages shall not be damaged during the drop such that they become useless.	Yes
The UAV shall be able to deliver a payload of 100 kg at least 3 times within 24 hours.	Yes
The UAV shall be identifiable as delivery vehicle for aid.	Yes
The UAV shall not harm anybody.	Yes
The UAV shall be able to perform in similar conditions as a UH-1 helicopter.	Partially
The UAV shall be able to delivery a package within in square of 25x25 m^2.	Yes
The delivery capacity of the UAV swarm shall be at least the same as a C-130 Hercules.	Yes
The UAV shall be traceable.	Yes
The UAV shall not damage the runways.	Yes
The cruise altitude of the UAV shall be limited to 10,000 ft.	Yes
The UAV shall not interfere with military missions.	Yes

12.4 Risk evaluation and management

It is important that all risks involved in the operation and design of the UAV are evaluated. After the evaluation a risk mitigation management strategy can be designed which will reduce the impact of the risks. A useful tool for this risk evaluation and mitigation is the so called risk matrix. This matrix visualises the impact of the risks clearly. In this section the risk matrices of all subsystems are presented.

Risk management of general operation.

Table 12.10: Ground phase take-off risk map with applied safety measures described in Section 12.5.

Likelihood of event	Consequence of event: Still successful mission	Partly mission failure	Mission failure	Harmful to environment
High				
			Engine failure Flight computer failure	
			Landing gear failure	
		Structural failure	Control surface failure	
Low				

In Table 12.10 the risks involved in the ground phase of the take-off are presented. As mentioned in the caption a couple of risks are already managed by the safety measures explained in Section 12.5. The likelihood of the events for the structural parts and control surfaces are relatively low due to the regular checks while a failure of the flight systems and engine is very likely to occur. The latter is due to the fact that both subsystems contain many single points of failure. Failure of the systems let the mission fail except for some structural failures that might let the UAV continue its mission. The reason that the engine has such a high likelihood of failure is due to it having many single points of failure which are listed here.

- Fuel pump
- Fuel piping leak
- Exhaust
- Carburetor
- Coolant piping leak
- Piston
- Throttle valve

If any one of these components fail, then the engine will stop, with the exception of the throttle valve which could get stuck in the open position and so leaving the engine running at the maximum setting until the fuel gets shut off. The exhaust gas temperature probe does not have any redundancy, however the engine can continue to function without it. Really the only component with redundancy in the engine is the spark plug, of which there are two.

To shift the events in Table 12.10 to the bottom left corner redundancy is to be added to the complete UAV. This will reduce the amount of single point failures. However due to requirement budget constraints redundancy is not an option. Another option is to use more reliable and certified systems. However, these are also more expensive.

The airborne phase of the take-off, shown in Table 12.11, is prone to the same risks as the ground phase. However, because of the fact that the UAV is in flight, the consequences of a failure are much more severe. Due to the low flight altitude the consequences are difficult to mitigate with the already installed safety systems such as the parachute. To shift the events to the down left corner the critical systems should be made more reliable or redundant.

The cruise phase of the mission in Table 12.12 is prone to the same risks as the take-off phase. With the current safety systems the UAV is made considerably safer to the environment. When critical systems fail the parachute will ensure a safe descent. If more sensors and instruments are available the UAV can recognize its flight condition and use this information to fly to a safe location or perform a less rigorous safety procedure. This would shift the events to the left. More reliable systems will of course decrease the likelihood but will increase the costs.

Table 12.11: Airborne phase take-off risk map with applied safety measures described in Section 12.5.

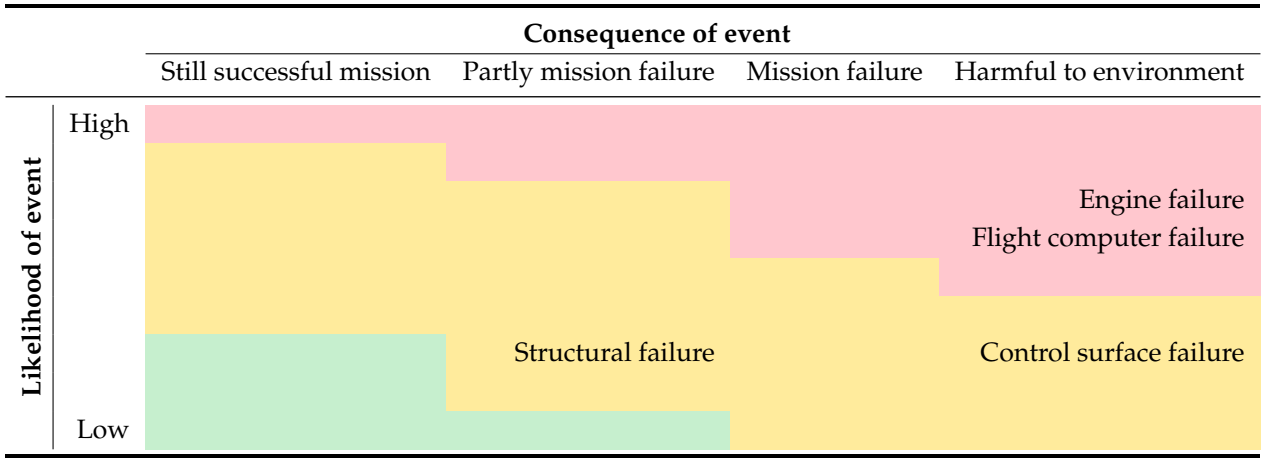

Table 12.12: Cruise phase risk map including applied safety measures described in Section 12.5.

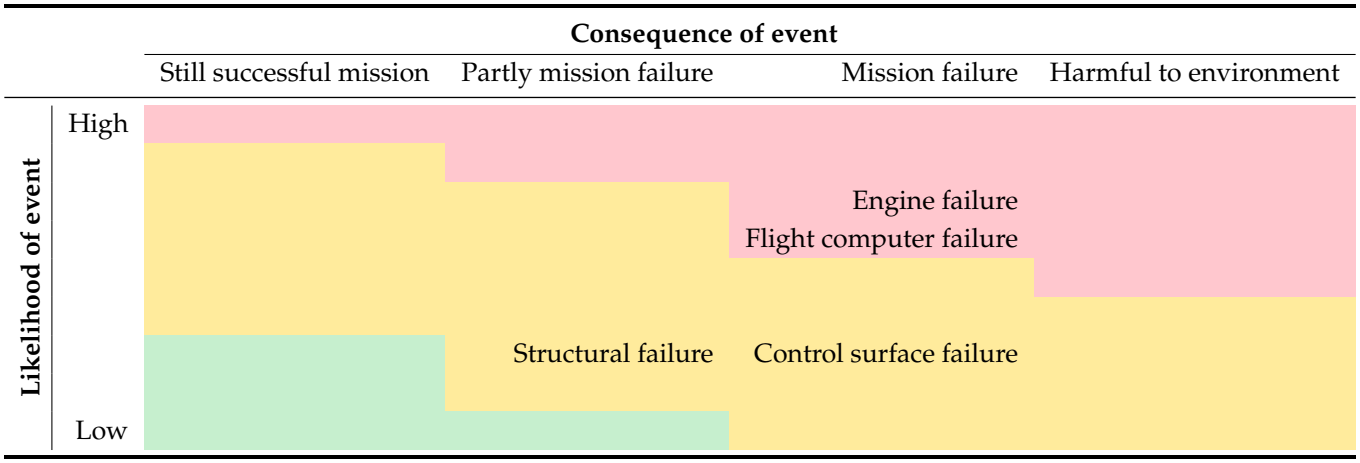

Table 12.13: Maneuver risk map including applied safety measures described in Section 12.5.

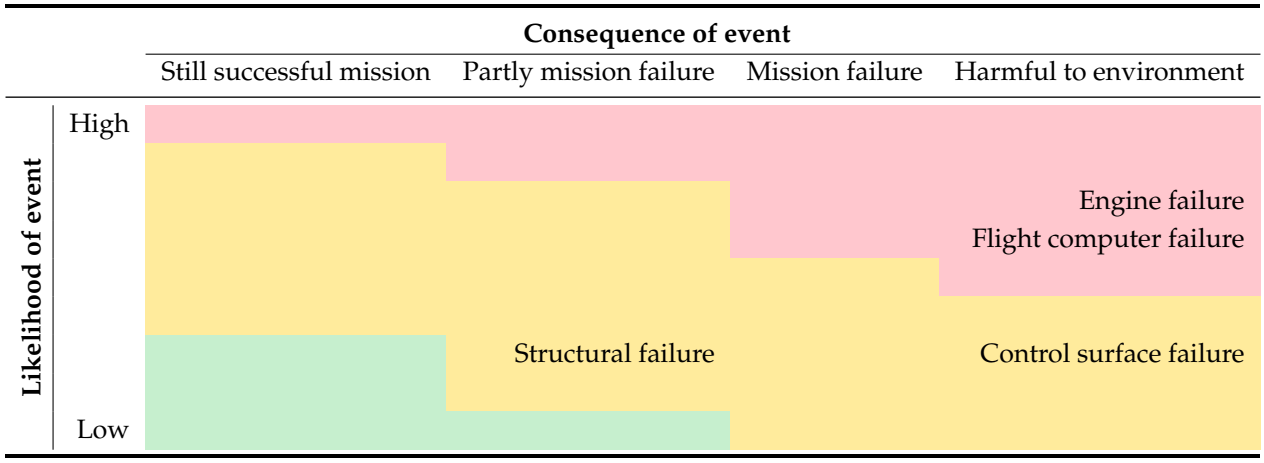

Table 12.13 is very similar to Table 12.11 due to the same flight conditions. At this low altitudes the safety options are very limited which is why many failures will lead to hazardous situations for the environment. In this particular situation the increase of redundancy and reliability of the systems would shift the events down. Evasive maneuvers can be programmed in the UAV because these maneuvers

can reduce the impact of the UAV when it is falling down. The latter requires more sensors and instruments and is therefore not included in the current UAV configuration.

Table 12.14: Airborne phase take-off risk map with applied safety measures described in Section 12.5.

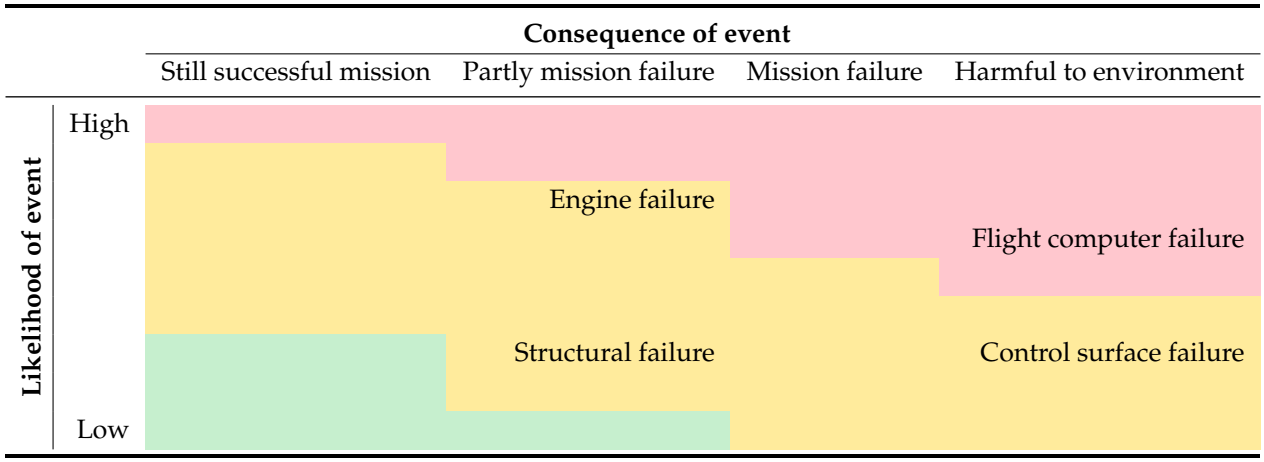

Table 12.14 is very similar to Table 12.11 due to the same conditions at that moment. Because the UAV flies at a very low altitude the safety options are limited which may lead to hazardous situations for the environment. Engine failure will not cause the mission to fail as the mission is already performed and the engine is not required during landing. A safety area is usually included as shown in Figure 12.1. This reduces the risk for the environment significantly. The impact of the event can be drastically reduced if, as stated before, redundant systems are present and/or the reliability of the systems is improved.

Table 12.15: Ground phase landing risk map with applied safety measures described in Section 12.5.

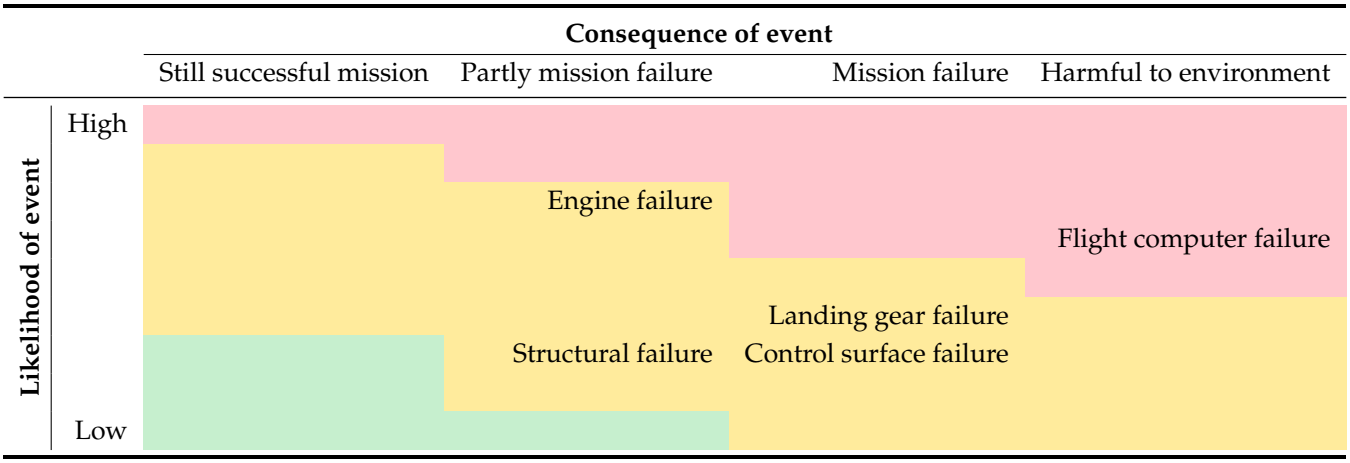

The risk map presented in Table 12.15 is similar to the risk map presented in Table 12.10. The flight conditions are namely very similar as well. An engine failure will not harm the mission as the engine is not required for landing. A flight computer or control surface failure will very likely lead to an uncontrollable UAV for which safety precautions are taken as explained in Section 12.5.

12.5 Reliability, availability, maintainability and safety

Reliability and availability

An important measure for a failure free operation of the Wings for Aid UAV is the reliability of the system. The higher the reliability the lower the downtime of the UAV, which means it can spend more time in the air delivering packages. The total reliability is equal to the multiplication of the reliability of its subsystems. An estimate of several subsystem reliabilities for general aviation as determined by

NASA[37] is given in Table 12.16.

Table 12.16: General aviation subsystem reliability estimates.

System	Reliability estimate
Airframe	0.99940
Electrical	0.99997
Powerplant	0.99986
Flight control	0.98476
Ground control	0.99598
Cockpit instrumentation	0.976

Of course cockpit instrumentation is not directly applicable in this case, however we can take it as an approximation of the reliability of the sense and avoid and communication systems. Multiplying all these values we get a first approximation of the reliability of 0.95653, or 95.65%. This does not mean that 1 in every 25 flights will result in a crash, as not all failures are fatal. Most reliability issues only require some extra maintenance and are often not noticed until the next inspection. The availability of the UAV is highly dependant not only on the system itself but also on the availability of all the other parts of the operation, such as the availability of fuel and goods to be dropped. Normally it is identified as a measure of up-time with respect to total time, however due to the irregularity of natural disasters it is difficult to give an estimation of the expected flight hours and therefore the availability. Furthermore the UAV will not be built using certified parts which will reduce the reliability further.

Maintainability

For maintenance the engine is the main concern as it has so many single points of failure. As mentioned in Section 6.7 and Table 6.6 every 50 flight hours a Type A check will be completed and every 100 hours a Type B check for the engine is performed. Furthermore every 100 flight hours the fuel filter and fuel line will be replaced, every 200 the spark plugs and after each 250 flight hours the air filter. These replacements can be done in coincidence with the Type A and B checks. Furthermore the TBO, or Time Between Overhaul, of the Victor 1 Super is 500 hours. This is when the engine is completely disassembled and many component replaced. Simonini advise that the engine gets sent back to them so that their experienced engineers can complete the overhaul in the correct fashion, however with the operation size of the Wings for Aid operation it will be significantly more cost effective to train Wings for Aid engineers who can operate from the main hubs so that the engines do not need to be sent back to Italy.

For the other components a quick visual check will be completed during the pre-flight check and more extended visual checks in the harder to see locations during the Type A maintenance and in the Type B maintenance the UAV will be disassembled to inspect the mounting points of the various modular components. Furthermore out-of-schedule maintenance will be conducted before each UAV enters storage to ensure that the UAV is ready for rapid deployment. If a part is damaged, then a certified engineer must decide if the UAV can continue flying, can be repaired on the spot, or is required to be sent back to the nearest main hub for difficult repairs. If repair is required then the damaged part will be replaced using the modular design and the rest of the UAV can continue operations. At location repairs can only be simple tasks due to minimal equipment being available. This could include covering minimal leading edge damage with speed tape or replacing a broken bolt.

Safety

Safety is of utmost importance in the Wings for Aid operation. Three different areas of safety are distinguished in this section: safety of ground operations, safety in flight and safety during dropping maneuvers. The risks involved in these areas are evaluated and analysed after which the chosen safety measures are described.

Safety of ground operation

During ground operation the safety of the ground personnel is of highest concern. This personnel is not trained or educated and the safety measures should take that into account. In general the following safety measures are applied:

- The noise level of the operative UAV is expected to be high. Above 90 dB hearing protection is required[5] and it is expected that the UAV will exceed this sound intensity level. Therefore hearing protection is mandatory for every person working with the operative UAV. This means that the people transporting the UAV on the ground will wear hearing protection as well as the people doing the maintenance of the engine. If the reloading and system test areas are close to the runway hearing protections for people working in these sections is recommended as well.
- For ATC it is very important that every person working on the groundsite is clearly visible at all times. This means that all people have to wear reflecting safety jacket or vest and carry lightdevices during nighttime.

On top of these general safety measures the following three hazards that are present during ground operation are analysed:

- Loading and refueling threats
- Threats due to unsuccessful take-off
- Threats due to unsuccessful landing

Before the reloading and refueling a systems check is conducted. In this check all the different systems are tested to make sure that everything works. The systems that are checked are:

- Avionics
- Control surfaces
- Cabling

Also a visual check is conducted. This procedure is described in Section 11.3.

During loading and refueling the fuel is the greatest source of possible accidents. The type of fuel used is gasoline which can catch fire easily. The FAA certifications extensively prescribe refuel procedures in [38]. Not all measures can be implemented due to the primitive airstrips the UAV will be operated from. A careful selection of procedures is made to make sure that the ground personnel is still safe while the procedures can still be implemented realistically. The following refueling procedure is recommended:

1. The fuel shall be stored at least 50 $feet$ (15.2 m) away from any operative aircraft and/or building. Due to the large amount of people walking around the aircraft the recommended distance is chosen to be at least 100 $feet$ (30.4 m). An example of a fuel storage located at a ground site can be seen in Figure 12.1.
2. The fuel storage shall be surrounded by a fence and locked to prevent abuse and to make sure non-authorized people are not allowed to enter the perimeter.
3. Refueling of the external fuel tanks is done at least 100 $feet$ (30.4 m) away from any operative aircraft.
4. Refueling is done by instructed people.
5. There shall be a distance of at least 10 $feet$ (3.3 m) between filled fuel tanks.
6. Smoking is prohibited at the operational site.
7. Clear, non-linguistic signs shall be placed to make people aware of the risks.

After refueling the fuel tank is connected to the aircraft. A single connection system is used to make sure that there are the least amount of connections in the fuel system. The connection is placed at an easy to reach location to make sure that any wear of the connection can easily be noticed.

An unsuccessful take-off is defined as a take-off that is not going according to the flight plan. For this instance the take-off also consists of the preparation for take-off which is the UAV systems check, taxiing and the engine start-up.

During the system check the connections between the different systems are checked. This is again explained in Section 11.3. After the systems check the UAV taxis to the runway and the engine is started. Starting the engine is done by pressing the start button located at the very aft of the tail of the UAV. This specific location is chosen as it is far away from the propeller to ensure maximum safety. Furthermore the start button is designed in such a way that it excludes misuse. From the moment of starting up the engine the ATC takes charge of the UAV and proceeds with the take-off procedure.

[5] URL `https://www.google.nl/webhp?sourceid=chrome-instant&ion=1&espv=2&ie=UTF-8#q=amount+of+dB+of+aircraft+engine` [Cited on 17/06/2016]

During take-off a lot of failures can occur. The ones that are expected to occur the most are listed below. These failures will be analysed even further to motivate the required safety measures. A distinction is made between the ground phase and airborne phase. In the current configuration the UAV will not send data to the ATC as the required communication system is not available. This means that for all safety measures during take-off the ATC relies on visuals and the onboard emergency systems in the UAV itself. Technical failures as described below are of course always possible but the likelihood of failure is already reduced because of the regular system checks that are performed after every flight.

- Engine failure
- Failure of control surfaces
- Failure of landing gear
- Failure of structure
- Flight computer failure

Engine failure during ground phase means end of mission as the UAV only has one engine. The ATC tower is equipped with an emergency stop system that allows the flight crew to send a stop signal to the UAV in the case of visual engine failure. This signal will activate the brakes and will shut down the engine if still on. When the engine loses power it might not have enough power to proceed with the take-off procedure. If the UAV does not reach V1 before a certain mark on the ground the ATC crew will terminate the mission of the UAV with the above mentioned stop procedure. As a safety measure a net will be placed at the end of the runway to make sure the UAV does not continue its path. During airborne phase the engine can fail as well. If there is a collision risk the flight crew will terminate the mission by the system described above. On top of this the UAV will use its in flight safety system. This system consists mainly of an emergency parachute that is able to carry the UAV down with a reasonable velocity. The choice of parachute is explained in Section 10.10. On top of this there is an alarm included that produces a high pitch 120 dB tone that warns people on the ground. In both cases the UAV will crash in an uncontrolled way.

Failure of control surfaces has its influence on the steering of the UAV both in ground phase and in airborne phase of the take-off. If the vertical tail surface control fails during ground phase the UAV will encounter a deviation to either the right or left. If the flight crew notices the failure during ground phase the mission of the UAV will be terminated via above mentioned system. Nets will be placed on the sides and in between the landing strips to catch uncontrollable UAVs. This improves the safety for the workforce significantly. During the airborne phase a failure of rudder can result in an uncontrolled turn if other control surfaces fail as well. If this is noticed by the flight crew the mission is terminated. The in flight system of the UAV will be active as well. If only the rudder fails it is still possible to do a go-around and land on the runway as the deviation caused by the vertical rudder can still be overcome by the ailerons. Other control surfaces like the elevators and ailerons can all fail individually. This has its effect on the steering of the UAV in a similar way as a failure of the vertical rudder. The safety measures will be the same except for the go-around as this will not be possible when these control surfaces fail.

The landing gear is one of the most critical systems and can fail due to structural failure, braking failure or due to a tire blowout. Structural failure results in terminating the mission as it can lead to either a crash or an offset. To prevent dangerous situations nets will be placed next to the runway. Braking failure is not expected to be an issue during take-off. Tire blow out will either cause a crash and will result in a termination of the mission in the same way as mentioned before. If the flight computer fails the UAV will continue in a safe mode making use of the small emergency computer. This computer activates the emergency parachute and alarm. At low altitude this safety system is not flawless and is considered to be the most dangerous situation in the mission life of the UAV.

During landing the same types of technical failures as the ones from take-off can occur. Due to this similarity the same safety precautions and emergency procedures apply to the landing. Some differences are stated below. During the ground phase of the landing the brakes can fail which can have the consequence that the UAV will not be able to stop before the end of the runway. Another option is that one of the brakes fail which will cause the UAV to deviate from the center line. To reduce the risks involved with this kind of failure safety nets will be placed next to each runway. On top of this the regular safety procedures as performed by the flight crew will be executed. If the landing is not performed well there is often the possibility of a go-around. This go-around procedure has its limits and has to be programmed in the UAV. The advantage of a go-around procedure is that it will safe the UAV from crashing into the ground.

The orientation and positioning of the runways and other facilities can improve the safety of the workforce considerably. The following aspects should be considered.

- No people should be in the respective fly-in or fly-out zone (marked area in Figure 12.1) during either take-off or landing. This measure has a negative effect on the turnaround time of the operation.
- Location of ATC tower is as such that it can oversee the compleet ground operations at the airstrip. This ATC tower is marked with the character A in Figure 12.1

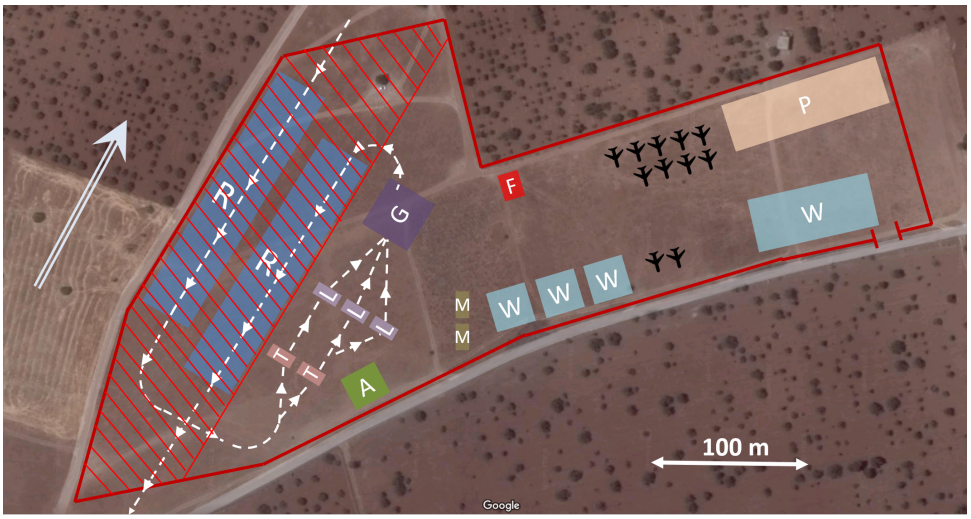

Figure 12.1: Safety measures taken on ground site.

Safety in flight

Cruise flight is in general the most safe phase of any flight[6]. However, technical failure is always an issue during this phase. It is expected that with the instruments available on the UAV in this configuration the UAV will not be able to perform an automated emergency landing without the guarantee that nobody on the ground is harmed. It is assumed that only a rudder defect can be compensated by the other control surfaces and that if this is the case the UAV will be programmed to return to the ground station. In case of any other failure of systems the UAV will execute its emergency protocol which consists of deploying the emergency parachute and activating the 120 dB alarm. This protocol is described in Section 10.10

Safety during dropping maneuvers

The dropping procedure is described in Section 9.2. During the dropping procedure the UAV descends to 15 m and flies into a certain fly-in zone, headed towards the dropzone. During this low-altitude flight the safety options are very limited and therefore other procedures are required. The emergency parachute can not be used as the altitude is too low. This means that in case of an engine failure the UAV executes an efficient climb maneuver to gain as much height as possible. If the UAV is still within the drop margin shown in Figure 9.6 the UAV will drop all its remaining packages to lose as much weight as possible because this will increase the climb performance significantly. If the highest altitude is reached the parachute will be deployed. When the maneuver starts the alarm will be triggered to notify the people on the ground that a failure occurred.

If the control surfaces fail the UAV will try to climb to higher altitudes and will execute the regular safety procedure. If the UAV loses its flight computer the UAV will immediately activate the regular safety procedure. It is expected that the parachute cannot be deployed fully at that altitude but the parachute will still help slowing the UAV down in its descent.

12.6 Sensitivity analysis

A sensitivity analysis was performed using the concept design tool. This tool is described in the Midterm report [5]. Using this tool the variations of the weight of the aircraft is displayed as a function

[6]URL `http://www.flyingmag.com/pilot-technique/instrument-flight-rules/keys-cruise-flight-safety` [Cited on 17/06/2016]

of various design parameters. The result of this can be seen in Table 12.17. The various parameters are all increased separately with 1% and then the increase in gross weight is measured as a percentage of change with respect to the old gross weight. From this it can be concluded that the parameter with the most influence is the aspect ratio.

Table 12.17: Sensitivity analysis for the Wings for Aid concept.

Parameter name	Percent change in MTOW
Aspect ratio wing	0.168 %
Climb rate	0.00175 %
Cruise altitude	-0.0037 %
Aspect ratio horizontal tail	0.00408 %
Aspect ratio vertical tail	0.00707 %
Length of the tail	0.0809 %
Wing position	0.00536 %
Runway length	0.0 %
Cruise speed	0.00262 %

12.7 Sustainability

The sustainability is a very important part of the design process. During the design sustainability is taken into account and furthermore the end-of-life solution is also a great part of the sustainability approach. Both the design sustainability and the end-of-life solutions are explained in this section.

Sustainability during design

The unit cost of €15,000 is a very constraining factor on our design and therefore it was difficult to implement the Cradle-to-Cradle methodology as explained in the Midterm report [5]. However the sustainability approach was not entirely sacrificed to cut costs.

First off, for the materials a comprehensive end-of-life solutions plan is created and can be found further in the section. Furthermore, all harmful materials for the environment are avoided and the need for de-icing fluids is removed by using an icephobic coating. De-icing fluids extract oxygen from the ground water during degradation and therefore very toxic to the ecosystem. During operation the material waste is minimized due to the modular design so that a broken component can be easily replaced and the rest of the UAV can be reused even if the correct tools for repair are not around. the modularity additionally allows for different parts of the UAV to have different lengths of usage, so maximizing the use of each component and preventing disposal of component which are not at their end-of-life yet. this can be obtained through keeping track of each component of a sold UAV separately, and so it is known for each component of each UAV how long it has left until its must be retired from use.

The energy use during operation has been minimized by optimizing the efficiency of aircraft design and choosing the most efficient engine. Furthermore, as the use of biofuels seems unfeasible due to lack of availability, the CO_2 emissions from burning fossil fuels could be offset by the future operator through investing in carbon offset projects.

Water stewardship should be considered in the manufacturing method selection as there are methods which use a significant amount of water. Social fairness has been considered in the ground operation set up where fair wages were used in calculating the operational costs of the local labours. Furthermore the safety of the laborers was extensively looked into to ensure a safe working environment. For final implementation of the Wings for Aid UAV system it should be verified that the components and materials are not sourced from factories that use child laborers or treat their employees unfairly.

For the future in the logistical setup of the manufacturing and operations there are still a significant amount of possibilities to improve the sustainability of the design. The waste of material during manufacturing should be considered, where it is preferred to select production methods where the residual material is minimized. One other way to reduce material waste is to improve the quality control methods during manufacturing to prevent faulty products. Additionally the electricity required by the ground operations could be generated by solar panel or small windmills instead of diesel generators.

However if this is the sole source of power, then large batteries will be required for during the periods when there is no sun or wind.

End-of-life solutions

At the end of the service life of the UAV the system will somehow have to be discarded, and therefore some end-of-life solutions need to be examined. After decommissioning of the aircraft it will be cleaned and all fuel, oil and coolant tanks will be drained of liquids. After this it is ready for disassembly in separate equipment and parts. The efficient dismantlement of the UAV requires a disassembly planning, as no two UAVs are equal. Therefore before each disassembly a plan must be made [39]. For each of the disassembled parts and components there are several end-of-life solutions:

- Reuse
- Reuse for different purpose
- Re-manufacture
- Recycling
- Disposal

Reuse is at the highest level, where parts are reused maintaining their original function. Different parts might have different lifetimes, and in order to be able to reuse parts it is essential that there is the possibility of easy disassembly. Besides full reuse the components could also be used for different purposes. If the components are at the end of their useful life structurally but still look sound, another option is to sell them to the growing market of refurbished decorative aircraft parts. Used wings and other structural parts are transformed into office desks, bookshelves or even beds[7].Not only entire parts but also components of parts might be reused, such as components of the main fuselage. The next level is re-manufacturing, where the parts are taken apart down to a component level and are used as parts in new aircraft. Again easy dismantlement is essential to making this a viable option. Third is recycling, where parts are disassembled to their material level where they can be remade into new parts or products. Depending on the material it is not always possible to match the performance characteristics of the original material after recycling. The final option is disposal, where the parts or material is not fit for any of the other categories.

Table 12.18: Recovery channels Wings for Aid UAVs.

UAV parts	Recovery channel
Engine, APU, landing gears, modular tail and wing surfaces, structural parts, control surfaces and payload mount.	Reuse or recycle based on condition
Safety equipment, avionics, tires	Recycle or Reuse according to regulations
Aluminium scrap parts, Foam, plastics	Recycle or dispose according to material

A summary of the end-of-life for the different parts can be seen in Table 12.18. Not all parts of the UAV will reach the end of their service life at the same time. Because of the modularity of the design any of the modular parts in sufficient condition can instantly be detached and reused on a different UAV, or kept as a spare part. This applies to the wing, wing tips, tail wing surfaces, landing gear, propeller and payload mount.

Parts such as the tires, the avionics and the safety equipment must be thoroughly check to verify that they still meet the regulations that apply to them before being reused on an aircraft. Otherwise they will have to be disposed of. Aluminium parts can be recycled provided there is no foam directly attached to it. Foam residue's would need to be burned off before the aluminium wing parts can be recycled. Large parts of the main fuselage are riveted they can relatively easily be dismantled, and can be re-manufactured into another UAV. The foam in wing parts will need to be removed from the skin. The large inner parts can be recycled, whilst scraps stuck to the skin will have to be disposed of. The foam recycling can happen in two different ways. Physical recycling is fast and cheap but affects the performance properties of the material, limiting its market applications. Chemical recycling of foam means the foam returns to its original state and can be re-used as raw material for original parts [40].

[7]URL `http://www.motoart.com/gallery/` [Cited on 17/06/2016]

Chapter 13

Post-DSE project plan

This chapter will explain the logical steps in bringing the project from preliminary design to implementation and production of the Wings for Aid UAV. To this end, Section 13.1 describes the development stages after preliminary design has ended, and Section 13.2 illustrates an initial assembly line plan. Additionally in Section 12.7 some ideas for the end-of-life solutions for the Wings for Aid UAV are discussed.

13.1 Post-DSE project development

After the DSE the design will have to be finalized and brought to the market. In doing so several steps have to be follow, as illustrated in Figure 13.1. A quick explanation of each step is as follows:

- **Step 1: Product development** The first step is the research and design phase in which the design goes through detailed design and prototyping several times before being deemed ready for manufacturing. When the prototype fits all requirements it is deemed ready for production, and can be taken to the next step.
- **Step 2: Manufacturing** During this phase the product assembly line and part manufacturing stations are set up. Each initial product is evaluated to see if it meets the specifications, once this is done, bulk production can start.
- **Step 3: Marketing** While product development is being done, it is a good idea to explore potential markets where the Wings for Aid UAV might be applied so that the initial product series can be enlarged, which leads to lower unit costs.
- **Step 4: Bulk production** At this stage the design and market is ready for full scale production, both for life-saving Wings for Aid UAVs and commercially employable UAVs.

13.2 Manufacturing and assembly plan

The production methods of the main components of the UAV have already been discussed independently in Chapter 8. The preliminary plan for the main assembly line can be seen in Figure 13.2. In the assembly plan a distinction is made between parts created in-house, and parts originating from external suppliers.

In the assembly flow it is specified at which point of the assembly these parts are brought in. Most metal parts will be manufactured in-house. These will include the main fuselage parts, wing and tail surface skins and landing gear struts. Other parts such as the engine, wheels, tires, foam core parts for the wings and plastic covers will created by partner companies. The landing gear, wing and tail surfaces are assembled at sub-assembly stations from where they can can be attached to the main assembly at the appropriate stage. The following activities will take place at each of the main stations:

- **Assembly station 1:** At this station the main fuselage structure is assembled from parts, including the tail boom, the firewall and engine support and the payload doors/covers at the bottom of the fuselage. The final stage at this station is that the fuselage is put onto the landing gear so that it can be easily rolled through the rest of the assembly line.
- **Assembly station 2:** At this station all the power, control, communication and emergency systems are installed into the main body of the fuselage, such as the flight control, the GNSS receiver and the emergency parachute among others.
- **Assembly station 3:** When arriving at this station the main wing and tail surfaces will be attached and the control system will be tested. Simultaneously the engine will be installed.
- **Assembly station 4:** At the final station the propeller will be mounted on the engine, the payload structure will be placed inside the fuselage and the nose and tail fuselage covers will be mounted. With this step complete the UAV is ready for full system testing, before being disassembled for storage or transport.

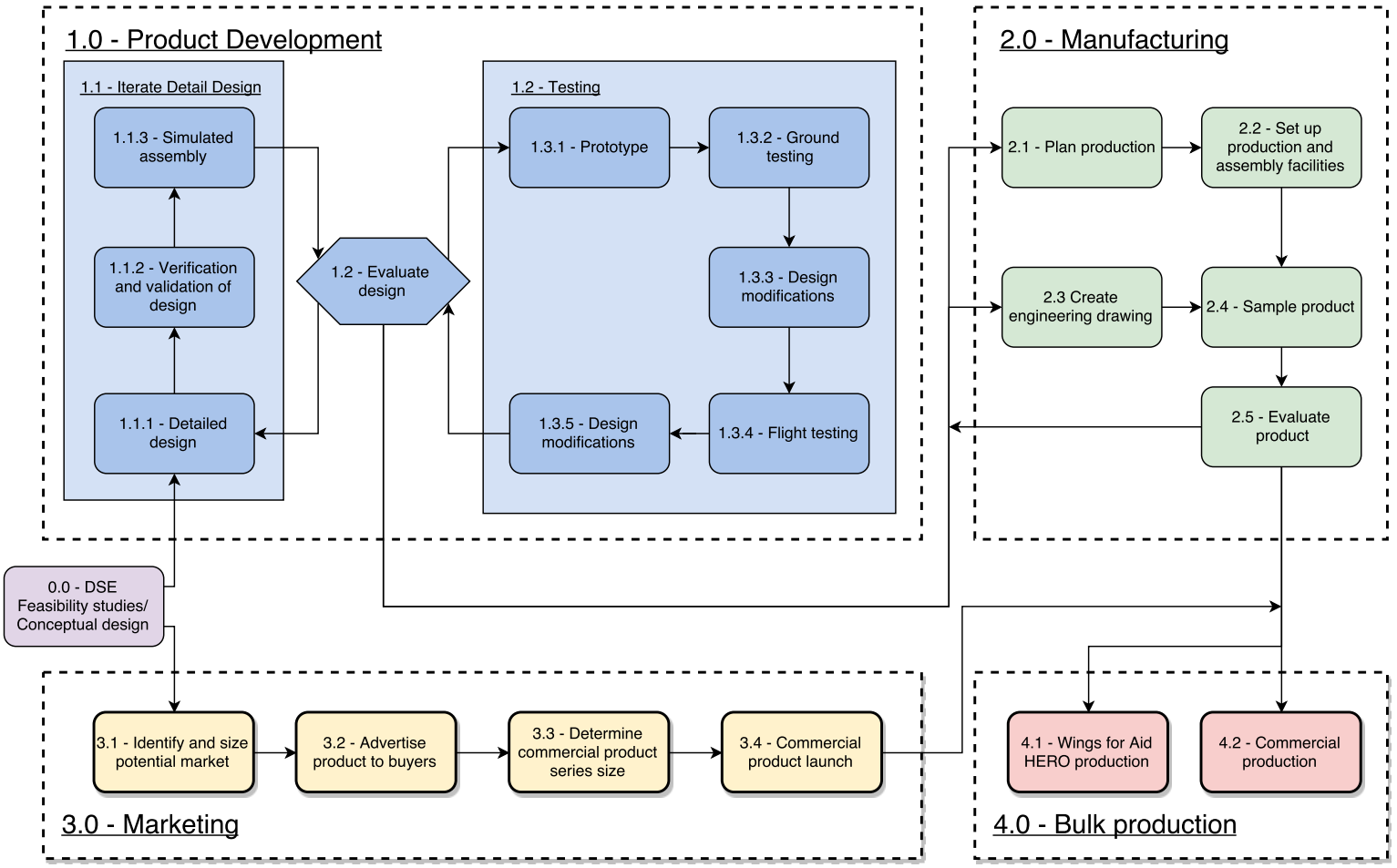

Figure 13.1: Flowchart of product development post-DSE.

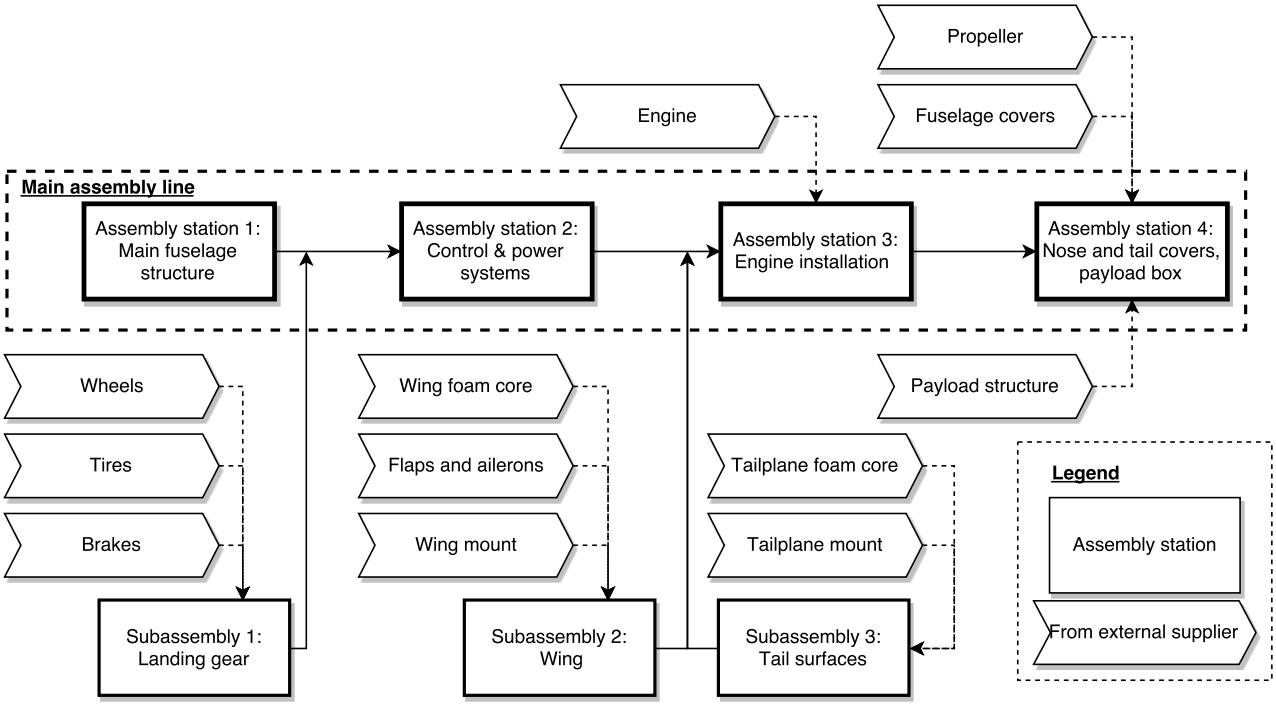

Figure 13.2: Assembly line layout for the Wings for Aid UAV.

Chapter 14

Conclusion and recommendations

14.1 Conclusion

The purpose of this technical report is to present and explain the design of the Wings for Aid concept with a focus on the Wings for Aid UAV. The aim of the Wings for Aid concept is to be able to transport five 20 kg packages over a distance of 500 km. The packages will contain food, water and blankets in sufficient amounts to provide relief to victims on the ground for several days. The Wings for Aid concept aims to compete with all traditional modes of transportation on different areas namely operational costs and ease of usage. Two different types of aid missions are considered namely a warzone mission and a regular mission.

Different concepts for both the operational aspect and the UAV aspect were considered to come to the design presented in this report. The Wings for Aid concept can operate at full capacity within 72 hr from any location within 3800 km of the central logistical hub using the ferry concept to transport the UAVs. The turnaround time of every UAV during operation is 29 min but because an assembly line strategy is used a UAV can take off and land every 6.4 min. This means that for a warzone mission a minimum of 50 UAVs and for a regular mission a minimum amount of 43 UAVs is required to reach the required capacity requirement of 22,500 kg delivered aid supply within 24 hours. The operational costs for the UAV are €28,000 to deliver 22,500 kg of goods to a location 500 km away from the ground site. This means that the Wings for Aid UAV can compete with the C-130 Hercules (€32,678) and the UH-1 Bell Huey (€897,000) from a cost perspective.

The Wings for Aid UAV has a maximum take-off weight of 350.4 kg, an operational empty weight of 211.6 kg, a wingspan of 7.9 m, a wing area of 9.0 m^2 and a total length of 5.9 m. With a fuselage width of 0.58 m and by placing two UAVs in an opposite direction both UAVs can be placed in a 20 ft container.

The UAV costs are expected to be €14,790 with uncertainty it should be between €13,163 and €16,670. This leads to the conclusion that the Wings for Aid concept is a financially feasible concept that will be a dominant competitor in the aerial aid delivery market by outperforming other competitors on aspects like delivery time, operating costs and effective distribution of aid supplies. However there is still room for improvement which is why recommendations are presented in Section 14.2.

14.2 Recommendations

Aerodynamics It is recommended to perform a CFD simulation on the landing gear and complete UAV to get a better estimation for the drag coefficient. 3D interactions between wing and fuselage were not analysed as it is beyond the scope of the DSE. The connection between the wing and fuselage has to be analyzed to minimize the lift loss due to interference between wing and fuselage. Secondly the air intake has to be optimised such that the flow can enter the radiator and the water can be cooled. This will be critical for the engine to operate and therefore very important to investigate.

Control surfaces For the control surfaces it is recommended to investigate if the assumed critical cases for the design of the control surfaces are actually critical. This can be done by also sizing the different control surfaces for other flight phases of the mission and not just the assumed critical one. The flaps for example can be sized by looking at the approach during landing or the drop maneuver, or the elevator by also looking at trim conditions during cruise flight and drop procedures. By doing this, it is expected to get a better sizing for the control surfaces which takes into account all the different flight phases.

Performance and propulsion For propulsion the first thing recommended is to do real world tests with the off-the-shelf parts chosen to validate that the used power level, propeller efficiency, thrust level, fuel consumption and component weights are correct. Variations in these parameters will greatly affect the take-off distance and range of the UAV. Additionally propellers with different pitches can be tested in flight tests to find an optimum between take-off cruise and climb performance. For performance it is also important to do real life tests to determine the actual landing, take-off, climb and cruise performance. The simulations used to verify the landing and take-off distance still include assumptions and so will differ from reality, which is something that needs to be checked.

Stability derivatives Because of the inaccuracies the DATCOM method experiences especially when modelling the lift curve slope of the different lift generating area's it is recommended that a CFD analysis is performed on the entire aircraft configuration. It is expected that the CD found after CFD analysis

will be higher than the CFD currently obtained from DATCOM. This is mainly due to the fact that the DATCOM method is not able to take into account a fixed landing gear. Also, the DATCOM method was not able to give a reasonable estimate for the lift curve slope of the various lift generating surfaces and therefore the values obtained from XFLR5 had to be used for some stability derivatives. Another disadvantage of the DATCOM method is that it is not possible to give a rudder as input. Therefore it is also recommended the control derivatives are analysed using CFD to give more accurate estimates.

Structures For the structure of the UAV the main load cases have been considered and analyzed in the main load carrying elements. In the detail design of the UAV more attention will have to be paid to the design of the connecting elements between the main structural components. Additionally we recommend that the trade-off for the different wing and fuselage structures be made at a stage where each concept is worked out into more detail. A more detailed design of the payload rack has to be performed. For the weight estimation it was assumed that the rack consists out of aluminium L-profiles. This is a suitable design solution as it is lightweight and can bear a lot of loads. The rack structure is likely to need enforcement at the location of the release mechanisms where the packages are carried. It is recommended to place this release mechanism with enforcement at the upper side of the rack.

Air intake Currently the air intake is external which provides for good air intake, however the air intake is therefore prone to debris and other impact sources. Furthermore it creates the risk of flooding the engine with water in heavy rain. To prevent this it is recommended to create a small cover to enclose the air intake as much as possible, while not restricting the air flow for the intake.

Communications We recommend fitting the UAV with a communications device, such as a long wave radio antenna, strong enough to be able to remotely pilot the UAV, or providing this as an optional extra. Being able to remotely take control of the UAV in every stage of flight will almost certainly be required by CS-LUAS when it is released. It will also greatly increase the safety. If something abnormal happens, the UAV will need to deploy the emergency parachute as rapidly as a human could possibly judge. It should judge the surroundings of the UAV to better guide it to an empty space and then deploy the parachute or even perform an emergency landing to preserve the UAV.

De-icing Currently the lack of de-icing limits the operating environments of the UAV. Most disasters have historically been in warmer areas and these are generally more densely populated. Therefore for most cases de-icing will not be needed, however it could be an optional extra for that the colder regions of the earth could also receive aid if a disaster happens. This could for example be the higher regions of Nepal, Alaska or Japan or Chili in the winter. These are all earthquake prone regions which could not be reached with the current UAV. This will however add significant cost and weight to the UAV as not only do the wing, empennage and propeller leading edges need to be kept ice free, but additionally will require a carburettor heater, pitot tube heater and an overhaul of the electronics as currently most of the electronics will only be rated for positive temperatures.

Lightning strikes Lightning strikes have not been looked into. The complete outside is built up out of metal, with the exception of the tail cone, which could cause issues. Another issue is the foam core of the wings. If the wing is hit by lightning, then there will be a local increase in temperature which could damage the foam and the adhesive. Therefore it is not recommended to fly through lightning storms.

Parachute When the parachute is deployed the nose of the UAV will pitch up as the parachute is mounted in front of the CG. To prevent the propeller damaging the parachute lines the parachute was mounted as close to the CG as possible and the elevator will additionally help keep the nose down. Furthermore a system should be implemented in the avionics to stop the fuel flow to the engine when the parachute is deployed. However it is still possible that the propeller can windmill, so the orientation of the UAV when falling below the parachute should be check to prevent damage to the parachute. It is expected that the current parachute deployment system will not deploy fast enough for low altitude deployment, so for more safety, and reliability, a parachute system that makes use of pyrotechnics to ensure a fast deployment could be looked into.

Operational aspect From an operational aspect it would be beneficial if the UAVs would drop all packages at once as this will reduce the mission time per UAV significantly which will reduce the amount of UAVs required significantly. As stated in Section 11.1 the ferry concept should be thoroughly investigated as it will be a very beneficial method of UAV transportation. However it is still prone to many issues which will have to be solved before it can be applied in real life.

Cost When calculating the unit cost of the UAV the development and mould costs are not included. If the development cost is divided over the UAVs the unit cost will increase. This increase in unit cost depends on how many UAVs are ordered. In order to be able to calculate the unit cost more accurately it is recommended to estimated how many UAVs are ordered and how much the development cost will be. For the operational costs the cost of insurance was not included, however the UAV is designed to meet as many regulations as possible to increase the insurability.

Bibliography

[1] van Wassenhoven, L., "Humanitarian aid logistics: supply chain management in high gear," *Journal of the Operational Research Society*, Vol. 57, 2006, pp. 475–489.

[2] Balcik, B., Beamon, B. M., and Smilowitz, K., "Last Mile Distribution in Humanitarian Relief," *Journal of Intelligent Transportation Systems*, Vol. 12:2, 2016, pp. 51–63.

[3] Borton, J., Brusset, E., and Hallam, A., "The International Response to Conflict and Genocide: Lessons from the Rwanda Experience; Study III: Humanitarian Aid and Effects," Tech. rep., Overseas Development Institute, March 1996.

[4] Gunasekaran, A. and Ngai, E., "The successful management of a small logistics company," *International Journal of Physical Distribution & Logistics Management*, Vol. 33, 2003, pp. 825–842.

[5] Y.Bunk, M.J.Faber, Jong, D., L.N.Lodder, Loo, M., M.J.Mollema, N.Pynaert, B.Slangen, B.Smit, and L.Vertonghen, "DSE - Wings for Aid Midterm Report, Design an unmanned aircraft that can deliver 5 aid pack-ages of 20 kg each with a range of 250 km." Tech. rep., TU Delft, May 2016.

[6] Raymer, D. P., *Aircraft Design: A Conceptual Approach*, Educ Series, American Institute of Aeronautics and Astronautics, 1989.

[7] John D. Anderson, J., *Fundamentals of aerodynamics*, McGraw-Hill, 2011.

[8] Schlichting, H., *Boundary-Layer Theory*, 7th ed., McGraw Hill, 1979.

[9] ANSYS, I., *ANSYS Fluent Theory Guide*, ANSYS,Inc., 2014.

[10] Ahmed, S.R., R. G., "Some Salient Features of the Time-Averaged Ground Vehicle Wake," Tech. rep., SAE Technical Paper 840300, 1984.

[11] M. Nita, D. S., "Estimating The Oswald Factor From Basic Aircraft Geometrical Parameters," Tech. rep., Hamburg University of Applied Sciences, May 2012.

[12] European Aviation Safety Agency, "Certification Specifications for Very Light Aeroplanes," 2016, CS-VLA.

[13] J.A. Melkert, R. Vos, B. Z., "Aircraft Preliminary Sizing," 2014, AE1222-II Aircraft Preliminary Sizing (T/W-W/S diagram) Part 1 of 2, TU Delft.

[14] Gundlach, J., *Designing Unmanned Aircraft Systems: A Comprehensive Approach*, AIAA education series, American Institute of Aeronautics and Astronautics, 2014.

[15] Gudmundsson, S., *General Aviation Aircraft Design: Applied Methods and Procedures*, Elsevier Science, 2013.

[16] McCormick, B., *Aerodynamics, Aeronautics, and Flight Mechanics*, John Wiley & Sons, Inc., 1979.

[17] Roskam, J., *Airplane Design: Determination of Stability, Control and Performance Characteristics: FAR and Military Requirements*, Airplane Design, DARcorporation, 1985.

[18] Roskam, J., *Airplane Design: Preliminary Calculation of Aerodynamic, Thrust and Power Characteristics*, Airplane Design, Roskam Aviation and Engineering Corporation, 1985.

[19] Ruijgrok, G. J., *Elements of airplane performance*, Delft Academic Press, 2013.

[20] Noon, R. K., *Engineering analysis of vehicular accidents*, CRC Press, 1994.

[21] Sadraey, M. H., *Aircraft Design: A Systems Engineering Approach*, Aerospace Series, Wiley, 2012.

[22] in 't Veld, A., *Flight dynamics Lecture Notes*, TU Delft, 2015.

[23] Foster, T., *Dynamic Stability and Handling Qualities of Small Unmanned-Aerial-Vehicles*, Brigham Young University, 2004.

[24] Edupack, C., 2016.

[25] Armao, F., "Aluminium Workshop: Choosing an alminium alloy," *Practical welding today*, 2015.

[26] "Urethane Pour Foam Overview," online, 2012.

[27] Sinke, J., *Riveting and Bolting*, Production of Aerospace Systems, TU Delft.

[28] Saunders-Smits, G. and Rans, C., "Transverse Shear Stresses in Bending," 2014, AE1108-II Aerospace Mechanics of Materials, TU Delft.

[29] T.H.G. Megson, *Aircraft Structures for Engineering Students*, Elsevier, 4th ed., 2007.

[30] Hoerner, S. F., *Fluid-Dynamic Drag*, Sighard F. Hoerner, 1965.

[31] Steenhuizen, D., "Wing design," 2015, Aerospace Design and Systems Engineering Elemens II (AE211-II).

[32] Kundu, A. K., *Aircraft Design*, Cambridge University, 32 Avenua of the Americas, New York, USA, 2010.

[33] Association for Unmanned Vehicle Systems International, *Airspace Integration Alternatives for Unmanned Aircraft*, 2010.

[34] Administration, F. A., "Automatic Dependent Surveillance Broadcast (ADSB) Out Performance Requirements To Support Air Traffic Control (ATC) Service; Final Rule," 2010.

[35] Pham, H., Smolka, S. A., Stoller, S. D., Phan, D., and Yang, J., "A survey on unmanned aerial vehicle collision avoidance systems," *arXiv preprint arXiv:1508.07723*, 2015.

[36] Y.Bunk, M.J.Faber, Jong, D., L.N.Lodder, Loo, M., M.J.Mollema, N.Pynaert, B.Slangen, B.Smit, and L.Vertonghen, "DSE - Wings for Aid Baseline Report, Design an unmanned aircraft that can deliver 5 aid pack-ages of 20 kg each with a range of 250 km." Tech. rep., TU Delft, May 2016.

[37] Pettit, D. and Turnbull, A., "General Aviation Aircraft Reliability Study," Tech. rep., 2001.

[38] FAA, *International and FAA Fuel Fire Safety ICAO Annex 14, Chapter 9*, 2012.

[39] 12th Global Conference on Sustainable Manufacturing, *Proposed framework for End-Of-Life aircraft recycling*, 2015.

[40] The 7th International Conference on Waste Management and Technology, *Recycling and disposal methods for polyurethane foam wastes*, 2012.

Appendix A
Total operational cost

Table A.1: Total operational cost.

Warzone			**Natural disaster**		
Workforce	38	people	Workforce	38	people
Salary	€3.00		Salary	€3.00	
Total costs workforce per hour	€114.00		Total costs workforce per hour	€114.00	
Total cost workforce/day	€2,736.00		Total cost workforce/day	€2,736.00	
Total cost workforce/mission	€12.16		Total cost workforce/mission	€12.16	
Experts	6	people	Experts	6	people
Salary	€40.00		Salary	€40.00	
Total costs experts/hour	€240.00		Total costs experts/hour	€240.00	
Total cost experts/day	€5,760.00		Total cost experts/day	€5,760.00	
Total cost experts/mission	€25.60		Total cost experts/mission	€25.60	
Total salary per day	€8,496.00		Total salary per day	€8,496.00	
Engine cost per mission	€84.12		Engine cost per mission	€68.30	
Total salary per mission	€37.76		Total salary per mission	€37.76	
Total costs per mission	€121.88		Total costs per mission	€106.06	
Total costs per person in need	€0.61		Total costs per person in need	€0.53	
Salary costs	0.76	€/*ton*/*km*	Salary costs	0.76	€/*ton*/*km*
Engine and fuel costs	1.68	€/*ton*/*km*	Engine and fuel costs	1.62	€/*ton*/*km*
Total operational cost	2.44	€/*ton*/*km*	**Total operational cost**	2.38	€/*ton*/*km*

Appendix B
DATCOM input file

Listing B.1: Input file used for the USAF DATCOM programme.

```
  $FLTCON NMACH=1., MACH(1)=0.128,
    NALPHA=13.0,ALSCHD(1)=-2.,-1.,0.,1.0,2.0,3.0,4.0,6.0,9.0,12.0,16.0,20.0,22.,
    RNNUB(1)=2717928.62$
 $SYNTHS XCG=1.897, ZCG=0.494, XW=1.0,
    ZW=0.806,
    ALIW=0.0, XH=4.786,ZH=0.750, ALIH=0.0,
    XV=4.786, VERTUP=.TRUE., ZV=0.80$
 $OPTINS SREF=9.0, CBARR=1.204,
    BLREF=7.9$
 $BODY NX=5.0,BNOSE=2.0,BTAIL=2.,BLN=0.545,BLA=2.927,
    X(1)=0.0,0.545,2.985,4.645,5.809,
    S(1)=0.0050,0.464,0.464,0.0050,0.0050,
    P(1)=0.251,2.76,2.76,0.251,0.251,
    R(1)=0.04,0.345,0.345,0.04,0.04,
    ZU(1)=0.440,0.80,0.80,0.80,0.80,
    ZL(1)=0.360,0.,0.,0.72,0.72$
NACA-W-4-1312
 $WGPLNF CHRDTP=0.65, SSPNE=3.66,
    SSPN=3.95,
    CHRDR=1.62, SAVSI=13.8, CHSTAT=0.0,
    TWISTA=0.0, DHDADI=0.0, TYPE=1.0$
NACA-H-4-0012
 $HTPLNF CHRDR=1.02, CHRDTP=0.46,
    SSPNE=1.023,
    SSPN=1.055, SAVSI=26.8,
    CHSTAT=0.0, TWISTA=0.0, DHDADI=0.0, TYPE=1.0$
NACA-V-4-0012
 $VTPLNF CHRDTP=0.46, SSPNE=1.023,
    SSPN=1.055,
    CHRDR=1.02, SAVSI=26.8,CHSTAT=0.0,
    TWISTA=0.0, DHDADI=0.0, TYPE=1.0$
 $SYMFLP FTYPE=1.0, NDELTA=9.0,
    DELTA(1)= -4.0,-3.0,-2.0,-1.0,0.0,1.0,2.0,3.0,4.0,
    PHETE=0.13, PHETEP=0.10, SPANFI=0.12,
    SPANFO=0.95,
    CHRDFI=0.25, CHRDFO=0.193,
    CB=0.0795, TC=0.038, NTYPE=1.0,$
DERIV RAD
TRIM
DAMP
DIM M
CASEID CONCEPT WINGS FOR AID
SAVE
NEXT CASE
 $ASYFLP STYPE=4.0, NDELTA=8.0, DELTAL(1)=1.,6.,9.,10.,12.,15.,17.5,20.,
    DELTAR(1)=-1.,-6.,-9.,-10.,-12.,-15.,-17.5,-20.,SPANFI=2.300,SPANFO=3.555,
    CHRDFI=0.468, CHRDFO=0.414$
DERIV RAD
DIM M
CASEID CONCEPT WINGS FOR AID AILERONS
NEXT CASE
```